THE UNIVERSITY OF MICHIGAN

INDUSTRY PROGRAM OF THE COLLEGE OF ENGINEERING

IRRADIATION INDUCED ATOMIC DISPLACEMENTS IN METALS

Jean Michel Planeix

A dissertation submitted in partial fulfillment
of the requirements for the degree of
Doctor of Philosophy in the
University of Michigan
1958

September, 1958

IP-315

Doctoral Committee:

Professor H. J. Gomberg, Chairman
Assistant Professor B. A. Galler
Professor E. H. Rothe
Professor M. J. Sinnott
Assistant Professor G. L. West, Jr.
Professor E. F. Westrum, Jr.

ACKNOWLEDGEMENTS

The author wishes to express his gratitude to the members of his Doctoral Committee for their interest in this work and their understanding, and particularly to Professors H. J. Gomberg, M. J. Westrum, and M. J. Sinnott for frequent and fruitful discussions.

Many thanks are due to Mr. R. White for his very competent work in building the components of the cryostat under construction and to Mr. J. Mannlein for his accurate job on an unusual liquid helium transfer.

Finally, the author is indebted to the Industry Program of the College of Engineering for having accepted this dissertation for distribution.

TABLE OF CONTENTS

TABLE OF CONTENTS (CONT'D)

NOTE: The following signs are used throughout this dissertation:

$\sim$ meaning proportional to

$\cong$ meaning approximately equal to

LIST OF TABLES

LIST OF FIGURES

LIST OF FIGURES (CONT'D)

LIST OF DIAGRAMS

LIST OF APPENDICES

LIST OF APPENDICES (CONT'D)

LIST OF APPENDICES (CONT'D)

CHAPTER I

INTRODUCTION

Of the two broad categories of the effects of radiations on matter, namely atomic displacements and ionization, the first one is of basic importance in solid state studies, since it is closely dependent on the interaction of identical atoms of the irradiated sample. Atomic displacements constitute the only permanent radiation damage in non fissile metals and they are only produced to an important extent by massive particles, those coming into consideration being neutrons for pile irradiation and protons, deuterons, alpha-particles for cyclotron irradiation. The present status of theoretical and experimental research in this field has been summarized in a previous paper.(1) Some indications relative to this status will be given in Chapter II, Background. Much more experimental work has been done than theoretical work. The two most important recent pieces of theoretical work are Brinkman theory of displacement spikes(2) and Snyder and Neufeld(3) calculation of the total number of atoms displaced per atom displaced by bombarding particles, i.e. per primary knock-on. Brinkman assumes an interaction potential energy between a knock-on and a stationary lattice atom which is the electrostatic mutual potential energy of two rigid charge distributions having each a typical screened potential. This potential energy is negative deep within the atom, which stems from the fact that closed shell repulsion between the two atoms is neglected in this treatment, and leads to a discontinuity in the interaction when the separation of the two atoms drops below the value for

which the potential energy has its minimum. Brinkman uses an impulse approximation to assess energy transfer between moving and stationary atoms and obtains a mean free path between displacing collisions which is smaller than the interatomic distance when the knock-on energy falls below a certain transition value, typical of the metal. Hence he concludes to the existence of highly disturbed localized regions, which he calls "displacement spikes". This theory leads to a qualitative explanation of the phenomena observed when samples are thermally annealed after low temperature irradiation.

Snyder and Neufeld proposed the only calculational model allowing qualitative confrontation to be made with experimental results. This model assumes hard sphere scatter between moving and stationary atoms, at all energies. It is worth noting that a direct confrontation is impossible. It is necessary to adopt a theoretical value for the change in electrical resistivity due to a fraction of one percent of atoms displaced, i.e. of Frenkel pairs if we regard the sample as perfect before irradiation. This value has been calculated for some monovalent metals by Jongenburger[4], Blatt[5], and Dexter.[6] The author[1] has made an independent calculation, assuming a screened potential interaction between defect and conduction electron of the same form, but opposite sign, depending whether the defect considered is an interstitial atom or a vacancy. His result, for 1% Frenkel pairs in copper, is about the same as Dexter's estimate and about three times smaller than Jongenburger's. Dividing the observed change in

electrical resistivity by the adopted value of the influence of one percent Frenkel pairs on resistivity (2.7 $\mu \Omega$ x cm is generally admitted, after Jongenburger) furnishes a first estimate of the fraction of existing defect pairs. If the experiment shows radiation anneal, the tangent to the curve at the origin is extrapolated to replace the experimental curve. A second estimate is obtained by calculating the fraction of lattice atoms becoming primary knock-ons, from cross sections, and bombarding particle fluxes, and the number of atoms displaced per primary, using Snyder and Neufeld method. Such a confrontation made, in the case of pile neutron irradiation of copper and cyclotron deuteron irradiation of the same metal shows that the second estimate is 4 times and 6 times higher than the first one, for pile and cyclotron irradiation respectively. Similar treatment of other properties, such as changes in Hall coefficient and neutron scattering cross section of graphite during neutron irradiation and volume expansion of copper under deuteron bombardment, have shown deviations in the same direction, and of about the same magnitude, between the two estimates. It seems, therefore, that Snyder and Neufeld method over estimates the number of atoms displaced per primary knock-on.

Measurements of electrical resistivity have been performed during cyclotron irradiation(7), (8) and reactor irradiation(31), in both cases at very low temperature. The cyclotron experiments show that, as irradiation progresses, the line representing the change in resistivity versus integrated particle flux deviates from linearity,

bending downward. Thus some damage is recovered in this way and this process is called "radiation anneal". Seitz and Koehler[9] have investigated the problem of recombination between defects of various generations, i.e. corresponding to various primary displacing collisions between bombarding particles and lattice atoms and conclude that the values of knock-on range required for such process are higher than the values one would reasonably expect for a moving atom. But the case they considered was that of extreme recombination, i.e. saturation, when the rate of recombination equals that of formation.

The reactor experiments show that, for exposures of 150 hours in a fast flux of the order of 7×10^{11} neuts cm^{-1} sec^{-1}, the change in resistivity is proportional to irradiation time, in other words that no appreciable radiation anneal is taking place.

The aim of this dissertation is to study in an independent fashion the problems of interaction energy and energy transfer between knock-ons and lattice stationary atoms, knock-on displacement cross section and mean free path, radiation anneal, and number of atoms displaced per primary knock-on. The results are compared to those obtained from the existing theories and to experimental data, qualitatively and quantitatively. Comparison of expected damage in light and heavy metals, both for charged particle and neutron irradiation is drawn up. Basic principles are obtained for the design of a pile neutron irradiation experiment.

Assuming, subject to check by the results, that the problem at hand is a two body problem, the collision of two identical particles

interacting through a mutual potential energy and acted upon by an external field which is essentially the same at the position of both particles at any time of the interaction for the separations coming into consideration, is first reduced to a problem (in the center of mass frame) of scattering of a particle by a center of force, the potential energy in the reduced problem being the same as the interaction potential energy of the two identical particles.

The potential energy adopted for two interacting atoms is the sum of the electrostatic potential energy of two rigid charge distributions with screened potential and of a term corresponding to closed shell repulsion of the two atoms. It has the correct Coulombian form at small separation and takes a value with the correct positive sign (repulsion) and a magnitude consistent with compressibility data, at separations of about 5 to 7 times the screening distance.

The case of copper is treated numerically in detail. First, it is seen that, for E = 25 ev, the distance of closest approach is about the atomic radius. This tends to show that an atom receiving an energy of the order of 25 ev in a collision will not be able to pass through the nearest neighbors, but will be pushed back to its normal lattice site. At any rate, it is clear that low energy defect pairs have a small separation. It is shown that classical treatment is valid over the whole range of knock-on energies for pile neutron irradiation and for deuteron irradiation with deuteron energy up to at least 12 Mev. Instead of using the impulse approximation, the center of mass frame

reduced problem is treated as a Kepler problem. A strict first integral of the motion is obtained and more proper boundary conditions than a condition at infinity are employed. This result is quite general, independent of the form of potential energy. Angle of scatter, displacement cross section and displacement mean free path at various energies are then bracketed between an upper value and a lower value by replacing the potential energy by two functions of the separation, one overestimating the interaction, the other underestimating it and such that the only remaining integration giving the equation of motion can be performed. The lower value of the displacement mean free path is shown to be a good approximation at high knock-on energy. An advantage of this method over Brinkman's is that it yields an upper and a lower limit for the interaction parameters. The lower values of the displacement mean free path are close to the estimate of Brinkman at energies down to 10^{-3} Mev and are larger below. This is consistent with the conclusions of a critique of Brinkman model, namely of the form of interaction energy and the screening distance it uses, and of the impulse approximation, all of which tend to overestimate the interaction, especially at low energy. The results obtained essentially check the validity of the assumption made of a two body collision problem.

In the model of this paper and the case of copper, there is an energy region, estimated to lie between 10^{-1} and 10^{-3} Mev, where the displacement mean free path is comparable to the interatomic distance and where we may consider that a knock on creates a displacement spike.

But this model "attaches a tail" to Brinkman displacement spikes: a knock-on slowed down to 10^{-3} Mev within the spike can escape from it and travel quite a distance, creating displacements, before it is trapped as interstitial, or recombines with a vacancy. However, the low energy pairs formed toward the end of a track have a small separation. The region of the sample disturbed by a primary knock-on and its progeny is seen as a cylindrical region, along the track of the primary, essentially linear down to energy 10^3ev, which we call a "damage spike". It comprises the displacement spike in its middle. For a 1 Mev primary, its length, or about the range of the primary knock-on, is estimated of the order of 660 r_o for copper, i.e. 1.68×10^{-5} cm. This is still much less than the estimated range $\sim 4 \times 10^{-4}$ cm - of Uranium fission fragments in Uranium; it is also compatible with the number of secondaries for a primary of that energy. This shows another superiority of the method, namely the obtention of an analytical expression approximating the displacement cross section, manageable enough to permit the calculation of the average energy transfer in a collision, hence that of the approximate range.

Using results obtained later in the paper, the number of atoms displaced per primary is obtained for a copper knock-on having the average energy of a primary produced by a 1 Mev neutron and for a copper knock-on having the average energy of a primary produced by a 12 Mev deuteron; these average energies are 3.1×10^4 ev and 275 ev, respectively, the numbers of displacements per primary, about 600 and 6 respectively. Hence displacement spikes will occur in the neutron irradiation, not in the charged particle irradiation.

Consideration of the distance, from the point of birth of a primary knock-on, at which small separation defect pairs are formed, at the end of the track of the primary, of the number of defect pairs per primary, and of the separation of the points of birth of the various primaries, shows that, for irradiation of copper by 12 Mev deuterons(8), at one fourth the full irradiation used in the experiment, interaction of defects newly formed with defects previously formed can be appreciable. For neutron irradiation, a similar reasoning shows that such interaction would not be appreciable with the exposures coming into consideration in experiments. Hence, for charged particle irradiation, there is the possibility that the thermal or electron spikes of the knock-ons of a generation (i.e. corresponding to a primary collision) will cause appreciable recombination of low separation defects of a previous generation. This would explain the phenomenon of radiation anneal which, on this basis, is not expected in pile neutron irradiation, for the exposures and fast fluxes coming in consideration in experiments. As pointed out before, this last prediction is confirmed by reactor experiments.(31) The type of recombination proposed explains quite well the differential equation which Cooper(10) found to fit closely the curve of change in resistivity versus integrated flux in the deuteron experiment.

Classical treatment as used in the case of copper is still valid for pile neutron irradiation of beryllium and even cyclotron irradiation of beryllium by deuterons of more than 20 Mev. But, for low atomic number, the model is inadequate at high energy, where ionization is important. The potential energy of the form used, where a

screening distance depending on the atomic number is involved, is shown to decrease monotonically with the atomic number Z at all separations coming in consideration, so that energy transfer and displacement cross section decrease with Z and the displacement mean free path increases when Z decreases. For Z low enough, it is possible that no displacement spikes are formed at any knock-on energy.

For charged particle irradiation there will be less disturbed regions in light metals than in heavy metals, but the mean free paths will be larger, so that the chances of recombination will not be appreciably changed. Hence we expect radiation anneal to have approximately the same effect in various metals. This conclusion is borne out by the experimental results of Marx, Cooper, and Henderson.(8)

For neutron irradiation, the number of disturbed regions mainly depends on the scattering cross section. The number of defects in a region varies on the average as the reciprocal of the mass number, so that, although radiation anneal is not expected for "reasonable" irradiations, chances for its appearance are larger for light metals with high neutron scattering cross section. As said before, it it possible that, for an atomic number low enough, displacement spikes will not form.

These conclusions show the interest presented by in pile measurements for neutron irradiation.

If knock-on collisions with stationary atoms can be described at all energies by differential cross sections analytically known, an integral equation, replacing that of Snyder and Neufeld, but more general,

can be studied in the asymptotic case of a primary with high energy compared to the energy needed to displace an atom from a normal lattice site. The application of the method to the approximate interaction cross section in copper found earlier in this paper shows that a linear asymptotic solution is a possible approximation, i.e. number of atoms displaced per primary varying linearly with energy of the primary, the coefficient of the variable energy being almost equal to that found by Snyder and Neufeld (2×10^4 in this paper, against 2.24×10^4 from the Snyder and Neufeld equation, E in Mev). Since the approximate cross section used overestimates interaction at low energy and most primary knock-ons in charged particle irradiation and secondary knock-ons in neutron irradiation have low energy (say, below 10^3 ev), the estimate of the number of atoms displaced per primary is too high, hence, also the Snyder and Neufeld estimate is too high. This agrees with experimental results, as shown before in this Introduction. We also expect the estimate to be better for neutron irradiation, where an appreciable fraction of primaries have high energy, than for charged particle irradiation (at reasonable particle energies, say 20 Mev at most for deuterons) where most of the primaries have low energy. This trend seems to be followed by the results of experiment and of calculations for the 12 Mev deuteron experiment[8] already mentioned and a pile experiment[11] performed in the same conditions of temperature (liquid helium).

In summary, the interaction potential energy used yields collision and damage parameters qualitatively and quantatively compatible with experimental results and the method of investigation throws light into the

main processes of atomic displacements both in the case of neutron and charged particle irradiation. It allows for useful comparisons between these two modes of irradiation and shows the importance of the in pile measurement during neutron irradiation.

CHAPTER II

BACKGROUND

In this brief review, the most important pieces of theoretical and experimental work in the field will be described, with the exception of that by Brinkman and by Snyder and Neufeld, already described in the Introduction, and on which we shall spend some time, later in this dissertation.

a. Determination of the energy E_d needed to displace an atom permanently

E_d has been calculated theoretically by Huntington.[12] He employs an interaction potential energy between atoms, of the form $U = A \exp\left(-\rho \frac{r - r_0}{r_0}\right)$ where r is the separation of the interacting atoms, r_0 the normal spacing of the lattice, A and ρ constants. Depending on the direction in which the atom is displaced, it is found that, for copper, E_d should be bracketed between the two values 18 ev and 40 ev.

The above formula is of the Born-Mayer type. The constants A and ρ are chosen to fit compressibility data. In Appendix I it is shown that it is comparable to and yields values of the same order as the potential energy used in this dissertation for the interaction of two copper atoms, at large separation.

Eggen and Laubenstein[13] have measured E_d experimentally in copper by observing the threshold electron energy for which atomic displacements are evidenced by X-ray inspection. They found the value 25 ev.

Denny [unpublished work, quoted by Seitz and Koehler(9)] has studied the effect of electrons on precipitates of iron in a CuFe alloy with 2.4% iron and found that E_d should be 27± 1 ev in iron.

b. Irradiation of Cu_3Au by alpha-particles

Dixon and Bowen(14) irradiated Cu_3Au with 36 Mev alpha-particles. They found that the initial disordering rate, as measured by change in electrical resistivity, was proportional to the bombarding flux.

c. Irradiation of iron, nickel, and cobalt wires by 10 Mev deuterons

Wruck and Wert(15) irradiated iron, nickel, and cobalt wires by 10 Mev deuterons, at -150°C. For an integrated flux of 10^{17} deuts cm^{-2}, the relative change of electrical resistivity, measured at -150°C, was 0.5 for iron, body centered cubic, and 0.1 for nickel and cobalt, hexagonal close packed and face centered cubic.

d. Irradiation of copper wires by 20 Mev deuterons

Dieckamp and Crittenden(16) bombarded high purity (99.999%) polycrystalline copper wires by 20 Mev deuterons at -175°C. The recovery of the change in shear modulus was observed at close temperature intervals between -196°C and +300°C, with an allowed annealing time of 15 minutes at each temperature step. The shear modulus decreased by 1.5% upon irradiation (8μ A hr cm^{-2}). One third of this change annealed at -125°C, further very little recovery took place at -100°C and -75°C and practically the final two thirds were recovered continuously between -50°C and +100°C.

e. Irradiation of copper, silver, and gold by 12 Mev deuterons

Cooper, Koehler, and Marx[8,27] irradiated pure thin wires of copper, silver, and gold at 10°K, using 12 Mev deuterons. Measurement of electrical resistivity during irradiation showed the occurrence of radiation anneal. After irradiation, the samples were left to warm up. It was found that, for copper and silver, a very rapid recovery takes place near 43°K (40-50% anneal) and 30°K (13-24% anneal) for each of the two metals, respectively. Recovery continued gradually from 50 to 220°K, becoming more rapid above 220°K. At 300°K, the remaining changes were

8% of initial change for copper

10% of initial change for silver and gold.

f. Irradiation of copper by 19 Mev deuterons

McDonnell and Kierstead[17] irradiated a bent tube of commercial copper by 19 Mev deuterons, at -180°C. The volume expansion of the sample was measured by the change in bending. A relative volume change of 0.068% was found for 1.15×10^{17} deuts cm^{-2}.

g. Irradiation of copper, silver, gold, nickel, and tantalum

Marx, Cooper, and Henderson[7] irradiated thin foils of copper, silver, gold, nickel, and tantalum by 12 Mev deuterons at liquid nitrogen temperature. This experiment, performed, chronologically, before the experiment quoted in (e) above, gave results similar to those obtained in that experiment. The comparison of the two shows the influence of thermal annealing of the defects below liquid nitrogen temperature.

h. Isothermal annealing of irradiated copper

Overhauser[18] has followed the annealing of the damage induced in copper by 12 Mev deuterons at -145°C. He found that the activation energy for annealing varies linearly with temperature, at low temperature, and that there possibly exists also a single isolated recovery, at -30°C, of activation energy 0.68 ev.

i. Pile irradiation of copper and gold

Redman, Noggle, Coltman, and Blewitt[11] irradiated copper and gold in the Oak Ridge reactor, at 17°K, for 154 hours. The theoretical change in resistivity, obtained from Snyder and Neufeld method[3] for the fraction of defects formed, from Jongenburger value[4] of an increase of resistivity of 2.7μ Ω cm per one per cent Frenkel defects, and from relations by Holmes [unpublished, but quoted by Seitz and Koehler[9]] expressing the neutron flux $\Phi(E)$ in the experimental hole used, has been calculated in the Preliminary Study.[1] It is found that the theoretical value is about four times higher than the experimental one.

j. Pile irradiation of UCr

Tucker and Senio[19] used fission thermal spikes by bombarding uranium containing 2% chromium in the Brookhaven reactor. X-ray observation after irradiation failed to show the presence of beta-uranium, which should be retained by chromium if nucleation after melting took place in a thermal or displacement spike.

k. Pile irradiation of copper and aluminum

McReynolds, Augustyniak, McKeown and Rosenblatt[20] have irradiated copper and aluminum in the Brookhaven reactor, at liquid nitrogen temperature. Electrical resistivity and critical shear

stress changes were measured after irradiation, and their recovery was followed during thermal anneal. For copper, it was found that there is recovery of electrical resistivity in a lower temperature process, between -80 and +20°C, and in a higher temperature process, between 300 and 350°C, this last process being accompanied by the recovery of the critical shear stress. For aluminum, recovery of electrical resistivity and of critical shear stress takes place in a single process around -60°C.

l. Evidence of melted regions in the spikes.

Denney[21] has irradiated ferromagnetic samples of a FeCu alloy with 2.4% copper in a cyclotron. Such an alloy is metastable, iron precipates, the precipitate being paramagnetic, but going over to a ferromagnetic form under the influence of cold work or particle irradiation. The ferromagnetic precipitate is stable, except when the sample is heated above the two phase region. In the experiment, it was found that irradiation decreased the ferromagnetism of the sample, from what one can induce that melting has taken place in some regions.

m. Low temperature pile irradiation of various metals and alloys with measure of electrical resistivity during irradiation

Blewitt, Coltman, Holmes, and Noggle[31] have bombarded various metals and alloys, including copper, aluminum, nickel, iron, gold, cobalt, Cu_3Au, brass, around 22°K. The interesting result of these experiments, for the purpose of this dissertation, is that the increase of electrical resistivity varies, for all metals and alloys investigated, proportionally to the time of irradiation, i.e. that no radiation anneal is apparent.

This list is very incomplete but, nevertheless, contains more background than will be used in the study. It is believed it gives a fair cross section of the status of atomic displacement studies.

CHAPTER III

COLLISION BETWEEN TWO IDENTICAL PARTICLES INTERACTING THROUGH A MUTUAL POTENTIAL ENERGY AND ACTED UPON BY AN EXTERNAL FIELD

(Application to the collision of a knock on and a stationary atom in copper)

1. Generalities

Consider 2 particles of masses M_1, M_2, subjected to an external potential U such that, if $\underline{R}_1$ and $\underline{R}_2$ are the coordinates of the particles in the laboratory frame, the potential energy of the system of the 2 particles in the external field is

$$U\ (\underline{R}_1, \underline{R}_2) \quad .$$

Assume a potential energy of the system of the 2 particles, isolated from the external field, of the form

$$V\ (r)$$

where

$$r = |\ \underline{R}_1 - \underline{R}_2| \quad .$$

The Schroedinger equation defining the wave function $\Psi\ (\underline{R}_1, \underline{R}_2, t)$ representative of the system of 2 particles is:

$$\frac{\hbar}{i}\dot{\Psi} = \left[\frac{\hbar^2}{2m_1}\nabla^2_{R_1} + \frac{\hbar^2}{2m_2}\nabla^2_{R_2} - V(r) - U(\underline{R}_1, \underline{R}_2)\right]\Psi \quad . \quad (1)$$

Where the dot denotes derivation with respect to time and the Laplacians are taken with respect to the coordinates of each particle.

Defining $\underline{R} = \frac{\mu}{m_2}\underline{R}_1 + \frac{\mu}{m_1}\underline{R}_2$, where μ is the reduced mass of the system, equal to $\frac{m_1 m_2}{m_1+m_2}$, i.e. $\underline{R}$ is the coordinate of the center of mass in the

laboratory frame, and

$$\underline{r} = \underline{R}_1 - \underline{R}_2 \ ,$$

Equation (1) can be thrown into the form (see Appendix II),

$$\frac{\hbar}{i}\dot{\psi} = \left[\frac{\hbar^2}{2M}\nabla_R^2 + \frac{\hbar^2}{2\mu}\nabla_r^2\right]\psi - \left[V(r) + U(\underline{R}_1, \underline{R}_2)\right]\psi \ ,$$

where $M = m_1 + m_2$ and the Laplacians are taken with respect to the componenets of $\underline{R}$ and $\underline{r}$.

We now consider the interaction between two idenetical atoms, one a knock-on moving through the lattice, the other one stationary before collision. The potential energy U is due to the other atoms of the lattice, i.e. the nearest neighbors of the stationary atom:

$$U(\underline{R}_1, \underline{R}_2) = U(\underline{R}_1) + U(\underline{R}_2) \ .$$

For a typical screened potential interaction between the two atoms, it will be shown later that for r approximately equal to $r_o/2$, half the interatomic distance, the interaction is weak in copper. Hence we may assume that, during a "collision", r is small compared to the distance of the center of mass to any neighboring atom except the struck one and approximate the U's thusly, if both atoms are on the same side with respect to the minimum of the potential trough:

$$U(\underline{R}_1) = U(\underline{R}) + (\underline{R}_1 - \underline{R}) \cdot \nabla_R U$$
$$U(\underline{R}_2) = U(\underline{R}) + (\underline{R}_2 - \underline{R}) \cdot \nabla_R U \ .$$

Since

$$m_1 = m_2 = m,$$
$$(\underline{R}_1 - \underline{R}) + (\underline{R}_2 - \underline{R}) = 0 \ .$$

If the two atoms are not on the same side with respect to the minimum, they must be close to the minimum during the collision, and

$$U(\underline{R}_1) \cong U(\underline{R}_2) = U(\underline{R}) \ .$$

In both cases,

$$U(\underline{R}_1, \underline{R}_2) \cong 2U(\underline{\mathcal{R}}) \quad .$$

Hence the variables $\underline{\mathcal{R}}$, $\underline{r}$ of the spatial part ψ_s of ψ can be separated and a solution is

$$\psi_s(\underline{\mathcal{R}}, \underline{r}) = \psi_1(\underline{\mathcal{R}})\psi_2(\underline{r})$$

with ψ_1 and ψ_2 satisfying

$$\left[\frac{\hbar^2}{2M}\nabla_{\mathcal{R}}^2 - 2U(\underline{\mathcal{R}})\right]\psi_1(\underline{\mathcal{R}}) = -E_1\psi_1(\underline{\mathcal{R}}) \quad , \qquad (3)$$

$$\left[\frac{\hbar^2}{2\mu}\nabla_r^2 - V(r)\right]\psi_2(\underline{r}) = -E_2\psi_2(\underline{r}) \quad . \qquad (4)$$

Equation (3) is the equation of motion of the center of mass in the external field. (4) is the equation of relative motion and may be considered as the equation of motion of the reduced mass, about the center of mass, i.e. in the center of mass frame, at a distance $\underline{r} = \underline{R}_1 - \underline{R}_2$ from the center of mass. Substantially, this shows that a two body treatment is permissible.

The velocities $\underline{v}'_{1c}$ and $\underline{v}_{2c}$, in the center of mass frame, of the knock-on A_1 and the stationary atom A_2, after collision, are colinear and their support passes through the center of mass G (Figure 1). Since $\underline{r} = \underline{R}_1 - \underline{R}_2 = \underline{A_2A_1}$, the angle of scatter φ of the knock-on in the center of mass frame is equal to the angle of scatter of the particle P with reduced mass μ in its motion about G.

Hence the problem of finding φ, which furnishes the interaction cross section, is reduced to that of studying the motion of the mass μ about the center of force G, in a field giving the potential energy $V(r)$ to the particle P of mass μ.

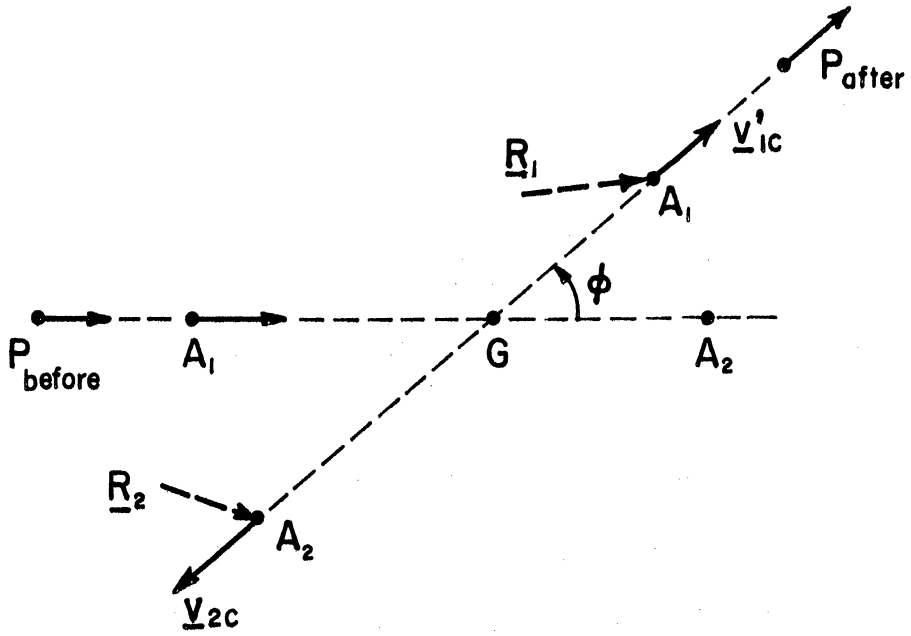

Figure 1. Diagram for the Collison of Two Particles.

If the velocity of the incoming knock-on, in the laboratory frame, is $\underline{v}$ before collision, the initial velocity of P (in the center of mass frame) is, since the atom A_2 is stationary and hence $\dot{\underline{R}}_2 = 0$ initially:

$$\dot{\underline{r}} = \dot{\underline{R}}_1 = \underline{v}$$

For elastic collisions, P, in its motion about G, keeps a constant total energy equal to

$$E_2 = \frac{M}{2} v^2 = \frac{1}{2}\left(\frac{m}{2} v^2\right) = \frac{E}{2} ,$$

where E is the absolute energy of the knock-on before collision.

It will be noticed that this treatment neglects ionization and atomic and conduction electron excitation. The second one is in effect, a case of inelastic scattering. It has been shown by Seitz[9] that the third one is negligible in all cases and by Cottrell,[22] on the basis of a classical criterion, that the first two are only significant in light metals (beryllium and aluminum). The release of an atom from a normal site is envisioned as a two stage process:

1. The incoming knock-on transfers energy to the stationary atom by elastic process.
2. If the energy transfer has been large enough, the initially stationary atom, by losing an energy E_d to the field of the neighboring atoms, escapes from its site. In this paper, E_d will be taken equal to 25 ev.[12, 13]

2. Choice of an Interaction Potential Energy

Brinkman[2] has studied the interaction of two similar atoms, considering a rigid atomic charge distribution corresponding to a

potential, at distance r from the atom,

$$V(r) = \frac{Z\epsilon}{r} \exp(-\frac{r}{a})$$

where $Z\epsilon$ is the charge of the nucleus and a the screening distance. This leads (see Appendix XIII) to a potential energy of interaction between two identical atoms

$$V(r) = \frac{Z^2\epsilon^2}{r} (1 - \frac{r}{2a}) \exp(-\frac{r}{a}) \quad . \qquad (5)$$

The force F, counted positively from O (center of force) to P (particle), is, for such a potential energy (Figure 2),

$$F = -\frac{dV}{dr} = Z^2\epsilon^2 \exp(-\frac{r}{a}) \frac{2a^2 + 2ar - r^2}{2a^2r^2}$$

i.e. F is $\geq$ o for $o < r < a(1 + \sqrt{3})$

F is $<$ o for $r > a(1 + \sqrt{3})$.

Hence V(r) is repulsive for $o < r < a(1 + \sqrt{3})$

and attractive for $r > a(1 + \sqrt{3})$.

The screening distance a is much smaller than r_o.

An accepted value for a is $a_h Z^{-1/3}$, where a_h is Bohr radius for hydrogen. For copper, this gives $a = 0.172$ Å. Hence such an interaction potential energy corresponds to no physical reality. V(r) should be repulsive up to $r = r_o$ and attractive only for values of r exceeding r_o. However, for $r \ll a$, Equation (5) gives the correct Coulomb unscreened form of interaction and, for $r \gg a$, the magnitude of V(r), i.e.

$$|V(r)| = \frac{Z^2\epsilon^2}{2a} \exp(-\frac{r}{a})$$

when employed for a repulsive interaction, leads to values agreeing well with compressibility data, after Huntington[12] and Brinkman[2], and as

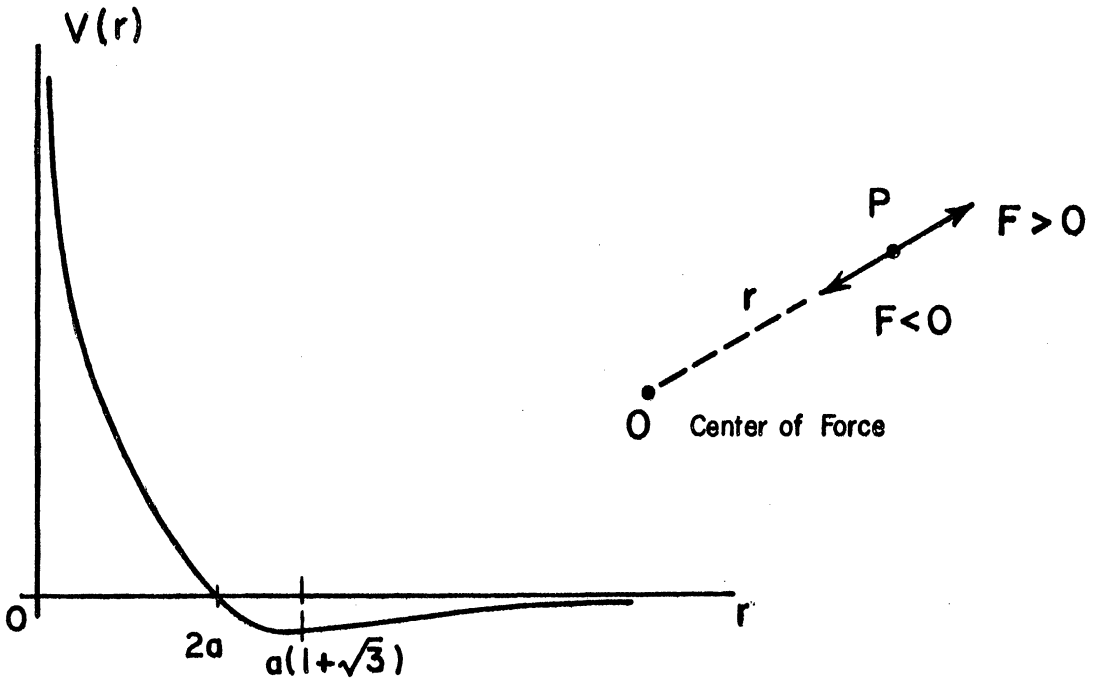

Figure 2. Brinkman Potential Energy.

further shown in Appendix I. Hence it appears that an interaction of the form

$$V(r) = \frac{Z^2\epsilon^2}{r}\ (1 + \frac{r}{2a})\ \exp(-\frac{r}{a}) \qquad (6)$$

is more realistic. It is derived from Equation (5) by adding to the interaction obtained from two rigid charge distributions with typical screened potential, a term

$$\frac{Z^2\epsilon^2}{a}\ \exp(-\frac{r}{a})$$

which would account for closed shell repulsion, admittedly neglected by Brinkman.

For copper, this potential energy is

$$V(r) = 1.21 \times 10^{-2}\ (\frac{1}{r} + \frac{1}{0.344})\ \exp(-\frac{r}{0.172}) \qquad (7)$$

where V is in Mev and r in $\mathring{A}$.

Table I gives numerical values of V for r = 2R (R nuclear radius), a/100, a/10, a/5, a/2 through 15a by increments equal to a/2, and 20a.

The problem at hand may be treated by the methods of classical mechanics provided the "dimension of the scatterer" is large compared to the wavelength of the incoming particle,

i.e.

$$b \gg \lambda\!\!\!^{-}$$

where b is the smallest value of the radius vector r in the motion of the particle with mass μ equal to the reduced mass around the center of mass G, $\lambda\!\!\!^{-}$ is the reduced wavelength of P when it has the speed of the incoming knock-on.

TABLE I. $V(r) = \frac{Z^2e^2}{r}\left(1+\frac{r}{2a}\right)\exp\left(-\frac{r}{a}\right)$;

for Cu, $V(r) = 1.21\times10^{-2}\left(\frac{1}{r}+\frac{1}{0.344}\right)e^{-\frac{r}{0.172}}$ Mev; r in Å

	r Å	u Å⁻¹	$\frac{r}{0.172}=\frac{r}{a}$	$e^{-\frac{r}{0.172}}$	u + 2.9	$e^{-\frac{r_o}{0.172}}(u+2.9)$	V(r) Mev	u^2 Å⁻²	$\frac{V(u)}{u^2}$	$V-V(\frac{r_o}{2})$ Mev	$\frac{V-V(\frac{r_o}{2})}{u^2}$ ← Mev Å²
2R	1.192×10^{-4}	8.37×10^{3}	6.92×10^{-4}	1.000	8.37×10^{3}	8.37×10^{3}	1.01×10^{2}	7.00×10^{7}	1.44×10^{-6}		
a/100	1.72×10^{-3}	5.80×10^{2}	1.00×10^{-2}	9.90×10^{-1}	5.83×10^{2}	5.78×10^{2}	7.00	3.35×10^{5}	2.09×10^{-5}		
a/10	1.72×10^{-2}	5.80x10	1.00×10^{-1}	9.05×10^{-1}	6.09x10	5.50x10	6.65×10^{-1}	3.35×10^{3}	1.99×10^{-4}	6.65×10^{-1}	1.99×10^{-4}
a/5	3.44×10^{-2}	2.90x10	2.00×10^{-1}	8.19×10^{-1}	3.19x10	2.60x10	3.14×10^{-1}	8.40×10^{2}	3.74×10^{-4}	3.14×10^{-1}	3.74×10^{-4}
a/2	8.60×10^{-2}	1.16x10	5.00×10^{-1}	6.07×10^{-1}	1.45x10	8.80	1.07×10^{-1}	1.34×10^{2}	8.00×10^{-4}	1.07×10^{-1}	8.00×10^{-4}
a	1.72×10^{-1}	5.80	1.00	3.68×10^{-1}	8.80	3.20	3.86×10^{-2}	3.35x10	1.15×10^{-3}	3.86×10^{-2}	1.15×10^{-3}
3a/2	2.58×10^{-1}	3.88	1.50	2.23×10^{-1}	6.78	1.51	1.62×10^{-2}	1.50x10	1.08×10^{-3}	1.62×10^{-2}	1.08×10^{-3}
2a	3.44×10^{-1}	2.90	2.00	1.35×10^{-1}	5.80	7.82×10^{-1}	9.50×10^{-3}	8.40	1.13×10^{-3}	9.50×10^{-3}	1.13×10^{-3}
5a/2	4.30×10^{-1}	2.32	2.50	8.21×10^{-2}	5.22	4.28×10^{-1}	5.18×10^{-3}	5.39	9.60×10^{-4}	5.16×10^{-3}	9.60×10^{-4}
3a	5.16×10^{-1}	1.94	3.00	4.98×10^{-2}	4.84	2.40×10^{-1}	2.90×10^{-3}	3.75	1.75×10^{-4}	2.88×10^{-3}	7.75×10^{-4}
7a/2	6.02×10^{-1}	1.66	3.50	3.02×10^{-2}	4.56	1.38×10^{-1}	1.67×10^{-3}	2.75	6.08×10^{-4}	1.65×10^{-3}	6.08×10^{-4}
4a	6.88×10^{-1}	1.45	4.00	1.83×10^{-2}	4.35	7.95×10^{-2}	9.65×10^{-4}	2.10	4.60×10^{-4}	9.40×10^{-4}	4.48×10^{-4}
9a/2	7.74×10^{-1}	1.29	4.50	1.11×10^{-2}	4.19	4.65×10^{-2}	5.64×10^{-4}	1.66	3.40×10^{-4}	5.49×10^{-4}	3.26×10^{-4}
5a	8.60×10^{-1}	1.16	5.00	6.74×10^{-3}	4.06	2.72×10^{-2}	3.30×10^{-4}	1.34	2.46×10^{-4}	3.05×10^{-4}	2.28×10^{-4}
11a/2	9.46×10^{-1}	1.06	5.50	4.09×10^{-3}	3.96	1.62×10^{-2}	1.96×10^{-4}	1.12	1.75×10^{-4}	1.71×10^{-4}	1.53×10^{-4}
6a	1.032	9.70×10^{-1}	6.00	2.48×10^{-3}	3.87	9.60×10^{-3}	1.16×10^{-4}	9.40×10^{-1}	1.23×10^{-4}	9.10×10^{-5}	9.70×10^{-5}
13a/2	1.118	8.95×10^{-1}	6.50	1.50×10^{-3}	3.795	5.68×10^{-3}	6.88×10^{-5}	8.00×10^{-1}	8.60×10^{-5}	4.42×10^{-5}	5.53×10^{-5}
7a	1.204	8.30×10^{-1}	7.00	9.12×10^{-4}	3.730	3.40×10^{-3}	4.12×10^{-5}	6.90×10^{-1}	6.00×10^{-5}	1.66×10^{-5}	2.41×10^{-5}
15a/2	1.290	7.75×10^{-1}	7.50	5.53×10^{-4}	3.675	2.03×10^{-3}	2.46×10^{-5}	6.00×10^{-1}	4.10×10^{-5}	0	0
8a	1.376	7.26×10^{-1}	8.00	3.35×10^{-4}	3.626	1.21×10^{-3}	1.46×10^{-5}	5.30×10^{-1}	2.76×10^{-5}		
17a/2	1.462	6.85×10^{-1}	8.50	2.03×10^{-4}	3.585	7.30×10^{-4}	8.85×10^{-6}	4.70×10^{-1}	1.88×10^{-5}	$V(\frac{r_o}{2}) \cong V(\frac{15a}{2})$	
9a	1.548	6.45×10^{-1}	9.00	1.23×10^{-4}	3.545	4.37×10^{-4}	5.30×10^{-6}	4.15×10^{-1}	1.28×10^{-5}	$= 2.46\times10^{-5}$ Mev	
19a/2	1.634	6.11×10^{-1}	9.50	7.48×10^{-5}	3.511	2.62×10^{-4}	3.17×10^{-6}	3.74×10^{-1}	8.50×10^{-6}		
10a	1.720	5.80×10^{-1}	1.00x10	4.54×10^{-5}	3.480	1.57×10^{-4}	1.90×10^{-6}	3.35×10^{-1}	5.70×10^{-6}		
21a/2	1.806	5.55×10^{-1}	1.05x10	2.75×10^{-5}	3.455	9.50×10^{-5}	1.15×10^{-6}	3.07×10^{-1}	3.75×10^{-6}		
11a	1.892	5.30×10^{-1}	1.10x10	1.67×10^{-5}	3.430	5.72×10^{-5}	6.95×10^{-7}	2.80×10^{-1}	2.48×10^{-6}		
23a/2	1.978	5.05×10^{-1}	1.15x10	1.01×10^{-5}	3.405	3.44×10^{-5}	4.16×10^{-7}	2.55×10^{-1}	1.64×10^{-6}		
12a	2.064	4.85×10^{-1}	1.20x10	6.14×10^{-6}	3.385	2.08×10^{-5}	2.52×10^{-7}	2.35×10^{-1}	1.07×10^{-6}		
25a/2	2.150	4.65×10^{-1}	1.25x10	3.72×10^{-6}	3.365	1.25×10^{-5}	1.52×10^{-7}	2.16×10^{-1}	7.05×10^{-7}		
13a	2.236	4.48×10^{-1}	1.30x10	2.26×10^{-6}	3.348	7.57×10^{-6}	9.15×10^{-8}	2.00×10^{-1}	4.57×10^{-7}		
27a/2	2.322	4.20×10^{-1}	1.35x10	1.37×10^{-6}	3.320	4.55×10^{-6}	5.50×10^{-8}	1.76×10^{-1}	3.13×10^{-7}		
14a	2.408	4.15×10^{-1}	1.40x10	8.31×10^{-7}	3.315	2.76×10^{-6}	3.34×10^{-8}	1.72×10^{-1}	1.95×10^{-7}		
29a/2	2.494	4.00×10^{-1}	1.45x10	5.04×10^{-7}	3.300	1.66×10^{-6}	2.01×10^{-8}	1.60×10^{-1}	1.26×10^{-7}		
r_o	2.557	3.90×10^{-1}	≅1.50x10	3.06×10^{-7}	3.290	≅1.00×10^{-6}	1.22×10^{-8}	1.52×10^{-1}	≅8.15×10^{-8}		
15a	2.580	3.88×10^{-1}	1.50x10	3.06×10^{-7}	3.288	1.00×10^{-6}	1.22×10^{-8}	1.50×10^{-1}	8.15×10^{-8}		
20a	3.440	2.90×10^{-1}	2.00x10	2.06×10^{-9}	3.190	6.60×10^{-9}	8.00×10^{-11}	8.40×10^{-2}	9.50×10^{-10}		

If b_o is the "distance of closest approach", i.e. the minimum value of r for a particle shot directly at the center of force (p = o) with the same speed v, it is clear that (Figure 3),

$$b \geq b_o$$

for

$$V(b_o) = \frac{E}{2} \quad \text{and} \quad V(b) = \frac{E}{2} + \frac{\mu}{2} w^2(b)$$

E being the initial energy of the incoming knock-on, w(b) the speed of P at distance b from G. Hence $V(b) \leq V(b_o)$ and $b \geq b_o$. Naturally, for p = o, $b = b_o$.

For pile neutron irradiation of metals, the energy of a primary knock-on is practically always smaller than 0.72 Mev, which is the maximum energy transfered by a 2 Mev neutron to a Be 9 atom in an elastic collision.

For copper, with the interaction potential energy (7), Table I shows that

for E/2 = 0.72 Mev, $\quad b_o = a/10 = 1.72 \times 10^{-2}$ Å

for E/2 = 25 ev, $\quad b_o = 10a = 7.5a = 1.29$ Å

In Appendix III, the following reduced wavelengths are obtained:

for E/2 = 0.72 Mev, $\quad \lambda\!\!\!^{-} = 1.35 \times 10^{-13}$cm $\ll = 1.72 \times 10^{-10}$cm

for E/2 = 25 ev, $\quad \lambda\!\!\!^{-} = 3.0 \times 10^{-11}$cm $\ll = 1.29 \times 10^{-8}$cm .

For smaller energies, the same inequality will hold, even more so. It also holds for E = 1.5 Mev, maximum energy transferred by a 12 Mev deuteron to a copper atom.

Hence, classical treatment is applicable over the whole range of energy of the knock-ons, for a potential energy such as (7) between two copper atoms and in the case of pile neutron irradiation. It remains

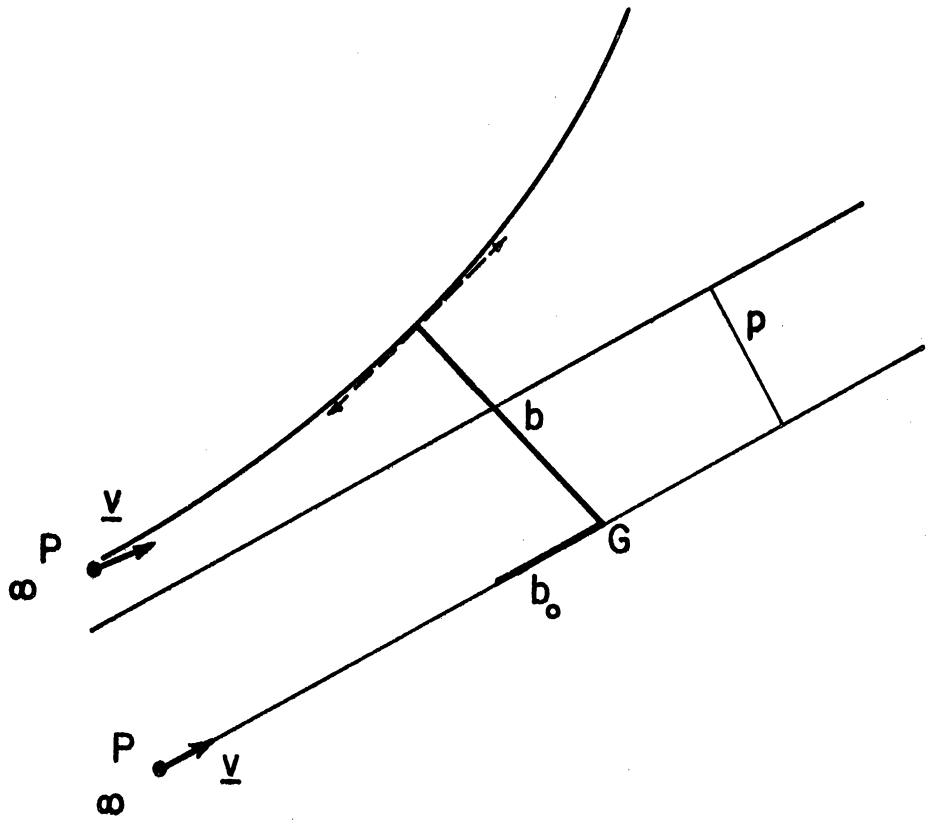

Figure 3. Distance of Closest Approach.

applicable, in the case of deuteron irradiation, for a deuteron energy of 12 Mev.

In Table I, it is worth noting that $V(r) = 2.46 \times 10^{-5}$ Mev for $r = 15\ a/2 \cong r_o/2$, so that an atom receiving in a collision an energy smaller than $E_d = 25$ ev will not approach another atom closer than $r_o/2$. It is then plausible that this atom will be pushed back to its site. It is clear that an atom receiving an energy slightly in excess of 25 ev will at most become interstitial at the interstitial position closest to the site from which it has been ejected. Hence a knock-on becoming interstitial at low energy will have a small separation from its vacancy and should recombine easily with it.

3. Classical Treatment of Scattering by a Center of Force Giving Rise to an Interaction Potential Energy Depending on the Distance Only

Use polar coordinates (Figure 4) with pole at the center of force G and arbitrary axis $G\infty$ for the origin of angles. The equations of conservation of energy and momentum for the motion of the particle P of mass μ about G are:

$$\frac{1}{2}\mu w^2 + V(r) = \frac{1}{2}\mu v^2 = \frac{E}{2} \qquad (8)$$

where w is the speed of P at the point considered, r the distance GP, V(r) the potential energy of P at distance r from P, assuming $V(\infty) = 0$, v the speed of P at infinite separation and E the initial energy of the incoming atom in the laboratory frame,

and

$$r^2 \frac{d\theta}{dt} = K = pv$$

p being the impact parameter.

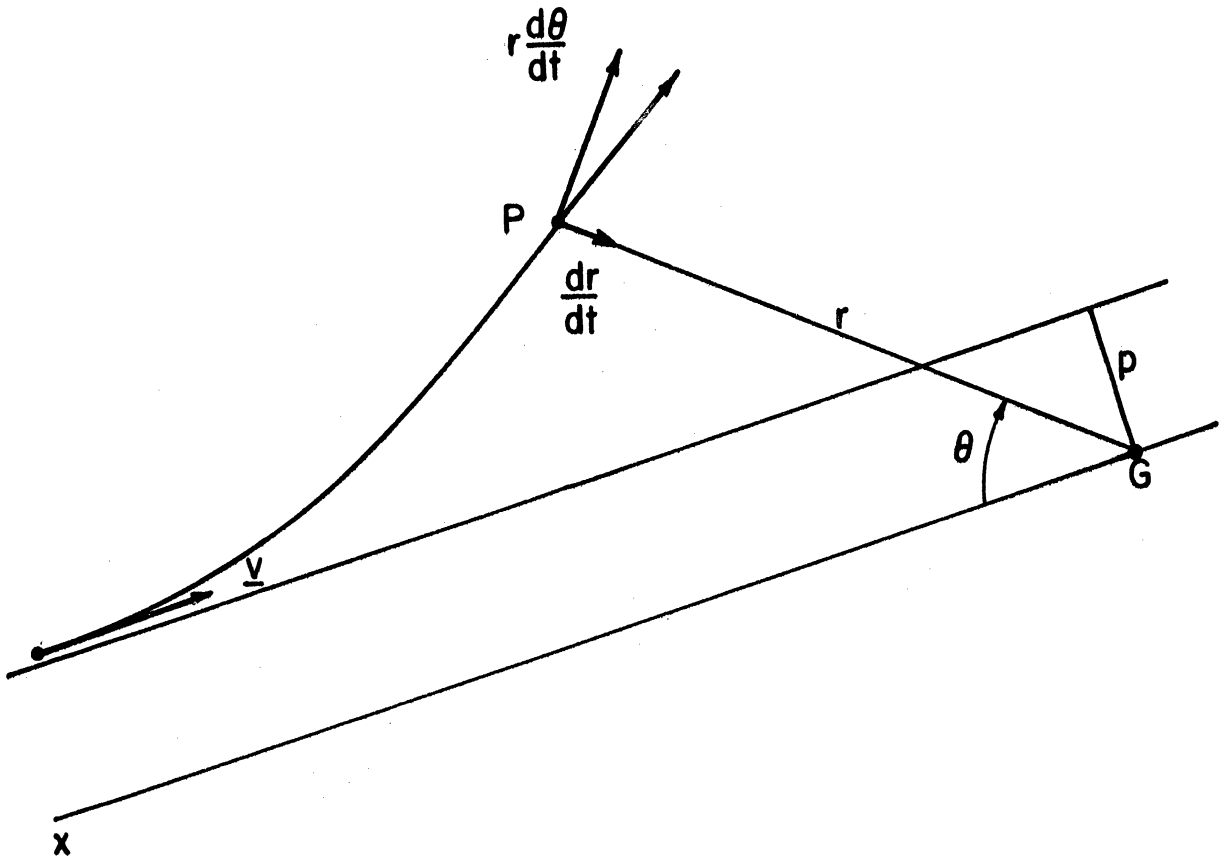

Figure 4. Polar Diagram for the Kepler Problem.

We have

$$w^2 = \left(\frac{dr}{dt}\right)^2 + \left(r\frac{d\theta}{dt}\right)^2 = \left(\frac{dr}{d\theta}\frac{d\theta}{dt}\right)^2 + \left(r\frac{d\theta}{dt}\right)^2$$

$$= \left(\frac{dr}{d\theta}\frac{hv}{r^2}\right)^2 + \left(r\frac{hv}{r^2}\right)^2 .$$

Putting into (8),

$$\frac{E}{2}\frac{h^2}{r^4}\left(\frac{dr}{d\theta}\right)^2 + \frac{E}{2}\frac{h^2}{r^2} + V(r) = \frac{E}{2} \;,$$

$$\left(\frac{dr}{d\theta}\right)^2 = \frac{r^4}{h^2}\left[1 - \frac{h^2}{r^2} - 2\frac{V(r)}{E}\right] .$$

Let $\frac{1}{r} = u$, then the above relation becomes

$$\frac{d\theta}{du} = \frac{\pm 1}{\sqrt{\frac{1}{h^2}\left[1 - 2\frac{V(u)}{E} - u^2\right]}} \qquad (10)$$

For a repulsive potential, with origin of θ selected so that θ is counted positive clockwise, and for a trajectory such as AB (Figure 5), θ increases from $u = o$ to $u = u_m$, (maximum, vertex O of the trajectory). Then it is clear that the + sign is to be taken in (10) for the branch AO. For a trajectory such as CD, the + sign applies to the branch O'D. A minus sign would correspond to the branches OB and CO', with a same positive direction for the angles. We shall remove any uncertainty in sign by taking the + sign and the positive direction for the angles such that, initially, θ increases with u and considering only the first half branch. It is clear then, that only a configuration such as AB is to be considered and (10) is to be taken with the + sign.

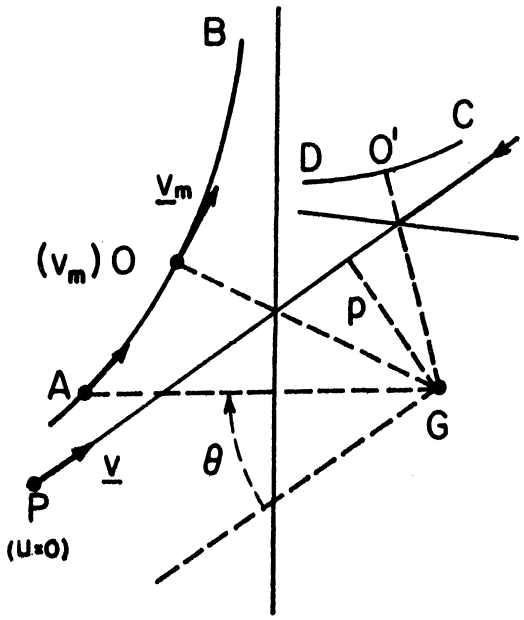

Figure 5. Branches of the Trajectory.

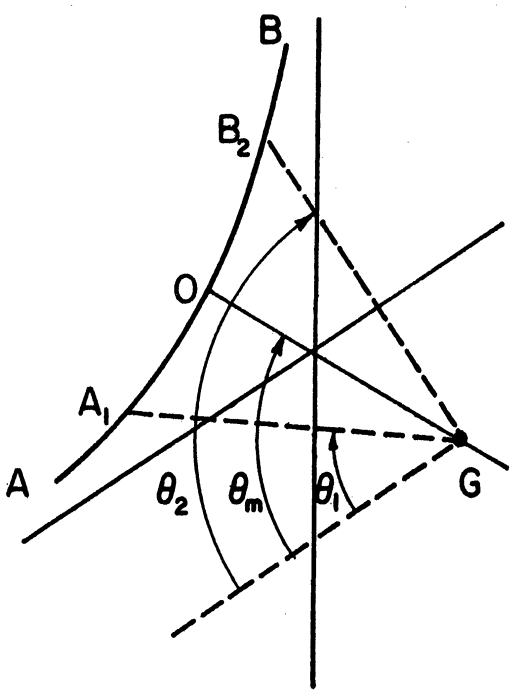

Figure 6. Symmetry of the Trajectory.

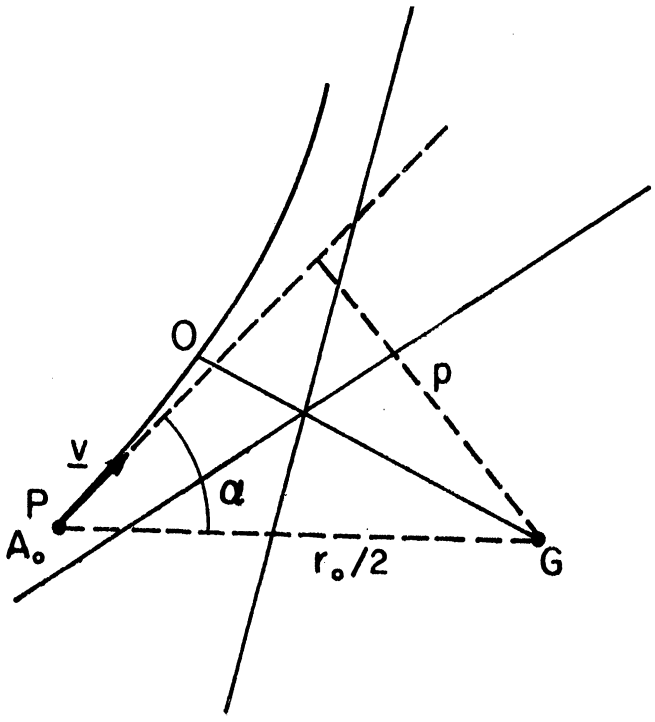

Figure 7. Boundary Conditions at $r_o/2$, or for $r = r_o/2$.

There is obviously symmetry with respect to GO. For, consider two points, A_1 on AO and B_2 on OB (Figure 6), both with the same u and respective angles θ_1 and θ_2; call θ_m the angle corresponding to point o. Let

$$R = \frac{1}{p^2}\left[1 - 2\frac{V(u)}{E}\right] - u^2,$$

then

$$\theta_1 = \int_0^u \frac{du}{\sqrt{R}} \quad ; \quad \theta_2 = \theta_m - \int_{u_m}^u \frac{du}{\sqrt{R}} \quad ;$$

$$\theta_2 = \int_0^{u_m} \frac{du}{\sqrt{R}} + \int_{u_m}^u \frac{du}{\sqrt{R}} - 2\int_{u_m}^u \frac{du}{\sqrt{R}} = \theta_1 + 2(\theta_2 - \theta_m),$$

i.e. $\theta_1 + \theta_2 = 2\theta_m$, hence the symmetry claimed.

Point O, i.e., u_m, is determined by the condition

$$\left(\frac{du}{d\theta}\right)_{u=u_m} = 0 \text{ , i.e. } \left(\frac{d\theta}{du}\right)_{u=u_m} = \infty,$$

in other words, u_m is a physically acceptable root of $R = 0$. It is easy to see that V(u) is a monotonically increasing function of u (Appendix V), since $F = \frac{dV}{dr}$ is always positive for repulsive potential. Hence the curve $Z_1(u) = \frac{2}{p^2E}V(u) + u^2$ intersects only at one point with the parallel $Z_2(u) = \frac{1}{p^2}$ to the u axis. Hence R = o has only one root, u_m. It is acceptable, since R is positive for $u \leq u_m$, as may be seen as follows:

$$V(u_m) = \frac{E}{2}(1 - p^2u_m^2) = \text{maxi. of } V \quad ;$$

hence

$$u \leq u_m \quad ; \qquad 1 - p^2u^2 \geq 1 - p^2u_m^2 \quad ;$$

$$V(u) \leq \frac{E}{2}(1 - p^2u_m^2) \leq \frac{E}{2}(1 - p^2u^2)$$

and

$$o \leq 1 - \frac{2}{E} V(u) - p^2 u^2 \quad ;$$

hence

$$R \geq o \quad .$$

It is interesting to treat now the case where the initial conditions cannot be taken as w = v for u = o ($r = \infty$). For example, consider the case where it is necessary to consider the interaction beginning at $r = r_o/2$, r_o interatomic distance. Use the notations of Figure 7.

Equation (8) now becomes

$$\frac{1}{2} \mu w^2 + V(r) = \frac{1}{2} \mu v^2 + V(r_o/2) \quad ,$$

where v is the initial speed.

Equation (9) remains unchanged, but p is now the distance of G to the support of velocity $\underline{v}$ at the initial point considered. Equation (8) being only altered by changing V(r) into $V(r) - V(r_o/2)$, $\frac{d\theta}{du}$ is obtained from (10) by replacing V(u) by $V(u) - V(2/r_o)$. Hence, for the initial branch of the trajectory:

$$\frac{d\theta}{du} = \frac{p}{\sqrt{1 - \frac{2}{E}\left[V(u) - V\left(\frac{2}{r_o}\right)\right] - p^2 u^2}} \quad . \qquad (11)$$

4. Application to the Selected Potential Energy

$$V(r) = Z^2 \epsilon^2 \left(\frac{1}{r} + \frac{1}{2a}\right) \exp\left(-\frac{r}{a}\right)$$

In the case of copper:

$$V(r) = 1.21 \times 10^{-2} \ (1/r + 2.9) \exp(-r/a) \text{ Mev, r Å}$$

We have assumed that the problem of collisions between knock-ons and stationary atoms is a two body problem, i.e. that the knock-on is scattered by only one stationary atom at a time. We shall show later

that the results of the calculation are reasonably consistent with this assumption. This is equivalent to saying the V(r) varies sharply enough around $r = r_o/2 = 15a/2$ so that, say $V(\frac{r_o}{2} - a)$ is appreciably higher than $V(\frac{r_o}{2})$. From Table I is is seen that $V(r_o/2) = 2.5 \times 10^{-5}$ Mev, while $V(\frac{r_o}{2} - a) = 7 \times 10^{-5}$ Mev, i.e. $V(\frac{r_o}{2} - a)$ is 2.8 time greater than $V(\frac{r_o}{2})$. Therefore, we consider that a knock-on 1, being at a point A (Figure 8), with velocity $\underline{v}$, will collide with the stationary atom 2 if the impact parameter p relative to 2 is smaller than $r_o/2$. 1 would collide with 2*, nearest neighbor of 2, if its velocity $\underline{v}^*$ were such that p* were smaller than $r_o/2$. It is clear that there is only one close stationary atom for which p is smaller than $r_o/2$. In our assumption, this is the only atom with which the knock-on 1 will experience its next collision. Then, we can assume that collision of 1 with 2 begins at a point such as B, on a sphere of radius to $r_o/2$ centered on 2 and that the interaction of 1 with any nearest neighbor 2* is negligible compared to that with 2 when 1 is at point B or closer to 2 (Figure 9).

In the equivalent problem of scattering of a particle of mass μ (reduced mass) by a center of force G, this means that we consider the interaction beginning when P is at distance $r_o/2$ from G.

It remains now to select an appropriate criterion for the end of the interaction. When atom 1, after collision, reaches the surface of the sphere of radius $r_o/2$ centered on the site of atom 2, it is ready to enter a region where it is at a distance of less than $r_o/2$ from a nearest neighbor of 2, that is where the predominant interaction with 1 will be that of the nearest neighbor, provided, at that time, the distance between 1 and 2 is greater than $r_o/2$ (2 is in motion!). Hence, it is satisfactory

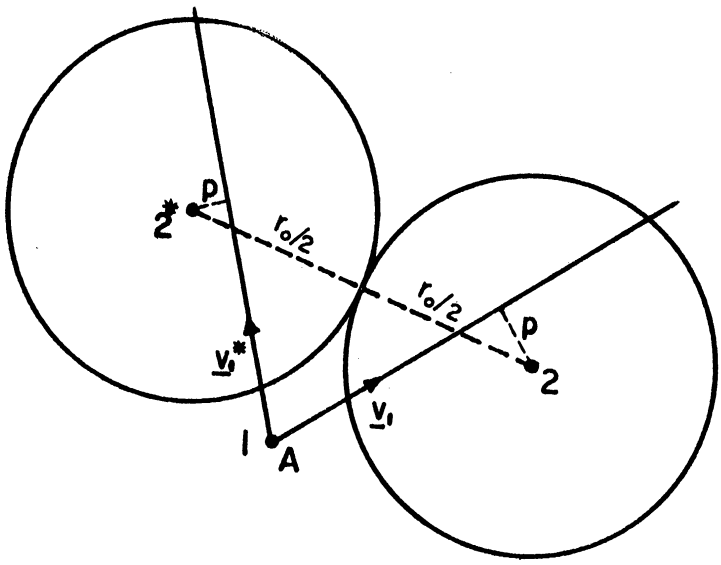

Figure 8. Preferential Interaction.

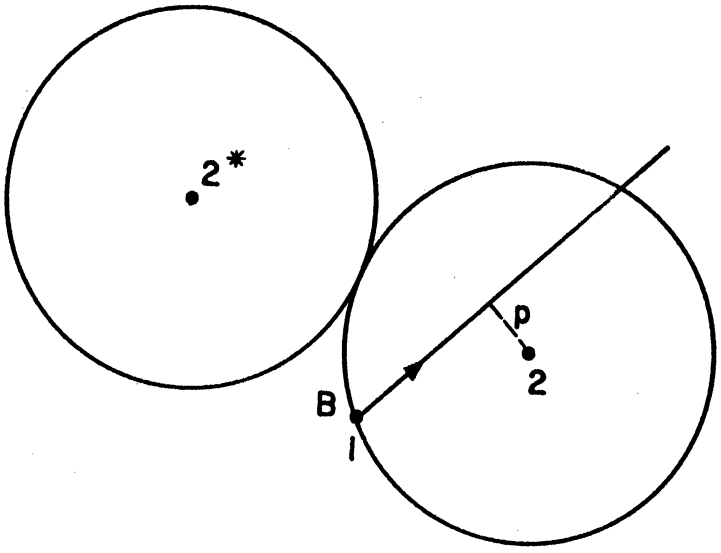

Figure 9. Beginning of Interaction.

to consider that collision between atoms 1 and 2 ends at distance $r_o/2$ from the lattice site of atom 2 when this corresponds to a distance between 1 and 2 greater than $r_o/2$.

The two diagrams of Figure 10 indicate the two configurations possible after collision. It is shown in Appendix VIII that, for elastic collision of two particles of the same mass, the two particles fly off at 90 degrees from each other, in the laboratory frame, after collision (Figure 10). Generally, the particles interacting are considered in zero field before and after collision. This leads, for two particles of identical mass M to one energy balance and two momentum balance equations, namely (Figure 11),

$$\left.\begin{aligned} &\tfrac{1}{2} M v_1^2 = \tfrac{1}{2} M v_1'^2 + \tfrac{1}{2} M v_2^2 \\ &M v_1' \sin\omega = M v_2 \sin\psi \\ &M v_1 = M v_1' \cos\omega + M v_2 \cos\psi \end{aligned}\right\} \qquad (12)$$

in the laboratory frame.

If we consider that the collision of 1 and 2 ends when the distance between the two is equal to $r_o/2$, and since we have assumed that collision begins when 1 comes at distance $r_o/2$ of 2, we can write the energy balance equation

$$\tfrac{1}{2} M v_1^2 + V\left(\tfrac{r_0}{2}\right) = \tfrac{1}{2} M v_1'^2 + \tfrac{1}{2} M v_2^2 + V\left(\tfrac{r_0}{2}\right)$$

and two momentum balance equations identical to those in (12), v_1' and v_2 being taken when the separation of the 2 colliding atoms is $r_o/2$, i.e. at the the "end" of the collision (Figure 12). Hence, this choice will preserve the usual results for two identical particles (See Appendix VIII) namely:

$$\omega + \psi = \pi/2 \quad ; \quad T = E \sin^2 \varphi/2 ,$$

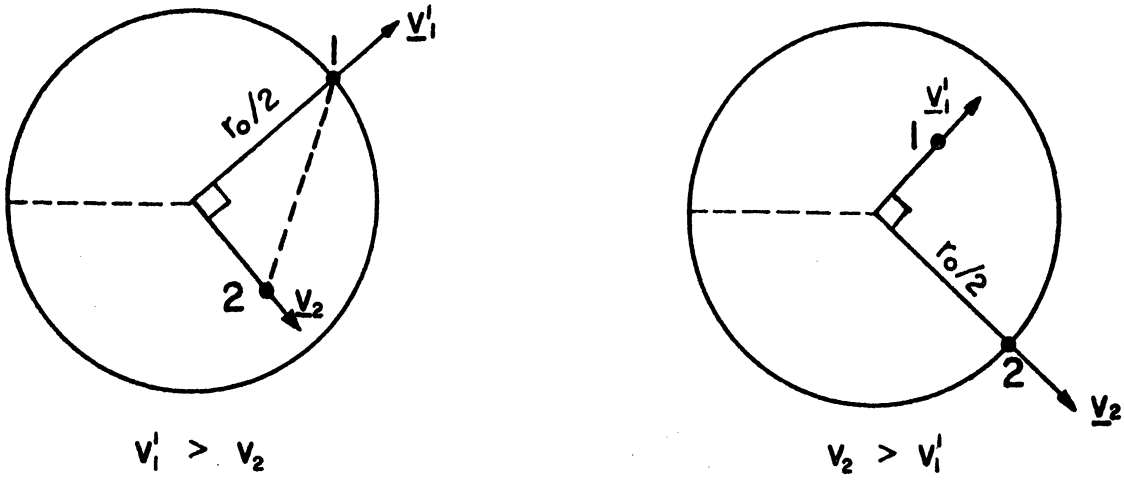

Figure 10. Possible Configurations When the First Particle Reaches Distance $r_o/2$ From the Center of Collision.

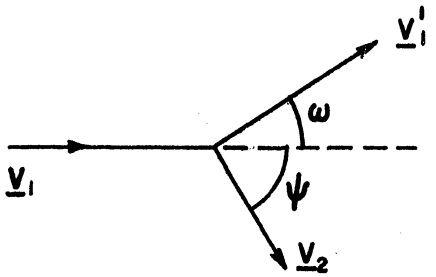

Figure 11. Diagram of Angles and Speeds in Laboratory Frame.

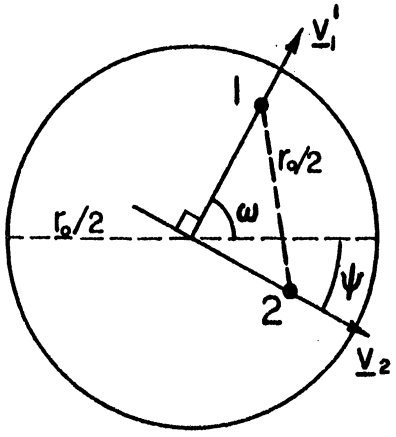

Figure 12. End of Collision.

where ω and ψ are the angles to the initial velocity $\underline{v}_1$ of the incoming knock-on 1 at which this knock-on and the initailly stationary atom 2 fly off at the end of collision (i.e. when their separation is $r_o/2$) in the laboratory frame, T is the kinetic energy transferred to 2, E the kinetic energy of 1 before collision, both in the laboratory frame, and φ is the angle of scattering of 1, in the center of mass frame, corresponding to ω . In the equivalent problem of the scattering of a particle P of mass μ equal to the reduced mass by a center of force G, this means that φ is the angle with $\underline{v}_1$ for which P is at distance $r_o/2$ (after collision).

From Figure 12, it is seen that 1 and 2 have to travel some distance, after their separation has reached $r_o/2$, to reach the surface of the sphere of radius $r_o/2$ centered on the lattice site of 2. This they do practically free of interaction between each other or with any nearest neighbor. Hence, it is essentially equivalent to consider the end of the interaction when 1 or 2 has reached the surface of this sphere, at which time the separation of the two atoms is larger than $r_o/2$ and the sum of the angles ω and ψ is still about $\pi/2$, or when their separation is $r_o/2$.

In summary, for the problem in the center of mass frame, we shall consider that interaction begins and ends when P is at distance $r_o/2$ from G. We therefore adopt formula (11).

It will be recalled that Rutherford scattering formula[23] was established considering the beginning and the end of the collision when the moving atom is at infinity from the scattering atom 2, this corresponding to single scattering of the alpha-particles when they pass through the foil. The assumption was justifiable since 1) the foil was assumed

very thin (practically, Geiger and Marsden[28] used a gold foil only 2.1×10^{-5} cm thick in their experiments to check Rutherford formula); 2) the incoming particles fell perpendicularly on the foil; 3) the incoming particles were energetic. On the contrary, in the problem being studied, the knock-ons move in all directions and their energy can be quite small, so that they experience multiple collisions in the sample. For energetic knock-ons, say E=0.75 Mev, which is practically too high for neutron irradiation of copper, r is always greater than a/10, so that $r/(r_o/2)$ is always greater than $\frac{a/10}{7.5a} = 1/75$. Hence $r_o/2$ cannot be considered as infinite. However, it will be shown shortly that taking the boundary conditions at infinity yields a justifiable approximation.

It will also be noted that Rutherford treatment of the scattering of alpha-particles assumes a two body situation: it is implicitly postulated that, when 1 crosses the foil (Figure 13) through two nearest neighbors 2 and 2*, only one of the two scatters 1; otherwise the simultaneous deviation of a particle by two centers of force would have to be studied. At $r = r_o/2$, the Coulomb energy between two copper nuclei,

$$V_c(r) = 1.21 \times 10^{-2}/r \text{ (Mev, Å)},$$

is about 10^{-2} Mev. The interaction potential energy used here is 2.46×10^{-5} Mev. Hence, we should be justified in using a two body approximation. Calculations of the displacement cross section, using this model, give results reasonably consistent with the two body assumption, as will be seen later.

Now, relation (11) is not integrable. Appropriate approximations to

$$R = 1 - \frac{2}{E}\left[V(u) - V(2/r_o)\right] - p^2u^2$$

are looked for, at various values of E.

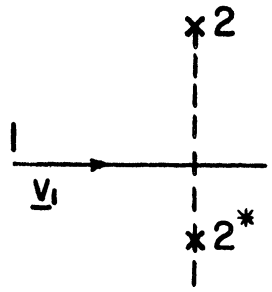

Figure 13. Two Body Interaction.

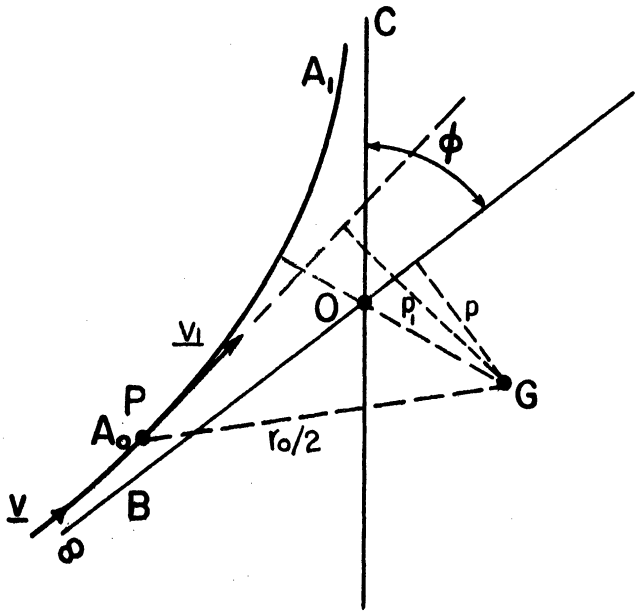

Figure 14. Equivalent Condition at Infinity.

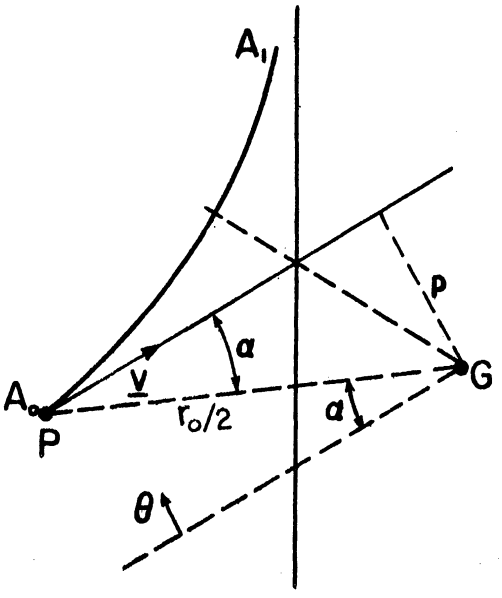

Figure 15. Origin of Angles.

If an acceptable approximation of the form

$$V(u) - V(2/r_0) \cong \alpha(E)\, u^2$$

can be found for each E, then (11) can be approximated by

$$d\theta/du = \gamma \cong p/\sqrt{1-\left[\frac{2}{E}\alpha(E)+p^2\right]u^2}\ , \qquad (12a)$$

which can be written

$$d\theta \cong \left[p/\sqrt{\frac{2}{E}\alpha(E)+p^2}\right] d\left[\sin^{-1}\sqrt{\frac{2}{E}\alpha(E)+p^2}\ u\right], \qquad (13)$$

hence θ is then obtained analytically.

(12a) is the differential equation for the motion of a particle P of mass μ, speed $v=\sqrt{\frac{E}{\mu}}$ at infinity from the center of force G (Figure 14), the asymptote OB passing at distance p from G and the potential energy being $\alpha(E)u^2$. Actually, the velocity of P at $r_o/2$ from G should be such that its support is at distance p from G and its magnitude is v. In the approximation (12a), if we call $\underline{v}_1$ the velocity of P at A_o and p_1 the distance from G of the support of $\underline{v}_1$, we have

$$\frac{1}{2}\mu v_1^2 + \alpha\left(\frac{2}{r_o}\right)^2 = \frac{1}{2}\mu v^2,$$

hence

$$v_1 = v\sqrt{1-\frac{2}{E}\alpha(E)\left(\frac{2}{r_o}\right)^2}\ ,$$

$$p_1 = p\Big/\sqrt{1-\frac{2}{E}\alpha(E)\left(\frac{2}{r_o}\right)^2},$$

with $E = \mu v^2$.

It will be seen later that the maximum values of $(2/E)\alpha(E)$ are 1.20, 6.52×10^{-1}, 1.92×10^{-1} for $E = 10^{-4}$, 10^{-3}, 10^{-2} Mev. Hence,

$$\sqrt{1-\frac{2}{E}\alpha(E)\left(\frac{2}{r_o}\right)^2}$$

takes the values 0.517, 0.785, 0.940, respectively, for these three values of E. It follows that, down to $E = 10^{-3}$ Mev, it is not a serious error to

consider that the angle of scattering is the angle φ of the asymptotes OB and OC. To gain an idea of the error of doing so when E is smaller than 10^{-3} Mev, the following analysis is made. Consider the correct conditions at A_o, i.e. velocity $\underline{v}$ and $\underline{v}$ passing at distance p from G. Count θ clockwise, from a parallel to $\underline{v}$, in a configuration as shown in Figure 15. Then the integration of (13) between $(\alpha, 2/r_o)$ and (θ, u), yields (See Appendix VII):

$$u = \left[1\Big/\sqrt{\frac{2}{E}\alpha(E)+p^2}\right] \sin\left[\frac{1}{p}\sqrt{\frac{2}{E}\alpha(E)+p^2}\left(\theta - \sin^{-1}\frac{2p}{r_o}\right) + \sin^{-1}\sqrt{\frac{2}{E}\alpha(E)+p^2}\frac{2}{r_o}\right]$$

for

$$\theta_o \leq \theta \leq \theta_m,$$

θ_o corresponding to the asymptote of the first part of the trajectory, θ_m to the center of the trajectory.

Let

$$\beta = \sin^{-1}\sqrt{\frac{2}{E}\alpha(E)+p^2}\,\frac{2}{r_o} - \frac{1}{p}\sqrt{\frac{2}{E}\alpha(E)+p^2}\,\sin^{-1}\frac{2p}{r_o}\,.$$

In Appendix X it is shown that

$$0 < \beta < \frac{\pi}{2} - 1,$$

in the range

$$0 \leq \frac{2}{r_o} \leq 1\Big/\sqrt{\frac{2}{E}\alpha(E)+p^2}$$

which limits p to

$$p \leq \sqrt{\left(\frac{r_o}{2}\right)^2 - \frac{2}{E}\alpha(E)}\,.$$

We write

$$u = \left[1 \Big/ \sqrt{\frac{2}{E}\alpha(E)+p^2}\right] \sin\left[\frac{1}{p}\sqrt{\frac{2}{E}\alpha(E)+p^2}\;\theta + \beta\right]. \qquad (14)$$

Now, the approximation

$$V(u) - V(r_o/2) \cong \alpha(E)u^2$$

can only be valid for $u > 2/r_o$, i.e. for the branch $A_o A_1$. If we use it for the branch between infinity and A_o, this means that $V(u) > V(\frac{r_o}{2})$ for $u < \frac{2}{r_o}$, i.e. that the potential corresponding to V(u) is attractive for $0 < u < 2/r_o$, has a minimum around $u = \frac{2}{r_o}$ (the approximation is, of course, wrong for $u = \frac{2}{r_o}$), and is repulsive for $u > \frac{2}{r_o}$. Hence the trajectory of P resulting from (14) starts with P below the asymptote OB (attractive portion). It is shown in Figure 16.

We have

$$\theta_o = -\left[p \Big/ \sqrt{\frac{2}{E}\alpha(E)+p^2}\right]\beta. \qquad (15)$$

Asymptote OC is defined by the angle

$$\theta_1 = \left[p \Big/ \sqrt{\frac{2}{E}\alpha(E)+p^2}\right](\pi - \beta), \qquad (15a)$$

and the angle φ is given by:

$$\varphi = \pi - (\theta_1 - \theta_o) = \pi\left[1 - p \Big/ \sqrt{\frac{2}{E}\alpha(E)+p^2}\right]. \qquad (16)$$

The angle of scatter to consider is

$$\varphi' = \pi - [(\theta_1 - \theta_o) + 2\theta_o] = \varphi - 2\theta_o. \qquad (17)$$

Appendix XI gives θ_o for $E = 10^{-1}$ Mev and $E = 10^{-4}$ Mev, for the two values $p = a/100$ and $p = \sqrt{r_o^2/4 - (2/E)\alpha(E)}$. The values $\alpha(E)$ taken are what will be called later α_u, i.e. a maximum leading to a too strong interaction (too large displacement cross-section, too small

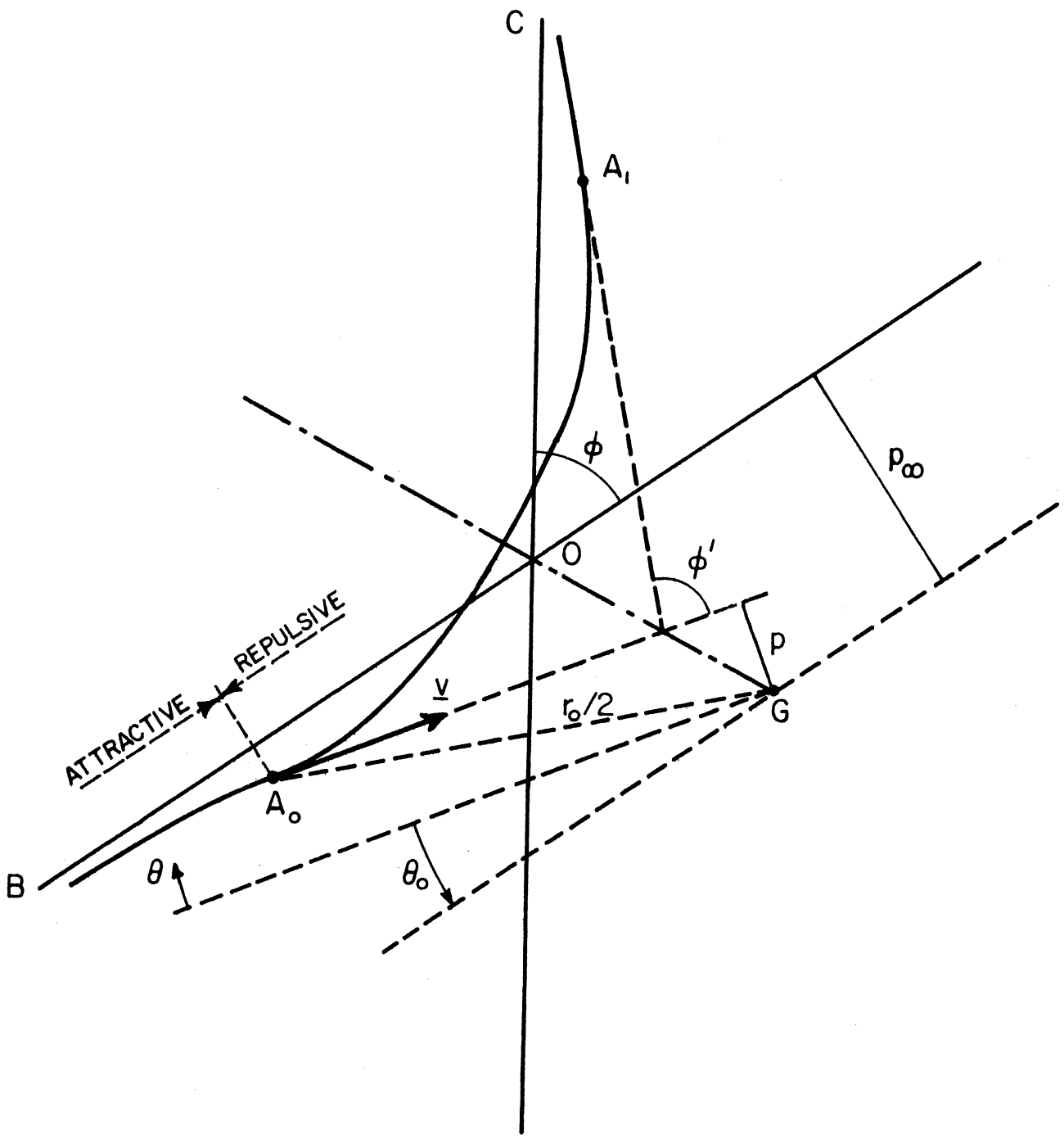

Figure 16. Prolongation of Trajectory to Infinity.

displacement mean free path).

It is found that:

for $E = 10^{-1}$ Mev and $p = a/100$,

$\theta_o \cong 0$, while $\varphi \cong \pi$;

for $E = 10^{-1}$ Mev and $p = \sqrt{r_o^2/4 - (2/E)\alpha_u} = 1.270 \cong 7.5\ a$,

$\theta_o \cong -0.019$ rad, while $\varphi \cong 2.20 \times 10^{-2}$ rad,

i.e., although $-2\theta_o$ is larger than φ, $\varphi' = 0.240$ rad, remains small.

For $E = 10^{-4}$ Mev and $p = a/100$,

$\theta_o = 2.72 \times 10^{-4}$ rad while $\varphi \cong \pi$;

for $E = 10^{-4}$ Mev and $p = \sqrt{r_o^2/4 - (2/E)\alpha u} = 0.655 \cong 3.8\ a$,

$\theta_o = -0.265$ rad while $\varphi = 1.54$ rad.

In summary, the approximation $\varphi' \cong \varphi$ is worse for large p ($\varphi' > \varphi$), the displacement cross section so calculated will be slightly too small. On the other hand, using the upper value α_u overestimates scatter, so that, for cross sections calculated with α_u, there should be some compensation of the two errors and we expect the result to come about right, somewhat too large, probably, for $E < 10^{-1}$ Mev, since the approximation $V - V(r_o/2) \cong \alpha_u u^2$ appears worse than the approximation $\varphi' \cong \varphi$ for such energies. On the contrary, cross sections calculated using a lower value α_ℓ, as will be explained shortly, should come out too small, since both errors are underestimating the interaction.

Then, we accept, for scattering angle, in the center of mass frame, an angle φ given by (16). In other words this discussion has shown that it is a permissible approximation to consider the boundary condition at $r = \infty$. Equation (16) has the general required form, since it gives

no interaction ($\varphi = 0$) for $p = \infty$ or $\alpha(E) = 0$, i.e. $V(u) = V(2/r_o)$, and backscatter ($\varphi = \pi$) for $p = 0$, i.e. head on collision.

From (12a), it is seen that the maximum value of p for which it is possible to have the trajectory pass through a point at distance $r_o/2$ from G is (Figure 17):

$$p_o = \sqrt{\left(\frac{r_o}{2}\right)^2 - \frac{2}{E}\alpha(E)} \quad .$$

This is entirely due to the mathematical approximation made. Actually, P is not scattered by G, but by another center of force, corresponding to a nearest neighbor of the atom considered, if its initial velocity (at A_o), $\underline{v}$, is tangent to the sphere centered about G of radius $r_o/2$. Hence, the maximum value of p for scattering is

$$p_s = r_o/2$$

and the scattering cross section

$$\sigma_s = \pi p_s^2 = \pi (r_o/2)^2 \quad .$$

For copper,

$$p_s = 1.278 \text{ Å}$$
$$p_s^2 = 1.628 \text{ Å}^2$$
$$\sigma_s = 5.11 \text{ Å}^2 \quad .$$

In order to find what value of $\alpha(E)$ to select for the approximation

$$V(u) - V(r_o/2) \cong \alpha(E)u^2,$$

two values were considered, a lower value α_ℓ and an upper value α_u.

α_u is such that

$$R_u = 1 - \frac{2}{E}\alpha_u(E)u^2 - p^2u^2 \leq 1 - \frac{2}{E}\left[V(u) - V\left(\frac{r_o}{2}\right)\right] - p^2u^2 = R$$

for all $u \leq u_1$, u_1 being defined by

$$1 - \frac{2}{E}\alpha_u(E)u_1^2 - p^2u_1^2 = 0 \quad .$$

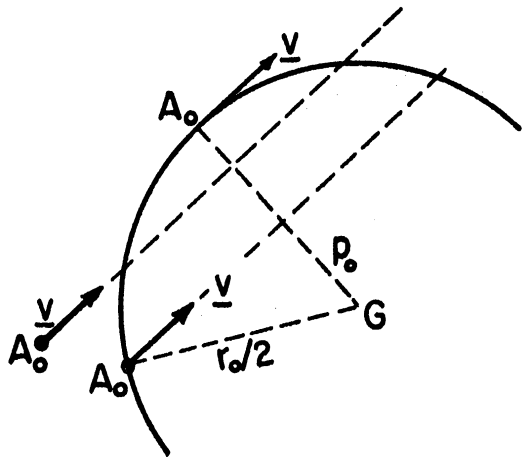

Figure 17. Maximum Value of p due to Approximation.

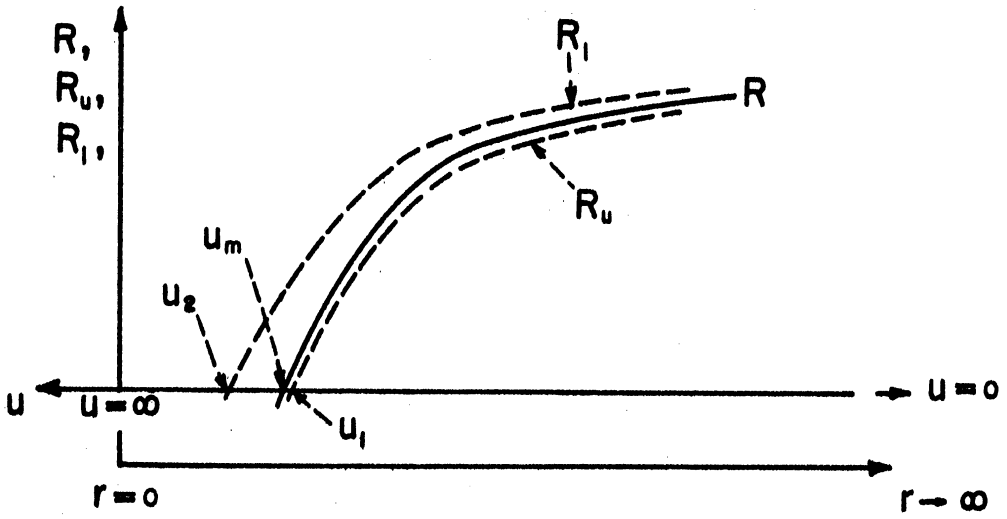

Figure 18. Upper and Lower Approximations.

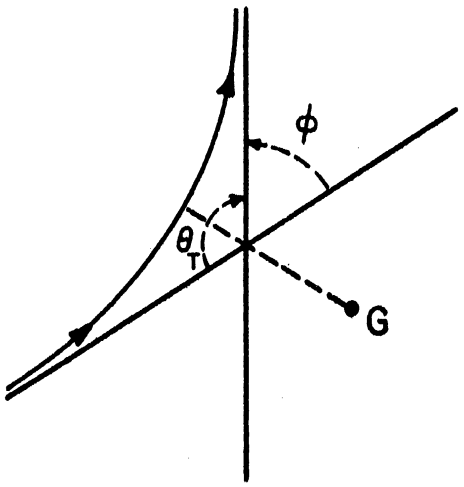

Figure 19. Angle of Asymptotes.

α_ℓ is such that

$$R_\ell = 1 - \frac{2}{E}\alpha_\ell(E)u^2 - p^2u^2 \geq 1 - \frac{2}{E}\left[V(u) - V\left(\frac{r_0}{2}\right)\right] - p^2u^2 = R$$

for all $u \leq u_2$, u_2 being defined by

$$1 - \frac{2}{E}\alpha_\ell(E)u_2^2 - p^2u_2^2 = 0 .$$

It follows that u_2, is greater than u_m. Figure 18 illustrates the situation. α_u and α_ℓ are chosen by inspecton of tables giving R as a function of u for various values of E. Strictly, α_ℓ is not chosen so that $R_\ell \geq R$ for all $u \leq u_2$, which would lead to very small values of α_ℓ, but so that $R_\ell \geq R$ in the portion of the R(u) line which has an appreciable curvature--i.e. the range of u where scattering takes place--and that $R_\ell \cong R$ in the portion where there is no appreciable curvature.

Disregard the approximation on φ' for the time being and consider φ' defined by the asymptotes. Call $(\theta_T)_u$ and $(\theta_T)_\ell$ the two values of θ_T obtained by selecting the approximation corresponding to α_u and α_ℓ, respectively (Figure 19). $(\theta_T)_u$ corresponds to scattering by a stronger potential than the actual one. Since the initial conditions are the same in the three cases, it follows that

$$(\theta_T)_u < \theta_T < (\theta_T)_\ell ,$$

hence,

$$\varphi_\ell < \varphi < \varphi_u .$$

We assume elastic collisions, hence the kinetic energy T transferred to the stationary atom by the incoming knock-on of energy E is (Appendix VIII),

$$T = E \sin^2 \varphi/2 .$$

This and Equation (16) give p_d, maximum of p for displacing collision, when T is equal to E_d. Thus,

$$p_d^2 = (2\alpha/E)(1 - \varphi_d/\pi)^2 / [1 - (1 - \varphi_d/\pi)^2] , \quad (20)$$

$$\sin^2 \varphi_d/2 = E_d/E \quad . \tag{21}$$

Call $(p_d)_u$ and $(p_d)_\ell$ the values of p_d obtained by selecting α_u and α_ℓ for α. In the same way, call $(\sigma_d)_u$ and $(\sigma_d)_\ell$, $(\Sigma_d)_u$ and $(\Sigma_d)_\ell$, $(\lambda_d)_u$ and $(\lambda_d)_\ell$ the corresponding microscopic and macroscopic cross sections and mean free path for displacing collisions, assuming $\varphi' = \varphi$. Call σ_d, ... the true values of these parameters. From Equation (20), since φ_d is fixed by Equation (21), and recalling that

$$\sigma_d = \pi (p_d)^2,$$

it follows that

$(\sigma_d)_u$, $(\Sigma_d)_u$ are proportional to α_u

$(\lambda_d)_u$ is inversely proportional to α_u

$(\sigma_d)_\ell$, $(\Sigma_d)_\ell$ are proportional to α_ℓ

$(\lambda_d)_\ell$ is inversely proportional to α_ℓ .

Hence,

$$(\sigma_d)_\ell < \sigma_d, \quad (\Sigma_d)_\ell < \Sigma_d \quad , \quad \lambda_d < (\lambda_d)_\ell$$

However, since, for α_u, the two approximations $V = V(r_o/2) \cong \alpha_u u^2$ and $\varphi' \cong \varphi$ partly compensate each other, we shall write

$$\left.\begin{aligned} (\sigma_d)_\ell < \sigma_d \lesssim (\sigma_d)_u, \quad (\Sigma_d)_\ell < \Sigma_d \leq (\Sigma_d)_u, \\ (\lambda_d)_u \leq \lambda_d < (\lambda_d)_\ell \end{aligned}\right\} \tag{22}$$

Diagram 1 shows the variations of V, $V-V(r_o/2)$, and u^2. This diagram is discussed in Appendix IX.

Tables II through VIII give the result of the numerical calculations made for E = 10^{-1} Mev, 10^{-2} Mev, 5 x 10^{-3} Mev, 10^{-3} Mev, 10^{-4} Mev, 25 ev and for p = a/100 (in addition, also p = a for E = 10^{-1} Mev), in order to select $\alpha_u(E)$ and $\alpha_\ell(E)$.

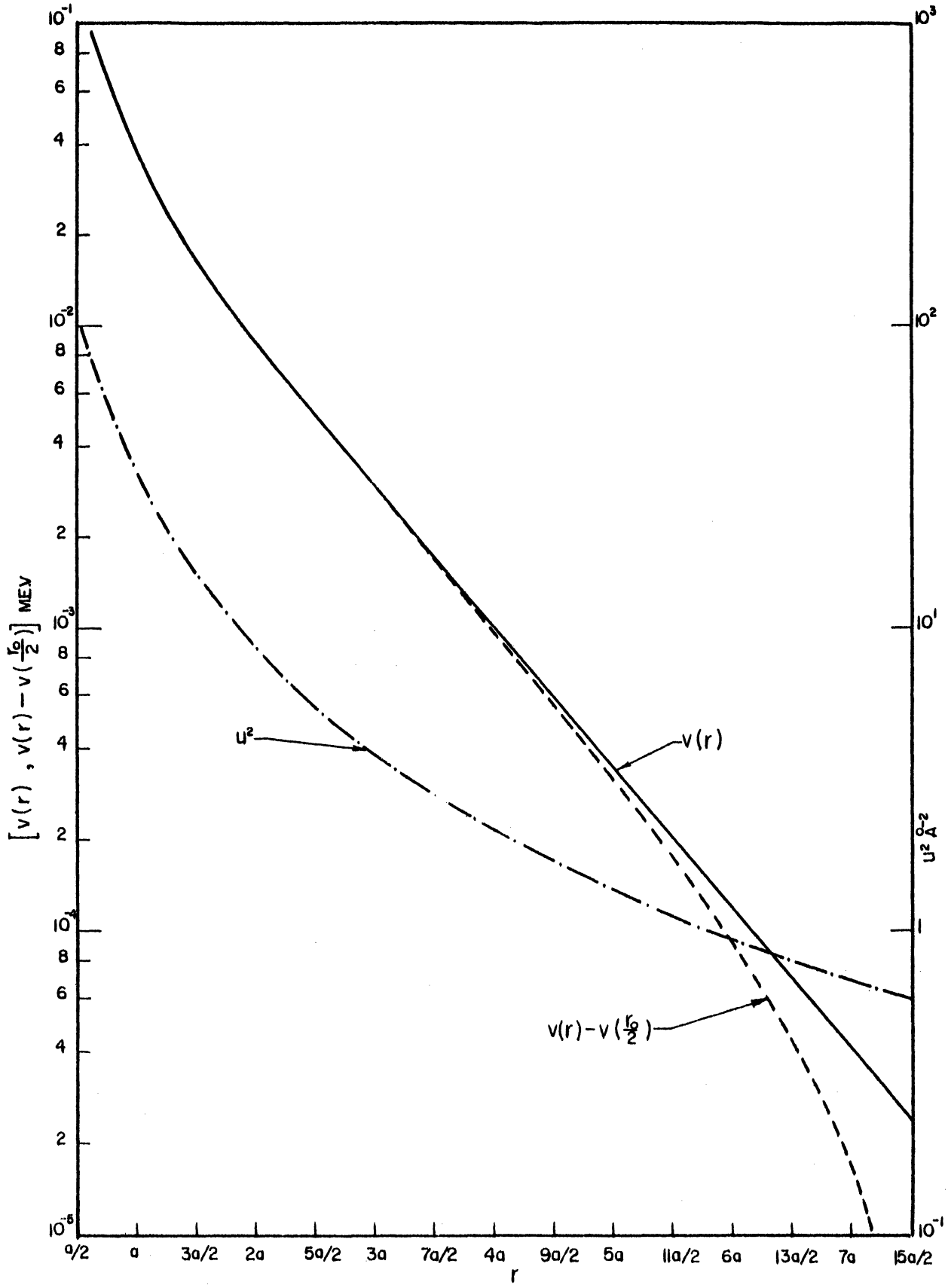

Diagram 1. $V(r)$, $V(r) - V(\frac{r_o}{2})$, and u^2 vs r. r Expressed in Fractions of Screening Distance a.

TABLE II. $E = 10^{-1}$ Mev; $p = a/100$

$p^2 = 2.98 \times 10^{-6}\ \text{Å}^2$; $\frac{1}{p^2} = 3.35 \times 10^{5}\ \text{Å}^2$; $\frac{2}{E} = 20$

$\alpha_u = 1.15 \times 10^{-3}$; $\frac{2}{E}\alpha_u = 2.30 \times 10^{-2}$; $\alpha_\ell = 6.00 \times 10^{-4}$; $\frac{2}{E}\alpha_\ell = 1.20 \times 10^{-2}$

r	u^2	$V-V(\frac{r_0}{2})$	$\frac{V-V(\frac{r_0}{2})}{u_2}$	$\frac{2}{E}[V-V(\ )]$	$1-\frac{2}{E}[\ ]$	p^2u^2	R	$\frac{2}{E}\alpha_u u^2$	$1-\frac{2}{E}..$	R_u	$\frac{2}{E}\alpha_\ell u^2$	$1-\frac{2}{E}..$	R_ℓ	$\sqrt{R}$	$\sqrt{R_u}$	y	y_u
a/2	1.34×10^{2}	1.07×10^{-1}	8.00×10^{-4}	2.14	1.14	$\cong 0$	1.14										
a	3.35×10	3.86×10^{-2}	1.15×10^{-3}	7.72×10^{-3}	2.28×10^{-1}		2.28×10^{-1}	7.71×10^{-1}	2.29×10^{-1}	2.29×10^{-1}	4.01×10^{-1}	5.99×10^{-1}	5.99×10^{-1}	4.78×10^{-1}	4.78×10^{-1}	3.60×10^{-3}	3.60×10^{-3}
3a/2	1.50×10	1.62×10^{-2}	1.08×10^{-3}	3.24×10^{-1}	6.76×10^{-1}		6.76×10^{-1}	3.45×10^{-1}	6.55×10^{-1}	6.55×10^{-1}	1.80×10^{-1}	8.20×10^{-1}	8.20×10^{-1}	8.20×10^{-1}	8.10×10^{-1}	2.10×10^{-3}	2.12×10^{-3}
2a	8.40	9.50×10^{-3}	1.13×10^{-3}	1.0×10^{-1}	8.10×10^{-1}		8.10×10^{-1}	1.3×10^{-1}	8.07×10^{-1}	8.07×10^{-1}	1.01×10^{-1}	8.99×10^{-1}	8.99×10^{-1}	9.00×10^{-1}	8.98×10^{-1}	1.91×10^{-3}	1.92×10^{-3}
5a/2	5.39	5.16×10^{-3}	9.60×10^{-4}	1.12×10^{-1}	8.80×10^{-1}		8.80×10^{-1}	1.24×10^{-1}	8.76×10^{-1}	8.76×10^{-1}	6.45×10^{-2}	9.36×10^{-1}	9.36×10^{-1}	9.40×10^{-1}	9.35×10^{-1}	1.83×10^{-3}	1.84×10^{-3}
3a	3.75	2.88×10^{-3}	7.75×10^{-4}	5.76×10^{-2}	9.42×10^{-1}		9.42×10^{-1}	8.61×10^{-2}	9.14×10^{-1}	9.14×10^{-1}	4.48×10^{-2}	9.55×10^{-1}	9.55×10^{-1}	9.70×10^{-1}	9.57×10^{-1}	1.77×10^{-3}	1.80×10^{-3}
7a/2	2.75	1.65×10^{-3}	6.08×10^{-4}	3.30×10^{-2}	9.67×10^{-1}		9.67×10^{-1}	6.32×10^{-2}	9.37×10^{-1}	9.37×10^{-1}	3.30×10^{-2}	9.67×10^{-1}	9.67×10^{-1}	9.84×10^{-1}	9.68×10^{-1}	1.75×10^{-3}	1.78×10^{-3}
4a	2.10	9.40×10^{-4}	4.48×10^{-4}	1.88×10^{-2}	9.81×10^{-1}		9.81×10^{-1}	4.83×10^{-2}	9.52×10^{-1}	9.52×10^{-1}	2.52×10^{-2}	9.75×10^{-1}	9.75×10^{-1}	9.90×10^{-1}	9.76×10^{-1}	1.74×10^{-3}	1.76×10^{-3}
9a/2	1.66	5.40×10^{-4}	3.26×10^{-4}	1.08×10^{-2}	9.89×10^{-1}		9.89×10^{-1}	3.82×10^{-2}	9.62×10^{-1}	9.62×10^{-1}	1.99×10^{-2}	9.80×10^{-1}	9.80×10^{-1}	9.95×10^{-1}	9.80×10^{-1}	1.73×10^{-3}	1.76×10^{-3}
5a	1.34	3.05×10^{-4}	2.28×10^{-4}	6.10×10^{-3}	$\cong 1.00$		1.00	3.08×10^{-2}	9.69×10^{-1}	9.69×10^{-1}	1.61×10^{-2}	9.84×10^{-1}	9.84×10^{-1}	1.00	9.85×10^{-1}	1.72×10^{-3}	1.75×10^{-3}
11a/2	1.12	1.71×10^{-4}	1.53×10^{-4}		$\cong 1.00$		1.00	2.58×10^{-2}	9.74×10^{-1}	9.74×10^{-1}				1.00	9.87×10^{-1}	1.72×10^{-3}	1.74×10^{-3}
6a	9.40×10^{-1}	9.10×10^{-5}	9.70×10^{-5}	1.82×10^{-3}	$\cong 1.00$		1.00	2.16×10^{-2}	9.78×10^{-1}	9.78×10^{-1}				1.00	9.89×10^{-1}	1.72×10^{-3}	1.74×10^{-3}
13a/2	8.00×10^{-1}	4.42×10^{-5}	5.53×10^{-5}		$\cong 1.00$		1.00	1.84×10^{-2}	9.82×10^{-1}	9.82×10^{-1}				1.00	9.91×10^{-1}	1.72×10^{-3}	1.73×10^{-3}
7a	6.90×10^{-1}	1.66×10^{-5}	2.41×10^{-5}	3.32×10^{-4}	$\cong 1.00$		1.00	1.58×10^{-2}	9.84×10^{-1}	9.84×10^{-1}				1.00	9.93×10^{-1}	1.72×10^{-3}	1.73×10^{-3}
15a/2	6.00×10^{-1}	0	0	0	1.00		1.00	1.38×10^{-2}	9.86×10^{-1}	9.86×10^{-1}				1.00	9.94×10^{-1}	1.72×10^{-3}	1.73×10^{-3}

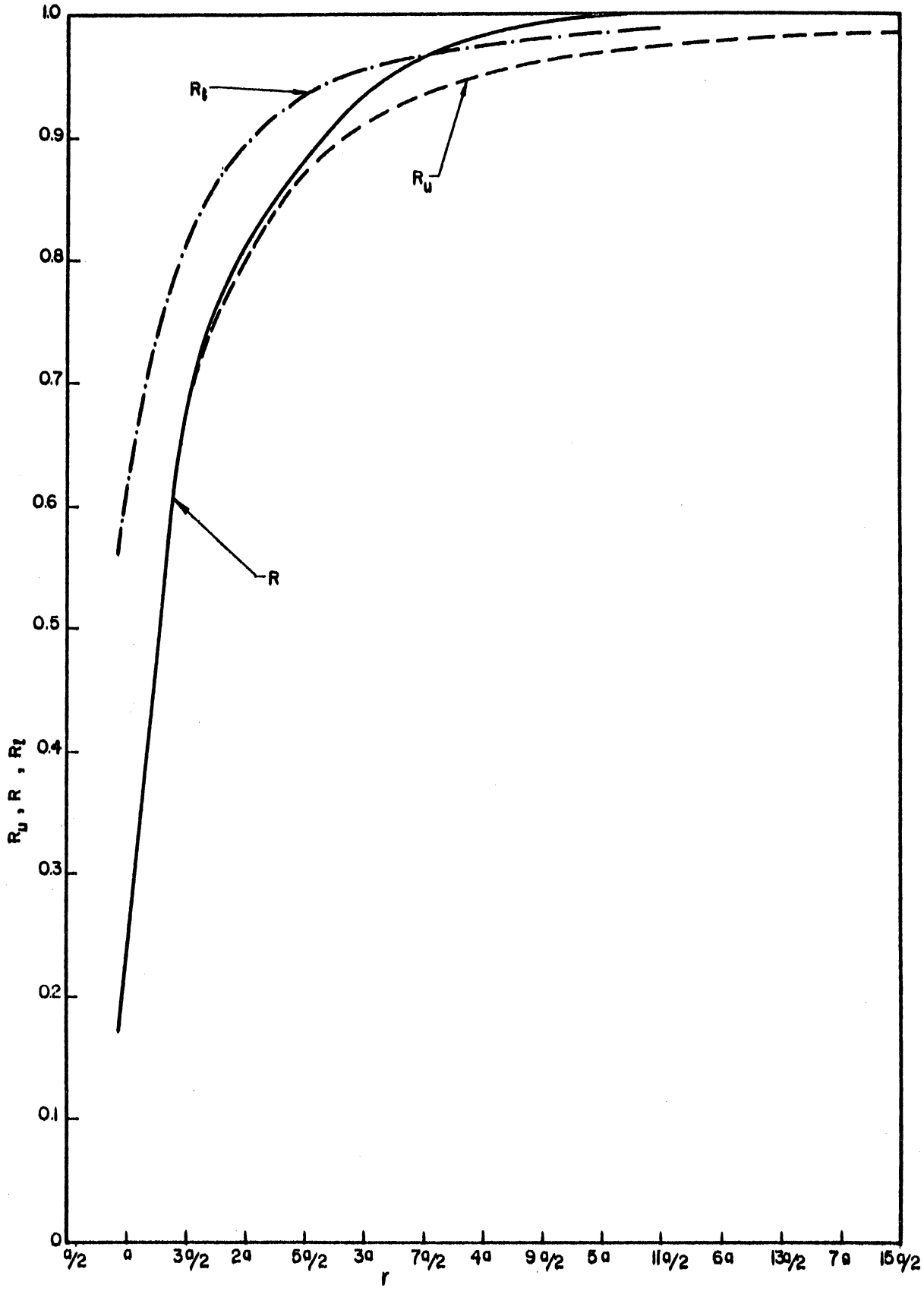

Diagram 2. $R(r)$, $R_u(r)$, $R_\ell(r)$. r Expressed in Fractions of Screening Distance a. $E = 10^{-1}$ Mev, $p = a/100$.

TABLE III. $E = 10^{-1}$ Mev; $p = a$

$p^2 = 2{\cdot}95 \times 10^{-2}\ \mathring{A}^2$

$\alpha_u = 1{\cdot}15 \times 10^{-3}$; $\frac{2}{E}\alpha_u = 2{\cdot}30 \times 10^{-2}$

r	u^2	$V-V(\frac{r_o}{2})$	$\frac{V-V(\frac{r_o}{2})}{u^2}$	$\frac{2}{E}[V-V(\ )]$	$1-\frac{2}{E}[\ ]$	p^2u^2	R	$\frac{2}{E}\alpha_u u^2$	$1-\frac{2}{E}..$	R_u
a/2	$1{\cdot}34 \times 10^{2}$	$1{\cdot}07 \times 10^{-1}$	$8{\cdot}00 \times 10^{-4}$	2·14	1·14	3·95	5·09			
a	3·35 x 10	$3{\cdot}86 \times 10^{-2}$	$1{\cdot}15 \times 10^{-3}$	$7{\cdot}72 \times 10^{-1}$	$2{\cdot}28 \times 10^{-1}$	$9{\cdot}85 \times 10^{-1}$	$7{\cdot}57 \bar{\times} 10^{-1}$	$7{\cdot}71 \times 10^{-1}$	$2{\cdot}29 \times 10^{-1}$	$7{\cdot}56 \bar{\times} 10^{-1}$
3a/2	1·50 x 10	$1{\cdot}62 \times 10^{-2}$	$1{\cdot}08 \times 10^{-3}$	$3{\cdot}24 \times 10^{-1}$	$6{\cdot}76 \times 10^{-1}$	$4{\cdot}43 \times 10^{-1}$	$2{\cdot}33 \dot{\times} 10^{-1}$	$3{\cdot}45 \times 10^{-1}$	$6{\cdot}55 \times 10^{-1}$	$2{\cdot}12 \times 10^{-1}$
2a	8·40	$9{\cdot}50 \times 10^{-3}$	$1{\cdot}13 \times 10^{-3}$	$1{\cdot}90 \times 10^{-1}$	$8{\cdot}10 \times 10^{-1}$	$2{\cdot}48 \times 10^{-1}$	$5{\cdot}62 \times 10^{-1}$	$1{\cdot}93 \times 10^{-1}$	$8{\cdot}07 \times 10^{-1}$	$5{\cdot}59 \times 10^{-1}$
5a/2	5·39	$5{\cdot}16 \times 10^{-3}$	$9{\cdot}60 \times 10^{-4}$	$1{\cdot}12 \times 10^{-1}$	$8{\cdot}80 \times 10^{-1}$	$1{\cdot}59 \times 10^{-1}$	$7{\cdot}21 \times 10^{-1}$	$1{\cdot}24 \times 10^{-1}$	$8{\cdot}76 \times 10^{-1}$	$7{\cdot}17 \times 10^{-1}$
3a	3·75	2.88×10^{-3}	7.75×10^{-4}	5.76×10^{-2}	9.42×10^{-1}	1.11×10^{-1}	8.31×10^{-1}	8.61×10^{-2}	9.14×10^{-1}	8.03×10^{-1}
7a/2	2.75	1.65×10^{-3}	3.30×10^{-2}	9.67×10^{-1}	9.67×10^{-1}	8.10×10^{-2}	8.85×10^{-1}	6.32×10^{-2}	9.37×10^{-1}	8.56×10^{-1}
4a	2.10	9.40×10^{-4}	4.48×10^{-4}	1.88×10^{-2}	9.81×10^{-1}	6.20×10^{-2}	9.19×10^{-1}	4.83×10^{-2}	9.52×10^{-1}	8.90×10^{-1}
9a/2	1.66	5.40×10^{-4}	3.26×10^{-4}	1.08×10^{-2}	9.89×10^{-1}	4.9×10^{-2}	9.40×10^{-1}	3.82×10^{-2}	9.62×10^{-1}	9.13×10^{-1}
5a	1.34	3.05×10^{-4}	2.28×10^{-4}	6.10×10^{-3}	$\cong 1.00$	3.95×10^{-2}	9.61×10^{-1}	3.08×10^{-2}	9.68×10^{-1}	9.30×10^{-1}
11a/2	1.12	1.71×10^{-4}	1.53×10^{-4}		$\cong 1.00$	3.30×10^{-2}	9.67×10^{-1}	2.58×10^{-2}	9.74×10^{-1}	9.41×10^{-1}
6a	9.40×10^{-1}	9.10×10^{-5}	9.70×10^{-5}	1.82×10^{-3}	$\cong 1.00$	2.77×10^{-2}	9.72×10^{-1}	2.16×10^{-2}	9.78×10^{-1}	9.51×10^{-1}
13a/2	8.00×10^{-1}	4.42×10^{-5}	5.53×10^{-5}		$\cong 1.00$	2.36×10^{-2}	9.76×10^{-1}	1.84×10^{-2}	9.82×10^{-1}	9.58×10^{-1}
7a	6.90×10^{-1}	1.66×10^{-5}	2.41×10^{-5}	3.32×10^{-4}	$\cong 1.00$	2.09×10^{-2}	9.79×10^{-1}	1.58×10^{-2}	9.84×10^{-1}	9.63×10^{-1}
15a/2	6.00×10^{-1}	0	0	0	1.00	1.77×10^{-2}	9.82×10^{-1}	1.38×10^{-2}	9.86×10^{-1}	9.69×10^{-1}

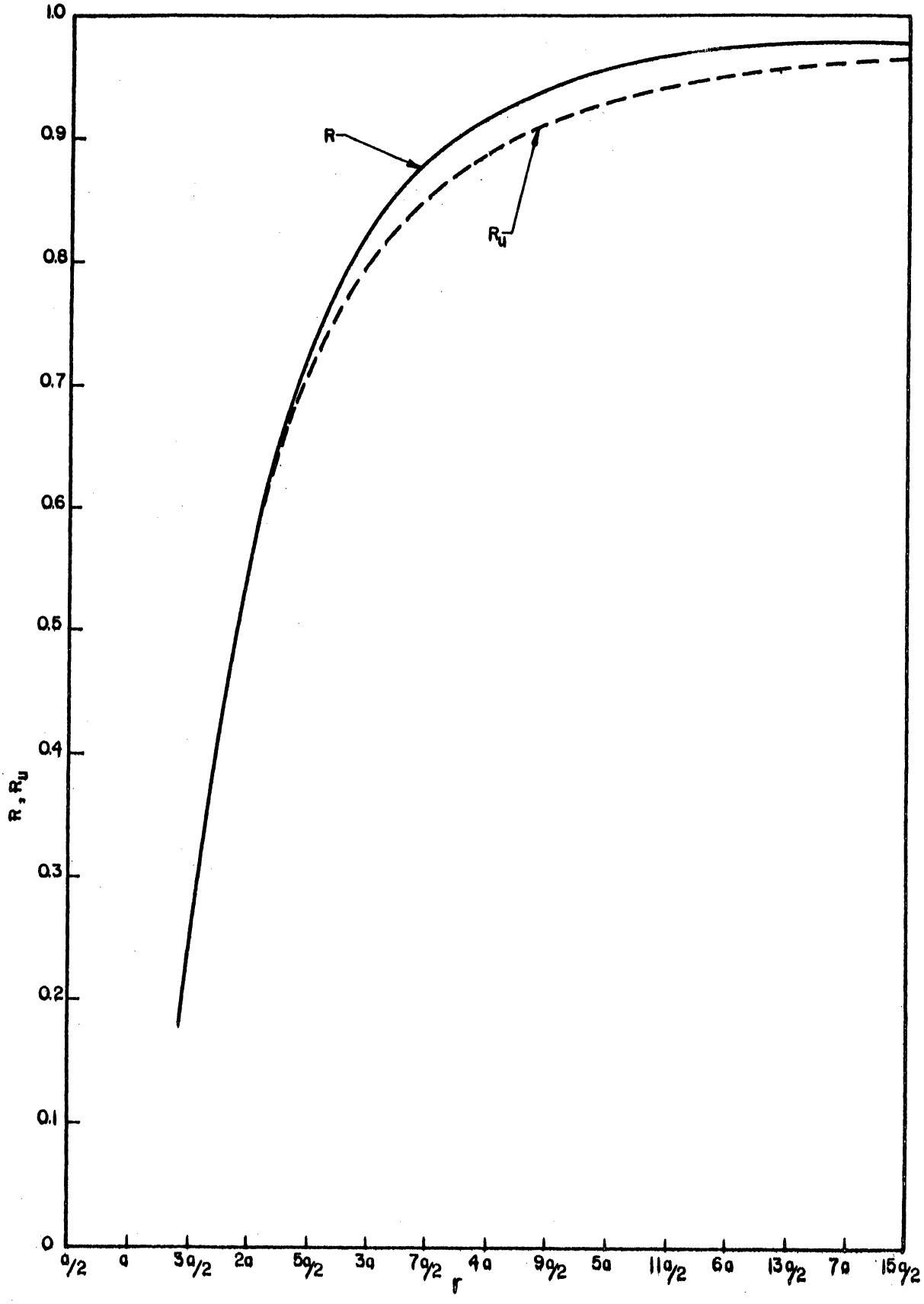

Diagram 3. R(r) and $R_u(r)$. r Expressed in Fractions of Screening Distance a. $E = 10^{-1}$ Mev, $p = a$.

TABLE IV. $E = 10^{-2}$ Mev; $p = a/100$

$p^2 = 2.98 \times 10^{-6}$ Å^2 $\alpha_u = 9.60 \times 10^{-4}$;

$\frac{2}{E}\alpha_u = 1.92 \times 10^{-1}$; $\alpha_\ell = 2.28 \times 10^{-4}$; $\frac{2}{E}\alpha_\ell = 4.56 \times 10^{-2}$

r	u^2	$V-V(\frac{r_o}{2})$	$\frac{V-V(\ )}{u^2}$	$\frac{2}{E}[V-V(\ )]$	$1-\frac{2}{E}[\ ]$	p^2u^2	R	$\frac{2}{E}\alpha_u u^2$	$1-\frac{2}{E}..$	R_u	$\frac{2}{E}\alpha_\ell u^2$	$1-\frac{2}{E}..$	R_ℓ
5a/2	5.39	5.16×10^{-3}	9.60×10^{-4}	1.03	-3.20×10^{-2}	$\cong 0$	<0	1.03	-3.00×10^{-2}	<0			
3a	3.75	2.88×10^{-3}	7.75×10^{-4}	5.76×10^{-1}	$+4.24\times10^{-1}$		4.24×10^{-1}	7.21×10^{-1}	$+2.79\times10^{-1}$	2.79×10^{-1}	1.70×10^{-1}	8.30×10^{-1}	8.30×10^{-1}
7a/2	2.75	1.65×10^{-3}	6.08×10^{-4}	3.30×10^{-1}	6.70×10^{-1}		6.70×10^{-1}	5.28×10^{-1}	4.72×10^{-1}	4.72×10^{-1}	1.25×10^{-1}	8.75×10^{-1}	8.75×10^{-1}
4a	2.10	9.40×10^{-4}	4.48×10^{-4}	1.88×10^{-1}	8.12×10^{-1}		8.12×10^{-1}	4.04×10^{-1}	5.96×10^{-1}	5.96×10^{-1}	9.60×10^{-2}	9.04×10^{-1}	9.04×10^{-1}
9a/2	1.66	5.40×10^{-4}	3.26×10^{-4}	1.08×10^{-1}	8.92×10^{-1}		8.92×10^{-1}	3.20×10^{-1}	6.80×10^{-1}	6.80×10^{-1}	7.57×10^{-2}	9.24×10^{-1}	9.24×10^{-1}
5a	1.34	3.05×10^{-4}	2.28×10^{-4}	6.10×10^{-2}	9.39×10^{-1}		9.39×10^{-1}	2.58×10^{-1}	7.42×10^{-1}	7.42×10^{-1}	6.11×10^{-2}	9.39×10^{-1}	9.39×10^{-1}
11a/2	1.12	1.71×10^{-4}	1.53×10^{-4}	2.70×10^{-2}	9.73×10^{-1}		9.73×10^{-1}	2.16×10^{-1}	7.84×10^{-1}	7.84×10^{-1}	5.11×10^{-2}	9.49×10^{-1}	9.49×10^{-1}
6a	9.40×10^{-1}	9.10×10^{-5}	9.70×10^{-5}	1.82×10^{-2}	9.82×10^{-1}		9.82×10^{-1}	1.81×10^{-1}	8.19×10^{-1}	8.19×10^{-1}	4.29×10^{-2}	9.57×10^{-1}	9.57×10^{-1}
13a/2	8.00×10^{-1}	4.42×10^{-5}	5.53×10^{-5}	4.84×10^{-3}	9.95×10^{-1}		9.95×10^{-1}	1.54×10^{-1}	8.46×10^{-1}	8.46×10^{-1}	3.66×10^{-2}	9.63×10^{-1}	9.63×10^{-1}
7a	6.90×10^{-1}	1.66×10^{-5}	2.41×10^{-5}	3.32×10^{-3}	9.97×10^{-1}		9.97×10^{-1}	1.33×10^{-1}	8.67×10^{-1}	8.67×10^{-1}	3.14×10^{-2}	9.69×10^{-1}	9.69×10^{-1}
15a/2	6.00×10^{-1}	0	0	0	1.00		1.00	1.15×10^{-1}	8.85×10^{-1}	8.85×10^{-1}	2.74×10^{-2}	9.73×10^{-1}	9.73×10^{-1}

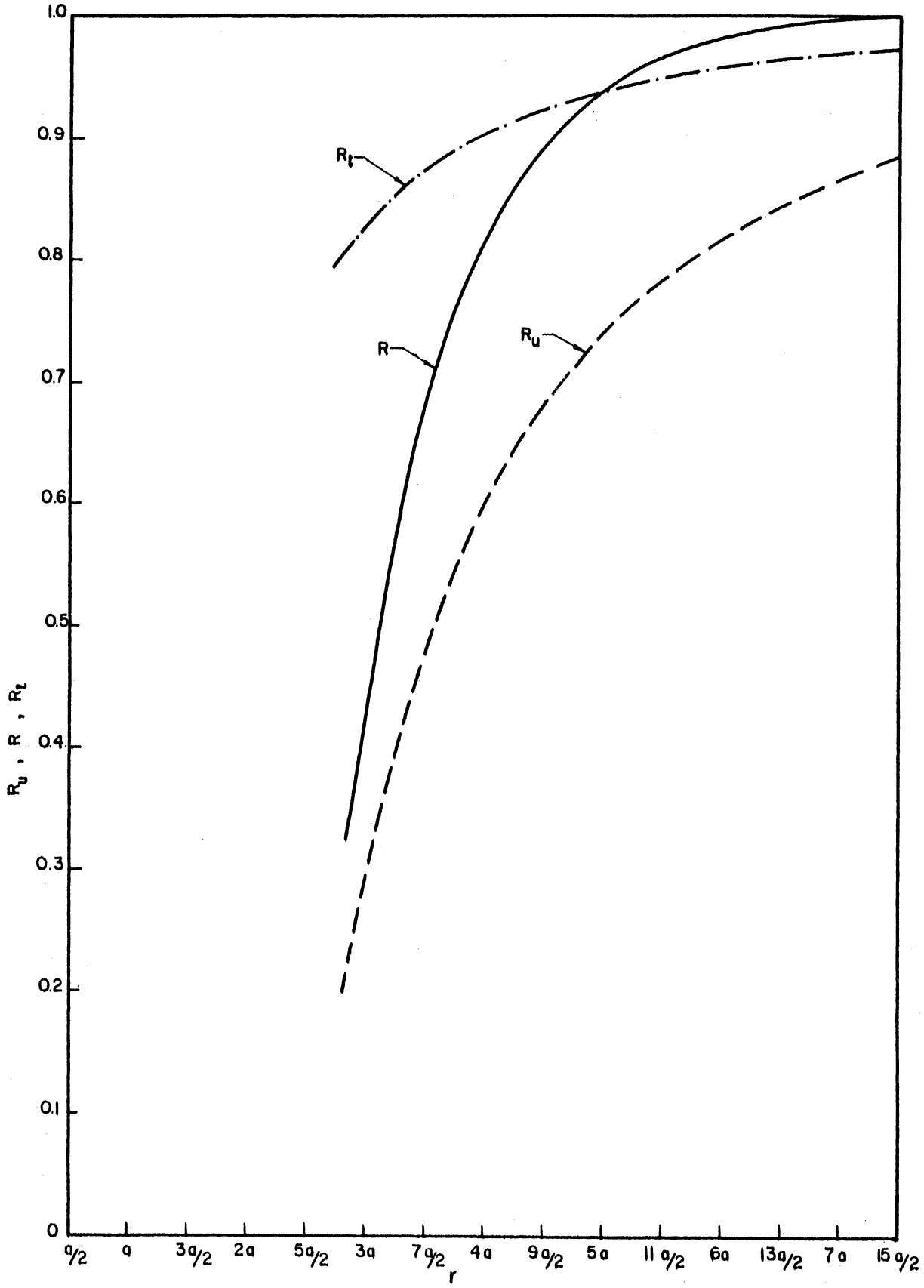

Diagram 4. R(r), $R_u(r)$, $R_\ell(r)$. r Expressed in Fractions of Screening Distance a. E = 10^{-2} Mev, p = a/100.

TABLE V. $E = 5 \times 10^{-3}$ Mev; $p = a/100$

$p^2 = 2.98 \times 10^{-6}$ Å^2; $\alpha_u = 7.75 \times 10^{-4}$;

$\frac{2}{E}\alpha_u = 3.1 \times 10^{-1}$; $\alpha_\ell = 1.53 \times 10^{-4}$; $\frac{2}{E}\alpha_\ell = 6.12 \times 10^{-2}$

r	u^2	$V-V(\frac{r_o}{2})$	$\frac{V-V(\ )}{u^2}$	$\frac{2}{E}[V-V(\ )]$	$1-\frac{2}{E}[\ ]$	p^2u^2	R	$\frac{2}{E}\alpha_u u^2$	$1-\frac{2}{E}..$	R_u	$\frac{2}{E}\alpha_\ell u^2$	$1-\frac{2}{E}..$	R_ℓ
3a	3.75	2.88×10^{-3}	7.75×10^{-4}	1.15	-1.52×10^{-1}	$\cong 0$	< 0	1.16	-1.60×10^{-1}	-1.60×10^{-1}	2.29×10^{-1}	$+7.71\times10^{-1}$	$+7.71\times10^{-1}$
7a/2	2.75	1.65×10^{-3}	6.08×10^{-4}	6.60×10^{-1}	3.40×10^{-1}		3.40×10^{-1}	8.51×10^{-1}	$+1.49\times10^{-1}$	$+1.49\times10^{-1}$	1.68×10^{-1}	8.32×10^{-1}	8.32×10^{-1}
4a	2.10	9.40×10^{-4}	4.48×10^{-4}	3.76×10^{-1}	6.24×10^{-1}		6.24×10^{-1}	6.51×10^{-1}	3.49×10^{-1}	3.49×10^{-1}	1.28×10^{-1}	8.72×10^{-1}	8.72×10^{-1}
9a/2	1.66	5.40×10^{-4}	3.26×10^{-4}	2.16×10^{-1}	7.84×10^{-1}		7.84×10^{-1}	5.15×10^{-1}	4.85×10^{-1}	4.85×10^{-1}	1.02×10^{-1}	8.98×10^{-1}	8.98×10^{-1}
5a	1.34	3.05×10^{-4}	2.28×10^{-4}	1.22×10^{-1}	8.78×10^{-1}		8.78×10^{-1}	4.15×10^{-1}	5.85×10^{-1}	5.85×10^{-1}	8.20×10^{-2}	9.18×10^{-1}	9.18×10^{-1}
11a/2	1.12	1.17×10^{-4}	1.53×10^{-4}	6.12×10^{-2}	9.39×10^{-1}		9.39×10^{-1}	3.48×10^{-1}	6.52×10^{-1}	6.52×10^{-1}	6.85×10^{-2}	9.32×10^{-1}	9.32×10^{-1}
6a	9.40×10^{-1}	9.10×10^{-5}	9.70×10^{-5}	3.64×10^{-2}	9.64×10^{-1}		9.64×10^{-1}	2.92×10^{-1}	7.08×10^{-1}	7.08×10^{-1}	5.75×10^{-2}	9.43×10^{-1}	9.43×10^{-1}
13a/2	8.00×10^{-1}	4.42×10^{-5}	5.53×10^{-5}	2.21×10^{-2}	9.78×10^{-1}			2.48×10^{-1}	7.52×10^{-1}	7.52×10^{-1}	4.90×10^{-2}	9.51×10^{-1}	9.51×10^{-1}
7a	6.90×10^{-1}	1.66×10^{-5}	2.41×10^{-5}	6.64×10^{-3}	9.93×10^{-1}		9.93×10^{-1}	2.14×10^{-1}	7.86×10^{-1}	7.86×10^{-1}	4.22×10^{-2}	9.58×10^{-1}	9.58×10^{-1}
15a/2	6.00×10^{-1}	0	0	0	1.00		1.00	1.86×10^{-1}	8.14×10^{-1}	8.14×10^{-1}	3.68×10^{-2}	9.63×10^{-1}	9.63×10^{-1}

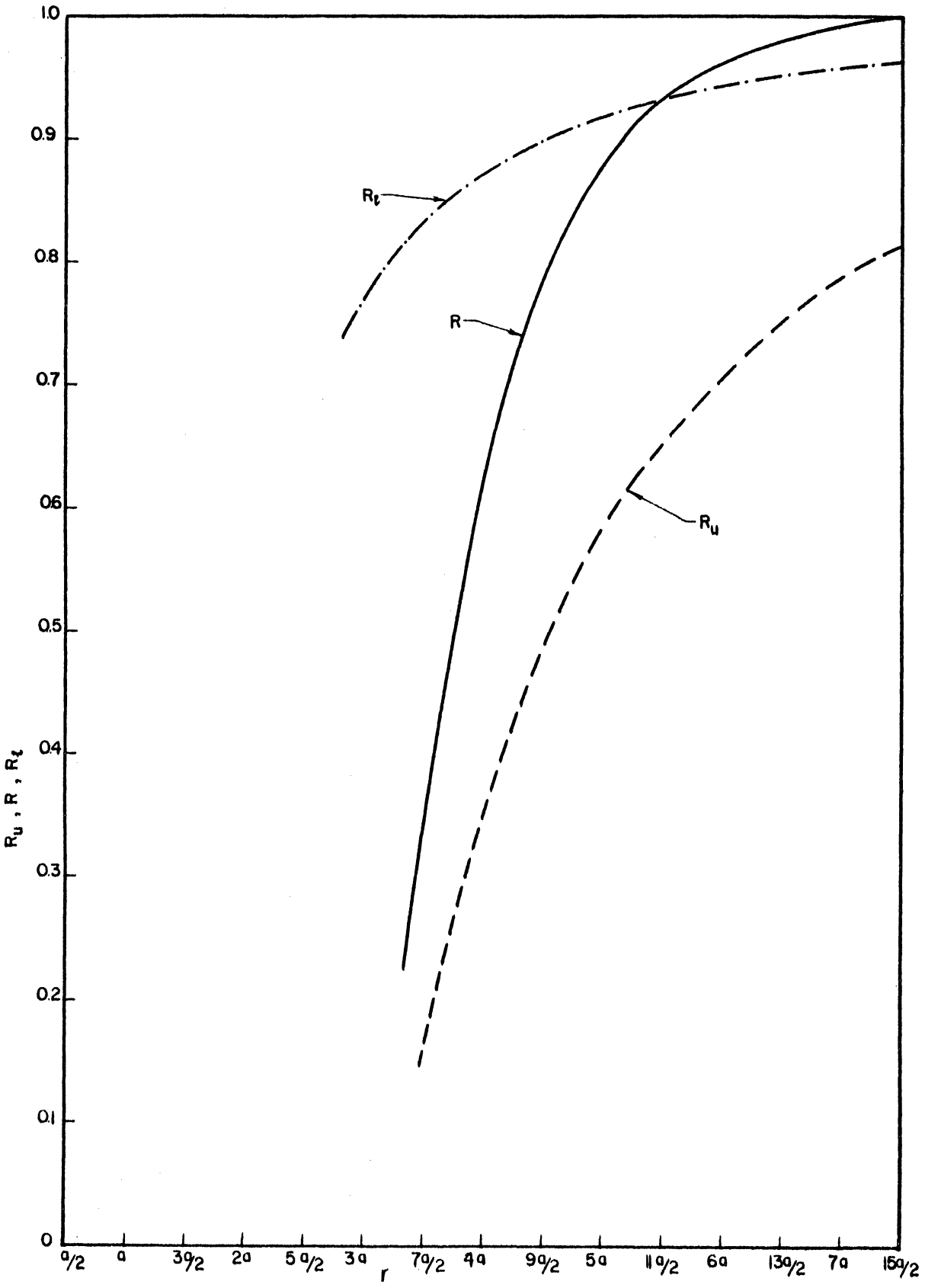

Diagram 5. $R(r)$, $R_u(r)$, $R_\ell(r)$. r Expressed in Fractions of Screening Distance a. $E = 5 \times 10^{-3}$ Mev, $p = a/100$.

TABLE VI. $E = 10^{-3}$ Mev; $p = a/100$

$p^2 = 2.98 \times 10^{-6}$ Å^2; $\alpha_u = 3.26 \times 10^{-4}$;

$\frac{2}{E}\alpha_u = 6.52 \times 10^{-1}$; $\alpha_\ell = 3.03 \times 10^{-5}$; $\frac{2}{E}\alpha_\ell = 6.06 \times 10^{-2}$

r	u^2	$V-V(\frac{r_o}{2})$	$\frac{V-V(\ )}{u^2}$	$\frac{2}{E}[V-V(\ )]$	$1-\frac{2}{E}[\ ]$	p^2u^2	R	$\frac{2}{E}\alpha_u u^2$	$1-\frac{2}{E}..$	R_u	$\frac{2}{E}\alpha_\ell u^2$	$1-\frac{2}{E}..$	R_ℓ
9a/2	1.66	5.40×10^{-4}	3.26×10^{-4}	1.08	-8.00×10^{-2}	$\cong 0$	< 0	1.08	< 0	< 0			
5a	1.34	3.05×10^{-4}	2.28×10^{-4}	6.10×10^{-1}	$+3.90\times10^{-1}$		$+3.90\times10^{-1}$	8.75×10^{-1}	1.25×10^{-1}	1.25×10^{-1}	8.12×10^{-2}	9.19×10^{-1}	9.19×10^{-1}
11a/2	1.12	1.71×10^{-4}	1.53×10^{-4}	3.42×10^{-1}	6.58×10^{-1}		6.58×10^{-1}	7.30×10^{-1}	2.70×10^{-1}	2.70×10^{-1}	6.80×10^{-2}	9.32×10^{-1}	9.32×10^{-1}
6a	9.40×10^{-1}	9.10×10^{-5}	9.70×10^{-5}	1.82×10^{-1}	8.18×10^{-1}		8.18×10^{-1}	6.13×10^{-1}	3.87×10^{-1}	3.87×10^{-1}	5.70×10^{-2}	9.43×10^{-1}	9.43×10^{-1}
13a/2	8.00×10^{-1}	4.42×10^{-5}	5.53×10^{-5}	8.84×10^{-2}	9.12×10^{-1}		9.12×10^{-1}	5.22×10^{-1}	4.78×10^{-1}	4.78×10^{-1}	4.85×10^{-2}	9.52×10^{-1}	9.52×10^{-1}
7a	6.90×10^{-1}	1.66×10^{-5}	2.41×10^{-5}	3.32×10^{-3}	9.97×10^{-1}		9.97×10^{-1}	4.50×10^{-1}	5.50×10^{-1}	5.50×10^{-1}	4.18×10^{-2}	9.58×10^{-1}	9.58×10^{-1}
15a/2	6.00×10^{-1}	0	0	0	1.00		1.00	3.92×10^{-1}	6.08×10^{-1}	6.08×10^{-1}	3.64×10^{-2}	9.64×10^{-1}	9.64×10^{-1}

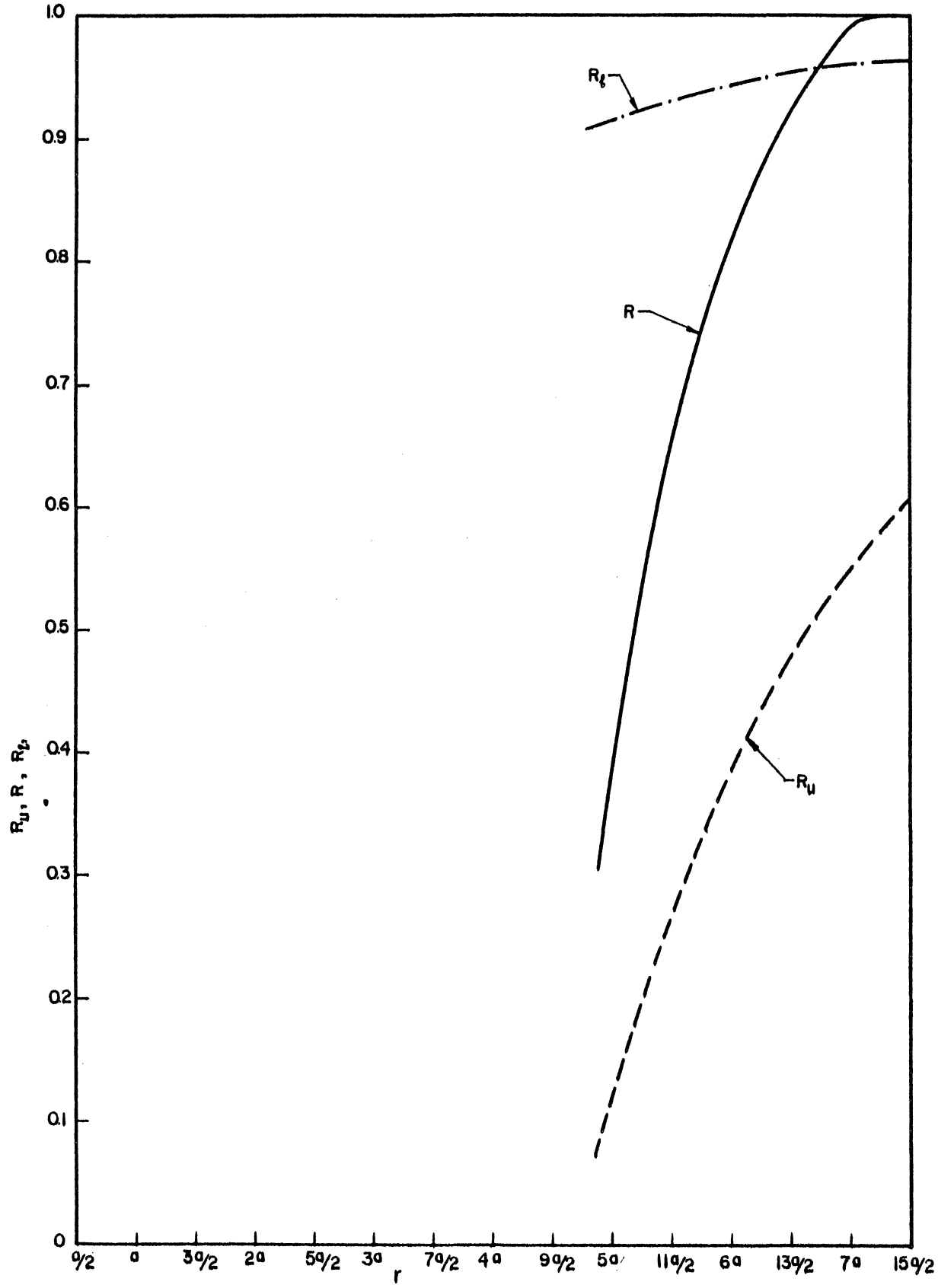

Diagram 6. $R(r)$, $R_u(r)$, $R_\ell(r)$. r Expressed in Fractions of Screening Distance a. E = 10^{-3} Mev, p = a/100.

TABLE VII. $E = 10^{-4}$ Mev; $p = a/100$

$p^2 = 2.98 \times 10^{-6}$ Å^2; $\alpha_u = 6.00 \times 10^{-5}$;

$\alpha_u = 1.20$; $\frac{2}{E}\alpha = 10^{-5}$; $\frac{2}{E}\alpha_\ell = 2.00 \times 10^{-1}$

r	u^2	$V-V(\frac{r_o}{2})$	$\frac{V-V(\ )}{u^2}$	$\frac{2}{E}[V-V(\ )]$	$1 - \frac{2}{E}[\ ]$	p^2u^2	R	$\frac{2}{E}\alpha_u u^2$	$1 - \frac{2}{E}..$	R_u	$\frac{2}{E}\alpha_\ell \cdot 2$	$1 - \frac{2}{E}..$	R_ℓ
6a	9.40×10^{-1}	9.10×10^{-5}	9.70×10^{-5}	1.82	$0.82 + 5.16\times10^{-1}$	$\cong 0$	$0.82 + 5.16\times10^{-1}$	1.13	$0.13 + 4.00\times10^{-2}$	$0.13 + 4.00\times10^{-2}$	1.60×10^{-1}	8.40×10^{-1}	8.40×10^{-1}
13a/2	8.00×10^{-1}	4.42×10^{-5}	5.53×10^{-5}	4.84×10^{-1}	9.67×10^{-1}		9.67×10^{-1}	8.28×10^{-1}	1.72×10^{-1}	1.72×10^{-1}	1.38×10^{-1}	8.62×10^{-1}	8.62×10^{-1}
7a	6.90×10^{-1}	1.66×10^{-5}	2.41×10^{-5}	3.32×10^{-2}	1		1.00	7.20×10^{-1}	2.80×10^{-1}	2.80×10^{-1}	1.20×10^{-1}	8.80×10^{-1}	8.80×10^{-1}
15a/2	6.00×10^{-1}	0	0	0									

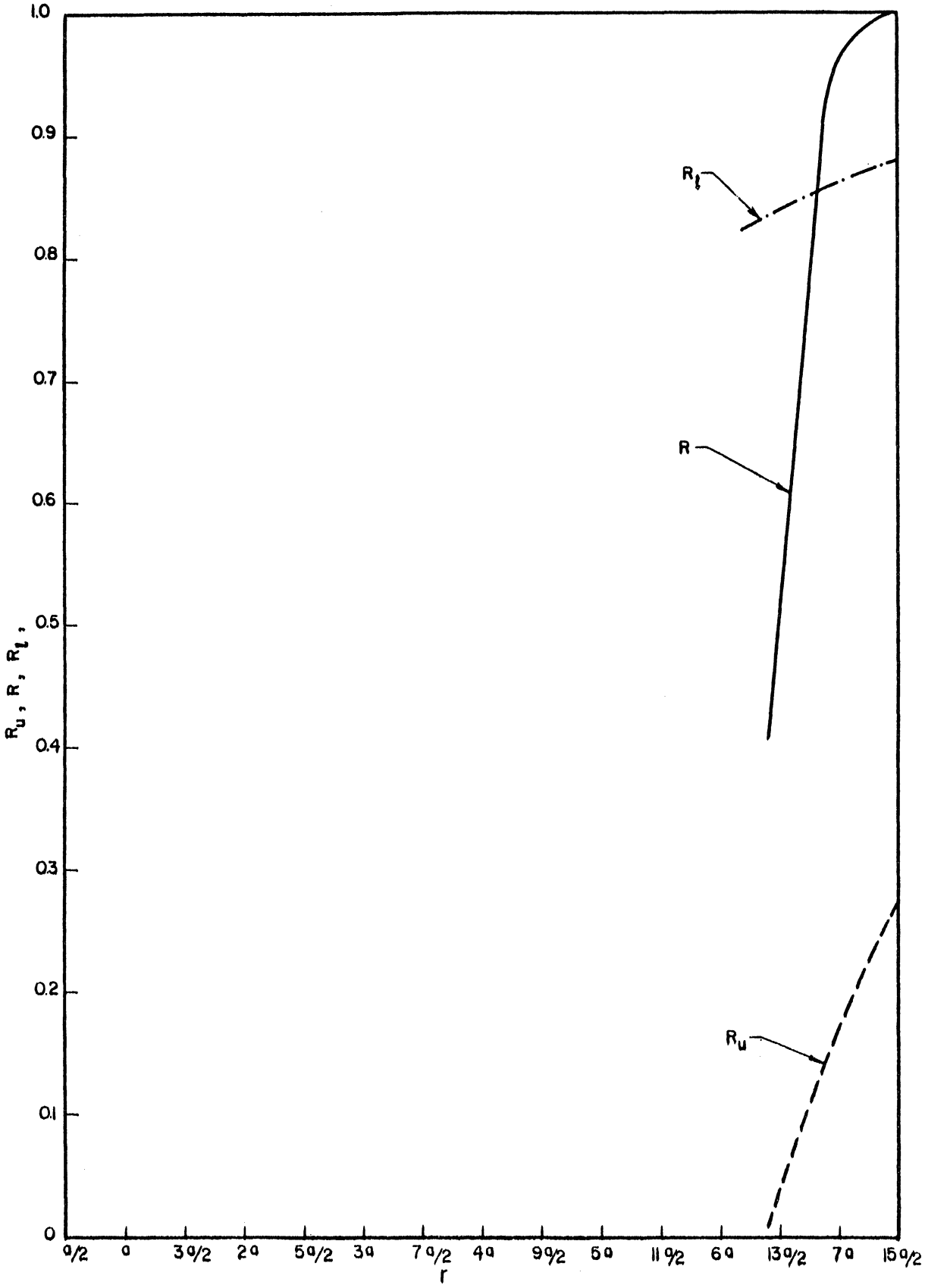

Diagram 7. $R(r)$, $R_u(r)$, $R_\ell(r)$. r Expressed in Fractions of Screening Distance a. $E = 10^{-4}$ Mev, $p = a/100$.

TABLE VIII. $E = 25$ ev; $p = a/100$

$p^2 = 2.98 \times 10^{-6}$ Å^2; $\alpha_u = 1.90 \times 10^{-5}$; $\frac{2}{E}\alpha_u = 1.52$

r	u^2	$V-V(\frac{r_o}{2})$	$\frac{V-V(\ )}{u^2}$	$\frac{2}{E}[V-V(\ )]$	$1 - \frac{2}{E}[\ ]$	p^2u^2	R	$\frac{2}{E}\alpha_u u^2$	$1 - \frac{2}{E}..$	R_u
7a	6.90×10^{-1}	1.66×10^{-5}	2.41×10^{-5}	1.33	-0.33	$\simeq 0$	< 0	1.05	-5.00×10^{-2}	< 0
15a/2	6.0×10^{-1}	0	0	0	0		1	9.5×10^{-1}	$+5.00\times10^{-2}$	5×10^{-2}

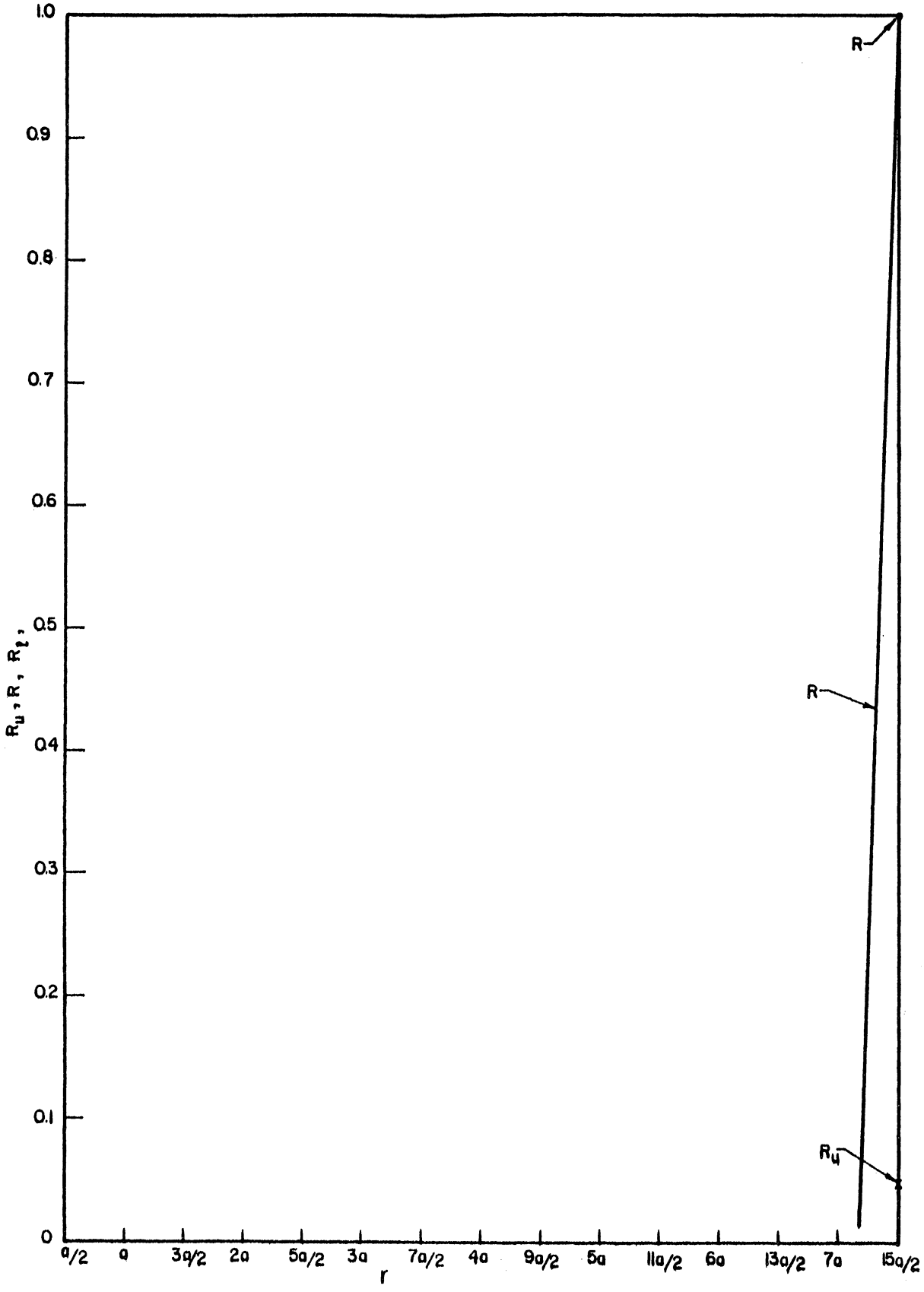

Diagram 8. R and R_u for E = 25 ev; p = a/100.

Diagrams 2 through 8 show the variations of $R(u)$, $R_u(u)$, $R_l(u)$, for the same energies and $p = a/100$ (also $p = a$ for $E = 10^{-1}$ Mev). The approximation $V - V(r_o/2) \cong \alpha_u u^2$ is very good at high energy (10^{-1} and 10^{-2} Mev), acceptable at medium energy (10^{-3} Mev), and mediocre at low energy (10^{-4} Mev). But, in any case, lower and upper limits for σ_d and λ_d are obtained from the relations (22).

The results for the values of α are summarized in the following Table.

TABLE IX

E	$\alpha_u(E)$	$\frac{2}{E}\alpha_u(E)$	$\alpha_l(E)$	$\frac{2}{E}\alpha_l(E)$
25 ev	1.90×10^{-5}	1.52		
10^{-4} Mev	6.00×10^{-5}	1.20	10^{-5}	2.00×10^{-1}
10^{-3} Mev	3.26×10^{-4}	6.52×10^{-1}	3.03×10^{-5}	6.06×10^{-2}
5×10^{-3} Mev	7.75×10^{-4}	3.10×10^{-1}	1.53×10^{-4}	6.12×10^{-2}
10^{-2} Mev	9.60×10^{-4}	1.92×10^{-1}	2.28×10^{-4}	4.56×10^{-2}
10^{-1} Mev	1.15×10^{-3}	2.30×10^{-2}	6.00×10^{-4}	1.20×10^{-2}

It must be noted that, at very low energy, close to 25 ev, the moving atom cannot approach the stationary one closer than about $r_o/2$, since from Table I, $V(r) = 2.46 \times 10^{-5}$ Mev for $r = 15a/2 \cong r_o/2$. Then, the approximation $V - V(r_o/2) \cong \alpha u^2$ is, of course, very poor and will overestimate the interaction, whatever the value of α selected.

5. Numerical Calculation of Knock-on Displacement Cross Section and Mean Free Path in Copper

The value φ_d of φ for displacement is obtained by

$$\varphi_d = 2 \sin^{-1} \sqrt{E_d/E} \quad ,$$

with $E_d = 25$ ev.

From this

$$(p_d)^2_{u,\ell} = (2/E)\,\alpha_{u,\ell}\,(1-\varphi_d/\pi)^2/[1-(1-\varphi_d/\pi)^2]\ ,$$

$$(\sigma_d)_{u,\ell} = \pi\,(p_d)^2_{u,\ell}\ ,\quad (\Sigma_d)_{u,\ell} = N\,(\sigma_d)_{u,\ell}\ ,$$

with $N = 8.5 \times 10^{22}$ atom cm^{-3} for copper.

Finally

$$(\lambda_d)_{u,\ell} = 1/(\Sigma_d)_{u,\ell}\ .$$

This is done for $E = 10^{-1}$, 10^{-2}, 5×10^{-3}, 10^{-3} and 10^{-4} Mev.

For E 25 ev, $\varphi_d = \pi$ and

$$(\sigma_d)_{u,\ell} = (\Sigma_d)_{u,\ell} = \sigma_d = \Sigma_d = 0\ ,$$

naturally.

The numerical details are carried out in Appendix XII. The results are as follows.

TABLE X

E	$(p_d)_u$	$(p_d)_\ell$	$(\lambda_d)_u$	$(\lambda_d)_\ell$
10^{-4} Mev	0.384 r_o	0.157 r_o	1.510 r_o	9.060 r_o
10^{-3} Mev	0.653 r_o	0.199 r_o	0.525 r_o	5.620 r_o
5×10^{-3} Mev	0.691 r_o	0.308 r_o	0.465 r_o	2.350 r_o
10^{-2} Mev	0.675 r_o	0.329 r_o	0.502 r_o	2.110 r_o
10^{-1} Mev	0.415 r_o	0.300 r_o	1.290 r_o	2.510 r_o

Diagrams 9 and 10 illustrate the situation.

It is seen that, in the region roughly limited by the energies 2.5×10^{-4} and 5.6×10^{-2} Mev, the problem may be one of many body collision, since in this region.

$$(\lambda_d)_u < r_o \qquad \text{and } (p_d)_u > r_o/2$$

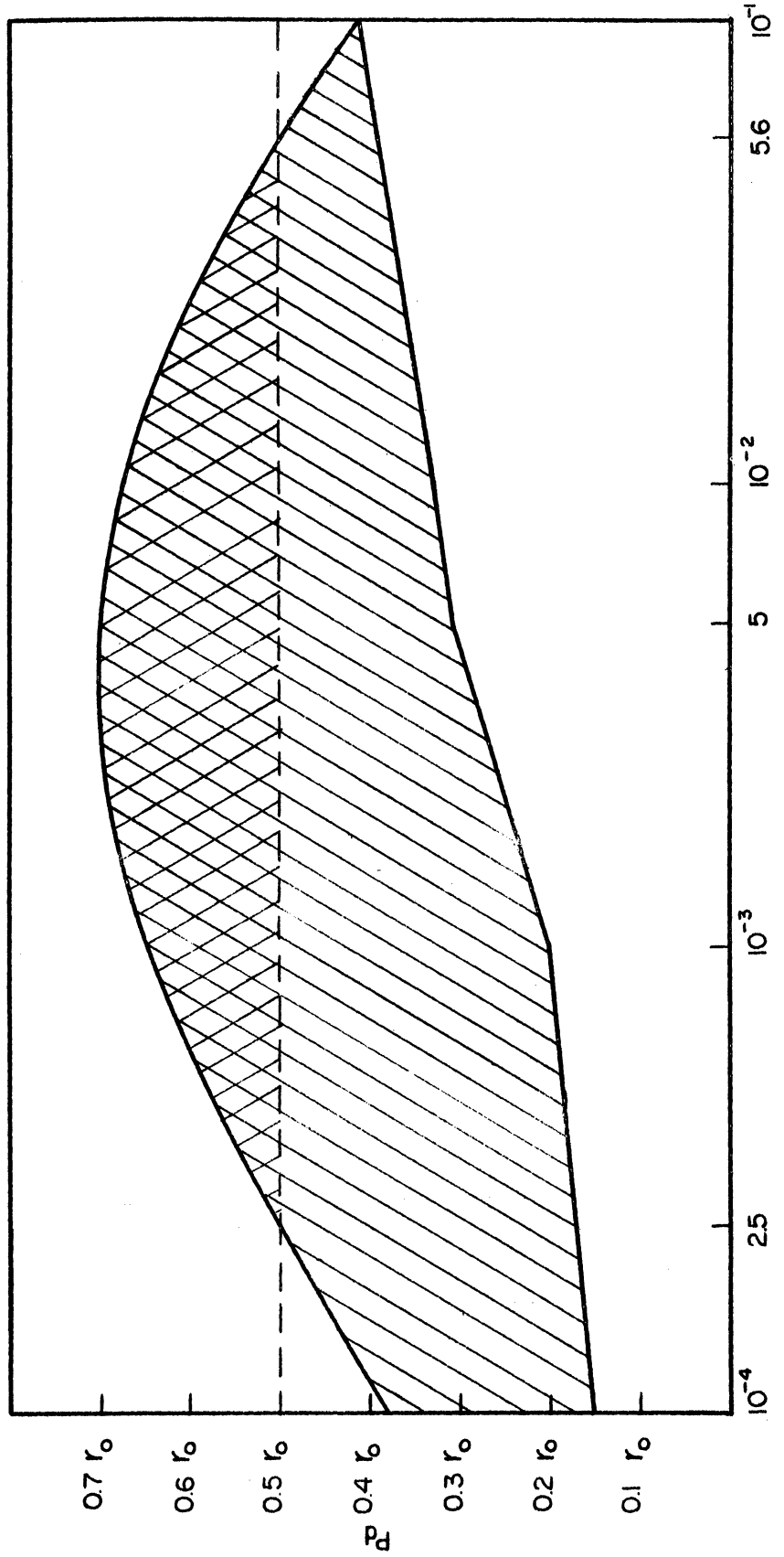

Diagram 9. Limits of p_d ///// and Possible Region of Many Body Collision XXXXX.

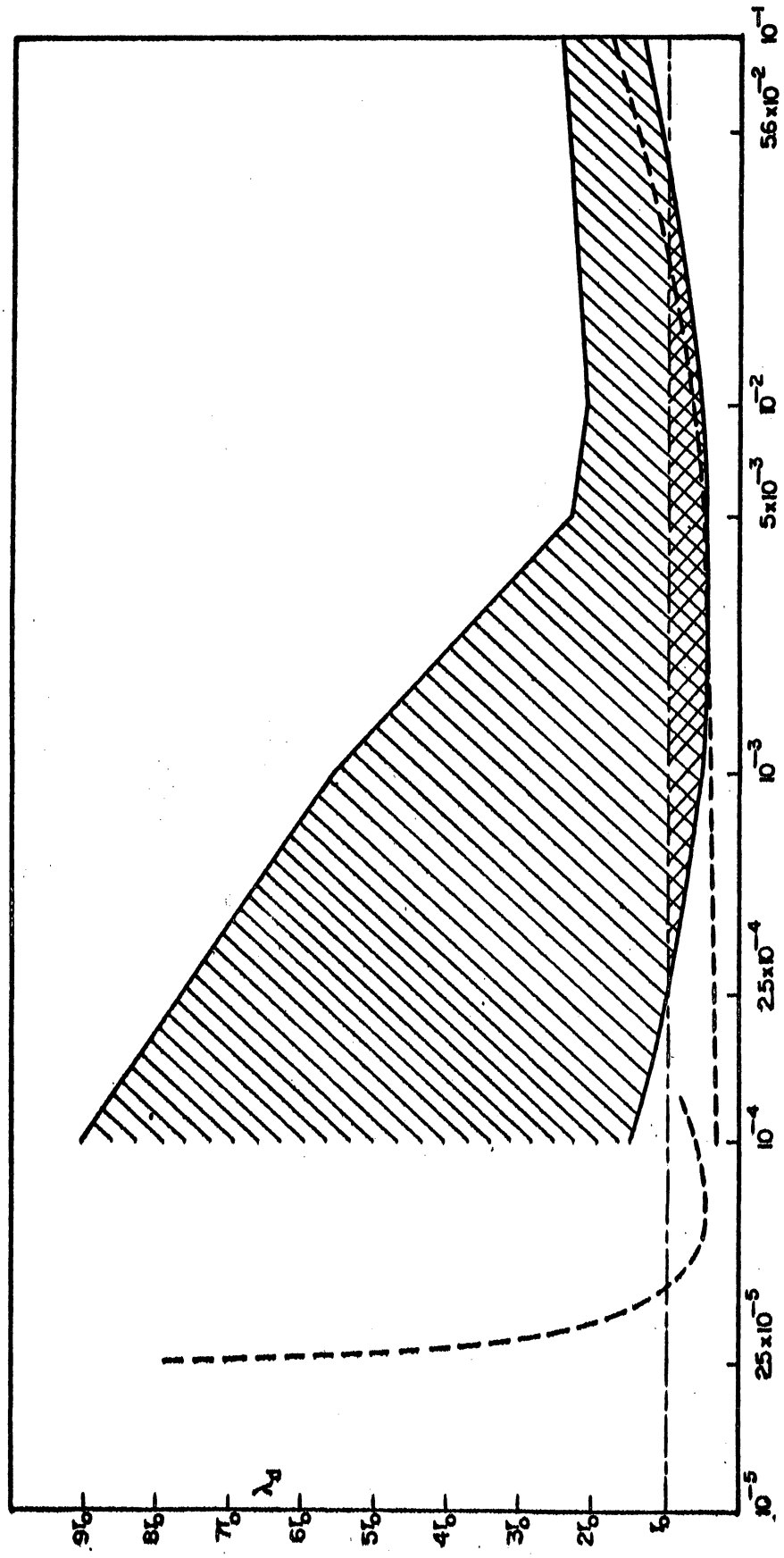

Diagram 10. Limits of λ_d //////. Possible Region of Many Body Collision XXXXX. Brinkman Estimate of λ_d ----;all for Cu.

However, the approximations made to obtain $(p_d)_u$ and $(\lambda_d)_u$ have been shown to be mainly good at high energies, specially at 10^{-1} Mev. We can then expect that $(p_d)_u$ is actually too large and $(\lambda_d)_u$ actually too small at smaller energies and the the two body approximation is a meaningful one over the whole range of energy. This justifies the two body treatment.

The above results will now be discussed by comparing them to those of the most recent existing theory of atomic displacement, namely Brinkman theory of displacement spikes.

CHAPTER IV

DISCUSSION OF MODEL. COMPARISON WITH BRINKMAN THEORY

1. Brinkman Theory

Brinkman[2] has treated the problem of atomic displacements by using an interaction potential energy between two identical atoms of the form (5). How this formula is obtained from two rigid distributions of charge with potential

$$\frac{Z\varepsilon}{r}\exp\left(-\frac{r}{a}\right)$$

is shown in Appendix XIII. Brinkman uses an impulse approximation, similar to the original Bohr approximation, for energies $E \gg E_d$. In Appendix XIV, it is shown that the use of such an approximation for an interaction of the form (5) yields an analytical expression for the displacement cross section, namely,

$$\sigma_d = \pi a^2 \left[F^{-1}\left(\frac{c^2 E E_d}{4 R_h^2 Z^{14/3}}\right)\right]^2 , \qquad (23)$$

where

$$a = c\, a_h\, Z^{-1/3} , \qquad (24)$$

a_h being Bohr radius of hydrogen, R_h Rydberg energy for hydrogen, c taken equal to 2.09, and F^{-1} the inverse of the function

$$F(x) = \left[K_1(x) - \frac{x}{2} K_0(x)\right]^2 , \qquad (25)$$

K_n denoting the modified Bessel function of the second kind of order n.

For E of the order of E_d, Brinkman notices that the absolute value of (5) for the asymptotic case where $r \gg a$, namely,

$$V(r) = \frac{Z^2\varepsilon^2}{2a} \exp\left(-\frac{r}{a}\right) \quad , \tag{24a}$$

gives an approximate representation of the interaction. It is of the Born-Mayer type

$$V(r) = A \exp(-Br) \quad , \tag{25a}$$

representing closed shell repulsion at distances of the order of 7a, A and B being chosen to fit compressibility data. Numerical values from (25a) agree well with values obtained from (24a). He assumes hard scatter for E of the order of E_d, which yields

$$\sigma_d = \pi b^2 \left(1 - \frac{E_d}{E}\right)$$

with b, minimum value of r, determined by

$$V(b) = \frac{Z^2\varepsilon^2}{2a} \exp\left(-\frac{b}{a}\right) = E$$

The resulting variations of λ_d versus E are shown in Diagram 10, where they are compared to $(\lambda_d)_u$. It is seen that Brinkman values almost coincide with the values of $(\lambda_d)_u$ for $10^{-3} \leqslant E \leqslant 10^{-1}$ Mev. On the contrary Brinkman value is much smaller that $(\lambda_d)_u$ at 10^{-4} Mev. The two portions of the curve λ_d vs E do not exactly join, due to the fact that two different potentials have been used: (5) at high energy and (5) changed sign at low energy, hence a discontinuity has been introduced.

Brinkman calls "transition energy", E_{tr}, the energy for which, while the knock-on slows down, its displacement mean free path becomes approximately equal to r_o. He proposes that, for $E > E_{tr}$, the displacement

cross section being comparatively small, the knock-on mainly loses its energy in setting stationary atoms into vibration, i.e. in furnishing the lattice thermal energy. Frenkel defects formed in this energy region should be enough spaced to remain stable. He calls the disordering effect along the corresponding path of the knock-on, a "thermal spike". For $E < E_{tr}$, Brinkman sees the displacement process as an intensive, localized one: the displacement cross section is comparatively large and practically all atoms of the region affected are displaced. He calls such a region a "displacement spike". However, since high temperatures are attained in a displacement spike, and since they endure long enough for appreciable relaxation to take place, it is postulated that most Frenkel defects do not persist in such a region, the damage being speculated to consist mainly, for example, of dislocation loops. In addition, it is recognized that the relaxation of Frenkel pairs may progress only until the fraction of interstitials is decreased to the order of 10^{-3}, the remaining defects, with large separation, becoming "frozen in" as the displacement spike cools off.

Brinkman theory does not attempt to furnish a quantative estimate of the number of stable interstitials remaining after irradiation. Furthermore, it postulates such defects as dislocations, whose effects on physical properties are unpredictable quantitively. Therefore, it cannot be tested against experimental results. However, although this has not been done in the literature, it can furnish reasonable qualitative explanation of some experimental results. This will be discussed now.

First, consider the case of the low temperature cyclotron irradiation of copper by 12 Mev deuterons.(8) Since E_{tr} is about 2.3×10^4 ev for copper(2) and since the maximum energy transfered by a 12 Mev deuteron to a copper atom in an elastic, center of mass isotropic collision, is about 1.5 Mev, it follows that, according to Brinkman views, knock-ons with energies between 1.5×10^6 and 2.3×10^4 ev will create atomic vibrations and Frenkel pairs and those with energy below 2.3×10^4 will induce displacement spikes. A typical value of the heat of fusion for a metal, at atmospheric pressure, is 0.1 to 0.2 ev per atoms. Assuming that the melting point is raised because the displacement spike is held at high pressure by the surrounding lattice, we accept a value of the order of 0.5 ev in our case.

Finally, taking into account heat losses to the unmelted lattice, we could expect that about 1 ev is needed to melt one atom of the lattice in the spike. All the atoms of the spike are assumed melted, hence the number of atoms in a displacement spike starting at energy E_{tr} is of the order $E_{tr}/1$, which, for copper gives about 2×10^4 atoms. With the figure, advanced above, of a fraction of 10^{-3} of these atoms remaining in interstitial positions, we find that there would be

$$2 \times 10^4 \times 10^{-3} = 20$$

Frenkel pairs per displacement spike starting at E_{tr}.

It has been shown in a previous paper (Preliminary Study(1)), that the differential scattering cross section for Rutherford collision between a charged particle and an atom may be placed in the form

$$\sigma(E', E)\, dE = \frac{\pi b_0^2}{4} E_m \frac{dE}{E^2} \qquad 0 \leq E \leq E_m,$$
$$= 0 \qquad \text{otherwise,}$$

where E' is the energy of the bombarding particle, E the energy of the atom after collision, E_m its maximum (i.e. a function of E'), and b_o the distance of closest approach between atom and particle. If we admit that, in the range 1.5 Mev - 2.3×10^4 ev, the Snyder - Neufeld model[3] describes sufficiently well collisions between knock-ons and stationary atoms, we are led to accept a number of displacements per primary knock-on given by

$$\nu(x_1) = 0.561\,(1 + x_1)$$

for $x_1 \gg 1$, where $x_1 = (E - E_d)/E_d$.

If we also admit that all progeny knock-ons of a primary with energy in this range do not appreciably participate in displacement spikes, we can write for average of ν for these primaries

$$\bar{\nu} = \frac{\int_{x_{1tr}}^{x_{1m}} \nu(x_1)\, G(E',E)\, dE}{\int_{0}^{x_{1m}} G(E',E)\, dE} \quad ,$$

where

$$x_{1m} = \frac{1.5 \times 10^6 - E_d}{E_d} \quad \text{and} \quad x_{1tr} = \frac{2.3 \times 10^4 - E_d}{E_d} \, .$$

This yields (see Appendix XV) $\bar{\nu} = 2.34$

All knock-ons with initial energy $E < E_{tr}$ only create displacement spikes, the number of atoms per spike being of order E ev. Hence the total number of atoms remaining interstitial in displacement spikes, per primary knock-on, is

$$\nu_1 = \frac{20 \int_{E_{tr}}^{E_m} G(E',E)\,dE}{\int_{E_d}^{E_m} G(E',E)\,dE} + 10^{-3} \frac{\int_{E_d}^{E_{tr}} E\, G(E',E)\,dE}{\int_{E_d}^{E_m} G(E',E)\,dE} ,$$

where the first term is term is the contribution of the primaries with initial energy greater than E_{tr}, the second one that of the primaries with initial energy smaller than E_{tr}.

Hence

$$\nu_1 = \frac{20(1/E_{tr} - 1/E_m)}{1/E_d - 1/E_m} + 10^{-3} \frac{\mathrm{Ln}\,(E_{tr}/E_d)}{1/E_d - 1/E_m} .$$

The numerical calculation is carried out in Appendix XVI.

The result is

$$\nu_1 \cong 1.9 \times 10^{-1} ,$$

so that the total number of surviving Frenkel pairs is, per primary knock-on

$$\bar{\nu} + \nu_1 = 2.34 \times 0.19 = 2.53 .$$

Now if the Snyder and Neufeld model is assumed over the whole range of energy, the average value of $\bar{\nu}$ is

$$\bar{\nu} = \frac{\int_0^{x_{1m}} \nu(x_1)\, G(E',E)\,dE}{\int_0^{x_{1m}} G(E',E)\,dE} = 0.561 \frac{\int_0^{x_{1m}} (1+x_1) \frac{dx_1}{(1+x_1)^2}}{\int_0^{x_{1m}} \frac{dx_1}{(1+x_1)^2}}$$

$$= 0.561 \frac{\mathrm{Ln}\,(1+x_{1m})}{1 - 1/(1+x_{1m})} = 0.561 \frac{1+x_{1m}}{x_{1m}} \mathrm{Ln}\,(1+x_{1m}) ,$$

i.e. with $\alpha_{1m} \cong 6 \times 10^4$,

$$\bar{\nu} \cong 0.561 \text{ Ln } 6 \times 10^4 = 6.16$$

Hence the fraction of Frenkel defects expected from Brinkman model would be 2.53/6.16 = 0.41 times the fraction calculated with the Snyder an Neufeld method. Using Jongenburger[4] value of 2.7 $\mu\Omega$ cm for the increase in electrical resistivity caused by 1% point defects in copper, it has been shown by Seitz and Koehler[9] that the Snyder and Neufeld method gives a result of change in resistivity by 12 Mev deuteron irradiation 6 times higher than the value obtained by replacing the experimental curve by its tangent at the origin, in order to account for radiation anneal. Hence, Brinkman model would give a numerical result closer to the actual change, about 2.4 times too high.

In the deuteron experiment[8] discussed, anneal was conducted after irradiation and, at 300°K, the fraction of initial change in resistivity still remaining was 8%. One may assume that this residual change is due widely spaced Frenkel pairs which have not annealed, i.e. presumably, the Frenkel pairs surviving the cooling off of displacement spikes. The remaining fraction of initial change expected from Brinkman model is then

$$\frac{\nu_1}{\bar{\nu}+\nu_1} = \frac{0.19}{2.53} = 7.5\ \%\ ,$$

which agrees well with the experimental result of 8%. Consider now the neutron irradiation of copper and aluminum at 80°K. Changes in electrical resistivity and in critical shear stress were followed during anneal after irradiation. It was found that, for copper, the increase in electrical

resistivity anneals in two stages: between -80 and +20°C (2/3 of initial $\Delta\rho$) and between 300 and 350°C, while the increase in critical shear stress is removed only at the stage between 300 and 350°C. In aluminum, increase in electrical resistivity and increase in critical shear stress both anneal in a single stage at -60°C. Brinkman model furnishes an acceptable qualitative explanation for these results. In copper, most of the stable (at irradiation temperature) Frenkel pairs are produced by knock-ons in their high energy range (corresponding to the $\bar{\nu}$ calculated above in the case of deuteron irradiation), a lesser fraction are produced in displacement spikes (ν_1), these are assumed to be more separated than the former ones. In addition, dislocation loops are presumably formed in displacement spikes. Anneal is then seen to proceed in the following way. During the low temperature annealing stage (-80; +20°C) the high energy range Frenkel pairs ($\bar{\nu}$), less separated, anneal out. Since, conceivably, in this case also $\bar{\nu} > \nu_1$, it is quite understandable that 2/3 of the initial increase in electrical resistivity may be recovered in this stage. During the high temperature annealing stage (300; 350°C), the displacement spike Frenkel pairs (ν_1) recombine and the dislocation loops they pinned down until then anneal out. Hence the residual increase in electrical resistivity and the whole increase in critical shear stress (presumably mainly due to the dislocations) are recovered in this stage. In aluminum, E_{tr} is very low, about 1200 ev, so that the displacement spikes contain at the most (see above) of the order of 1200 atoms. Practically all defect pairs are high energy range ones,

they anneal at low temperature (-60°C) in a single process and, with them, the small dislocation loops corresponding to the small displacement spikes created.

Despite the apparent quantitative agreement with experiment shown above in the case of the residual increase in electrical resistivity at room temperature, it is clear that too many assumptions have been made, so that only relative significance can be attached to quantitative results obtained by such interpretations of Brinkman's model. First, the figure of 10^{-3} atoms remaining interstitial in a displacement spike was adopted arbitrarily, on the assumption that pairs in which the defects are separated by 10 r_o or more would survive and not recombine during the cooling off period of the spike. Secondly, the treatment given above is incorrect in that knock-ons produced in the high energy range must enter the spike range while slowing down, unless we admit that, energy transfer being small for fast primaries (which is not in accord with Snyder and Neufeld model), the secondaries only produce negligible spikes. Thirdly, the model used to treat the interaction of two atoms has weaknesses in several respects. The interaction potential energy used becomes negative (attractive potential) in a region where, physically, it must be positive (repulsion of the interacting atoms). This leads to adopting a discontinuity in energy transfer and displacement cross section. The energy transfered to the stationary atom is found to be (see Appendix XIV),

$$T = 4 \frac{Z^{14/3} R h}{c^2 E} F\left(\frac{b}{a}\right) ,$$

where Z is the common atomic number of the two atoms, R_h Rydberg energy for hydrogen, E the energy of the incoming knock-on, C the constant of formula (24) giving the screening distance a, and F the function defined by (25). The variations of F are shown by the full line in Figure 20. It is seen that T = 0 for $\ell = 2.4$ a, meaning that there is no interaction for an incoming knock-on with an impact parameter having the value 2.4 a. This is due to the fact that the potential used makes a transition from repulsive to attractive for $r = a(1 + \sqrt{3}) \simeq 2.73$ a, as explained earlier. Brinkman then "bridges the gap" between the two branches of F by the broken line shown in Figure 20. The impulse approximation itself, valid when collisions with small impact parameters or collisions between a fast massive particle and a much lighter one are considered, is certainly less correct when comparatively slow particles experience with particles of the same mass encounters where the impact parameter may be large (here, of the order of $r_o/2$) and, consequently, the path of interaction comparatively small. The use of such an approximation tends to overestimate the interaction and the displacement cross section, hence to underestimate the displacement mean free path. At high knock-on energy, this approximation is justifiable, in the case of copper, since as has been seen in discussing the Kepler problem, boundary conditions at infinity are acceptable and since, as will be seen later, the knock-on path is then closely a straight line. Finally, the value C = 2.09 of (24) used by Brinkman was a value used by Ozeroff[24] for a Thomas-Fermi atomic model. Seitz[9] considers it too high for this application and Bohr[25] adopted the value C = 1 to

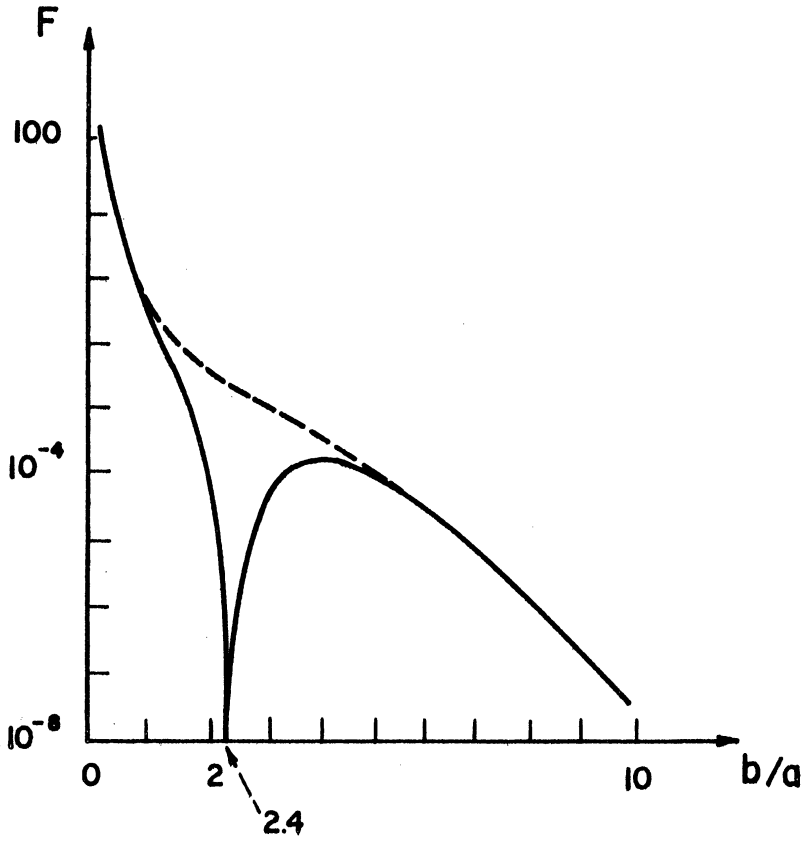

Figure 20. The Function F(b/a) .
Full Line: F .
Dotted Line: Bridging of Gap .

treat problems of atomic interactions. A value of 2.09 for C leads to a screening distance a about twice then the one used in this paper. The potential energy

$$V(r) = Z^2\varepsilon^2\left(\frac{1}{r} - \frac{1}{2a}\right)\exp\left(-\frac{r}{a}\right)$$

becomes larger, for all r, if a becomes larger. Hence, on this score also, it appears that Brinkman's treatment tends to overemphasize the interaction and the displacement cross section. The limiting values of displacement mean free path λ_d found in this paper are consistent with these observations, since the lower ones almost coincide or are larger than those of Brinkman. This is perhaps a good check for the model used.

One of the most important assets of Brinkman's work is to have shown that the displacement mean free path may become comparable to r_o and to have introduced the concept of "displacement spike", i.e. of a region of high disturbance.

2. Main Features of the Proposed Model Application to Deuteron Irradiation of Copper

The results of the calculations made using the proposed model (Diagram 10) show that there is also an energy region of the knock-ons for which the displacement mean free path is close to r_o. This region can be taken, for the case of copper considered, as extending from 10^5 ev (E_{tr1}) down to 10^3 ev (E_{tr2}). Any knock-on born with energy larger than E_{tr1} experiences first spaced displacing collisions in which it produces, a) secondary knock-ons with energy larger than E_{tr1}, b) secondary knock-ons with energy in the range $E_{tr1} - E_{tr2}$, and c) secondary knock-ons with

energy smaller than E_{tr2}. Group a) knock-ons have collisions of the type just under discussion until they reach energy E_{tr1}. Group b) knock-ons are in the displacement spike region; they and their progeny, while their energy is larger than E_{tr2}, move in a confined highly disturbed region. When their energy becomes smaller than E_{tr2} (but larger than E_d), they may move out of the highly disturbed region and, like Group c) knock-ons, they create point defects of various separations. The process through which the primary knock-on considered undergoes slowing down when its energy becomes smaller than E_{tr1}, then E_{tr2} is, of course, identical to that discussed above. In any case, defect pairs created with energy transfer of order 25 ev have small separation.

Hence, we see the displacement spike as a region in which perhaps a majority of the atoms have received substantial energy. The atoms remaining at their normal site may have received up to 25 ev, so the region may have melted. This region comprises vacancies corresponding to the departed atoms, i.e. those which have left the spike with energy between 10^3 and 25 ev. Those create defect pairs within and outside the spike and lodge themselves as interstitials or fill a vacancy at a distance from the spike's periphery which may be large, as will be seen shortly.

The whole pattern of the damage would then be as follows. Narrow regions with holes and possibly dislocations formed upon resolidification, with also Frenkel pairs of various separations, depending on the energy transfered during their formation. Around these regions,

Frenkel pairs with various separations and interstitials far away from their corresponding vacancies within the spike.

The process of knock-on collisions and diffusion through the lattice should perhaps be treated by stochastic methods and a Monte Carlo approach may be a profitable one. This is out of the scope of this paper, but an attempt will be made to picture a disturbed region and to find an order of magnitude of its size. In Appendix XVII, the average energy transfered in a displacing collision is calculated approximately, the collision being described by the cross section established earlier in this paper, namely,

$$2\pi p\,dp = \pi \frac{2\alpha}{E}\, d\, \frac{(1-\varphi_T/\pi)^2}{1-(1-\varphi_T/\pi)^2} = \pi \frac{2\alpha}{E}\, d\, \frac{\left(1-\frac{2}{\pi}\sin^{-1}\sqrt{\frac{T}{E}}\right)^2}{1-\left(1-\frac{2}{\pi}\sin^{-1}\sqrt{\frac{T}{E}}\right)^2} .$$

It is found that this average transfer is approximately

$$\overline{T} \cong \sqrt{E_d}\sqrt{E} = 5\sqrt{E} ,$$

E, in ev, being the energy of the colliding knock-on. The approximation underestimates $\overline{T}$ for $E \gg E_d$. It is not valid for $E \cong E_d$, for which values it seriously overestimates T.

Hence, a knock-on with energy $E = \left(\frac{100}{5}\right)^2 = 400$ ev will displace little. The secondaries of a knock-on with energy 10^6 ev will have, on the average, an energy smaller than 5×10^3 ev $= E_{tr2} = 10^3$ ev. Hence, most of them will not create displacement spikes, which shows that, perhaps, Brinkman's treatment gives too much importance to these chaotic regions.

Consider a fast primary knock-on with energy 10^6 ev, Figure 21, in copper. First, notice that the angles of scatter for transfer of $\bar{T}$ remain small down to E = 10^3 ev, so that we may consider the track as straight in the high energy region.

At E = 10^4 ev, $\bar{T}$ = 5 x 10^2 ev. To transfer this energy, the angle of scatter in the center of mass frame must be

$$\varphi = 2 \sin^{-1} \sqrt{\bar{T}/E} = 2 \sin^{-1} \sqrt{5 \times 10^{-2}} \cong 0.452 \text{ rad} \cong 26^\circ .$$

The angle of scatter in the laboratory system must be

$$\varphi_L = \varphi/2 \cong 13^\circ .$$

(see Appendix VIII, where φ is the angle of scatter in the laboratory frame, θ the angle of scatterin the center of mass frame.)

At E = 10^3 ev, $\bar{T}$ = 5 x 3.16 x 10 = 158 ev

$$\varphi = 2 \sin^{-1} \sqrt{0.158} \cong 0.801 \text{ rad} = 46^\circ ; \varphi_L = 23^\circ .$$

At E = 400 ev, $\bar{T}$ = 100 ev

$$\varphi = 2 \sin^{-1} 0.5 \cong 60^\circ ; \varphi_L = 30^\circ .$$

Let us reason on collisions in which the average energy is transfered.

Between 10^6 and 10^5 ev, the energy transfered is large enough so that either defect pairs with comparatively large separation are formed or the secondary knock-ons can form pairs with comparatively large separation (say several r_o). The displacement mean free path will be taken equal to 2 r_o in this energy region. The track is linear. An order of magnitude of its length can be gained by the following reasoning. In λ_d, the primary loses energy $5\sqrt{E}$, as a good approximation, since every other collision is a displacing collision.

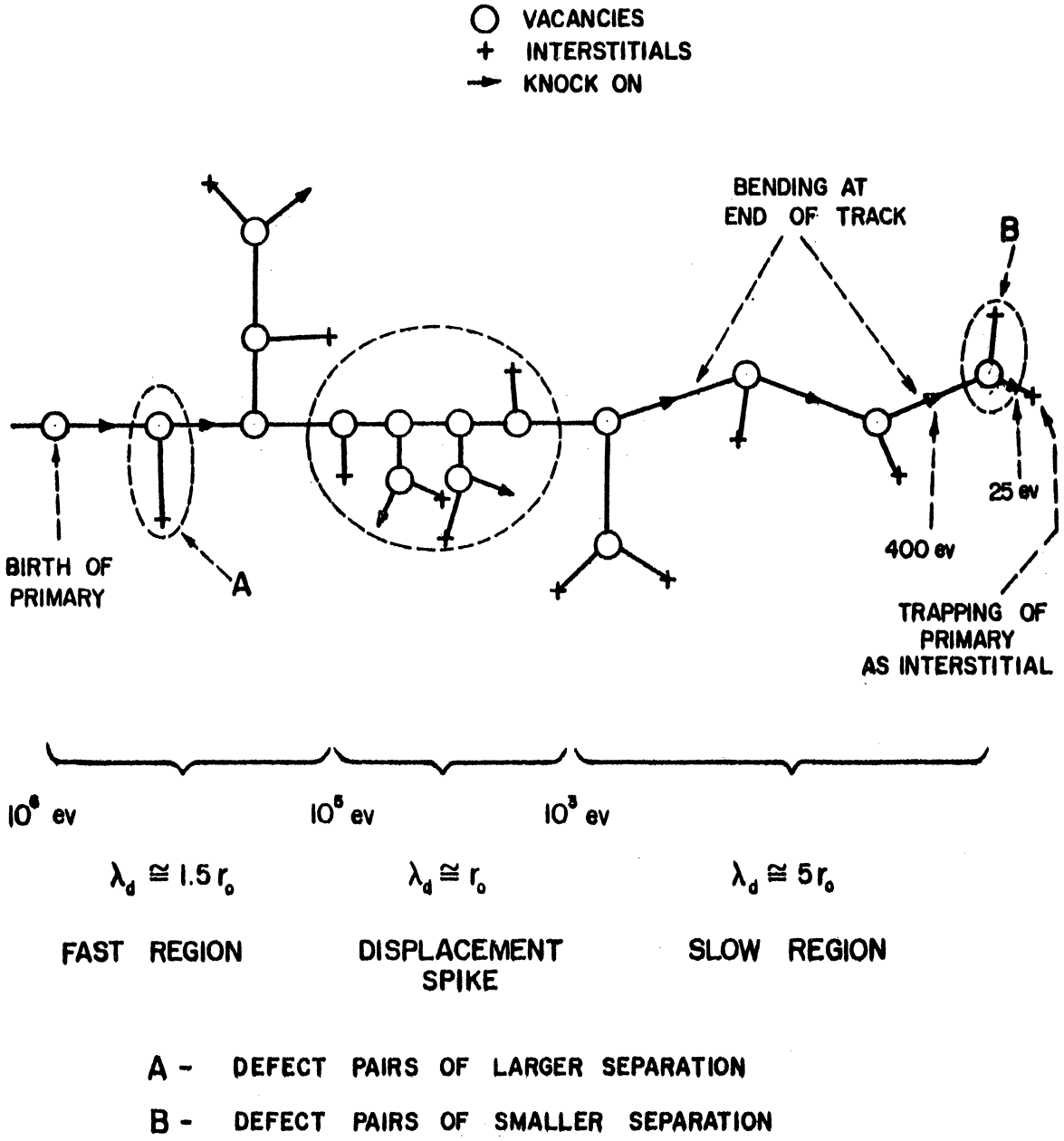

Figure 21. Track of an Energetic Primary Knock-On (1 Mev).

The loss per unit path is $5\sqrt{E}/\lambda_d$. Hence,

$$-dE(x) = (5/\lambda_d)\sqrt{E(x)}\,dx \quad .$$

And the track length between E = 10^6 ev and E = 10^5 ev is,

$$x_1 = (2\lambda_d/5)(10^3 - 3.16 \times 10^2) = 5.45 \times 10^2 r_o \quad .$$

Between 10^5 and 10^3 ev, the primary is in the displacement spike region, λ_d is about equal to r_o. Displacing collisions are close. The region is intensely disturbed around the track. Defect pairs formed by the primary or the secondaries may still have an appreciable separation. The track may still be considered linear. Its length in this region may be approximated to

$$x_2 = (2\,r_o/5)(3.16 \times 10^2 - 3.16 \times 10) = 114\,r_o \quad .$$

From 10^3 ev down to 400 ev, λ_d will be taken of order 5 r_o (Diagram 10). Displacing collisions are spaced. Secondaries have small energies. Defect pairs formed have small separation, of the order of r_o. They should recombine easily. The track is bent appreciably. From 400 ev to 25 ev, the primary practically does not displace any more. It may travel appreciably, before it is trapped when its energy reaches 25 ev. To obtain an estimate of the total crow flight of the primary, we take the total track length for the "linear" portion of the track, i.e.,

$$x_1 + x_2 \cong 6.6 \times 10^2\, r_o$$

With r_o = 2.556 Å, this gives, in copper, a range of 1.68×10^{-5} cm. This may appear high, but can be compared to an estimated range[22] of 4×10^{-4} cm for fission fragments of uranium in uranium and a range of 1.83×10^{-3} cm[26] for RaC' alpha-particles in copper. It is true that

fission fragments have an energy of about 160 Mev, but uranium has a high atomic number, so that the interaction should be strong, and, in addition, for fission fragments, ionization is important, due to the high value of the speed. RaC' alpha-particles have four energies between 7.6 and 10 Mev, about. Alpha-particles of this energy mainly ionize and lose energy fast. It may also be observed that the order of magnitude found for the range is compatible with the number of secondary knock-ons per primary knock-on. This may be seen as follows. The number of secondaries directly formed by the primary while it has energy between 1 Mev and 10^3 ev, would be

$$\frac{x_1}{(\lambda_d)_1} + \frac{x_2}{(\lambda_d)_2} = 545/2 + 114 = 330$$

The total number of secondaries produced as a result of collisions of the primary between 1 Mev and 10^3 ev is, using the Snyder and Neufeld method.

$$0.561\ (10^6/25 - 10^3/25) = 2.24 \times 10^4$$

So that, on the average, each secondary produced by a collision of the primary, would, in turn, produce about 70 secondaries, which is reasonable.

Finally, it is interesting to remark that the range of fission fragments has been experimentally found[32] to vary as the square root of the energy. The same energy dependence obtained, at high energy, for the range of a copper knock-on thus appears plausible. It should be noted that non-displacing collisions have not been taken into account, but this does not introduce large errors, since the average energy transfer is very small for such collisions.

If we use the approximation, found later in this paper, of a total number of displacements per primary given by

$$\nu(\alpha_1) = 0.5\ (1+\alpha_1),$$

where $\alpha_1 = E/E_d$, which should still have some validity at $E = 10^3$ ev, as will be seen later, we see that the number of defect pairs formed along the portion of the track of the primary corresponding to $E \leqslant 10^3$ ev should be about

$$0.5\ (1 + 40) \cong 20$$

Hence, we see a region disturbed by a fast primary knock-on (1 Mev) and its progeny as some sort of cylindrical portion of the sample, around the track of the primary. Pairs with large separation, but close to each other, are formed in the first and longer part of the disturbed region. Pairs with still appreciable separation, but very close to each other, are formed in the middle part, i.e. the displacement spike. Pairs with low separation and at appreciable distance (say, 5 r_o) away from each other are formed in the last part, at maximum distance from the point of birth of the primary. There should be about 20 pairs with small separation, located at distance of the order of 660 r_o from the point of birth of the primary.

We shall call this cylindrical disturbed region a "damage spike". It comprises the displacement spike in its middle. In Figure 21, it will be noted that the tracks of the secondaries have been drawn perpendicular to that of the primary. This is intentional, since, as observed in Chapter III, Section 4, and shown in Appendix VIII, two

particles of equal mass should leave from an elastic collision at 90 degrees from each other, in the laboratory frame.

Now, consider the case of the bombardment of copper by 12 Mev deuterons.(8) It is shown in Appendix XVIII that on the basis of the Snyder and Neufeld model(3), for an integrated flux of $\Phi = 7 \times 10^{16}$ deuts x cm^{-2}, the fraction of atoms becoming primary knock-ons being

$$\eta_{prim} = 4.90 \times 10^{-4},$$

the fraction of atoms displaced is

$$C \cong 3.04 \times 10^{-3}$$

and the average number of displacements per primary

$$\overline{\nu} \cong 6.16$$

These values agree rather well with experimental results, giving a change in resistivity about six times that found experimentally, if the value 2.7 $\mu\Omega$ cm of Jongenburger(4) is adopted for the change in resistivity due to C = 0.01.

On the grounds that a deviation of the same order is found between calculation and experiment for neutron irradiation and for changes in other properties under cyclotron irradiation, it may be presumed that the deviation is due an overestimate of $\overline{\nu}$ by the Snyder and Neufeld model. It will be shown in Chapter V, Section 2 that the overestimate is a fact, but its magnitude will not be found. We must consider possible, therefore, that most primaries may produce no secondaries in the case of irradiation under discussion.

It has been already mentioned that the energy transfer cross section between a charged particle and an atom may be placed in the form

$$\sigma(E',E)\,dE \sim \frac{dE}{E^2},$$

where E' is the charged (bombarding) particle energy, E the energy transferred to the atom hit. The frequency function, Figure 22, has therefore small values for E large, i.e. small energy transfers are favored. The average energy of a primary knock-on is

$$\bar{E} = \frac{\int_{E_d}^{E_m} E\,\sigma(E',E)\,dE}{\int_{E_d}^{E_m} \sigma(E',E)\,dE} = \frac{\ln(E_m/E_d)}{\frac{1}{E_d} - \frac{1}{E_m}} \cong E_d \ln \frac{E_m}{E_d},$$

E_m being the maximum energy transferred to an atom (in an elastic collision). For $E_m = 1.5 \times 10^6$ ev, corresponding to 12 Mev deuterons in copper, this gives

$$\bar{E} = 275 \text{ ev}$$

We recall now the remark, made earlier, that in most instances, a knock-on with energy smaller than 400 ev will not displace atoms. This is in keeping with the observation that most primaries may not produce secondaries in the case at hand. However, some primaries will have enough energy to displace atoms, but the secondary pairs formed will have small separation. The number of such pairs is impossible to obtain. In the low energy region, we may take $\lambda_d = 5\ r_o$, so that the small separation pairs will be formed, on the average, at distance $5\ r_o$ from the point of birth of the primary.

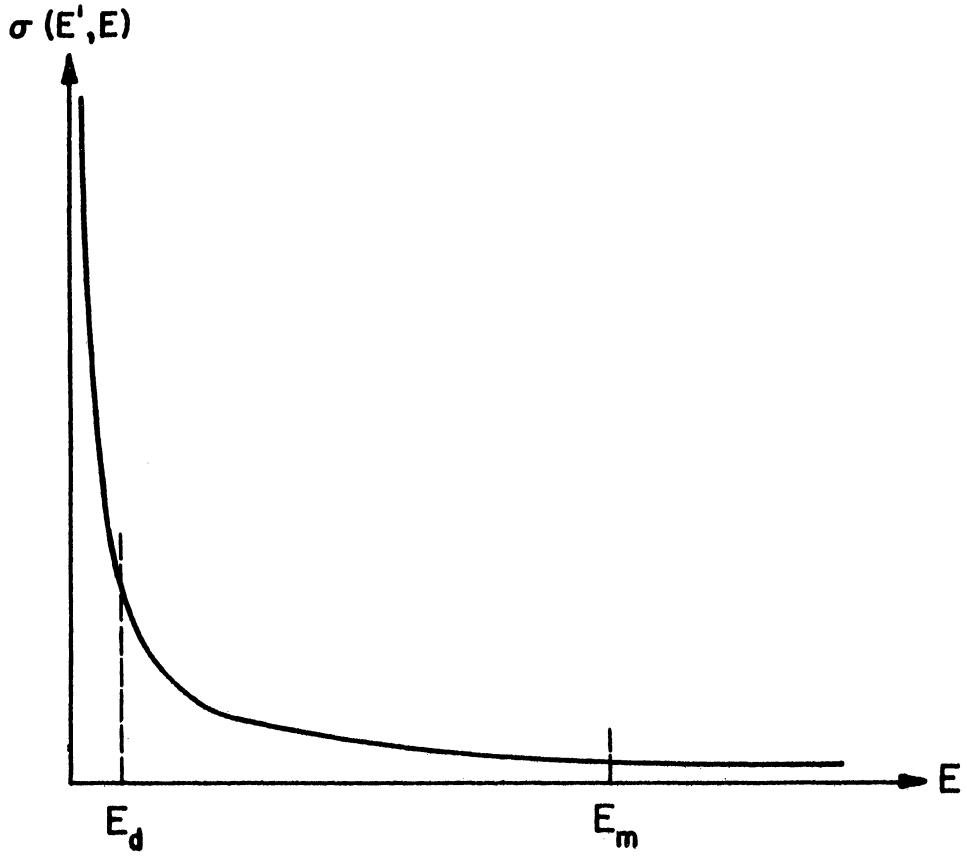

Figure 22. Frequency Function σ(E', E) of the Cross Section for Energy Transfer by Charged Particles.

Let us divide the sample in equal spherical cells centered at the point of birth of each primary. At one fourth full irradiation, i.e. $\Phi \cong 1.75 \times 10^{16}$ deuts x cm^{-2}, there are

$$Nn_{prim} = (4.90/4) \times 10^{-4} N$$

such cells, N being the number of atoms in the sample. The atomic radius is $r_o/2$. The radius a of each cell is given by

$$(1/4) \times 4.90 \times 10^{-4} \times Na^3 = N(r_o/2)^3$$

i.e., $$a \cong 10\ r_o$$

Imagine, Figure 23, that in cell 1, corresponding to primary 1, or generation 1, there is the primary vacancy, point of birth of the primary, the primary as interstitial, and a small separation pair A, at distance 5 r_o from the point of birth. In cell 2, of generation 2, take only a primary pair. The knock-on B, before becoming interstitial, causes a thermal perturbation, or "thermal spike" which may be felt by the pair A with enough strength to cause its recombination. Assume a spherical thermal spike, originated at the center of cell 2, with the release of 275 ev. Take 20 r_o for radius of the spike, which then would comprise the pair A. There would be

$$(20\ r_o)^3/(r_o/2)^3 = 6.4 \times 10^4$$

atoms in the spike. If thermal equilibrium were attained, each atom would receive an energy

$$275/6.4 \times 10^4 \cong 4 \times 10^{-3} \text{ ev} = 6.4 \times 10^{-15} \text{ ergs},$$

corresponding to a temperature increase

$$T = 6.4 \times 10^{-15}/1.4 \times 10^{-16} = 46°K.$$

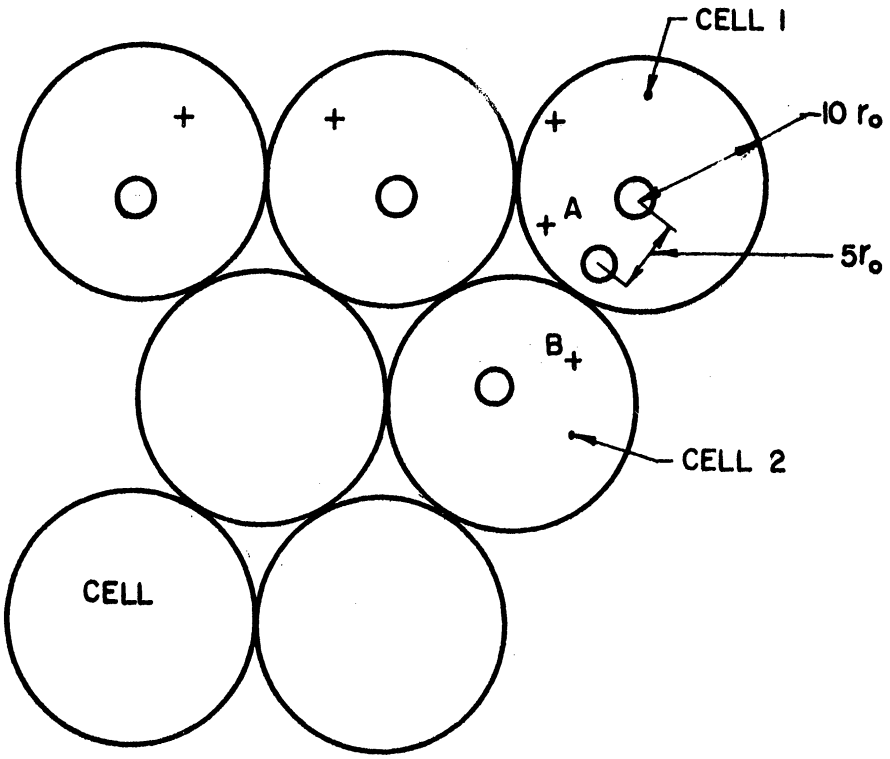

Figure 23. Illustrating the Possible Interaction of Defects of Different Generations in Charged Particle Irradiation.

It is found, experimentally, that an important thermal annealing occurs at 30°K, so that although the treatment is by no means rigorous, recombination of close pairs by thermal spikes due to knock-ons of later generations appears as a possibility.

It is clear that no displacement spikes will be formed in this particular case of irradiation, or is any expected, in general, for charged particle irradiation with the usual energies (say, smaller than 20 Mev).

Note, finally, that electrons displaced in cell 2, for example, by ionization may well transfer enough energy to the interstitial of the small separation pair A to force recombination of the pair.

3. A Possible Explanation of the Phenomenon of Radiation Anneal. Comparison of Charged Particle and Neutron Irradiation

First we describe the phenomenon of radiation anneal. For two experiments[7,8] made by bombarding thin foils and thin wires, respectively, by 12 Mev deuterons, the temperature was that of liquid nitrogen and liquid helium, respectively. The change $\Delta\rho$ in electrical resistivity was measured during irradiation. It was found (see Diagram 11) that the line $\Delta\rho$ versus Φ, integrated deuteron flux, is not straight, but possesses a downward curvature. Hence, some damage is recovered while irradiation progresses. This process is called "radiation anneal". The recovery is apparently not due to thermal anneal at the temperature of irradiation, at least for the lower temperature experiment, since the workers who performed this experiment report that the damage is stable when irradiation is turned off, but the low temperature maintained.

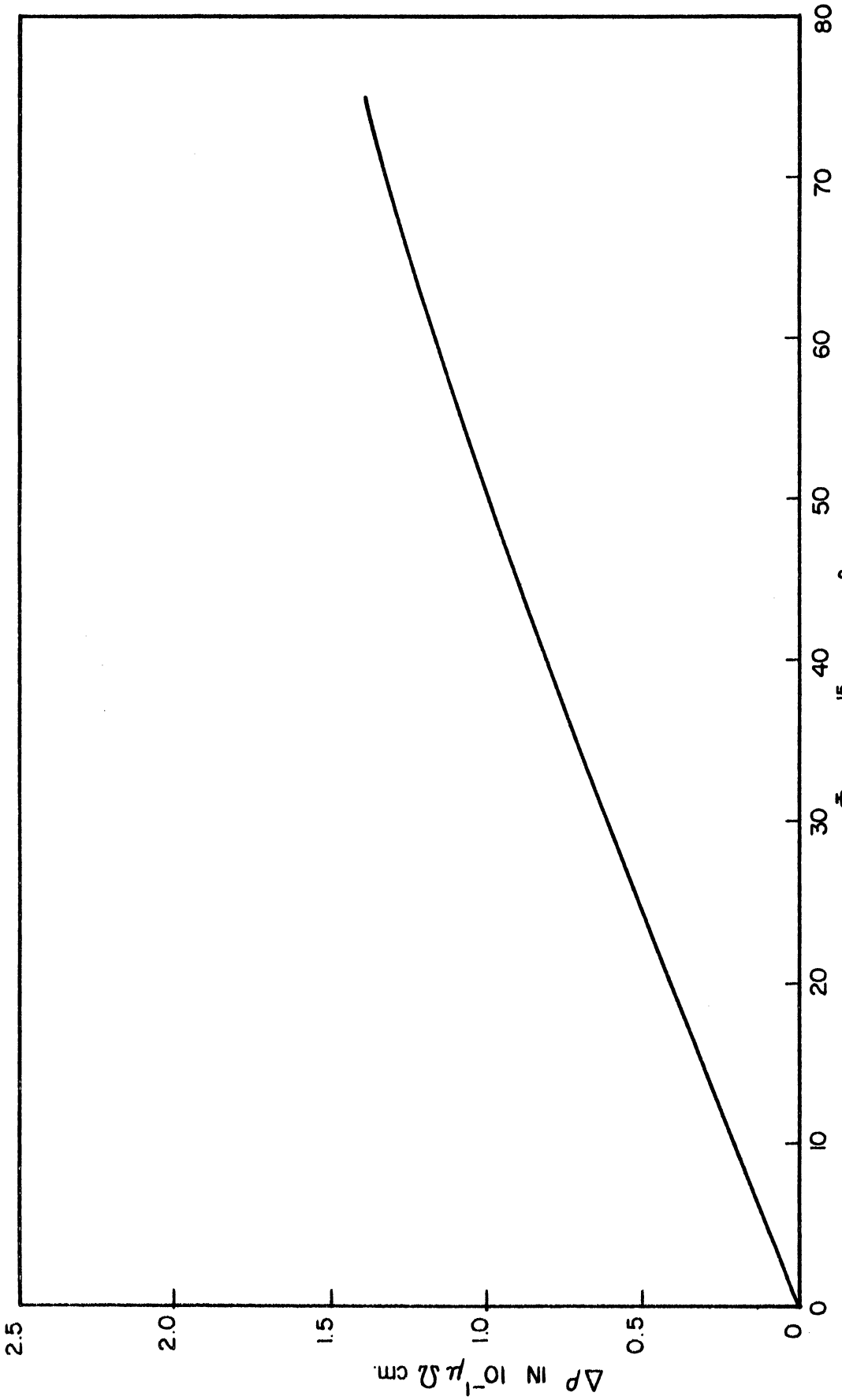

Diagram 11. Change Δρ in Electrical Resistivity Versus Integrated Flux Φ for Cyclotron Irradiation of Cu with 12 Mev Deuterons at Liquid He.

On the basis of what has been said at the end of the last Section, we see a possible explanation to the phenomenon, namely the interaction of new defects, in the form of thermal spikes or electrons, with defects already formed. Although, no strict proof can be given, the root of the argument is the smallness of the separation of the (few) secondary pairs and the closeness of the "disturbed regions". If this is correct, radiation annealing should be noticeable only after a minimum integrated flux has been attained. Although the experiment has been performed with great care by Cooper, Koehler and Marx[8] and eight experimental points have been obtained between $\Phi = 0$ and $\Phi = 20 \times 10^{15}$ deuts x cm^{-2}, it is doubtful that the slight curvature shown by the curve (given also by Seitz and Koehler[9]), for $\Phi < 20 \times 10^{15}$ is meaningful, so that the reasoning made above remains valid.

Diagram 11 is a reproduction of the curve obtained by Cooper, Koehler and Marx for copper. Cooper[10] observed that such a curve fitted very exactly into the appropriate integral curve of the equation

$$dC = \alpha\, d\Phi - \beta C\, d\Phi , \qquad (26)$$

with Φ deuteron integrated flux, C fraction of atoms displaced for the value Φ, α and β constants. α and β will now be determined approximately. Integration of (26) with the boundary condition C = 0 for $\Phi = 0$ yields

$$C = (\alpha/\beta)(1 - e^{-\beta\Phi}) . \qquad (26a)$$

Hence

$$(dC/d\Phi)_0 = \alpha .$$

On Diagram 11, we see that, for $\Phi = 2 \times 10^{16}$, $\Delta\rho = 5 \times 10^{-2}$ $\mu\Omega$ cm. Since, for C = 1%, we accept a value $\Delta\rho = 2.7$ $\mu\Omega$ cm, it follows that

$$C = (5 \times 10^{-2})/(2.7 \times 100) \text{ for } \Phi = 2 \times 10^{16} .$$

Hence

$$\alpha \cong (5/2.7) \times 10^{-4}/(2 \times 10^{16}) \cong 10^{-20} .$$

And (26a) yields

$$\Delta\rho = 2.7 \times 100 \times (10^{-20}/\beta)(1 - e^{-\beta\Phi})$$

For $\Phi = 70 \times 10^{15}$, i.e. $\Delta\rho = 1.32 \times 10^{-1}$, this gives (see Appendix XIX),

$$\beta \cong 0.5 \times 10^{-17} .$$

In (26), βC is the fraction of defects (number of defects per lattice atom) which recombine, per unit Φ, at time corresponding to the value of Φ for which the value $C(\Phi)$ obtains.

To obtain the value of the ratio

$$r = \frac{\text{defects recombined}}{\text{defects produced}}$$

about the value Φ, we observe that $N\alpha$, where N is the number of lattice atoms, is the number of defects produced per unit Φ. Hence above ratio is

$$r = N\beta C(\Phi)/N\alpha = 1 - e^{-\beta\Phi}$$

For $\Phi = 7 \times 10^{16}$, i.e. about maximum irradiation of experiment, then

$$e^{-\beta\Phi} = e^{-7 \times 0.5 \times 10^{-1}} \cong 0.7; \; r = 0.3$$

For $\Phi = 2 \times 10^{16}$,

$$e^{-\beta\Phi} = e^{-2 \times 0.5 \times 10^{-1}} = 0.9; \; r = 0.1$$

These two values, one for extreme irradiation, the other one at about one quarter of the total irradiation, are reasonable.

From what has been said before, it is quite conceivable that one third of the defects in a disturbed region produced after long irradiation will recombine with defects of another region, and that one tenth of the defects of a disturbed region produced after light irradiation will do so, on the average. The qualificatives "long" and "light" apply, of course, only to the experiment discussed.

It is also seen that saturation ($r = 1$) can only be attained for $\Phi = \infty$, so that, if one attempts[9] to determine the required order of magnitude of the range of a knock-on so that saturation be attained for a finite Φ, the range obtained appears too large.

Now it is interesting to see what the situation is for neutron irradiation. In this case, the differential cross section for energy transfer from a neutron to an atom of the sample is, for elastic, center of mass isotropic collisions (conditions wholly justifiable),

$$\sigma(E',E)\,dE = \sigma_s(E')\,\frac{dE}{E_m}\,, \quad 0 \leq E \leq E_m,$$

$$= 0 \quad \text{otherwise},$$

where E' is the energy of the neutron, E the energy transferred to the atom, $\sigma_s(E')$ the scattering cross section of the atom for neutrons of energy E, and E_m the maximum of E, namely

$$E_m = [4A/(A+1)^2]E',$$

where A is the mass number of the atoms considered. Hence the frequency

function $\sigma(E',E)$ is independent of E; all energy transfers are equally likely, in the meaningful range $(0; E_m)$, Figure 24. The average energy transferred in displacing collisions by neutrons of energy E is

$$\bar{E} = \int_{E_d}^{E_m} E\,dE \Big/ \int_{E_d}^{E_m} dE = \frac{E_m + E_d}{2} ,$$

i.e., for the same E_m, it is much larger than in the case of bombardment by charged particles. For comparable energies of the bombarding particles, the cross section σ_d is higher for charged particles than for neutrons. Another difference is that pile neutrons have a spectrum of energies and that a flux of very energetic neutrons, say, E larger than 1 Mev, i.e.,

$$\phi = \int_{1\,Mev}^{\infty} \phi(E)\,dE$$

of order 10^{11} neuts cm^{-2} sec^{-1} is difficult to obtain, while it is easily obtainable with a cyclotron. This value corresponds to an integrated flux of $\Phi = 5.5 \times 10^{16}$ particles cm^{-2} for one week irradiation ($\cong 5.5 \times 10^5$ sec), which was exceded in the deuteron experiment previously discussed.

For E = 1 Mev, in copper,

$$E_m = (4 \times 63)/(64)^2 \text{ Mev} = 6.25 \times 10^4 \text{ ev.}$$

The average energy of primary knock-ons produced by a 1 Mev neutron is, therefore,

$$\bar{E} \cong 3.1 \times 10^4 \text{ ev} .$$

For this energy, a knock-on is in the range E_{tr1}; E_{tr2}, and will produce a displacement spike. But as seen in Chapter IV, Section 2, only few of its secondaries will create displacement spikes.

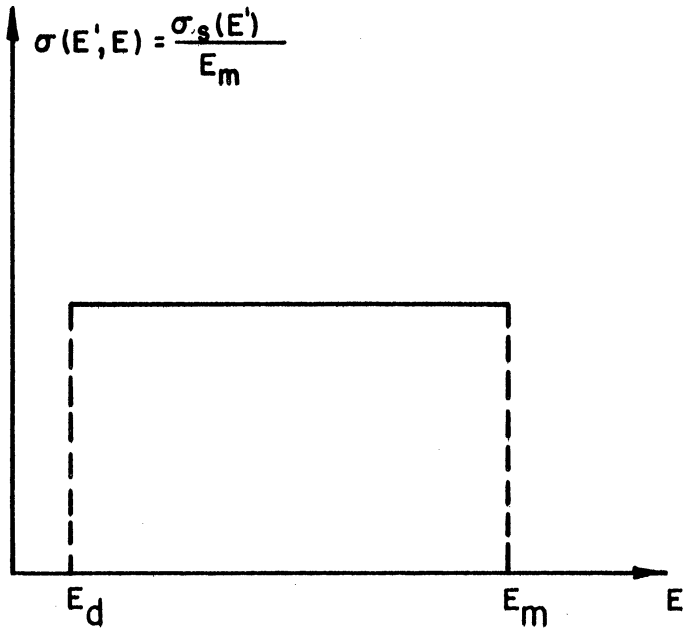

Figure 24. Frequency function σ(E', E) of the Cross Secton for Energy Transfer by Neutrons, in Elastic Collisions, Isotropic in the Center of Mass Frame.

Assume now, for the purpose of comparison, a monoenergetic neutron flux of energy 1 Mev and magnitude $\phi = 10^{11}$ neut cm^{-2} sec^{-1} and an irradiation of one week, i.e. about 5.5×10^5 sec. The cross section of copper for 1 Mev neutrons is $\sigma_s = 3$ barns.

Since, practically, all collisions of 1 Mev neutrons displace copper atoms, the number of primaries produced during the whole irradiation, per lattice atom, is about

$$n_{prim} = 3 \times 10^{-24} \times 10^{11} \times 5.5 \times 10^5 = 1.65 \times 10^{-7}.$$

If as before, we divide the sample in spherical cells round the point of birth of each primary, the radius a of these cells is then

$$a = (10/1.65)^{1/3} \times 10^2 \times (r_o/2) = 91\ r_o$$

Repeating the reasoning made in Chapter IV, Section 2, but for a primary with energy 3.1×10^4 ev, this time, we find that an order of magnitude of the length of the damage spike is

$$(2\ r_o/5)(1.76 \times 10^2 - 3.16 \times 10) = 58\ r_o$$

If we consider the damage spikes as cylindrical, Figure 25, of radius $5\ r_o$, which is probably too large (see Figure 21), and length $58\ r_o$, they occupy, at full irradiation, a volume

$$\pi \times (5\ r_o)^2 \times 58\ r_o \times N \times 1.65 \times 10^{-7},$$

N being the total number of atoms in the sample. Compare this to the volume of the sample, i.e.,

$$N \times (4/3) \times (r_o/2)^3.$$

This is comparing

$$2.4 \times 10^{-4}$$

to

$$1.7 \times 10^{-1}.$$

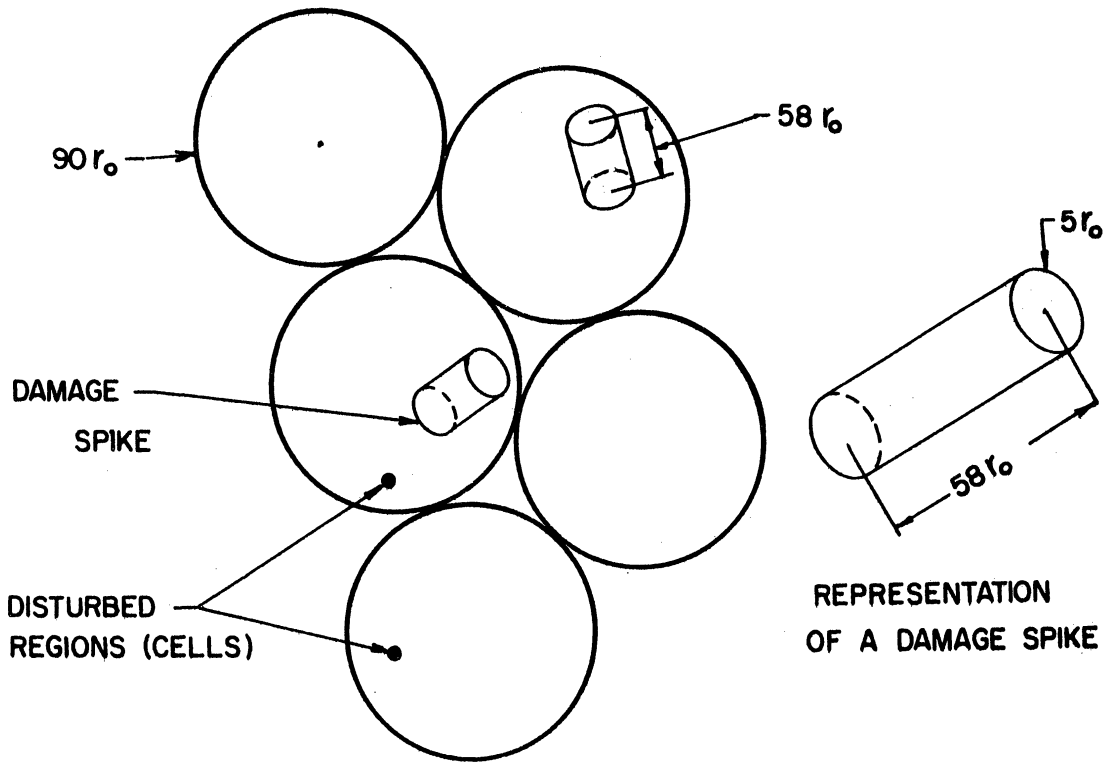

Figure 25. Illustrating the Possible Interaction of Defects of Different Generations in Neutron Irradiation.

This shows that the total volume of the damage spikes, at full irradiation, is less than 2/1000 of the total volume of the sample. Add the fact that, in the first part of the spike, the defect pairs have relatively large separation, the pairs in the displacement spike (center of the damage spike) still have appreciable separation, and only the pairs at the end of the damage spike have small separation and are highly susceptible to recombination, there being 20 such pairs, compared to

$$0.5 \times (3.1 \times 10^4/25 + 1) \cong 620$$

pairs in the whole damage spike, then it can be concluded that there should be little interaction between defects of different generations, for the case considered (see Figure 25).

Hence, for a typical metal like copper, except for extremely long irradiations, of the order of one year, which generally do not come into consideration in experiments, with fluxes of the order 10^{11} - 10^{12} (radius of cells 90 r_o, 30 r_o, respectively) above 1 Mev, we do not expect radiation anneal. Displacement spikes will form and contain many atoms.

The number of atoms displaced for a knock-on energy 3.1×10^4 ev will be 620, as just seen. Hence, the distrubed regions will contain many displaced atoms. The typical damage spike considered covers more than 8×10^3 lattice sites.

As it has been noted earlier, the conclusion just reached concerning the absence of radiation annealing in pile neutron irradiation, for reasonable exposures, is completely confirmed by the results

of the only reactor experiment[31] (to the best knowledge of this author) for which the temperature was near that of liquid helium and which, at the same time, incorporated the measurement of electrical resistivity during irradiation.

In this experiment, conducted at Oak Ridge, several metals and alloys were irradiated in a cryostat maintaining a temperature of 14.5°K within $\pm$ 1.5°K. Diagram 12, reproduced from the report on the experiment, shows that no radiation anneal took place, for any of the materials irradiated, for an exposure of 150 hrs, corresponding to a fast neutron integrated flux of 3.78×10^{17} neuts cm^{-2}. The accuracy and reproducibility of the measurements were good. The experimenters concluded, in line with the numerical results obtained in this dissertation, that it can be inferred that there is only slight, if any, interaction between adjacent damaged regions.

It is interesting, in connection with this experiment, to make an approximate calculation of the predicted change in electrical resistivity, in the case of copper.

For this we use the result, which we shall establish in the next section, that the fraction of atoms displaced is approximately given by

$$c \cong \frac{t \sigma_s}{E_d} \frac{A}{(A+1)^2} \int_{(A+1)^2 E_d/4A}^{\infty} E \phi(E) dE,$$

where t is the time of irradiation, in seconds, σ_s the scattering cross section of the irradiated material and A its mass number.

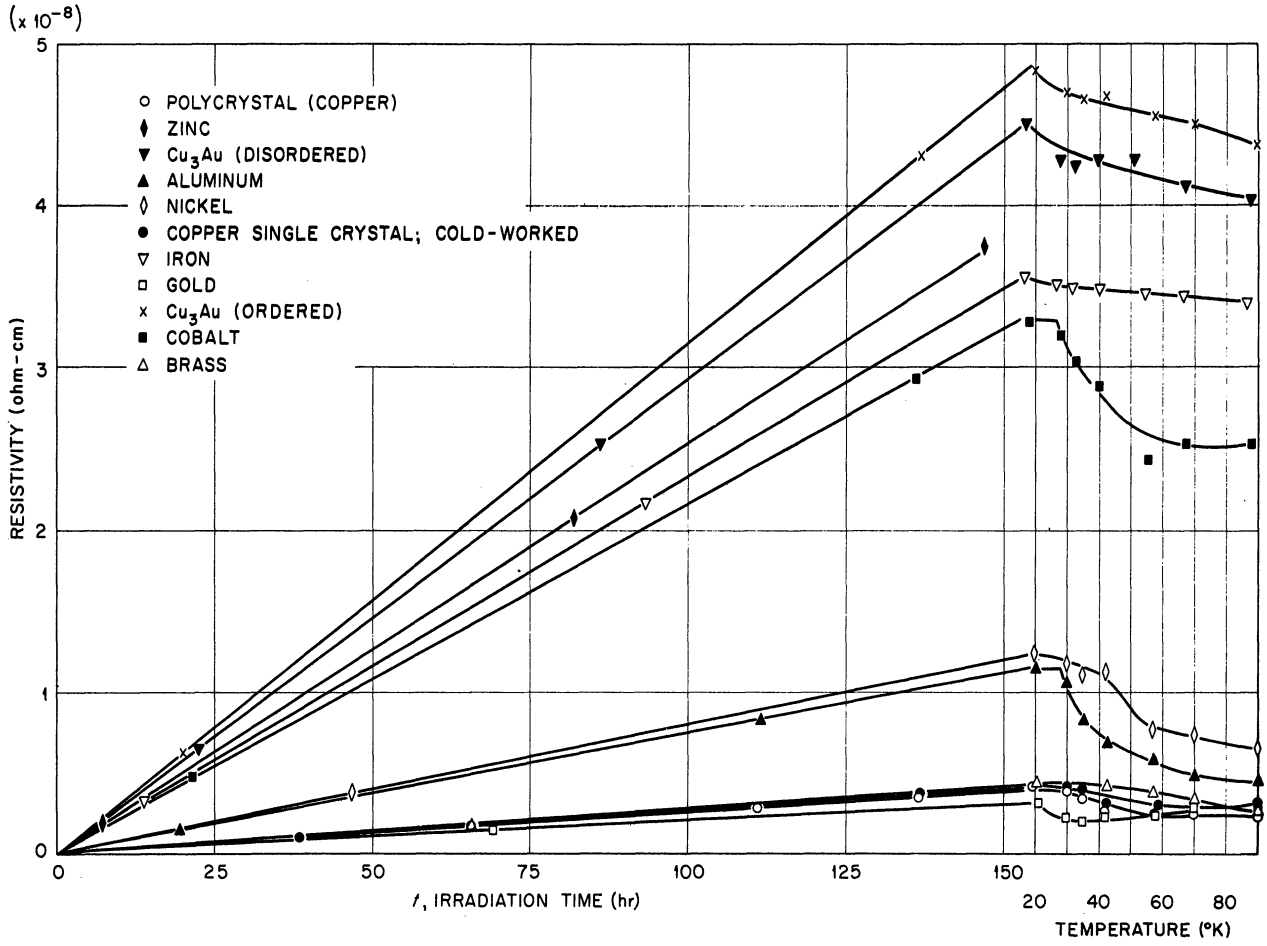

Diagram 12. Near Liquid Helium Temperature Reactor Irradiation of Various Metals and Alloys.(31)

For copper, A = 63 and we can take σ_s = 3 barns. In the experiment discussed,

$$t = 150 \text{ hrs} = 5.4 \times 10^5 \text{ sec}$$

An analytical expression for the neutron flux in hole 12 of the Oak Ridge reactor, which is the hole in which the cryostat is installed has been given by Seitz and Koehler[9], from unpublished data furnished by Holmes. It is the following:

$$\Phi(E) = \frac{0.414 \times 10^{11}}{E} \qquad \text{for } 0.025 < E < 2.5 \times 10^4 \text{ ev},$$

$$\Phi(E) = 1.508 \times 10^{11}(16.7e^{-20.5E} + 1.02e^{-1.51E}) \quad \text{for}$$

$$2.5 \times 10^{-2} \text{ Mev} \quad E,$$

with E in ev in the first formula and in Mev in the second one.

With this,

$$C \cong \frac{5.4 \times 10^5 \times 3 \times 10^{-24} \times 10^{11}}{25 \times 10^{-6} \times 64} \left\{ \left[0.414 \int_{400}^{2.5 \times 10^4} dE \right] \times 10^{-6} + 1.508 \left[16.7 \int_{2.5 \times 10^{-2}}^{\infty} E\, e^{-20.5E} dE + 1.02 \int_{2.5 \times 10^{-2}}^{\infty} E e^{-1.51E} dE \right] \right\},$$

$$C \cong 10^{-4} \left\{ 0.414 \times 2.5 \times 10^{-2} + \frac{1.508 \times 16.7}{20.5} e^{-0.51} \left[2.5 \times 10^{-2} + \frac{1}{20.5} \right] + \frac{1.508 \times 1.02}{1.51} e^{-3.78 \times 10^{-2}} \left[2.5 \times 10^{-2} + \frac{1}{1.51} \right] \right\},$$

$$C \cong 10^{-4} \left(10^{-2} + 1.23 \times 0.61 \times 7.4 \times 10^{-2} + 2.5 \times 10^{-2} + 0.66 \right),$$

$$C \cong 10^{-4} \left(10^{-2} + 5.56 \times 10^{-2} + 2.5 \times 10^{-2} + 0.66 \right),$$

$$C \cong 7.5 \times 10^{-5}.$$

With Jongenburger estimate of $\Delta\rho = 2.7\ \mu\Omega\,cm$ for C = 1% in copper, we obtain for estimate of increase in electrical resistivity after 150 has irradiation,

$$(\Delta\rho)_{th} = 7.5 \times 2.7 \times 10^{-3} = 2.02 \times 10^{-2}\ \mu\Omega\,cm.$$

On the line for copper in Diagram 12, we read,

$$(\Delta\rho)_{exp} = 3.75 \times 10^{-3}\ \mu\Omega\,cm.$$

Hence

$$\frac{(\Delta\rho)_{th}}{(\Delta\rho)_{exp}} = \frac{20.2}{3.75} = 5.4$$

Thus, we see that the theoretical estimate is about 5.4 times the observed change. This is consistent with the remark which will be made in Chapter V that the model used to calculate the number of secondary displacements per primary knock-on leads to an overestimate. This is also true of estimates made by the Snyder and Neufeld method. If anything, this may tend to prove that Jongenburger value of the increase in resistivity due to one percent displaced atoms has the correct order of magnitude.

The comparison between charged particle and neutron irradiation may be summarized as follows.

Charged Particle - Many primaries. The disturbed regions are small and contain few defects. Even for a reasonable irradiation, their distance apart is not large, compared to their size. Radiation anneal is expected to take place for such irradiation. Displacement spikes are not likely. "Dislocations" are not expected.

Neutron - Comparatively few primaries. The damage spikes are far apart for a reasonable irradiation. They contain many defects. Radiation anneal is not expected. Displacement spikes are formed and "dislocations" are expected.

4. Extension of the Model to Other Metals Than Copper. Expected Effects of Charged Particle and Neutron Irradiation as a Function of Atomic Number and Mass Number.

It is out the scope of this paper to make for other metals the same analysis as made for copper of the scattering by a potential leading to an interaction potential energy of the form (6). However, we shall now attempt to extend to other metals the results just obtained for copper and to see to what measure they must be modified. In Appendix XX it is shown that classical treatment is valid for pile irradiation of beryllium and even for cyclotron irradiation of beryllium with deuterons up to more than 20 Mev. However, the model is limited to probably $Z \geqslant 13$, because of the importance of ionization for lower atomic numbers. In the interaction energy (6)

$$V(r) = (Z^2\varepsilon^2/r)(1 + r/2a) \exp(-r/a),$$

with $a = a_h Z^{-1/3}$, we see that, the smaller Z, the larger the screening distance a (the potential remains Coulombian at larger distances).

It is clear that

$$F(a) = (1 + r/2a) \exp(-r/a)$$

is a monotonically increasing function of a, for

$$dF/da = (-r/2a^2 + r/a^2) \exp(-r/a)$$

is always greater than zero. Hence, F increases when Z decreases, monotonically, for all values of r.

Since $V(r) = (\varepsilon^2/r)\, Z^2 F$, it is possible for V(r) not to vary monotonically with Z. Let us study the function G(Z), such that

$$V(r) = (\varepsilon^2/r)\, G(Z),$$

i.e., $$G(Z) = Z^2 \left[1 + (r/2a_h) Z^{1/3}\right] \exp\left[-(r/a_h) Z^{1/3}\right],$$

or, with $Z^{1/3} = \varphi$,

$$G(\varphi) = [\varphi^6 + (r/2a_h)\varphi^7] \exp[-(r/a_h)\varphi] ,$$

$$dG/d\varphi = [6\varphi^5 + (7r/2a_h)\varphi^6 - r/a_h] \exp[-(r/a_h)\varphi] .$$

For the metals susceptible of being studied under neutron irradiation the smallest value of Z is 4, hence that of φ is 1.59, for which $\varphi^5 = 10.12$. All the values of r considered are smaller than r_o, which, in turn, is smaller than 4 Å, for all metals. Hence

$$6\varphi^5 > 6 \times 10.12$$

$$r/a_h < 4/0.5 = 8$$

i.e., in the range of r coming into play, we have

$$6\varphi^5 > r/a_h$$

for all r, and

$$dG/d\varphi > 0 .$$

In other words, G and V are monotonically increasing functions of φ and Z. With an interaction energy of the form (6), for all r in consideration, the interaction will be weaker for Z small than for Z large. In lighter metals, energy transfer and displacement cross section between knock-on and stationary atom will be smaller, displacement mean free path larger, at the same energy of the knock-on. For Z low enough, Diagram 10 may be altered to give a variation of $(\lambda_d)_u$ such as shown in Figure 26, i.e. such that it would be possible to conclude that no displacement spikes are formed. This is in accordance with Brinkman views, which are that, the transition energy being small for light metals, their displacement spikes will be small.

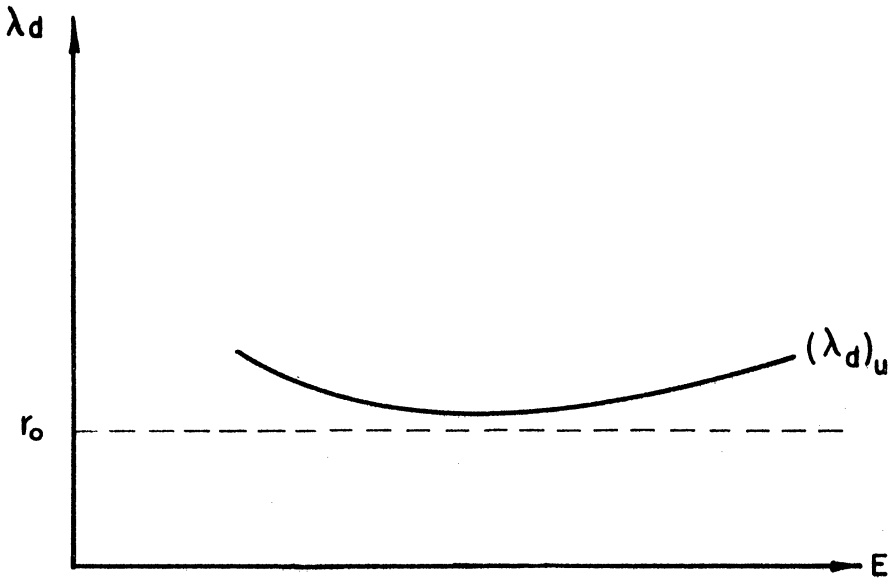

Figure 26. Possible Variation of λ_d for Light Metals.

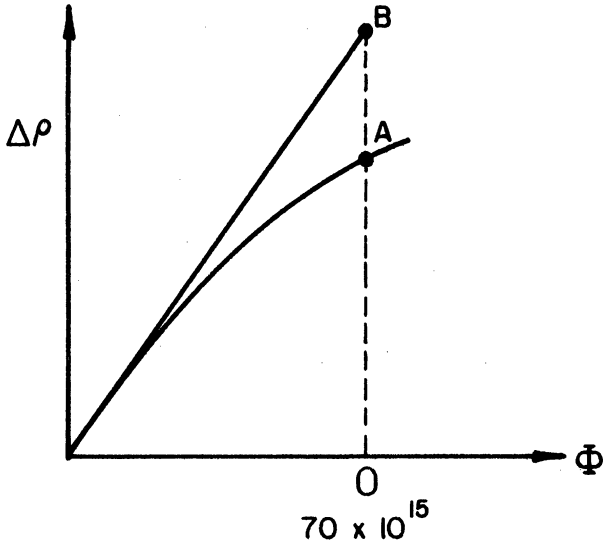

Figure 27. Effect of Radiation Anneal.

Consider first charged particle irradiation. In Appendix XXI, it is shown that, for a given type of particle, energy and integrated flux, the fraction of primary knock-ons p_{prim} varies like

$$Z^2/A$$

where Z is the atomic number and A the mass number of the metal irradiated. In Appendix XVIII it is shown that the average number $\overline{\nu}$ of atoms displaced per primary varies like

$$Ln\ (1+\chi_{1m})$$

where

$$\chi_{1m} = \left(\frac{E-E_d}{E_d}\right)_{max} \cong \frac{E_m}{E_d} = \frac{4MA}{(M+A)^2}\,\frac{E'}{E_d}\ ,$$

M being the mass number of the bombarding particle, E' its energy. Hence, $\overline{\nu}$ varies little from metal to metal, for the same conditions of irradiation. Take M = 2, E' = 12 Mev.

For Be 9,

$$\chi_{1m} = \frac{72}{121} \times \frac{12 \times 10^6}{25} = 29 \times 10^4;\ Ln\ (1+\chi_{1m}) = 12.6$$

For Au 197,

$$\chi_{1m} = \frac{8 \times 197}{(2+197)^2} \times 48 \times 10^4 = 1.95 \times 10^4;\ Ln\ (1+\chi_{1m}) = 9.85$$

Hence, for a light metal, we have less disturbed regions than for a heavy metal since n_{prim} is smaller, but each region does not contain appreciably more defects than a region in a heavy metal. The overall damage is greater in a heavy metal. This is borne out by experiment, in particular by the results of Cooper et al. However, the knock-on mean free path will be larger for the same energy and the small separation defect pairs will be farther away from the

point of birth of the primary. Hence, there is compensation on the change of the two parameters which influence recombination in the form of "radiation anneal" when one goes from irradiation of a heavy metal to that of a light metal and we expect that the effect of radiation annealing will not change appreciably from metal to metal, in charged particle irradiation. This checks with the few experimental results available. In the helium temperature deuteron irradiation(8), samples of gold (Z = 79), silver (47), and copper (29), were irradiated. For $\Phi = 70 \times 10^{15}$ deut cm^{-2}, the ratio OA/OB (see Figure 27), where A is on the $\Delta\rho$ vs Φ curve and B on its tangent at the origin, was

$$49.36/63.6 = 0.78 \text{ for Au}$$

$$34/45.5 = 0.75 \text{ for Ag}$$

$$30.5/38.7 = 0.79 \text{ for Cu}$$

(the numbers, such as 49.6, ... were measured in mm on the curves given by Seitz and Koehler.(9))

Consider now neutron irradiation. Denote by $\underline{r}$ (a vector) the position of a point A of the sample, Figure 27a. Define $n(r,E',\underline{\Omega}')$ $dE'\, d\underline{\Omega}'$ the volumetric density, at $\underline{r}$, of neutrons with energy in dE' about E', going within a small solid angle $d\underline{\Omega}'$ about the direction $\underline{\Omega}'$. Call $\underline{v}'$ the velocity corresponding to E' and $\underline{\Omega}'$ and v' the modulus of $\underline{v}'$. The number of such neutrons which cross unit area perpendicular to $\underline{\Omega}'$ at A, in the direction $\underline{\Omega}'$, per second, is

$$v' n(r, E', \underline{\Omega}')\, dE' d\underline{\Omega}' = \phi(r, E', \underline{\Omega}')\, dE' d\underline{\Omega}',$$

by usual definition of the angular neutron flux. Here ϕ is the flux in the sample, not the original flux before the introduction of the samples.

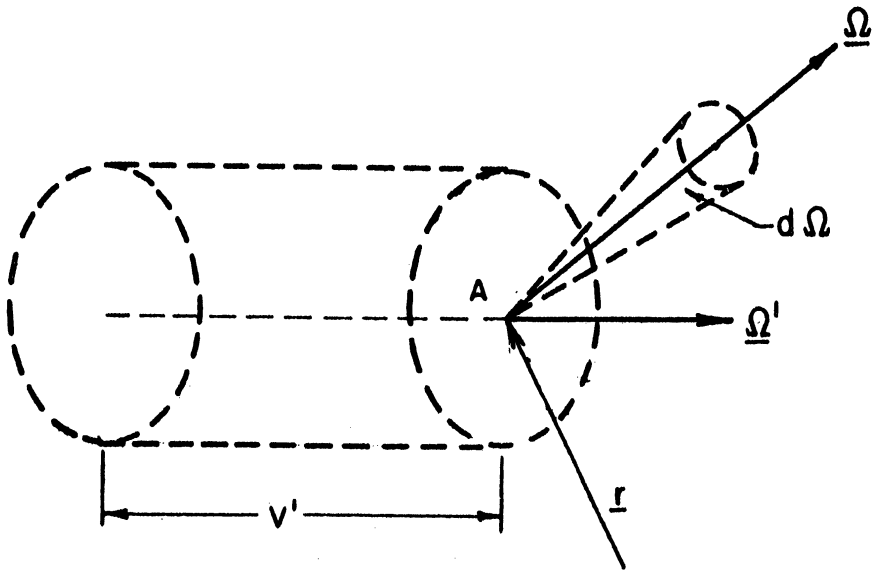

Figure 27a. Neutron Collision.

The number of neutrons, from those in dE', $d\Omega'$ before collision, deflected by collision in $d\Omega$ about $\underline{\Omega}$, per second, per atom present at A is, from definition of the microscopic differential cross section,

$$\phi(\underline{r}, E', \underline{\Omega}')\, dE'\, d\Omega'\, \sigma(E', \underline{\Omega})\, d\underline{\Omega} \,.$$

$\sigma(E', \underline{\Omega})\, d\Omega$ may be written in the form of an energy transfer cross section, by the condition of conservation of momentum and energy (elastic scattering assumed here), and the above number written as

$$\phi(\underline{r}, E', \underline{\Omega}')\, dE\, d\Omega'\, \sigma(E', E)\, dE, \qquad (27)$$

where E is the energy transmitted to the atom hit. This number is then seen to be the fraction of atoms present at A which receive energy in dE about E, per second, from neutrons with energy in dE' about E', moving in directions in $d\Omega'$ about $\underline{\Omega}'$.

Coherent scatter (crystal effect) is assumed not to take place and the lattice nuclei are considered at rest before the neutron collision. These two assumptions are perfectly valid for displacing collisions, where E_d = 25 ev, at least, is transmitted to the atom. Hence, σ is independent of $\underline{\Omega}'$.

Integrate (27) over all $\underline{\Omega}'$, calling

$$\phi(\underline{r}, E') = \int_{\text{all } \underline{\Omega}'} \phi(\underline{r}, E', \underline{\Omega}')\, d\Omega',$$

i.e., the "normal" flux, to obtain

$$\phi(\underline{r}, E')\, dE'\, \sigma(E', E)\, dE \qquad (28)$$

as the fraction of atoms present at A which receive energy in dE about E,

per second, from neutrons with energy in dE' about E'. The samples used are small (for example, 0.005 inch diameter metal wires, 1 to 3 inches long), hence we may take Φ as constant over the sample, for the purpose of calculating the fraction of atoms displaced. Then

$$\Phi(E')\,dE'\,\sigma(E',E)\,dE \qquad (29)$$

is now the fraction of atoms in the sample which receive energy in dE about E, per second, from neutrons with energy in dE' about E'.

If we add the assumption of center of mass isotropic scattering to that of elastic collision, which is also justified here at least for small and medium mass numbers, and a good first approximation for heavy metals (Preliminary Study[1]), (29) can be written

$$\sigma_s(E')\,\frac{dE}{E_m}\,\Phi(E')\,dE', \quad 0 \leq E \leq E_m \qquad (30)$$

$$0, \quad \text{otherwise,}$$

where E_m is the maximum of E.

The fraction of primaries formed per second is obtained by integrating (30) between $E = E_d$ and $E = E_m$, and between $E' = E'_{thr}$ and $E' = \infty$, where E'_{thr}, threshold energy for atomic displacement, is defined by

$$E_d = \frac{4A}{(A+1)^2}\,E'_{thr} .$$

After an irradiation time t sec, the fraction of primaries is

$$n_{prim} = t \int_{\frac{(A+1)^2}{4A}E_d}^{\infty} \sigma_s(E')\,\Phi(E')\,dE' \int_{E_d}^{\frac{4A}{(A+1)^2}E'} \frac{(A+1)^2}{4AE'}\,dE .$$

It is not seriously wrong to take $\sigma_s(E') \cong \sigma_s = ct$, neglecting resonance scattering.

Hence we may write

$$n_{prim} \cong t\sigma_s \int_{(A+1)^2 E_d/4A}^{\infty} \left[1 - \frac{(A+1)^2}{4A}\frac{E_d}{E'}\right] \phi(E')dE'.$$

Now, the frequency function ϕ is not peaked around E_{thr}, which is far above thermal. Hence, since

$$\frac{(A+1)^2}{4A}\frac{E_d}{E'} \leq 1, \text{ and since } \frac{(A+1)^2}{4A}\frac{E_d}{E'} \ll 1 \text{ for } E' \gg E'_{thr},$$

the term of the integral corresponding to $\phi(E')dE'$ will predominate over that corresponding to $\frac{(A+1)^2}{4A}\frac{E_d}{E'}\phi(E')dE'$ and another justifiable approximation is

$$n_{prim} \cong t\sigma_s \int_{(A+1)^2 E_d/4A}^{\infty} \phi(E')dE' \quad . \qquad (31)$$

ϕ is the disturbed flux, i.e., after introduction of the experimental device and the samples.

$\int_{(A+1)^2 E_d/4A}^{\infty} \phi(E')dE'$ decreases when A increases.

$\frac{(A+1)^2}{4A}E_d \cong \frac{AE_d}{4}$ takes the value $\frac{9 \times 25}{4} = 56.5$ ev for Be 9 and the value $\frac{197 \times 25}{4} = 1230$ ev for Au 197.

If, for the purpose of estimate, we assume $\phi(E') \sim 1/E'$, and adopt a cut off energy of 2 Mev, the integral is proportional to

$$\text{Log } (2 \times 10^6/56.5) \cong 2.3 \text{ Ln } 3.54 \times 10^4 \text{ for Be 9}$$

and to Log $(2 \times 10^6/1230) \cong 2.3$ Ln 1.63×10^3 for Au 197, so that the

ratio of the values for beryllium and gold is about 4/3. At any rate, it appears clear that n_{prim} is fairly insensitive to A, for irradiation in a thermal reactor.

If we compare two metals irradiated in the same conditions, i.e same reactor core configuration and neutron level, same experimental device, and presumably to a lesser degree of importance, since the samples will be small and very thin, same flux distortion, we can say, from (31), that n_{prim} varies like σ_s. However, in fact, about same size of different samples is adopted and flux distortion by the samples will depend on σ_s. Hence, it must be emphasized that, only if the flux distortion by the samples (not by the experimental device) is small, and this may be said to be true for such dimensions as mentioned above, can we say that $n_{prim} \sim \sigma_s$, approximatively.

The scattering cross section for neutrons of energy above, say 1 Kev, does not vary drastically from metal to metal. Hence, even for lighter metals, in which λ_d will be larger, no radiation anneal is expected.

It will be seen later that an approximation (overemphasizing displacements, however) for the number of knock-ons (including primary) per primary knock-on formed with energy E is

$$\nu(\alpha_1) \cong 0.5\,(1+\alpha_1)$$

where $\alpha_1 = E_1/E_d$ and $E_1 = E - E_d$, E being the same energy as used above. Hence,

$$\nu(E) \cong 0.5\, E/E_d$$

and the fraction of atoms displaced after irradiation t sec is

$$C \cong \frac{0.5}{E_d} t \sigma_s \int_{(A+1)^2 E_d/4A}^{\infty} \phi(E')\, dE' \int_{E_d}^{\frac{4A}{(A+1)^2}E'} \frac{(A+1)^2}{4AE'} E\, dE ,$$

or

$$C \cong \frac{0.5}{E_d} t \sigma_s \frac{1}{2} \int_{\frac{(A+1)^2}{4A}E_d}^{\infty} \frac{(A+1)^2}{4AE'} \left\{ \left[\frac{4A}{(A+1)^2} \right]^2 E'^2 - E_d^2 \right\} \phi(E')\, dE'.$$

Following the reasoning made before, we can neglect, in the integrand, E_d^2 in comparison to $\left[\frac{4A}{(A+1)^2}\right]^2 E'^2$. Hence, we have

$$C \cong \frac{t\sigma_s}{E_d} \frac{A}{(A+1)^2} \int_{(A+1)^2 E_d/4A}^{\infty} E' \phi(E')\, dE' \qquad (32)$$

For a $1/E'$ fast flux, and neglecting the lower limit, the integral is a constant, so that, for irradiation in a thermal reactor, and since $A/(A+1)^2 = 1/A$, we expect C to be approximately proportional to σ_s/A. Since n_{prim} is approximately proportional to σ_s, $\overline{\nu}$ is approximately inversely proportional to A.

Hence, the damage spikes will contain more point defects for A small than A large and, since λ_d will be larger, there will be more chances for recombination of defects by radiation anneal for A small.

We shall now summarize the comparison of light metals and heavy metals for both charged particle and neutron irradiation.

Charged Particle

Smaller number of primaries (i.e. of disturbed regions) for a light metal than for a heavy metal ($n_{prim} \sim Z^2/A$). About the same number

of point defects per region ($\overline{\nu}$ = ct). The regions are larger for the light metal, but the displacement mean free path, λ_d , is larger. Hence, radiation anneal is expected to be of the same order for light and heavy metals. Displacement spikes and "dislocations" are not expected.

Neutron

The number of primaries depends mainly on σ_s, to which it is roughly proportional. The number of point defects per region is approximately inversely proportional to A, hence is higher for light metals. Radiation is not expected to take place for "reasonable" irradiations (order of a few weeks with a flux of order 10^{11} -10^{12} above 1 Mev). For heavy irradiations, chances for radiation anneal are higher for metals with high σ_s and low A (n_{prim}, λ_d, and $\overline{\nu}$ all large). For Z (i.e. also A) low enough, displacement spikes may not form.

The above conclusions are borne out by experiments in which property changes have been measured during irradiation, insofar as radiation annealing is concerned, both in the case of charged particle and neutron irradiation.(7,8,31) Mechanical properties such shear strength, which should be sensitive to dislocations, hence, presumably, to the formation of displacement spikes, have not been measured for charged particle irradiation.

At least one reactor experiment (Reynolds et al.(20)) checks well with the picture of no displacement spikes produced in a light

metal. The results of this experiment have been discussed in connection with the critique of Brinkman's model.

Hence, the interest of measurements of change in properties -- then, practically, the only property which is manageable is electrical resistivity--during irradiation in a reactor is obvious.

We note also that such an experiment must be made at or near liquid helium temperature, so that possible radiation anneal is not masked by thermal anneal, incipient already below liquid nitrogen temperature.

We remark that, for purposes of checking the effect of irradiation, several metals should be irradiated in the same disturbed flux conditions.

Finally, the success of the experiment demands a comparatively high fast flux if the duration is to remain reasonable. Now, an attempt will be made to calculate the number of secondaries per primary, using a displacement cross section given by (20).

CHAPTER V

CALCULATION OF THE NUMBER OF ATOMS DISPLACED PER PRIMARY KNOCK-ON

1. Generalities-Obtention of the Primary Integral Equation

We consider a collision between a knock-on, called primary, and a lattice atom, called secondary, as happening in the following way. First the primary, of energy E, transfers energy T to the secondary. Then the secondary escapes from its lattice site if $T > E_d$, by losing energy E_d to the lattice, therefore retaining energy $T - E_d$ as a free secondary knock-on. After the collision, the primary has energy E. Since the collision is assumed elastic, we have

$$E = E' + T.$$

Call $P(E,T)dT$ the probability that, in a collision, i.e., given that a collision occurs, the primary transfers energy in dT about T to the secondary. Then

$$P(E,T)dT = \frac{\text{probability of having a collision w.transf.in dT ab.T}}{\text{probability of having a collision}}$$

Hence,

$$P(E,T)dT = \sigma(E, \varphi_T)d\Omega_T \,/\, \sigma_S(E) \ ,$$

where $\sigma(E, \varphi_T)d\Omega_T$ is the differential scattering cross section at angle φ_T, in the center of mass frame, such that φ_T corresponds to T; φ_T is the angle of scatter of the primary in the center of mass frame, Figure 28; $d\Omega_T$ is an element of solid angle of the center of mass frame, limited by the angles φ_T and $\varphi_T + d\varphi_T$, i.e.

$$d\Omega_T = 2\pi \sin\varphi_T \, d\varphi_T .$$

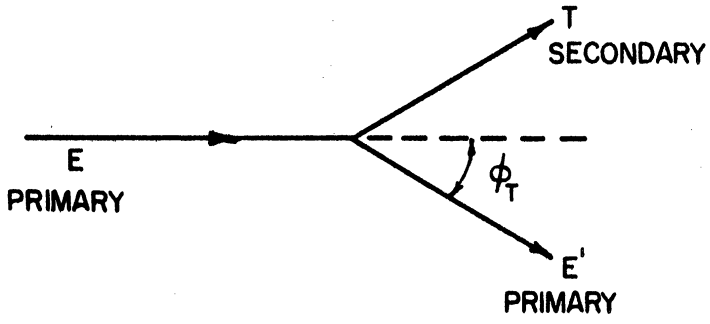

Figure 28. Angle of Scatter in the Center of Mass Frame.

We replace φ_T by its value in terms of T and E, from the relation (see Appendix VIII) expressing elastic scatter, namely

$$T = E \sin^2 \varphi_T/2, \tag{33}$$

from which we see that T increases with φ_T.

Hence, we can write

$$P(E,T)dT = \sigma(E,T)dT/\sigma_s(E) \tag{34}$$

T varying from 0 to E.

In the same way, if we call $P(E,E')dE'$ the probability that, in a collision, the primary will emerge with energy in dE' about E', we can write

$$P(E,E')dE' = \sigma(E,E')dE'/\sigma_s(E) \tag{35}$$

where $\sigma(E,E')dE'$ is obtained by replacing in $\sigma(E,\varphi_T)d\Omega_T$, φ_T by its value from

$$E' = E - T = E(1 - \sin^2 \varphi_T/2) \quad . \tag{36}$$

E' decreases when φ_T and Ω_T increase, and will be made to vary from E to 0.

Now, the following reasoning, generalized from Snyder and Neufeld[3] to various forms of cross section which may be considered, is made. Every knock-on will suffer at least one collision in the sample, since, in the model used, the collision cross section is $\pi(r_o/2)^2$. Note that this has been assumed by Snyder and Neufeld, for a model based on hard sphere scatter, center of mass isotropic, arbitrarily. We have seen before that the slowing down collisions of knock-ons in copper can be described by an approximate formula for the cross section

$$2\pi p\,dp = \pi \frac{2\alpha(E)}{E} d\left[\frac{(1-\varphi_T/\pi)^2}{1-(1-\varphi_T/\pi)^2}\right] \quad . \tag{37}$$

The approximation is much better at high energy than at low energy. Similar formulae would hold for other metals than copper.

The important point, for the time being, is that we can describe slowing down and energy transfer by appropriate differential cross sections

$$\sigma(E,E')dE' \text{ and } \sigma(E,T)dT, \text{ respectively.}$$

Call $\nu(E)$ the total number of atoms displaced by an knock-on (including the knock-on itself) of energy E after release, i.e. E is the quantity by which the energy transferred to it in the releasing collision exceeds E_d. Then, when the secondary receives energy T in the collision, the total number of atoms displaced as a result of its being released is

$$\nu(T - E_d),$$

and, when the primary emerges from the collision with energy E', the total number of atoms displaced as a result of this emergence is

$$\nu(E').$$

We can clearly write

$$\nu(E) = \int_{E_d}^{E} \nu(T-E_d) \frac{\sigma(E,T)dT}{\sigma_s(E)} + \int_{E}^{0} \nu(E') \frac{\sigma(E,E')dE'}{\sigma_s(E)} \qquad (38)$$

the limits of the integrals corresponding to values of T and E' which define the range of displacing collision, i.e.,

$$E_d \leq T \leq E$$

and

$$0 \leq E' \leq E \text{ , respectively, and E}$$

going from E to 0, while T goes from 0 to E and φ_T from 0 to π .

We first apply (38) to elastic, center of mass frame isotropic scatter. Then,

$$\sigma(E, \varphi_T)\, d\Omega_T = \sigma_s(E)\, d\Omega_T / 4\pi \ .$$

From $d\Omega_T = 2\pi \sin\varphi_T\, d\varphi_T$ and $dT = (E/2)\sin\varphi_T\, d\varphi_T$, we have

$$\sigma(E,\varphi_T)\, d\Omega_T = \sigma_s(E)\, dT/E = \sigma(E,T)\, dT.$$

In the same way,

$$dE' = -(E/2)\sin\varphi_T\, d\varphi_T$$

and

$$\sigma(E,\varphi_T)\, d\Omega_T = -\sigma_s(E)\, dE'/E = \sigma(E,E')\, dE'.$$

(38) becomes

$$\nu(E) = \frac{1}{E}\int_{E_d}^{E} \nu(T-E_d)\, dT - \frac{1}{E}\int_{E}^{0} \nu(E')\, dE'.$$

Let

$$E/E_d = x_1 \ , \ (T-E_d)/E_d = x_2 \ , \ E'/E_d = x'_1 \ .$$

The equation becomes finally,

$$x_1\, \nu(x_1) = \int_0^{x_1-1} \nu(x_2)\, dx_2 + \int_0^{x_1} \nu(x'_1)\, dx'_1 \ . \qquad (39)$$

This is Snyder and Neufeld primary equation, whose solution, and various associated problems, like treatment by Laplace transform, consideration of replacement and recombination of defects, are considered in Appendix XXII.

Return now to Equation(38). Call $\tilde{\sigma}_1(E,T)$ the primitive of $\sigma(E,T)$ with respect to T, and $\tilde{\sigma}_2(E,E')$ the primitive of $\sigma(E,E')$ with respect to E', defined by

$$\tilde{\sigma}_1(E,T) = \int_E^T \sigma(E,T^*)\, dT^*,$$

$$\tilde{\sigma}_2(E,E') = \int_0^{E'} \sigma(E,E^*)\, dE^* \ .$$

We then have the following relations:

$$\tilde{\sigma}_1(E,E_d) = \int_E^{E_d} \sigma(E,T)\,dT = -\sigma_d(E),$$
$$\tilde{\sigma}_1(E,E) = 0,$$
$$\tilde{\sigma}_2(E,0) = 0,$$
$$\tilde{\sigma}_2(E,E) = \int_0^E \sigma(E,E')\,dE' = -\sigma_s(E)$$

where σ_d is the displacement cross section, σ_s the scattering cross section.

Integrate Equation (38) by parts. This gives,

$$\nu(E) = \frac{1}{\sigma_s(E)} \left\{ \left[\nu(T-E_d)\tilde{\sigma}_1(E,T) \right]_{T=E_d}^{T=E} - \int_{E_d}^{E} \nu'(T-E_d)\tilde{\sigma}_1(E,T)\,dT \right\}$$
$$+ \frac{1}{\sigma_s(E)} \left\{ \left[\nu(E')\tilde{\sigma}_2(E,E') \right]_{E'=E}^{E'=0} - \int_{E}^{0} \nu'(E')\tilde{\sigma}_2(E,E')\,dE' \right\}$$

where the ν' are derivatives.

Using the relations established above, we obtain

$$\nu(E) = \frac{\sigma_d(E)}{\sigma_s(E)}\nu(0) + \frac{\sigma_s(E)}{\sigma_s(E)}\nu(E) - \frac{1}{\sigma_s(E)}\left[\int_{E_d}^{E} + \int_{E}^{0} \right],$$

or,

$$\frac{\sigma_d(E)}{\sigma_s(E)}\nu(0) = \frac{1}{\sigma_s(E)}\left[\int_{E_d}^{E} + \int_{E}^{0} \right]. \qquad (40)$$

For continuous scatter, i.e. for a differential cross section of the form pdp, with p going from zero to infinity, (40) is identically true, since $\sigma_s = \infty$.

2. Obtention of an Asymptotic Solution for the Model of Interaction Used.

Comparison with the Asymptotic Solution of the Snyder and Neufeld Equation.

Confrontation of Calculational and Experimental Results.

For the model used in this paper,

$$\sigma(E,\varphi_T)\,d\Omega_T = |2\pi p\,dp| \quad \text{for} \quad 0 \le p \le r_0/2$$

$$= 0 \qquad \text{otherwise.}$$

Hence, σ_s is finite and (40) can be used. By definition, $\nu(E) = 1$ for $E = 0$, since, when the primary emerges from the particle collision with energy 0, the total number of atoms displaced is reduced to that primary knock-on. Using this, (40) can be written,

$$\sigma_d(E) = \int_{E_d}^{E} \nu'(T-E_d)\,\tilde{\sigma}_1(E,T)\,dT + \int_{E}^{0} \nu'(E')\,\tilde{\sigma}_2(E,E')\,dE'. \quad (41)$$

Now, assume possible a solution of the form

$$\nu(E) = A + BE \qquad A,B \text{ constant.}$$

Then, we should have

$$\frac{\sigma_d(E)}{B} = \int_{E_d}^{E} \tilde{\sigma}_1(E,T)\,dT + \int_{E}^{0} \tilde{\sigma}_2(E,E')\,dE'.$$

Since p decreases (Figure 29) from ∞ to 0 when φ_T goes from 0 to π (while T goes from 0 to E and E' from E to 0), we have

$$\sigma(E,\varphi_T)\,d\Omega_T = \sigma(E,T)\,dT = \sigma(E,E')\,dE' = -\pi\,d(p^2).$$

From (20),

$$p^2 = (2\alpha/E)(1-\varphi_T/\pi)^2 \Big/ \left[1-(1-\varphi_T/\pi)^2\right]$$

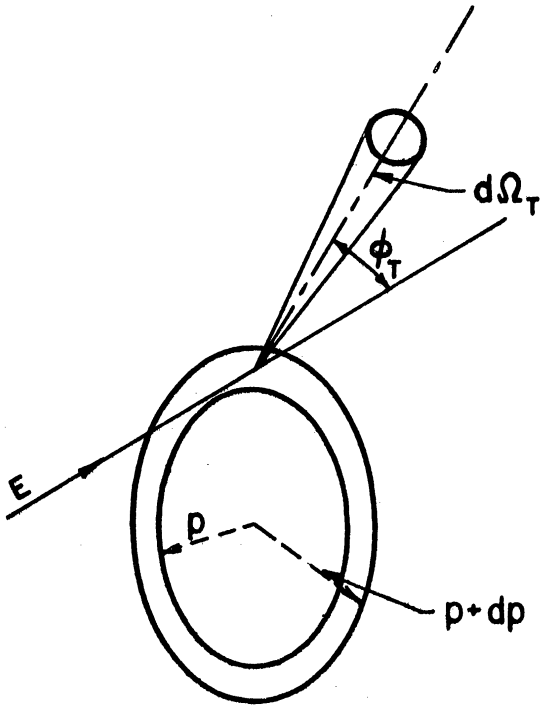

Figure 29. Variation of ϕ_T versus p.

with φ_T connected to T and E' by (33) and (36). Hence,

$$\sigma(E,T^*)\,dT^* = -\pi\frac{2\alpha}{E}\,d\left\{\left(1-\frac{2}{\pi}\sin^{-1}\sqrt{\frac{T^*}{E}}\right)^2\Big/\left[1-\left(1-\frac{2}{\pi}\sin^{-1}\sqrt{\frac{T^*}{E}}\right)^2\right]\right\},$$

$$\sigma(E,E^*)\,dE^* = -\pi\frac{2\alpha}{E}\,d\left\{\left(1-\frac{2}{\pi}\sin^{-1}\sqrt{\frac{E-E^*}{E}}\right)^2\Big/\left[1-\left(1-\frac{2}{\pi}\sin^{-1}\sqrt{\frac{E-E^*}{E}}\right)^2\right]\right\}.$$

From which,

$$\tilde{\sigma}_1(E,T) = -\pi\frac{2\alpha}{E}\left(1-\frac{2}{\pi}\sin^{-1}\sqrt{\frac{T}{E}}\right)^2\Big/\left[1-\left(1-\frac{2}{\pi}\sin^{-1}\sqrt{\frac{T}{E}}\right)^2\right],$$

$$\tilde{\sigma}_2(E,E') = -\pi\frac{2\alpha}{E}\left(1-\frac{2}{\pi}\sin^{-1}\sqrt{\frac{E-E'}{E}}\right)^2\Big/\left[1-\left(1-\frac{2}{\pi}\sin^{-1}\sqrt{\frac{E-E'}{E}}\right)^2\right].$$

Putting these expressions in (42), we obtain

$$\frac{E\sigma_d(E)}{2\alpha\pi B} = -\int_{E_d}^{E}\frac{\left(1-\frac{2}{\pi}\sin^{-1}\sqrt{\frac{T}{E}}\right)^2}{1-\left(1-\frac{2}{\pi}\sin^{-1}\sqrt{\frac{T}{E}}\right)^2}dT - \int_{E}^{0}\frac{\left(1-\frac{2}{\pi}\sin^{-1}\sqrt{\frac{E-E'}{E}}\right)^2}{1-\left(1-\frac{2}{\pi}\sin^{-1}\sqrt{\frac{E-E'}{E}}\right)^2}\cdot \quad (43)$$

Let E - E' = T in the integral at the right (dE' = - dT, limits 0 to E). Call f(T) dT the integrand , now common to both integrals. The right hand side of the equation becomes,

$$\left[-\int_{E_d}^{E}+\int_{0}^{E_d}+\int_{E_d}^{E}\right] f(T)\,dT = \int_{0}^{E_d} f(T)\,dT\,.$$

Now, assume $E \gg E_d$. We can make the approximation

$$\frac{E\sigma_d(E)}{2\alpha\pi B} \cong \int_0^{E_d}\frac{1-(4/\pi)\sqrt{T/E}}{(4/\pi)\sqrt{T/E}}\,dT = \frac{\pi}{2}\sqrt{E}\sqrt{E_d}-E_d\,,$$

$$\sigma_d(E) = \tilde{\sigma}_1(E,E_d) = \pi\frac{2\alpha}{E}\frac{\left(1-\frac{2}{\pi}\sin^{-1}\sqrt{E_d/E}\right)^2}{1-\left(1-\frac{2}{\pi}\sin^{-1}\sqrt{E_d/E}\right)^2}$$

$$\cong \pi\frac{2\alpha}{E}\,\frac{1-(4/\pi)\sqrt{E_d/E}}{(4/\pi)\sqrt{E_d/E}}\,.$$

Hence, the following must hold:

$$1 - \frac{4}{\pi}\sqrt{\frac{E_d}{E}} \cong B\frac{4}{\pi}\sqrt{\frac{E_d}{E}}\left(\frac{\pi}{2}\sqrt{E}\sqrt{E_d} - E_d\right),$$

and, since $E \gg E_d$ is assumed,

$$1 \cong B\frac{4}{\pi}\sqrt{E_d/E}\,\frac{\pi}{2}\sqrt{E}\sqrt{E_d},$$

which gives

$$B \cong 1/2E_d \qquad (44)$$

Since B, so determined, is effectively independent of E, an asymptotic solution, i.e. for $E \gg E_d$, of the form

$$\nu(E) \cong A + BE,$$

with E in Mev, is possible.

With E_d = 25 ev,

$$B = 10^6/(2 \times 25) = 2 \times 10^4 .$$

Snyder and Neufeld Equation (39) has an asymptotic solution

$$\nu(x_1) = 0.561\,(1 + x_1).$$

Since $x_1 = E/E_d$, we can write

$$\nu(E) = (0.561/E_d)(E + E_d) = 0.561 + (56.1 \times 10^4/25)E;\ E \text{ Mev}.$$

We see that the coefficient of E is practically identical with that found in this paper. Such solution leads to fractions of atoms displaced 4 to 6 times that shown by experiment on copper and gold, if Jongenburger[4] value of the change in electrical resistivity due to a fraction of 1% atoms displaced is employed. This is consistent with the observation that the model used in this paper overestimates displacements at low energy, from which we expected that ν so calculated would yield too large fractions of atoms displaced.

The approximation $E \gg E_d$ in the last calculation is good even for $E = 10^{-3}$ Mev, since, then,

$$E_d/E = 2.5 \times 10^{-2}; \quad (4/\pi)\sqrt{E_d/E} = 0.201.$$

Neglecting $(4/\pi)\sqrt{E_d/E}$ in comparison to 1 is not quite correct, but remains commensurate with other approximations made in the model used. At any rate, the estimate of $\nu(E)$ for this value of E is certainly too large.

We would expect the approximation on ν to be worse in the case of charged particle irradiation, where the primaries have low average energy, than in the case of neutron irradiation. However, we must remember that, in neutron irradiation, there is a large number of secondaries, most of them having low energy, so that most displacements must happen at low energy. Two experiments only allow comparison, the helium temperature cyclotron irradiation of copper by 12 Mev deuterons[8], and the helium temperature reactor irradiation of copper[11]. The deuteron experiment gives a change in electrical resistivity 6 times smaller and the reactor experiment a change 4 times smaller than the change calculated using the $\nu(E)$ furnished by the Snyder and Neufeld model.

Now, return to the approximation on $\nu(E)$. We cannot determine the constant A. Physically, if the solution were good over the whole range of E, we would have A = 1 for E = 0. A must be negligible in the range where the approximation is good, so that its value is of little importance. Since $E + E_d$ is the energy transferred to the

knock-on (primary; for example) before its release from its site, it is convenient to adopt

$$\nu(E) \cong B(E + E_d),\ E, E_d \text{ in Mev, that is } A = BE_d.$$

We can also write

$$\nu(x_1) = BE_d\ (1 + x_1) \tag{45}$$

with $B = 2 \times 10^4$, $BE_d = 0.5$.

Note that the study of $\nu(E)$ has proceeded on quite general lines, applicable to various types of cross sectional models, up to Equations (40) and (41). A direct treatment of the case of the model used in this paper is given in Appendix XXIII.

In summary, it will be said that the model of interaction between knock-ons and stationary atoms used in this paper leads to a number of secondaries per primary, at high primary energy, practically identical to that obtained by Snyder and Neufeld on the assumption of hard sphere scatter. The values so obtained, for the number of secondaries, are certainly too large, since the model overestimates interaction at low energy. This is conform to confrontation of experimental and calculational results.

CONCLUSION

The form of interaction potential energy used and the method of approach adopted in this paper have proved successful.

The values of displacement mean free path and fraction of atoms displaced obtained are quite compatible with experimental results. They show that recombination of defects by interaction with them of defects of a later generation can reasonably be expected in charged particle irradiation, but not in reactor neutron irradiation, for exposures coming into consideration in experiments.

The two extremely useful models of Brinkman and Snyder and Neufeld have been investigated critically, by comparison with the model used in this paper. The direction of the error in the parameters they arrive at has been defined. The method used has afforded useful comparisons between charged particle and neutron irradiation and shown the great interest of in pile measurements during low temperature neutron irradiation.

The design of a helium temperature cryostat which could be used, among various purposes, for experiments on neutron-induced atomic displacements in metals, has been made. Construction has begun and some development experiments have been carried out. Appendix XXIV gives a description of this work.

Low temperature neutron irradiation experiments help clarifying the problem of radiation annealing. It may be added that the study of the recovery of mechanical properties during thermal anneal after a low temperature charged particle irradiation should be helpful in the study of the problem of displacement spikes.

APPENDIX I

Correspondence between a Born-Mayer interaction and the potential energy used in the paper, at large separation

Born-Mayer interaction (Huntington[12]):

$$V_1(r) = A \exp\left(-\rho \frac{r - r_0}{r_0}\right)$$

with two sets of constants, for Cu,

$$\rho = 13, \qquad A = 0.053 \text{ ev}$$

$$\rho = 17, \qquad A = 0.038 \text{ ev}$$

which constitute a bracket for ρ and A. At $r \gg 2a$, (6) of the text becomes

$$V(r) \cong \frac{z^2\varepsilon^2}{2a} \exp\left(-\frac{r}{a}\right)$$

In fact, this will be a good approximation even for $r \cong 7a$. At $r = r_0$,

$$V_1(r) = A$$

$$V(r) = 1.22 \times 10^{-8} \text{ Mev. from}$$

Table I, so that the potential energy $V(r)$ used checks with the value of A, within a factor of at most 4.

Write $$V_1(r) = A\, e^{\rho} \exp\left(-\frac{r}{r_0}\rho\right) .$$

$$1 - \rho = 13; \quad \log_{10} e^{\rho} = \frac{13}{2.3} = 5.65; \quad e^{\rho} = 4.47 \times 10^5 ,$$

$$Ae^{\rho} = 5.3 \times 10^{-2} \times 4.47 \times 10^5 = 2.36 \times 10^4 \text{ ev} ,$$

$$\frac{z^2\varepsilon^2}{2a} = \frac{1.21}{0.344} \times 10^{-2} \text{ Mev} = 3.52 \times 10^4 \text{ ev},$$

$$\frac{r_0}{\rho} = \frac{2.556}{13} = 0.197 .$$

We can write $V_1(r) = 2.36 \times 10^4 \exp\left(-\frac{r}{0.197}\right)$ ev ,

compared to $V(r) = 3.52 \times 10^4 \exp\left(-\frac{\quad}{0.172}\right)$ ev .

For $r = \frac{r_0}{2}$

i) $\frac{r}{0.197} = \frac{2.556}{0.394} = 6.5$; $\log_{10} e^{6.5} = \frac{6.5}{2.3} = 2.83$;

$e^{6.5} = 6.77 \times 10^2$; $V_1\left(\frac{r_0}{2}\right) = \frac{2.36 \times 10^4}{6.77 \times 10^2} = 34.8$.

ii) $\frac{r}{0.172} = \frac{2.556}{0.344} = 7.45$; $\log_{10} e^{7.45} = \frac{7.45}{2.3} = 3.24$;

$e^{7.45} = 1.74 \times 10^3$; $V\left(\frac{r_0}{2}\right) = \frac{3.52 \times 10^4}{1.74 \times 10^3} = 20.5$.

At $r = \frac{r_0}{2} \simeq \frac{15a}{2}$, it is seen that $V(r)$ is sufficiently close to $V_1(r)$.

2- $\rho = 17$; $\log_{10} e^{\rho} = \frac{17}{2.3} = 7.40$; $e^{\rho} = 2.52 \times 10^7$;

$A e^{\rho} = 3.8 \times 10^{-2} \times 2.52 \times 10^7 = 9.55 \times 10^5$;

$\frac{r_0}{\rho} = \frac{2.556}{17} = 0.150$;

$V_1(r) = 9.55 \times 10^5 \exp\left(-\frac{r}{0.150}\right)$.

For $r = \frac{r_0}{2}$, $\frac{r}{0.150} = \frac{2.556}{0.3} = 8.52$;

$\log_{10} e^{8.52} = \frac{8.52}{2.3} = 3.7$; $e^{8.52} = 5.02 \times 10^3$;

$V_1\left(\frac{r_0}{2}\right) = \frac{9.55 \times 10^5}{5.02 \times 10^3} = 190$ ev .

Actually, from Table I, $V\left(\frac{r_0}{2}\right) = 2.46 \times 10^{-5}$ Mev. Hence, $V\left(\frac{r_0}{2}\right)$ is rather close to $V_1\left(\frac{r_0}{2}\right)$ for the lower value $\rho = 13$, but smaller, so that $V(r)$ is somewhat too small at large r, but yet takes acceptable values.

APPENDIX II

Reduction of the Schrödinger equation for a system of two particles

$$\frac{\hbar}{i}\dot{\psi} = \left[\frac{\hbar^2}{2m_1}\nabla_{R_1}^2 + \frac{\hbar^2}{2m_2}\nabla_{R_2}^2 - V(r) - U(\underline{R}_1, \underline{R}_2)\right]\psi \;;$$

$$\nabla_{R_1}^2 = \frac{\partial^2}{\partial x_1^2} + \text{---} \;;\quad \nabla_{R_2}^2 = \frac{\partial^2}{\partial x_2^2} + \text{---} \;;$$

$$\underline{R}_1 = (x_1, \text{---}) \;;\quad \underline{R}_2 = (x_2, \text{---}) \;.$$

Let $\underline{\mathcal{R}}$ be the coordinate of the center of mass, i.e.

$$\underline{\mathcal{R}} = \alpha\,\underline{R}_1 + \beta\,\underline{R}_2 = (X, Y, Z) \;.$$

Hence

$$X = \alpha x_1 + \beta x_2 \;;\quad \text{---} \;,$$

with

$$\alpha = \frac{m_1}{m_1+m_2} \;;\quad \beta = \frac{m_2}{m_1+m_2} \;.$$

Let

$$r = \underline{R}_2 - \underline{R}_1 = (x, y, z)\,,\ \text{i.e.}\ x = x_2 - x_1 \;; \text{---}$$

$$\frac{\partial}{\partial x_1} = \frac{\partial}{\partial X}\frac{\partial X}{\partial x_1} + \frac{\partial}{\partial x}\frac{\partial x}{\partial x_1} = \alpha\frac{\partial}{\partial X} - \frac{\partial}{\partial x} \;;$$

$$\frac{\partial^2}{\partial x_1^2} = \frac{\partial}{\partial X}\left(\alpha\frac{\partial}{\partial X} - \frac{\partial}{\partial x}\right)\alpha - \frac{\partial}{\partial x}\left(\alpha\frac{\partial}{\partial X} - \frac{\partial}{\partial x}\right)$$

$$= \alpha^2\frac{\partial^2}{\partial X^2} + \frac{\partial^2}{\partial x^2} - 2\alpha\frac{\partial^2}{\partial X\,\partial x} \;.$$

In the same way,

$$\frac{\partial^2}{\partial x_2^2} = \beta^2 \frac{\partial^2}{\partial X^2} + \frac{\partial^2}{\partial x^2} + 2\beta \frac{\partial^2}{\partial X \partial x} \quad .$$

$$\frac{1}{m_1}\nabla_{R_1}^2 + \frac{1}{m_2}\nabla_{R_2}^2 = \frac{1}{m_1}\left[\alpha^2 \nabla_R^2 + \nabla_r^2 - 2\alpha \sum_{\substack{x,y,z \\ X,Y,Z}} \frac{\partial^2}{\partial X \partial x}\right]$$

$$+ \frac{1}{m_2}\left[\beta^2 \nabla_R^2 + \nabla_r^2 + 2\beta \sum_{\substack{x,y,z \\ X,Y,Z}} \frac{\partial^2}{\partial X \partial x}\right]$$

$$= \nabla_R^2 \left[\frac{m_1}{(m_1+m_2)^2} + \frac{m_2}{(m_1+m_2)^2}\right] + \nabla_r^2 \left(\frac{1}{m_1} + \frac{1}{m_2}\right)$$

$$+ 2\left(\frac{1}{m_1+m_2} - \frac{1}{m_1+m_2}\right) \sum \frac{\partial^2}{\partial X \partial x}$$

$$= \frac{1}{M}\nabla_R^2 + \frac{1}{\mu}\nabla_r^2 \quad ,$$

where

$$\nabla_R^2 = \frac{\partial^2}{\partial X^2} + \text{---} \; ; \quad \nabla_r^2 = \frac{\partial^2}{\partial x^2} + \text{---} \; ;$$

$$M = m_1 + m_2 \; ; \quad \mu = \frac{m_1 m_2}{m_1 + m_2} \; , \text{ reduced mass.}$$

Hence, the original equation reduces to (2) of the text.

APPENDIX III

Wave length of a copper knock on "reduced" particle at various energies

1) $E = 7.2 \times 10^{-1}$ Mev

$$7.2 \times 10^{-1} \times 1.6 \times 10^{-6} = \frac{1}{2}\ 63 \times 1.67 \times 10^{-24} v^2,$$

in cm x sec^{-1} .

$$v^2 = \frac{1.44 \times 1.6 \times 10^{-6}}{6.3 \times 1.67 \times 10^{-23}} = \frac{2.305 \times 10^{-6}}{1.05 \times 10^{-22}} = 2.19 \times 10^{16} ,$$

$$v = 1.48 \times 10^{8} \text{ cm x } sec^{-1} ,$$

$$\lambda = \frac{1.05 \times 10^{-27}}{\frac{63}{2} \times 1.67 \times 10^{-24} \times 1.48 \times 10^{8}} = 1.35 \times 10^{-13} \text{ cm} .$$

2) $E = 25\ ev$

$$25 \times 1.6 \times 10^{-12} = \frac{1}{2}\ 63 \times 1.67 \times 10^{-24} v^2 ,$$

$$v^2 = \frac{50 \times 1.6 \times 10^{-12}}{63 \times 1.67 \times 10^{-24}} \cong 10^{12} ,$$

$$\lambda \cong \frac{1.05 \times 10^{-27}}{\frac{63}{2} \times 1.67 \times 10^{-24} \times 10^{6}} \cong 3 \times 10^{-11} \text{cm} .$$

APPENDIX IV

Constant of the law of areas and angular momentum

$$y = d\theta/du \; ; \; u = 1/r \; ; \; r^2 d\theta/dt = K$$

Hence $\left(\frac{d\theta}{dt}\right)_{\substack{r=\infty \\ u=0}} = 0$

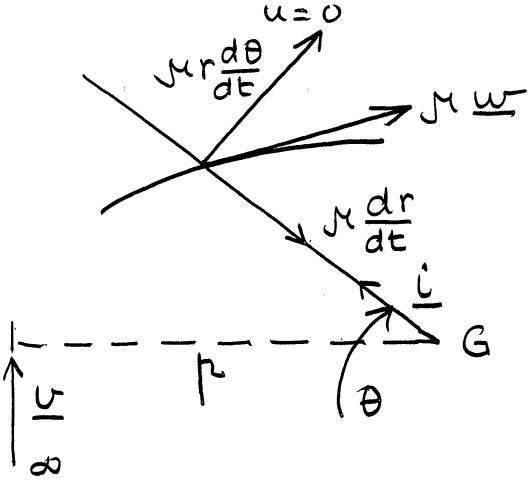

$$\frac{d\theta}{du} = \frac{d\theta}{dr}\frac{dr}{du} = -\frac{1}{u^2}\frac{d\theta}{dr}$$

$$= -\frac{1}{u^2}\frac{d\theta}{dt}\frac{dt}{dr} = -r^2\frac{d\theta}{dt}\frac{dt}{dr}$$

$$= -K\frac{dt}{dr}$$

Hence $$\left(\frac{d\theta}{du}\right)_{\substack{u=0 \\ r=\infty}} = -K\left(\frac{dt}{dr}\right)_{\substack{u=0 \\ r=\infty}}$$

$$\left(\frac{dt}{dr}\right)_{r=\infty} = 1\Big/\left(\frac{dr}{dt}\right)_{r=\infty}$$

For r very large, r decreases when t increases, since $r = |\underline{R}_1 - \underline{R}_2|$, i.e. the separation of the moving atom from the stationary one decreases. We have $v = -\left(\frac{dr}{dt}\right)_{r=\infty}$, speed at infinity, and $\left(\frac{d\theta}{du}\right)_{u=0} = -K \times \frac{-1}{v} = \frac{K}{v}$. From conservation of angular momentum, $\mu r^2 \frac{d\theta}{dt} = \mu K = \mu v p$, p impact parameter. Hence, $\frac{K}{v} = p$, $(y)_{u=0} = p$. Recall that $\mu r \frac{d\theta}{dt}$ is the component of momentum perpendicular to the radius vector $r\underline{i}$, since

$$\underline{w} = \frac{d}{dt}(r\underline{i}) = \underline{i}\frac{dr}{dt} + r\frac{d\theta}{dt}\frac{d}{d\theta}\underline{i} \quad .$$

APPENDIX V

Sign of dV/du

$$V(r) = z^2\varepsilon^2\left(\frac{1}{r} + \frac{1}{2a}\right)e^{-\frac{r}{a}} \quad ;$$

$$\frac{dV}{dr} = z^2\varepsilon^2 e^{-\frac{r}{a}}\left[-\frac{1}{r^2} - \frac{1}{a}\left(\frac{1}{r} + \frac{1}{2a}\right)\right] ;$$

$$\frac{dV}{du} = \frac{1}{u^2} z^2\varepsilon^2 e^{-\frac{r}{a}}\left[\frac{1}{r^2} + \frac{1}{a}\left(\frac{1}{r} + \frac{1}{2a}\right)\right] \geq 0$$

APPENDIX VI

First integral of the equation of motion. Boundary condition at $r = r_0/2$

$$y^{-2} = \frac{1-(2\rho/r_0)^2}{\rho^2} - u^2 + \left(\frac{2}{r_0}\right)^2 - \frac{1}{\rho^2 E}\left[V(u) - V\left(\frac{2}{r_0}\right)\right]$$

$$= \frac{1}{\rho^2} - u^2 - \frac{2}{\rho^2 E}\left[V(u) - V\left(\frac{2}{r_0}\right)\right] \quad ;$$

$$y = \frac{\pm \rho}{\sqrt{1 - \frac{2}{E}\left[V(u) - V\left(\frac{2}{r_0}\right)\right] - \rho^2 u^2}}$$

APPENDIX VII

Obtention of equation of motion

$$\frac{1}{p}\sqrt{\frac{2}{E}\alpha(E)+p^2}\left(\theta-\sin^{-1}\frac{2p}{r_0}\right)$$

$$=\sin^{-1}\sqrt{\frac{2}{E}\alpha(E)+p^2}\,u-\sin^{-1}\sqrt{\frac{2}{E}\alpha(E)+p^2}\,\frac{2}{r_0}\;;$$

$$u=\frac{1}{r}=\frac{1}{\sqrt{\frac{2}{E}\alpha(E)+p^2}}\sin\left[\frac{\sqrt{\frac{2}{E}\alpha(E)+p^2}}{p}\left(\theta-\sin^{-1}\frac{2p}{r_0}\right)\right.$$

$$\left.+\sin^{-1}\sqrt{\frac{2}{E}\alpha(E)+p^2}\,\frac{2}{r_0}\right].$$

APPENDIX VIII

General relations for elastic scattering

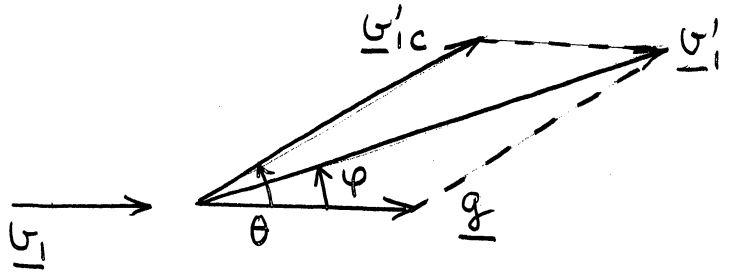

Incident particle: mass M_1, velocity $\underline{v}_1$, in laboratory frame, before collision; $\underline{v}'_1$ in lab frame, after collision;

$\underline{v}'_{1c}$ in center of mass frame, after collision.

$\underline{g}$ = velocity of center of mass in lab frame. Stationary particle: mass M_2, velocity $\underline{v}_2$ in lab frame, after collision.

θ = angle of scatter of incident particle in the center of mass frame, in the lab frame.

μ = reduced mass = $\dfrac{M_1 M_2}{M_1 + M_2}$.

We have

$$(M_1 + M_2)\,\underline{g} = M_1\,\underline{v}_1 \quad ;$$

$$\underline{g} = \frac{\mu}{M_2}\,\underline{v}_1 \quad ;$$

$$\operatorname{tg}\varphi = \frac{v'_{1c}\sin\theta}{v'_{1c}\cos\theta + g} \quad ;$$

where $g = |\underline{g}|$

For elastic scatter, there is no change of speed (the magnitude of the velocity vector) in the center of mass frame, hence

$$v'_{1c} = v_1 - g = v_1\left(1 - \frac{\mu}{M_2}\right) = \frac{\mu}{M_1} v_1$$

and

$$\operatorname{tg}\varphi = \frac{(\mu/M_1) v_1 \sin\theta}{(\mu/M_1) v_1 \cos\theta + (\mu/M_2) v_1} = \frac{M_2 \sin\theta}{M_2 \cos\theta + M_1} \quad (1)$$

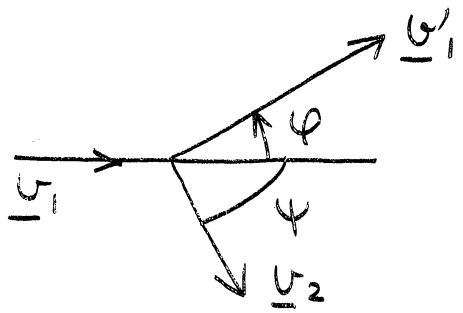

ψ being the angle of scatter (with respect to $\underline{v}_1$) of the stationary particle, in the lab frame, we also have,

$$M_1 v'_1 \sin\varphi = M_2 v_2 \sin\psi ,$$

$$\frac{v'^2_1}{v_1^2} = \frac{M_2^2 + 2M_1M_2\cos\theta + M_1^2}{(M_1+M_2)^2}$$

(see f. ex., Glasstone & Edlund, p. 149),

$$M_2 v_2^2 = M_1 (v_1^2 - v'^2_1) ,$$

$$\frac{M_2}{M_1} v_2^2 = v_1^2 - v'^2_1 \; ; \; \frac{M_2}{M_1}\frac{v_2^2}{v_1^2} = 1 - \frac{v'^2_1}{v_1^2} ,$$

$$\frac{M_2}{M_1}\frac{v_2^2}{v_1^2} = \frac{(M_1+M_2)^2 - (M_2^2 + 2M_1M_2\cos\theta + M_1^2)}{(M_1+M_2)^2} = \frac{2M_1M_2(1-\cos\theta)}{(M_1+M_2)^2} ,$$

$$\frac{v_2'^2}{v_1^2} = \frac{2M_1^2(1-\cos\theta)}{(M_1+M_2)^2} ,$$

$$\sin^2\psi = \frac{M_1^2 v_1'^2}{M_2^2 v_2^2}\sin^2\varphi = \frac{M_1^2}{M_2^2}\frac{v_1'^2}{v_1^2}\frac{v_1^2}{v_2^2}\sin^2\varphi$$

$$= \frac{M_1^2}{M_2^2}\,\frac{M_2^2+2M_1M_2\cos\theta+M_1^2}{(M_1+M_2)^2}\,\frac{(M_1+M_2)^2}{2M_1^2(1-\cos\theta)}\,\frac{tg^2\varphi}{1+tg^2\varphi}$$

$$= \frac{1}{2M_2^2}\,\frac{M_2^2+2M_1M_2\cos\theta+M_1^2}{1-\cos\theta}\,\frac{M_2^2\sin^2\theta}{M_2^2+2M_1M_2\cos\theta+M_1^2}$$

$$= \frac{1}{2}\,\frac{1}{2\sin^2\theta/2}\,4\sin^2\theta/2\cos^2\theta/2 ,$$

$$\sin^2\psi = \cos^2\frac{\theta}{2} .$$

Hence, since ψ and θ are both $\leq\pi$, it follows that

$$\psi = \frac{\pi}{2} - \frac{\theta}{2} \qquad (2)$$

1) $M_1 > M_2$, mass of moving particle greater than mass of stationary one

then φ goes from 0 to $\varphi_m < \frac{\pi}{2}$ when θ goes from 0 to π;

$(tg\varphi)_{\theta=\frac{\pi}{2}} = \frac{M_2}{M_1} < 1$; $(tg\varphi)_{\theta=\pi} = 0$; hence there is a maximum.

$$\frac{d}{d\theta}\,tg\varphi = \frac{M_2\cos\theta(M_2\cos\theta+M_1)+M_2^2\sin^2\theta}{(M_2\cos\theta+M_1)^2} = \frac{M_2^2+M_1M_2\cos\theta}{(M_2\cos\theta+M_1)^2}$$

for $\theta = 0$,

$$\frac{d}{d\theta}\,tg\varphi = \frac{M_2}{M_2+M_1} > 0 ;$$

for $\theta = \pi$

$$\frac{d}{d\theta}\,tg\varphi = -\frac{M_2}{M_1-M_2} < 0 .$$

$\frac{d}{d\theta} tg\varphi$ has a zero for

$$M_2^2 + M_1 M_2 \cos\theta = 0 ,$$

i.e. $$\cos\theta_m = -\frac{M_2}{M_1} \quad ; \quad \theta_m > \frac{\pi}{2} \quad ;$$

for $\theta < \theta_m$, $\cos\theta > -\frac{M_2}{M_1}$, $\frac{d}{d\theta} tg\varphi > 0$, and $tg\varphi$ increases with θ.

Maximum of $tg\varphi$:

$$tg\varphi_m = \frac{M_2 \sin\theta_m}{M_2\cos\theta_m + M_1} = \frac{M_2\sqrt{1-M_2^2/M_1^2}}{M_1 - M_2^2/M_1} = \frac{M_2}{\sqrt{M_1^2-M_2^2}} > \frac{M_2}{M_1}$$

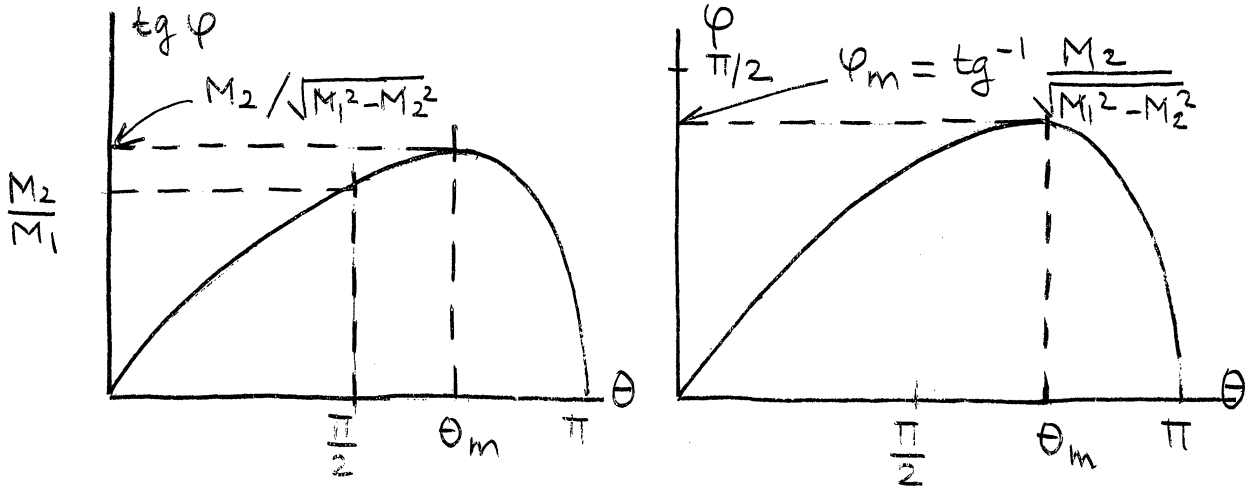

2) <u>$M_1 < M_2$, mass of moving particle smaller than mass of stationary one</u>

$M_2\cos\theta + M_1$ has a zero, for which $tg\varphi = \infty$ and $\varphi = \frac{\pi}{2}$. Call θ_∞ the corresponding value of θ. For $\theta > \theta_\infty = \cos^{-1}\left(-\frac{M_1}{M_2}\right)$, $M_2\cos\theta + M_1 < -M_1 + M_1 = 0$, hence $tg\varphi$ is < 0 and $\varphi > \frac{\pi}{2}$. For $\theta = \pi$, $tg\varphi = 0$ and $\varphi = \pi$. Hence φ goes from 0 to π . $tg\varphi$ varies monotically, since

$$\frac{d}{d\theta} tg\varphi = \frac{M_2(M_2 + M_1\cos\theta)}{(M_2\cos\theta + M_1)^2}$$ has no zero.

It increases with θ.

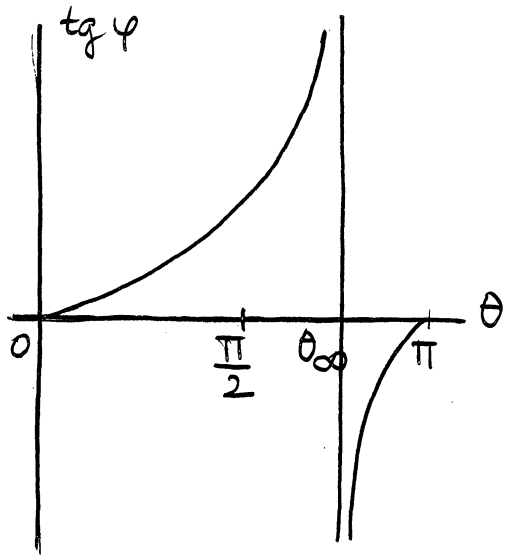

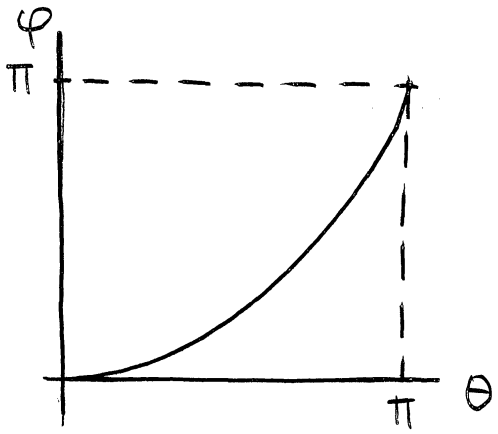

3) $M_1 = M_2$, $tg\varphi = \dfrac{\sin\theta}{1+\cos\theta} = tg\,\dfrac{\theta}{2}$

hence $$\varphi = \theta/2 \qquad (3)$$

and, from (2) $$\psi = \frac{\pi}{2} - \varphi \;, \quad \psi + \varphi = \frac{\pi}{2} \qquad (4)$$

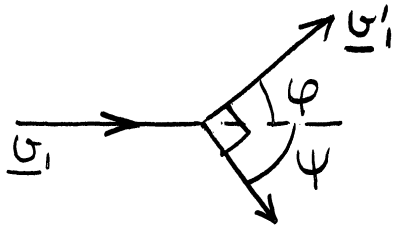

<u>The final velocities of two particles of equal mass, in the lab system, are perpendicular, for an elastic collision.</u>

Return now to the stationary particle after collision.

$$\frac{v_2^2}{v_1^2} = \frac{2M_1^2 2\sin^2\theta/2}{(M_1+M_2)^2} \quad ; \quad \frac{v_2}{v_1} = \frac{2M_1 \sin\theta/2}{M_1+M_2}$$

and

$$v_1 = \frac{M_1+M_2}{M_1}\, g \;;$$

hence

$$v_2 = 2g \sin\frac{\theta}{2} \;.$$

The kinetic energy transferred to the stationary particle is

$$T = \frac{1}{2} M_2 v_2^2 = \frac{1}{2} M_2 v_1^2 \frac{4M_1^2 \sin^2 \theta/2}{(M_1+M_2)^2}$$

$$= E \frac{4M_1M_2}{(M_1+M_2)^2} \sin^2 \frac{\theta}{2} .$$

The maximum of T is $T_m = E \frac{4M_1M_2}{(M_1+M_2)^2}$.

Hence $T = T_m \sin^2 \frac{\theta}{2}$

If $M_1 = M_2$, $T_m = E$ and $T = E \sin^2 \frac{\theta}{2}$.

APPENDIX IX

Discussion of plot of $V(r)$

$$V(r) = 1.21 \times 10^{-2}\left(\frac{1}{r} + 2.9\right) e^{-\frac{r}{0.172}}$$

$$= 1.21 \times 10^{-2}\left(\frac{1}{r} + \frac{1}{2a}\right) e^{-\frac{r}{a}}$$

For $r >> 2a$, $V(r) \cong \frac{1.21 \times 10^{-2}}{2a} e^{-\frac{r}{a}}$,

i.e. $V(r)$ is represented by a stratight line of slope $-1/a$ in semi-log paper ($\log V, r$). In fact, since $1/r + 1/2a = u + 2.9$ varies slowly with r for $r > 2a$, a straight line is practically obtained for $r \gtrsim 2a$. For $r \ll 2a$, $V(r) \sim \frac{1}{r}$, hence an hyperbolic branch for small r. Notice that $V(r) - V(r_0/2)$ varies sharply when r approaches $r_0/2$, but, up to $r = \frac{13a}{2}$, the approximation $V\left(\frac{r_0}{2}\right) \cong 0$ would be a justifiable one.

APPENDIX X

Maximum value of $\beta = \sin^{-1}\sqrt{\frac{2\alpha}{E}+\rho^2}\,\frac{2}{r_0} - \frac{1}{\rho}\sqrt{\frac{2\alpha}{E}+\rho^2}\,\sin^{-1}\frac{2\rho}{r_0}$

Let $A = y - z$

with

$$y = \rho \sin^{-1}\sqrt{\frac{2\alpha}{E}+\rho^2}\,\frac{2}{r_0} \quad ; \quad z = \sqrt{\frac{2\alpha}{E}+\rho^2}\,\sin^{-1}\rho\,\frac{2}{r_0} \; .$$

Study $y(x)$ and $z(x)$, with $x = 2/r_0$.

$$\frac{dy}{dx} = \frac{\rho\sqrt{2\alpha/E+\rho^2}}{\sqrt{1-\left(\frac{2\alpha}{E}+\rho^2\right)x^2}} \quad ; \quad \frac{dz}{dx} = \frac{\rho\sqrt{2\alpha/E+\rho^2}}{\sqrt{1-\rho^2x^2}} \; ,$$

hence $\frac{dy}{dx} > \frac{dz}{dx}$, for all x.

For

$$x = 0, \quad \frac{dy}{dx} = \frac{dz}{dx} = \rho\sqrt{\frac{2\alpha}{E}+\rho^2} \; , \quad y = z = 0 \; .$$

For

$$x = 1/\sqrt{2\alpha/E+\rho^2} \; , \quad \frac{dy}{dx} = \infty \; , \quad y = \rho\frac{\pi}{2} \; .$$

For

$$x = 1/\rho \; , \quad \frac{dz}{dx} = \infty \; , \quad z = \sqrt{\frac{2\alpha}{E}+\rho^2}\,\frac{\pi}{2} \; .$$

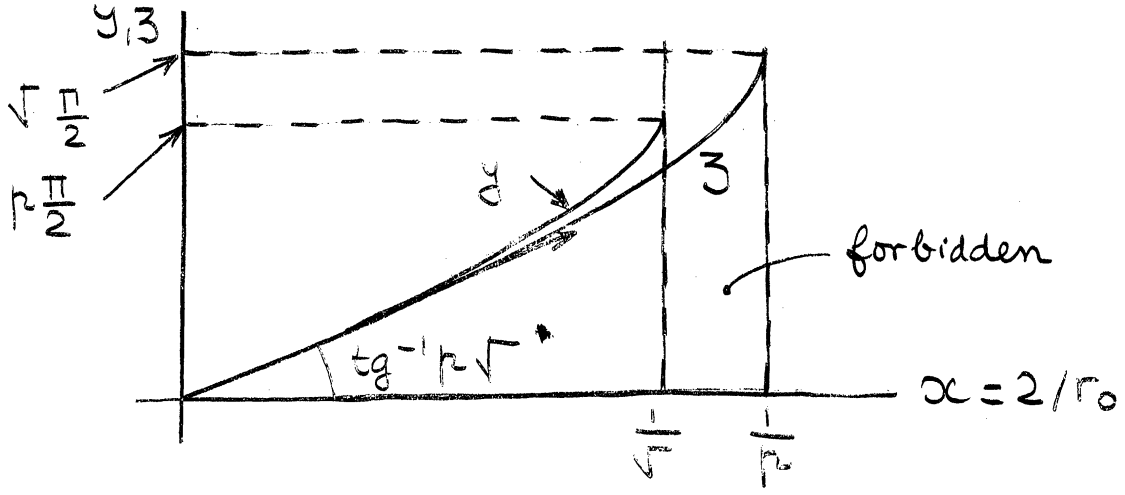

Since $dA/dx = dy/dx - dz/dx$ is > 0 for all x,

it follows that A has its highest value for

$$2/r_0 = 1/\sqrt{2\alpha/E + p^2},$$

which is

$$A_m = p\pi/2 - \sqrt{2\alpha/E + p^2}\,\sin^{-1}\left(p/\sqrt{2\alpha/E + p^2}\right).$$

Hence the highest value of β is

$$\beta_m = \frac{1}{p} A_m = \frac{\pi}{2} - \frac{1}{p}\sqrt{2\alpha/E + p^2}\,\sin^{-1}\left(p/\sqrt{2\alpha/E + p^2}\right).$$

Since

$$\sin^{-1}\left(p/\sqrt{2\alpha/E + p^2}\right) > p/\sqrt{2\alpha/E + p^2},$$

We have

$$\beta_m < \frac{\pi}{2} - \frac{1}{p}\sqrt{\quad}\,\frac{p^2}{\sqrt{\quad}} = \frac{\pi}{2} - 1.$$

Hence β is always smaller than $\frac{\pi}{2} - 1$.

APPENDIX XI

Calculation of θ_0, angle of asymptote OB with the velocity $\underline{v}_1$ at A_0 $(r = r_0/2)$

$$\theta_0 = -\left(p/\sqrt{2\alpha_u/E + p^2}\right)\beta ,$$

$$\beta = \sin^{-1}\left(\sqrt{2\alpha_u/E + p^2}\; 2/r_0\right) - (1/p)\sqrt{2\alpha_u/E + p^2}\,\sin^{-1} 2p/r_0 .$$

1) $E = 10^{-1}$ Mev; $2\alpha_u/E = 2.30 \times 10^{-2}$; $r_0 = 2.556$ Å $\cong 15a$.

i) $p = \pi/100$, $p^2 = 2.98 \times 10^{-6}$,

$2\alpha_u/E + p^2 \cong 2.30 \times 10^{-2}$; $\sqrt{(2\alpha_u/E + p^2)} \cong 1.54 \times 10^{-1}$,

$\beta \cong \sqrt{(2\alpha_u/E + p^2)}\,\frac{2}{r_0} - \frac{1}{p}\sqrt{(2\alpha_u/E + p^2)}\,\frac{2p}{r_0} = 0$,

hence $\theta_0 \cong 0$.

ii) $p = \sqrt{(r_0^2/4 - 2\alpha_u/E)}$,

$p^2 = 6.51/4 - 2.30 \times 10^{-2} = 1.605$,

$p = 1.270$,

$$\sqrt{(2\alpha_u/E + p^2)}\,\frac{2}{r_0} = 1; \quad \beta = \sin^{-1}\; 1 - \frac{1}{1.270}\;\frac{2.556}{2}\;\sin^{-1}\frac{2.540}{2.556},$$

$\beta = 1.571 - 1.007 \sin^{-1} 0.993 = 0.110$ rad;

$$\theta_0 = -\frac{1.270}{2.556/2} = -0.109 \text{ rad.}$$

$$\varphi = \pi\left(1 - \frac{1.270}{2.556/2}\right) = 2.199 \times 10^{-2} \text{ rad.}$$

Although, here, $\varphi' = 2.199 \times 10^{-2} + 0.218 = 0.240$ rad, compared to $\varphi = 2.199 \times 10^{-2}$ rad, it is probably not a very serious error to take φ instead of φ', since φ' remains a small angle. However, this treatment will slightly underestimate the interaction.

2) $E = 10^{-4}$ Mev; $\frac{2\alpha_u}{E} = 1.20$.

i) $p = \lambda/100 = 1.72 \times 10^{-3}$,

$2\alpha_u/E + p^2 \cong 1.20$; $\sqrt{(2\alpha_u/E + p^2)} = 1.095$,

$\sqrt{(2\alpha_u/E + p^2)}\,\frac{2}{r_0} = \frac{1.095 \times 2}{2.556} = 0.857$,

$\sin^{-1} 0.857 \cong 1.030$ rad .

$\beta \cong 1.030 - (1/1.72 \times 10^{-3})\, 1.095 \times 2 \times 1.72 \times 10^{-3}/2.556 =$

$1.030 - \frac{2.190}{2.556} = 0.173$ rad.

$\theta_0 = -\frac{1.72 \times 10^{-3}}{1.095}\ 0.173 = 2.72 \times 10^{-4}$ rad.

Since $\varphi = \pi\,(1 - 1.72 \times 10^{-3}/1.095) \cong \pi$, the approximation $\varphi' \cong \varphi$ is here fully justified.

ii) $p = \sqrt{(r_0^2/4 - 2\alpha_u/E)}$,

$p^2 = \frac{6.51}{4} - 1.20 = 0.428$; $p = 0.655$,

$\beta = \sin^{-1}\ 1 - \frac{1}{0.655}\ \frac{2.556}{2}\ \sin^{-1}\frac{2 \times 0.655}{2.556} \cong 0.518$ rad ,

$\theta_0 = -\frac{0.655}{2.556/2}\ 0.518 = -0.265$ rad.

$\varphi = \pi\,(1 - \frac{0.655}{2.556/2}) = 1.54$ rad.

Hence the error made by making the approximation $\varphi' \cong \varphi$ is not negligible, but still not large.

APPENDIX XII

Calculation of $(r_d)_{u,\ell}$, $(\sigma_d)_{u,\ell}$, $(\Sigma_d)_{u,\ell}$, $(\lambda_d)_{u,\ell}$ for various energies

1) $E = 10^{-4}$ Mev

$E_d/E = 25/10^2$; $\sqrt{(E_d/E)} = 1/2$; $\varphi_d = 2 \times 0.5236 = 1.0472$ rad;

$\varphi_d/\pi = 1.0472/3.1416 = 0.333$; $(1 - \varphi_d/\pi) = 0.667$;

$(1 - \varphi_d/\pi)^2 = 0.445$; $1 - (1 - \varphi_d/\pi)^2 = 0.555$;

$2\alpha_u/E = 1.20$; $(r_d)_u^2 = 1.20 \times 0.445/0.555 = 0.965$ Å^2

$(r_d)_u = 0.980$ Å $= 5.70\, a = \underline{0.384\, r_o}$

$(\sigma_d)_u = \pi \times 0.965 = 3.04$ Å$^2 = 3.04 \times 10^{-16}$ cm^2

$(\Sigma_d)_u = 8.5 \times 10^{22} \times 3.04 \times 10^{-16} = 2.58 \times 10^7$ cm^{-1}

$(\lambda_d)_u = 1/0.258$ Å $= 3.87$ Å $= 22.5\, a = \underline{1.51\, r_o}$

$(r_d)_\ell^2 / (r_d)_u^2 = 10^{-5}/6 \times 10^{-5} = 1/6$

$(r_d)_\ell = (5.7/2.45)\, a = 2.33\, a = \underline{0.157\, r_o}$

$(\lambda_d)_\ell = 6\, (\lambda_d)_u = \underline{9.06\, r_o}$

2) $E = 10^{-3}$ Mev

$E_d/E = 25/10^3$; $\sqrt{(E_d/E)} = 1.58 \times 10^{-1}$; $\varphi_d \cong 2 \times 0.1571 = 0.3142$;

$\varphi_d/\pi = 0.1$; $1 - \varphi_d/\pi = 0.9$; $(1 - \varphi_d/\pi)^2 = 0.81$; $1 - (1 - \varphi_d/\pi)^2 = 0.19$;

$$(r_d)_u^2 = \frac{6.52 \times 10^{-1} \times 0.81}{0.19} = 2.78\ \text{Å}^2;\quad (r_d)_u = 1.67\ \text{Å} = 9.7\, a = \underline{0.653\, r_o}$$

$(\sigma_d)_u = \pi \times 2.78 = 8.74$ Å$^2 = 8.74 \times 10^{-16}$ cm^2 ; $(\Sigma_d)_u = 8.5 \times 10^{22} \times 8.74 \times 10^{-16} = 7.44 \times 10^7$ cm^{-1}

$(\lambda_d)_u = 1/0.744$ Å $= 1.342$ Å $= 7.8\, a = \underline{0.525\, r_o}$

$(r_d)_\ell^2 / (r_d)_u^2 = 3.03 \times 10^{-5}/3.26 \times 10^{-4} = 9.3 \times 10^{-2}$

$(r_d)_\ell = 3.05 \times 10^{-1} \times 0.653\, r_o = \underline{0.199\, r_o}$

$(\lambda_d)_\ell = (\lambda_d)_u / 9.3 \times 10^{-2} = 10.7\, (\lambda_d)_u = \underline{5.62\, r_o}$

3) $E = 5 \times 10^{-3}$ Mev

$E_d/E = 25/5 \times 10^3 = 50 \times 10^{-4}$; $\sqrt{(E_d/E)} = 7.07 \times 10^{-2}$

$\varphi_d \cong 2 \times 0.0707 = 0.1414$; $\varphi_d/\pi = 0.045$; $1 - \varphi_d/\pi = 0.955$;

$(1 - \varphi_d/\pi)^2 = 0.910$; $1 - (1 - \varphi_d/\pi)^2 = 0.09$;

$(\rho_d)_u^2 = 3.1 \times 10^{-1} \times 0.91/9 \times 10^{-2} = 3.14$ Å^2;

$(\rho_d)_u = 1.77$ Å $= 10.3\, a = \underline{0.691\, r_o}$

$(\sigma_d)_u = \pi \times 3.14 = 9.9 \times 10^{-16}$ cm^2;

$(\Sigma_d)_u = 8.5 \times 10^{22} \times 9.9 \times 10^{-16} = 8.41 \times 10^7$ cm^{-1};

$(\lambda_d)_u = 1/0.841$ Å $= 1.188$ Å $= 6.9\, a = \underline{0.465\, r_o}$

$(\rho_d)_\ell^2/(\rho_d)_u^2 = 1.53 \times 10^{-4}/7.75 \times 10^{-4} = 1/5.06$;

$(\rho_d)_\ell = 0.691\, r_o/2.245 = \underline{0.308\, r_o}$

$(\lambda_d)_\ell = 5.06\, (\lambda_d)_u = \underline{2.35\, r_o}$

4) $E = 10^{-2}$ Mev

$E_d/E = 25/10^4$; $\sqrt{(E_d/E)} = 5 \times 10^{-2}$; $\varphi_d \cong 2 \times 5 \times 10^{-2} = 10^{-1}$;

$\varphi_d/\pi = 0.0318$; $1 - \varphi_d/\pi = 0.9682$; $(1 - \varphi_d/\pi)^2 = 0.938$;

$1 - (1 - \varphi_d/\pi)^2 = 0.062$; $(\rho_d)_u^2 = \dfrac{1.92 \times 10^{-1} \times 0.938}{0.062} = 2.91$ Å^2;

$(\rho_d)_u = 1.72$ Å $= 10\, a = \underline{0.675\, r_o}$

$(\sigma_d)_u = \pi \times 2.91 = 9.15$ Å^2;

$(\Sigma_d)_u = 8.5 \times 10^{22} \times 9.15 \times 10^{-16} = 7.78 \times 10^7$ cm^{-1};

$(\lambda_d)_u = 1/0.778$ Å $= 1.282$ Å $= 7.45\, a = \underline{0.502\, r_o}$

$(\rho_d)_\ell^2/(\rho_d)_u^2 = 2.28 \times 10^{-4}/9.60 \times 10^{-4} = 0.237$

$(\rho_d)_\ell = 0.488 \times 0.675\, r_o = \underline{0.329\, r_o}$

$(\lambda_d)_\ell = (\lambda_d)_u/0.237 = \underline{2.11\, r_o}$

5) $E = 10^{-1}$ Mev

$E_d/E = 25/10^5$; $\sqrt{(E_d/E)} = 1.58 \times 10^{-2}$; $\varphi_d \cong 2 \times 1.58 \times 10^{-2} = 0.0316$;

$\varphi_d/\pi = 0.01$; $1 - \varphi_d/\pi = 0.99$; $(1 - \varphi_d/\pi)^2 = 0.98$; $1 - (1 - \varphi_d/\pi)^2 = 0.02$

$(p_d)_u^2 = 2.3 \times 10^{-2} \times 0.98/0.02 = 1.13 \text{ Å}^2$

$(p_d)_u = 1.062 \text{ Å} = 6.18\, a = \underline{0.415\, r_o}$

$(\sigma_d)_u = \pi \times 1.13 = 3.56 \text{ Å}^2$

$(\Sigma_d)_u = 8.5 \times 10^{22} \times 3.56 \times 10^{-16} = 3.02 \times 10^7 \text{ cm}^{-1}$

$(\lambda_d)_u = 1/0.302 \text{ Å} = 3.3 \text{ Å} = 19.2\, a = \underline{1.29\, r_o}$

$(p_d)_\ell^2/(p_d)_u^2 = 6 \times 10^{-4}/1.15 \times 10^{-3} = 0.522$

$(p_d)_\ell = 0.724 \times 0.415\, r_o = \underline{0.300\, r_o}$

$(\lambda_d)_\ell = (\lambda_d)_u/0.522 = 1.94\, (\lambda_d)_u = \underline{2.51\, r_o}$

APPENDIX XIII

Mutual potential energy of two rigid charge distributions with screened potential.

Consider two non-identical atoms separated by a distance R, one at point $\underline{R}_1$, the second at point $\underline{R}_2$, with respective potentials at $\underline{r}$:

$$\phi_1 = Z_1 \varepsilon \frac{\exp -\left[\frac{|\underline{r} - \underline{R}_1|}{a_1}\right]}{|\underline{r} - \underline{R}_1|} ,$$

$$\phi_2 = Z_2 \varepsilon \frac{\exp \left[-\frac{|\underline{r} - \underline{R}_2|}{a_2}\right]}{|\underline{r} - \underline{R}_2|} .$$

The charge density is, for $|\underline{r} - \underline{R}| \neq 0$,

$$\rho = -\frac{1}{4\pi} \nabla^2 \phi \quad ; \quad \rho = \rho_1, \rho_2 \; ; \; \phi = \phi_1, \phi_2 ,$$

where

$$\nabla^2 = \frac{d^2}{d[|\underline{r} - \underline{R}|]^2} + \frac{2}{|\underline{r} - \underline{R}|} \frac{d}{d[|\underline{r} - \underline{R}|]}$$

since there is spherical symmetry.

For $\underline{r} = \underline{R}$, we can write

$$\rho_{\underline{r} = \underline{R}} = Z \varepsilon \, \delta(\underline{r} - \underline{R})$$

δ being the 3-dimensional Dirae function. This gives, correctly,

$$\int_{\text{all space}} \rho \, d^3r = \int_{\text{all space}} -\frac{1}{4\pi} \nabla^2 \phi \, d^3r + Z\varepsilon \int_{\text{all space}} \delta(\underline{r} - \underline{R}) \, d^3r$$

$$= -\frac{1}{4\pi} \int_{S \text{ at } \infty} \underline{\nabla} \phi \cdot \underline{n} \, dS + Z\varepsilon = -\frac{Z\varepsilon}{4\pi} 4\pi r^2 \frac{d}{dr} \frac{e^{-\frac{r}{a}}}{r} \Bigg|_{r=\infty} + Z\varepsilon$$

$$= Z\varepsilon .$$

Hence

$$\rho_1 = -\frac{Z_1\varepsilon}{4\pi}\left\{\frac{2\exp}{|\underline{r}-\underline{R}_1|^3} + 2\,\frac{-1}{|\underline{r}-\underline{R}_1|^2}\,\frac{-\exp}{a_1} + \frac{1}{|\underline{r}-\underline{R}_1|}\,\frac{\exp}{a_1^2}\right.$$

$$\left. + \frac{2}{|\underline{r}-\underline{R}_1|}\left[\frac{-1}{a_1}\,\frac{\exp}{|\underline{r}-\underline{R}_1|} - \frac{\exp}{|\underline{r}-\underline{R}_1|^2}\right]\right\} + Z_1\varepsilon\,\delta(\underline{r}-\underline{R}_1)$$

$$\rho_1 = -\frac{Z_1\varepsilon}{4\pi}\,\frac{\exp(-|\underline{r}-\underline{R}_1|/a_1)}{a_1^2\,|\underline{r}-\underline{R}_1|} + Z_1\varepsilon\,\delta(\underline{r}-\underline{R}_1)$$

$$\rho_2 = -\frac{Z_2\varepsilon}{4\pi}\,\frac{\exp(-|\underline{r}-\underline{R}_2|/a_2)}{a_2^2\,|\underline{r}-\underline{R}_2|} + Z_2\varepsilon\,\delta(\underline{r}-\underline{R}_2)\ .$$

The interaction energy is

$$V = \frac{1}{2}\int_{\text{all sp.}}(\phi_1\rho_2 + \phi_2\rho_1)\,d^3r = \int_{\text{all sp.}}\phi_1\rho_2\,d^3r = \int_{\text{all sp.}}\phi_2\rho_1\,d^3r \qquad (1)$$

$$V = \int_{\text{all sp.}} Z_1\varepsilon\,\frac{\exp(-|\underline{r}-\underline{R}_1|/a_1)}{|\underline{r}-\underline{R}_1|}\,\frac{-Z_2\varepsilon}{4\pi}\left[\frac{\exp(-|\underline{r}-\underline{R}_2|/a_2)}{a_2^2\,|\underline{r}-\underline{R}_2|} - 4\pi\,\delta(\underline{r}-\underline{R}_2)\right]d^3r$$

$$= -Z_1Z_2\varepsilon^2\left[-\frac{\exp\left(-\frac{R}{a_1}\right)}{R} + \frac{1}{4\pi a_2^2}\int_{\text{all sp.}}\frac{\exp\left(-\frac{|\underline{r}-\underline{R}_1|}{a_1}\right)}{|\underline{r}-\underline{R}_1|}\,\frac{\exp\left(-\frac{|\underline{r}-\underline{R}_2|}{a_2}\right)}{|\underline{r}-\underline{R}_2|}\,d^3r\right]$$

From (1), we also have

$$V = -Z_1Z_2\varepsilon^2\left[-\frac{\exp\left(-\frac{R}{a_2}\right)}{R} + \frac{1}{4\pi a_1^2}\int_{\text{all sp}}\right]\ .$$

Hence

$$\frac{1}{4\pi}\left(\frac{1}{a_1^2}-\frac{1}{a_2^2}\right)\int_{\text{all sp}} = \frac{1}{R}\left[\exp\left(-\frac{R}{a_2}\right) - \exp\left(-\frac{R}{a_1}\right)\right]$$

$$\int_{\text{all sp}} = \frac{4\pi a_1^2a_2^2}{R(a_2^2-a_1^2)}\left[\exp\left(-\frac{R}{a_2}\right) - \exp\left(-\frac{R}{a_1}\right)\right]$$

So that

$$V = -Z_1 Z_2 \varepsilon^2 \left\{ -\frac{\exp\left(-\frac{R}{a_1}\right)}{R} + \frac{a_1^2}{R(a_2^2-a_1^2)}\left[\exp\left(-\frac{R}{a_2}\right) - \exp\left(-\frac{R}{a_1}\right)\right]\right.$$

$$= \frac{Z_1 Z_2 \varepsilon^2}{R(a_2^2-a_1^2)}\left[a_2^2 \exp\left(-\frac{R}{a_1}\right) - a_1^2 \exp\left(-\frac{R}{a_2}\right)\right] .$$

Now make $Z_1, Z_2 \longrightarrow Z$; $a_1, a_2 \longrightarrow a$

$$\exp\left(-\frac{R}{a_1}\right) = \exp\left[-\frac{R}{(a_1-a)+a}\right] = \exp\left[-\frac{R}{a\left(1+\frac{a_1-a}{a}\right)}\right]$$

$$\xrightarrow[\varepsilon_1 = a_1 - a \to 0]{} \exp\left[-\frac{R}{a}\left(1-\frac{\varepsilon_1}{a}\right)\right]$$

$$= \exp\left(-\frac{R}{a}\right)\exp\left(\varepsilon_1 \frac{R}{a^2}\right)$$

$$\xrightarrow[\varepsilon_1 \to 0]{} \left(1+\varepsilon_1 \frac{R}{a^2}\right)\exp\left(-\frac{R}{a}\right) ;$$

call ε_2 the difference $a_2 - a$, then

$$V = \frac{Z^2\varepsilon^2}{R} \lim_{\varepsilon_1, \varepsilon_2 \to 0} \frac{a_2^2(1+\varepsilon_1 R/a^2) - a_1^2(1+\varepsilon_2 R/a^2)}{a_2^2 - a_1^2} \exp\left(-\frac{R}{a}\right)$$

$$= \frac{Z^2\varepsilon^2}{R}\exp\left(-\frac{R}{a}\right) \lim_{\varepsilon_1, \varepsilon_2 \to 0}\left[1 + \frac{R}{a^2}\frac{a_2^2\varepsilon_1 - a_1^2\varepsilon_2}{a_2^2 - a_1^2}\right] ;$$

$$a_2^2\varepsilon_1 - a_1^2\varepsilon_2 = a_2^2(a_1-a) - a_1^2(a_2-a)$$

$$= a_1 a_2 (a_2 - a_1) + a(a_1^2 - a_2^2) ;$$

$$\frac{R}{a^2}\frac{a_2^2\varepsilon_1 - a_1^2\varepsilon_2}{a_2^2 - a_1^2} = \frac{R}{a^2}\left(\frac{a_1 a_2}{a_2+a_1} - a\right) ;$$

$$\lim_{a_1, a_2 \to a} = \frac{R}{a^2}\left(\frac{a^2}{2a} - a\right) = -\frac{R}{2a}$$

Finally,

$$V(R) = \frac{Z^2\varepsilon^2}{R}\left(1 - \frac{R}{2a}\right)\exp\left(-\frac{R}{a}\right) .$$

Replacing R by r gives Equation (5) of the text.

APPENDIX XIV

Energy transfer in the impulse approximation, for the interaction energy used by Brinkman.

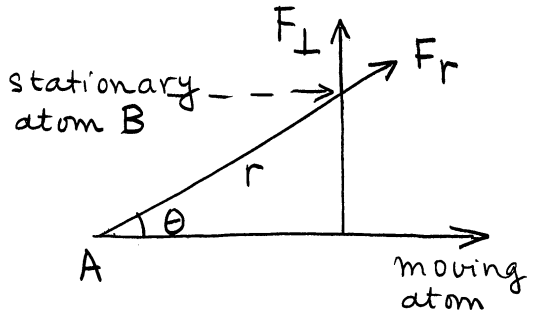

Impulse

$$I = \int_{-\infty}^{\infty} F_\perp \, dt = 2 \int_0^{\infty} \left(\frac{M}{2E}\right)^{\frac{1}{2}} F_\perp \, dx$$

M mass, E kinetic energy of disturbing particle.

$$F_r = -\frac{dV}{dr} \quad , \text{ with } V = \frac{Z^2\varepsilon^2}{r}\left(1-\frac{r}{2a}\right)\exp\left(-\frac{r}{a}\right) ;$$

$$F_r = -Z^2\varepsilon^2 \exp\left(-\frac{r}{a}\right)\left(-\frac{1}{r^2} - \frac{1}{ar} + \frac{1}{2a^2}\right) ;$$

$$F_\perp = F_r \sin\theta = \frac{b}{r} F_r \; ; \; x^2 = r^2 - b^2 \; ; \; dx = r(r^2-b^2)^{-\frac{1}{2}} dr ;$$

$$F_\perp \, dx = F_r \, b \, (r^2-b^2)^{-\frac{1}{2}} dr .$$

Hence

$$I = 2\left(\frac{M}{2E}\right)^{\frac{1}{2}} b \, Z^2\varepsilon^2 \left(J_1 + J_2 + J_3\right) ;$$

$$J_1 = -\frac{1}{2a^2} \int_b^{\infty} \frac{e^{-r/a}}{(r^2-b^2)^{1/2}} \, dr ;$$

$$J_2 = \frac{1}{a} \int_b^{\infty} \frac{e^{-r/a}}{r(r^2-b^2)^{1/2}} \, dr ;$$

$$J_3 = \int_b^{\infty} \frac{e^{-r/a}}{r^2(r^2-b^2)^{1/2}} \, dr .$$

Denote by L a LaPlace transform. Then

$$J_1 = -\frac{1}{2a^2} L\{G(r)\} \quad \text{, with transform variable } 1/a\text{, where}$$

$$G(r) = 0 \qquad 0 < r < b$$
$$= 1/(r^2-b^2)^{1/2} \qquad b < r < \infty .$$

From Churchill, Appendix III, p. 301,

$$f(s) = K_0(ks) = L\{F(t)\}$$
$$F(t) = 0 \qquad 0 < t < k$$
$$= (t^2-k^2)^{-1/2} \qquad k < t$$

Hence

$$L\{G(r)\} = K_0\left(\frac{b}{a}\right),$$

K_0, modified Bessel function, 2nd kind, zeroth order.

Now, let $1/a = x$. Then

$$J_2 = x\int_b^\infty \frac{e^{-rx}}{r(r^2-b^2)^{1/2}}\,dr \quad ; \quad J_1 = -\frac{x^2}{2}\int_b^\infty \frac{e^{-rx}}{(r^2-b^2)^{1/2}}\,dr$$
$$= -\frac{x^2}{2} K_0(bx).$$

We have $\frac{2J_1}{x^2} = \frac{d}{dx}\left(\frac{J_2}{x}\right)$; hence

$$J_2 = -x\int_\infty^x K_0(bx')\,dx' \quad \text{, where the limit } \infty \text{ is}$$

taken because $J_2 = 0$ at $x = \infty$.

From this,

$$J_2 = \frac{1}{a}\int_{1/a}^\infty K_0(bx)\,dx \quad .$$

We also see that

$$\frac{dJ_3}{dx} = -\frac{J_2}{x} = -\int_{1/a}^\infty K_0(bx)\,dx .$$

For $x=\infty$, $J_3 = 0$, hence

$$J_3 = -\int_{\infty}^{1/a} dy \int_{y}^{\infty} K_0(bx)\,dx .$$

But, it can be shown that

$$\int_{\alpha}^{\infty} dy \int_{y}^{\infty} f(x)\,dx = -\int_{\alpha}^{\infty} (\alpha - x) f(x)\,dx .$$

Hence

$$J_3 = -\int_{1/a}^{\infty} \left(\frac{1}{a} - x\right) K_0(bx)\,dx$$

$$J_2 + J_3 = \int_{1/a}^{\infty} x\, K_0(bx)\,dx = \frac{1}{ab} K_1\left(\frac{b}{a}\right) .$$

Finally,

$$I = 2\left(\frac{M}{2E}\right)^{1/2} b Z^2 \varepsilon^2 \left[-\frac{1}{2a^2} K_0\left(\frac{b}{a}\right) + \frac{1}{ab} K_1\left(\frac{b}{a}\right)\right]$$

$$= \frac{Z^2\varepsilon^2}{a}\left(\frac{2M}{E}\right)^{1/2}\left[K_1\left(\frac{b}{a}\right) - \frac{1}{2}\frac{b}{a} K_0\left(\frac{b}{a}\right)\right] .$$

The energy T transfered to the stationary atom is

$$T = \frac{I^2}{2M} = \frac{(Z^2\varepsilon^2)^2}{a^2}\frac{1}{E} F\left(\frac{b}{a}\right),$$

where $F(x) = \left[K_1(x) - (x/2) K_0(x)\right]^2$, which is Equation (25) of the text.

With $a = c a_h Z^{-1/3}$; a_h Bohr radius for hydrogen, i.e.

$$a_h = \frac{\varepsilon^2}{2R_h} \quad ; \qquad R_h \text{ Rydberg energy}$$

for hydrogen, we can write

$$\left(\frac{Z^2\varepsilon^2}{a}\right)^2 = \left(\frac{Z^2\varepsilon^2}{c a_h Z^{-1/3}}\right)^2 = \left(\frac{Z^{7/3}}{C} 2R_h\right)^2 .$$

Hence

$$T = 4 \frac{Z^{14/3}}{c^2} \frac{R_h^2}{E} F\left(\frac{b}{a}\right) \qquad (1)$$

The displacement cross section is

$$\sigma_d = \pi b^2$$

with b such that T, given by (1), equals E_d, i.e.

$$b = a F^{-1}\left(\frac{c^2 E E_d}{4 Z^{14/3} R_h^2}\right),$$

F^{-1} = inverse of F.

Hence

$$\sigma_d = \pi a^2 \left[F^{-1}\left(\frac{c^2 E E_d}{4 R_h^2 Z^{14/3}}\right)\right]^2,$$

which is Equation (23) of the text.

APPENDIX XV

Average number of atoms displaced per primary, for primary energy in the range 1.5 Mev - 2.3×10^4 ev.

$$x_{1m} = \frac{1.5 \times 10^6}{25} - 1 \cong 6 \times 10^4 ,$$

$$x_{1tr} = \frac{2.3 \times 10^4}{25} - 1 \cong 9.2 \times 10^2 ,$$

$$\sigma(E', x_1)\,dx_1 = \frac{\pi b_0^2}{4} E_d (1 + x_{1m}) \frac{E_d\, dx_1}{E_d^2 (1 + x_1)^2}$$

$$= \frac{\pi b_0^2}{4} (1 + x_{1m}) \frac{dx_1}{(1 + x_1)^2} ,$$

$$\bar{\nu} = \frac{\displaystyle\int_{9.2\times10^2}^{6\times10^4} 0.561 (1 + x_1) \frac{dx_1}{(1 + x_1)^2}}{\displaystyle\int_0^{6\times10^4} \frac{dx_1}{(1 + x_1)^2}} ,$$

the denominator being proportional to the total probability of displacing interaction.

$$\bar{\nu} = 0.561 \frac{\text{Log} \dfrac{6 \times 10^4 + 1}{9.2 \times 10^2 + 1}}{1 - \dfrac{1}{6 \times 10^4}} = 0.561 \times 4.175 = \underline{2.34}$$

APPENDIX XVI

Number of defect pairs per primary in displacement spikes.

$$J_1 = 20\,\frac{E_m - E_{tr}}{E_{tr}\,E_m} \Big/ \frac{E_m - E_d}{E_d\,E_m} + 10^{-3}\,E_d\,E_m\left[\mathrm{Ln}\,(E_{tr}/E_d)\right]/(E_m - E_d)\,,$$

$$J_1 = 20\,\frac{1.5 \times 10^6 - 2.3 \times 10^4}{1.5 \times 10^6 - 25} \times \frac{25}{2.3 \times 10^4} + 10^{-3} \times 25 \times 1.5 \times 10^6 \times \frac{\mathrm{Log}\ 2.3 \times 10^4/25}{1.5 \times 10^6 - 25}\,,$$

$$J_1 \cong 2 \times 10^{-2} + 2.5 \times 10^{-2}\ \mathrm{Log}\ 9.2 \times 10^2 =$$

$$10^{-2}\,(2 + 17) = \underline{1.9 \times 10^{-1}}$$

APPENDIX XVII

Average energy transfer in a displacing collision, for the interaction cross section adopted

The cross section adopted is

$$\sigma(E,T)dT = -2\pi p\,dp = -\pi \frac{2\alpha}{E}\, d\, \frac{\left(1-\frac{2}{\pi}\sin^{-1}\sqrt{T/E}\right)^2}{1-\left(1-\frac{2}{\pi}\sin^{-1}\sqrt{T/E}\right)^2} \quad ,$$

for transfer of energy in dT about T; p goes from ∞ to o, T from o to E (see Chapter IV of text). It is clear that the frequency function $\sigma(E,T)$ is infinite for T = o, i.e. for no energy transfered. Low energy transfers are strongly favored. Actually, we recall that our mathematical model does not allow p to go to infinity.

The average energy transfered in a displacing collision is

$$\bar{T} = \frac{\int_E^{E_d} T\, d\, \frac{\left(1-\frac{2}{\pi}\sin^{-1}\sqrt{T/E}\right)^2}{1-\left(1-\frac{2}{\pi}\sin^{-1}\sqrt{T/E}\right)^2}}{\int_E^{E_d} d\, \frac{\left(1-\frac{2}{\pi}\sin^{-1}\sqrt{T/E}\right)^2}{1-\left(1-\frac{2}{\pi}\sin^{-1}\sqrt{T/E}\right)^2}} \quad .$$

It is perhaps more convenient to place the differential element in the form

$$f(T)dT = \frac{-2}{\pi E}\, \frac{1}{\left[1-\left(1-\frac{2}{\pi}\sin^{-1}\sqrt{T/E}\right)^2\right]^2}\, \frac{1}{\sqrt{\frac{T}{E}\left(1-\frac{T}{E}\right)}} \left(1-\frac{2}{\pi}\sin^{-1}\sqrt{\frac{T}{E}}\right) dT \, .$$

Values of f (T)

T/E	0	10^{-6}	10^{-4}	10^{-2}	4×10^{-2}	1.6×10^{-1}	4.9×10^{-1}	8.1×10^{-1}	9.9×10^{-1}	1
$1 - \frac{2}{\pi}\sin^{-1}\sqrt{\ }$	1	0.999	0.994	0.934	0.87	0.75	0.51	0.38	0.06	0
$(1 - \frac{2}{\pi}\sin^{-1}\sqrt{\ })^2$	1	0.998	0.99	0.87	0.76	0.56	0.26	0.14	3.6×10^{-3}	0
$1 - (1 - \frac{2}{\pi}\sin^{-1}\sqrt{\ })^2$	0	0.002	0.01	0.13	0.24	0.44	0.74	0.86	1	1
$\left[1 - (1 - \frac{2}{\pi}\sin^{-1}\sqrt{\ })^2\right]^2$	0	2×10^{-6}	10^{-4}	1.7×10^{-2}	5.8×10^{-2}	1.9×10^{-1}	5.5×10^{-1}	7.4×10^{-1}	1	1
$\frac{1}{\sqrt{\ }}(1 - \sin^{-1}\sqrt{\ })$	∞	10^3	10^2	10	4.4	2.04	1	1	0.64	$\frac{2}{\pi}$
$\frac{\pi E}{2}$ f (T)	∞	5×10^8	10^6	6×10^2	76	10	2	1.4	0.64	$\frac{2}{\pi}$

For E = 1 Mev

for $T = 10^{-6}$ Mev, the integrand of the upper integral takes the value

$$10^{-6} \times 5 \times 10^{8} = 5 \times 10^{2} \ ,$$

for $T = 10^{-4}$ Mev,

$$10^{-4} \times 10^{6} = 10^{2} \ ,$$

for $T = 10^{-2}$ Mev,

$$10^{-2} \times 6 \times 10^{2} = 6 \ ,$$

for $T = 1.6 \times 10^{-1}$ Mev,

$$1.6 \times 10^{-1} \times 10 = 1.6 \ .$$

So that most of the contribution to the integrals is due to the range $T \ll E$.

Then we can approximate:

$$\bar{T} \cong \frac{\int_{E}^{E_d} -\frac{2}{\pi E} \frac{T}{\left(\frac{4}{\pi}\sqrt{T/E}\right)^2} \frac{dT}{\sqrt{T/E}}}{\int_{E}^{E_d} -\frac{2}{\pi E} \frac{1}{\left(\frac{4}{\pi}\sqrt{T/E}\right)^2} \frac{dT}{\sqrt{T/E}}} = \frac{\int_{E_d}^{E} dT/\sqrt{T}}{\int_{E_d}^{E} dT/(T\sqrt{T})}$$

$$= \frac{2\left(\sqrt{E} - \sqrt{E_d}\right)}{2\left(1/\sqrt{E_d} - 1/\sqrt{E}\right)} \ ,$$

i.e.

$$\bar{T} \cong \sqrt{E_d}\sqrt{E} = 5\sqrt{E} \ , \quad \bar{T}, E \text{ in ev.}$$

It is seen that the energy transfer is small, which justifies the approximation made. In fact, the denominator is better approximated then the numerator, so that $\bar{T}$ is somewhat underestimated for $E \gg E_d$.

For $E \overset{\sim}{=} E_d$, the approximation is not valid. If employed, it certainly overestimates $\bar{T}$ seriously, since $\bar{T}$ = 25 ev requires E = 25 ev.

APPENDIX XVIII

Fraction of primaries, average number of displacements per primary, and fraction of atoms displaced in the irradiation of copper by 12 Mev deuterons.

Differential cross section for energy transfer from charged particles to lattic atoms:

$$\sigma(E',E)\,dE = \frac{\pi b^2}{4} E_m \frac{dE}{E^2} \qquad (1),$$

where E' is the charged particle energy, E the energy transfered, E_m the maximum of E, b the distance of closest approach; b is given by

$$\frac{Z_0 Z \varepsilon^2}{b} = \frac{1}{2} \mu v^2 ,$$

μ = reduced mass = $\frac{MA}{M+A}$;

M mass of the charged particle;

A mass of the lattice atom;

Z atomic number of the lattice atoms;

Z_0 atomic number of the charged particle;

v intial velocity of the charged particle, i.e. related to E' by

$$E' = \frac{1}{2} M v^2 .$$

Since elastic collisions are assumed,

$$E_m = \frac{4MA}{(M+A)^2} E' .$$

Integrating (1) between E_d (minimum value of E for an atomic displacement) and E_m, one obtains the atom cross section for production

of primaries by charged particles, namely

$$\sigma_r = \frac{\pi b^2}{4} E_m \left(\frac{1}{E_d} - \frac{1}{E_m}\right) \cong \frac{\pi b^2}{4} \frac{E_m}{E_d} ,$$

$$\sigma_r = \frac{\pi}{4} 4 Z_0^2 Z^2 \varepsilon^4 \frac{1}{(Mv^2)^2} \frac{4MA}{(M+A)^2} \frac{E'}{E_d} .$$

We have $\varepsilon^2/2a_h = R_h$; a_h Bohr radius for hydrogen, R_h Rydberg energy for hydrogen.

Hence we can write

$$\sigma_r = \frac{\pi Z_0^2 Z^2}{\frac{A^2}{(M+A)^2} 4E'^2} R_h^2 4a_h^2 \frac{4MA}{(M+A)^2} \frac{E'}{E_d} ,$$

$$\sigma_r = 4\pi a_h^2 \frac{M}{A} \frac{Z_0^2 Z^2 R_h^2}{E' E_d} .$$

M and A can be taken as mass numbers, since they only enter through their ratio.

Write

$$\sigma_r = \frac{D}{E'},$$

with

$$D = 4\pi a_h^2 \frac{M}{A} \frac{Z_0^2 Z^2 R_h^2}{E_d} ,$$

M,A, mass numbers of particle and atom, respectively.

Now, admit, after Seitz and Koehler(9), the following formula for the range of the charged particles in the sample

$$X(E') = C E'^{\gamma}$$

with $\gamma = 1.63$ and C another constant.

If N is the atomic density, $N\sigma_r(x)$ is the probability, per unit path, for small paths, at x, that a bombarding particle will form a primary.

If Φ is the integrated charged particle flux (i.e. in particles x cm^{-2}), the number of primaries formed per unitvolume at x is $\Phi N \sigma_r(x)$.

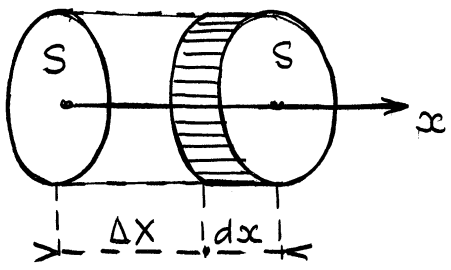

S being an area perpendicular to the beam, the number of primaries formed in the volume defined by S and a length equal to the drop ΔX of range is

$$\Phi N S \int_{X}^{X-\Delta X} \sigma_r(x)\, dx$$

The corresponding number per atom in the volume is obtained by dividing by $NS\Delta X$, so that

$$n_{prim} = \frac{\Phi}{\Delta X} \int_{X}^{X-\Delta X} \sigma_r(x)\, dx = \frac{\Phi}{\Delta X} \int_{X-\Delta X}^{X} \sigma_r(X')\, dX',$$

where X' is a range (hence $dX' = -dx$).

Using the formula for the range,

$$n_{prim} = b \frac{\Phi}{\Delta X} \int_{X-\Delta X}^{X} \frac{dX'}{E''} = b \frac{\Phi}{\Delta X} \int_{X-\Delta X}^{X} \left(\frac{X'}{c}\right)^{-\frac{1}{\gamma}} dX' \qquad (2)$$

Let ΔX be the thickness of the sample and assume it is smaller than the range X of the particles at energy E'.

Integrate (2)

$$n_{prim} = \frac{\Phi}{\Delta X} b \frac{c}{-\frac{1}{\gamma}+1} \left[\left(\frac{X'}{c}\right)^{-\frac{1}{\gamma}+1}\right]_{X-\Delta X}^{X}$$

$$= \frac{\Phi}{\Delta X} b \frac{c\gamma}{\gamma-1} \left[\left(\frac{X}{c}\right)^{\frac{\gamma-1}{\gamma}} - \left(\frac{X-\Delta X}{c}\right)^{\frac{\gamma-1}{\gamma}}\right],$$

$$n_{prim} = \frac{\Phi}{\Delta X} b \frac{c\gamma}{\gamma-1} \left(\frac{X}{c}\right)^{\frac{\gamma-1}{\gamma}} \left[1-\left(1-\frac{\Delta X}{X}\right)^{\frac{\gamma-1}{\gamma}}\right] ,$$

$$= \frac{\Phi}{\Delta X} b \frac{\gamma}{\gamma-1} \frac{X}{E'^{\gamma}} E'^{\gamma-1} \left[1-\left(1-\frac{\Delta X}{X}\right)^{\frac{\gamma-1}{\gamma}}\right] ,$$

$$= \frac{\Phi}{\Delta X} b \frac{\gamma}{\gamma-1} \frac{X}{E'} \left[1-\left(1-\frac{\Delta X}{X}\right)^{\frac{\gamma-1}{\gamma}}\right] .$$

Now expand the quantity between brackets, keeping up to terms in $\left(\frac{\Delta X}{X}\right)^3$;

$$n_{prim} = \frac{\Phi}{\Delta X} b \frac{\gamma}{\gamma-1} \frac{X}{E'} \left\{1-\left[1-\frac{\gamma-1}{\gamma}\left(\frac{\Delta X}{X}\right)+\frac{1}{2}\left(\frac{\gamma-1}{\gamma}\right)\left(\frac{\gamma-1}{\gamma}-1\right)\times\right.\right.$$

$$\left.\times\left(-\frac{\Delta X}{X}\right)^2+\frac{1}{6}\left(\frac{\gamma-1}{\gamma}\right)\left(\frac{\gamma-1}{\gamma}-1\right)\left(\frac{\gamma-1}{\gamma}-2\right)\left(-\frac{\Delta X}{X}\right)^3\right.$$

$$\left.+ \text{---}\right] ,$$

$$= \frac{\Phi}{\Delta X} b \frac{\gamma}{\gamma-1} \frac{X}{E'} \left[\frac{\gamma-1}{\gamma}\left(\frac{\Delta X}{X}\right)+\frac{1}{2}\frac{\gamma-1}{\gamma}\frac{1}{\gamma}\left(\frac{\Delta X}{X}\right)^2+\frac{1}{6}\frac{\gamma-1}{\gamma}\frac{1}{\gamma}\frac{\gamma+1}{\gamma}\left(\frac{\Delta X}{X}\right)^3\right.$$

$$\left.+ \text{---}\right] ,$$

$$n_{prim} = \Phi \frac{b}{E'} \left[1+\frac{1}{2\gamma}\left(\frac{\Delta X}{X}\right)+\frac{\gamma+1}{6\gamma^2}\left(\frac{\Delta X}{X}\right)^2+ \text{--}\right] \qquad (3) .$$

Recall that this is correct to the third power of $\left(\frac{\Delta X}{X}\right)$, and for a thin target, i.e. $\Delta X < X$; ΔX is the thickness of the sample, X the initial range of the bombarding charged particles.

Note an error, relative to the order which (3) is valid, in Seitz and Koehler's review article.(9)

Admit Snyder and Neufeld[3] result that, for $E \gg E_d$, the number of atoms displaced per primary of energy E before release is

$$\nu(E) = 0.561 \left(x_1 + 1 \right)$$

where $x_1 = (E - E_d)/E_d$.

The probability to get a primary with energy in dE about E in a collision of the bombarding particles is measured by

$$\sigma(E', E)\, dE = \frac{\pi b^2}{4} E_m \frac{dE}{E^2} .$$

So that the average of ν is

$$\bar{\nu} = 0.561 \int_{E_d}^{E_m} (x_1 + 1) \frac{dE}{E^2} \Big/ \int_{E_d}^{E_m} \frac{dE}{E^2}$$

$$= 0.561 \int_0^{x_{1m}} \frac{dx_1}{1 + x_1} \Big/ \int_0^{x_{1m}} \frac{dx_1}{(1 + x_1)^2})$$

where x_{1m} is the maximum of x_1, i.e.

$$x_{1m} = \frac{E_m}{E_d} - 1 \cong \frac{E_m}{E_d} .$$

This yields

$$\bar{\nu} = 0.561 \frac{1 + x_{1m}}{x_{1m}} \operatorname{Log} (1 + x_{1m}) = 0.561 \operatorname{Log} x_{1m} .$$

Note also an error in Seitz and Koehler's[9] review article, on this result.

The fraction of atoms displaced is

$$C = \bar{\nu}\, n_{prim} \cong 0.561 \operatorname{Log} x_{1m}\, \Phi \frac{D}{E'} \left[1 + \frac{1}{2\gamma} \left(\frac{\Delta X}{X} \right) + \frac{\gamma + 1}{6\gamma^2} \left(\frac{\Delta X}{X} \right)^2 \right] .$$

For the low temperature experiment[8], thin wires of 5 mils = 0.13 mm diameter, of Cu, placed perpendicularly to the beam, were irradiated by 12 Mev deuterons. The flux was $\Phi = 7 \times 10^{16}$ deuts x cm^{-2} at

maximum exposure. The range of 12 Mev deuterons in Cu is 0.2 mm, so that

$$\Delta X = 0.13 \text{ mm} < X = 0.2 \text{ mm}$$

and approximation (3) is certainly very good.

$$\mathfrak{H} = 4\pi (0.531 \times 10^{-8})^2 \frac{2}{63} \frac{1(29)^2(13.54)^2}{25} = 0.68 \times 10^{-19} \text{ Mev x cm}^2$$

The bracket has for value

$$1 + \frac{1}{2 \times 1.63} \frac{0.13}{0.2} \frac{1}{6} \frac{2.63}{(1.63)^2} \left(\frac{0.13}{0.2}\right)^2 = 1.25 ,$$

$$n_{prim} = \frac{7 \times 10^{16} \times 0.68 \times 10^{-19}}{12} \times 1.25 = \underline{4.9 \times 10^{-4}} ,$$

$$\alpha_{lm} = \frac{1}{25} \frac{4 \times 63 \times 2}{(63 + 2)^2} \times 12 \times 10^6 = 5.7 \times 10^4 ,$$

$$\overline{Q} = \underline{6.16} .$$

Hence $$C = \underline{3.04 \times 10^{-3}} .$$

APPENDIX XIX

Calculation of the coefficient β of radiation anneal

β is given by

$$1.32 \times 10^{-1} = 2.7 \times 10^{-18} \frac{1}{\beta} (1 - e^{-\beta \times 7 \times 10^{16}})$$

or

$$e^{-7 \times 10^{16} \beta} = 1 - 4.9 \times 10^{16} \beta$$

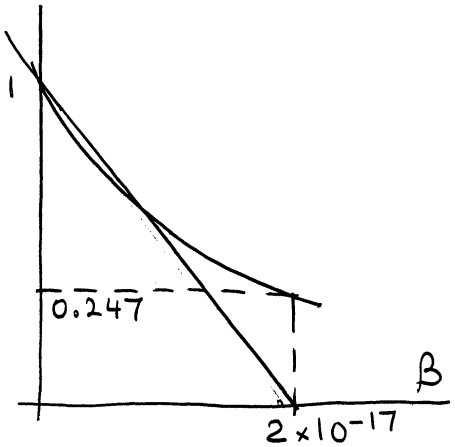

For $\beta = 0$, the two sides equal 1. The right side is zero for $\beta = \frac{1}{4.9} \times 10^{-16} \cong 2 \times 10^{-17}$. For this value of β, $e^{-7 \times 10^{16} \beta} = e^{-1.4} = 0.247$.

Try $\beta = 0.5 \times 10^{-17}$; $e^{-7 \times 10^{16} \beta} = e^{-0.35} \cong 0.7$,

$1 - 4.9 \times 10^{16} \beta = 1 - 4.9 \times 0.5 \times 10^{-1} = 0.755$.

Hence we can accept $\beta \cong \underline{0.5 \times 10^{-17}}$

APPENDIX XX

Upper energy at which classical approach remains valid in light metals

The condition of validity for classical approach is

$$\lambda \ll b_0 ,$$

where b_0 is the distance of closest approach.

Hence, since, at high energy, the potential must be practically Coulombian at closest approach,

$$Z^2\varepsilon^2 / b_0 = E .$$

The condition is $\hbar / \sqrt{(2A \times 1.67 \times 10^{-24} E)} \ll Z^2\varepsilon^2 / E$

A mass number, Z atomic number of metal, E energy of the knock-on (in ergs).

The maximum value of E is

$$E_m = \frac{4AM}{(A+M)^2} E'$$

M mass number of bombarding particle, E' its energy (ergs), assuming elastic collision.

Hence, we must have

$$\frac{\hbar}{\sqrt{3.34 \times 10^{-24} A}} \frac{2}{M+A} \sqrt{AM} \sqrt{E'} \ll Z^2\varepsilon^2 ,$$

or

$$E' \ll \frac{(M+A)^2}{4M} \frac{3.34 \times 10^{-24}}{\hbar^2} (Z^2\varepsilon^2)^2$$

For 4 Be 9 and deuterons (M = 2)

$$E' \ll \frac{(11)^2}{8} \frac{3.34 \times 10^{-24}}{1.1 \times 10^{-54}} \left[16 \times (4.8)^2 \times 10^{-20} \right]^2$$

$$= 46 \times 10^{32} \times 13.7 \times 10^{-36} \text{ ergs}$$

$$= 6.3 \times 10^{-2} \text{ ergs} = \frac{6.3 \times 10^{-2}}{1.6 \times 10^{-6}} = 3.94 \times 10^4 \text{ Mev}$$

Hence, classical treatment is valid, for deuteron irradiation be Be, even for deuteron energy of the order of, say, 20 Mev.

It is clear that it is also valid for pile neutron irradiation of Be.

APPENDIX XXI

Variation of the fraction of primary knock-ons with Z and A in charged particle irradiation.

Return to Appendix XVIII, Equation (3). We see that, for a given irradiation, i.e. the same Φ and E',

$$n_{prim} \sim \eta \sim \frac{M}{A} Z_0^2 Z^2,$$

M and Z_0 mass and atomic numbers of bombarding particle, A and Z mass and atomic numbers of the sample irradiated.

Hence, for the same bombarding particles and different samples,

$$n_{prim} \sim \frac{Z^2}{A}$$

which is the proportionality claimed in the text. This result was first obtained by Seitz.(30)

APPENDIX XXII

Solution of Snyder and Neufeld primary equation and associated problems.

Snyder and Neufeld primary equation is

$$x_1 \varphi(x_1) = \int_0^{x_1} \varphi(x_1')\, dx_1' + \int_0^{x_1-1} \varphi(x_2)\, dx_2 \qquad (1)$$

By differentiation, one obtains the equivalent differential equation with boundary condition:

$$x_1 \varphi'(x_1) = \varphi(x_1 - 1) \,, \qquad (2)$$

$$\varphi(x_1) = 1 \,, \quad 0 < x_1 < 1 \qquad (3)$$

where prime means derivative.

Take $1 < x_1 < 2$, hence $0 < x_1 - 1 < 1$, then, in this range,

$$\varphi'(x_1) = 1/x_1$$

and

$$\varphi(x_1) = \mathrm{Log}\, x_1 + C \,,$$

$$\varphi(1) = C = 1 \,,$$

$$\varphi(x_1) = 1 + \mathrm{Log}\, x_1 \,.$$

If the boundary condition (3) is disregarded, (2) admits a solution

$$\varphi(x_1) = a\,(1 + x_1) \,, \quad a \text{ ct},$$

which must be the asymptotic solution for $x_1 \gg 1$, since, then, (2) reduces to

$$\varphi'(x_1) / \varphi(x_1) = 1/x_1$$

which has the solution $\varphi(x_1) = C(x_1)$.

We can approximately determine the constant a in the following way $\psi(2) = 1 + \text{Log } 2 = 3a$, hence $a = \underline{0.564}$

A correct numerical treatment(3) yields $a = 0.561$.

The curve of $\psi(x_1)$ obtained numerically is reproduced in the diagram next page.

Note that (2) can be treated by LaPlace transform. Using the relations

$$L\{t^n Y(t)\} = (-1)^n y^{(n)}(s),$$

$$L\{t^n Y'(t)\} = (-1)^n \frac{d^n}{ds^n} L\{Y'(t)\},$$

$$L\{Y'(t)\} = s\,y(s) - Y(0)$$

between the function $Y(t)$ and its transform $y(s)$, calling $\mu(s)$ the transform of $\psi(x_1)$, (2) transforms into

$$-\mu(s) - s\mu'(s) = e^{-s}\mu(s).$$

The exponential term is obtained using the fact that

$\psi(x_1) = 0$ for $x_1 < 0$.

From this,

$$\text{Log}\frac{\mu}{c} = -\text{Log } s + \int_s^\infty \frac{e^{-s}}{s}\,ds$$

and, by inverse transformation,

$$\psi(x_1) = \frac{c}{2\pi}\int_{\delta-i\infty}^{\delta+i\infty} \frac{e^{-\lambda x_1}}{\lambda} \exp\left(\int_\lambda^\infty \frac{e^{-s}}{s}\,ds\right) d\lambda.$$

The expansion of the exponential integral around the pole yields a term in $e^{-\gamma} = 0.561$, where γ is Euler constant.

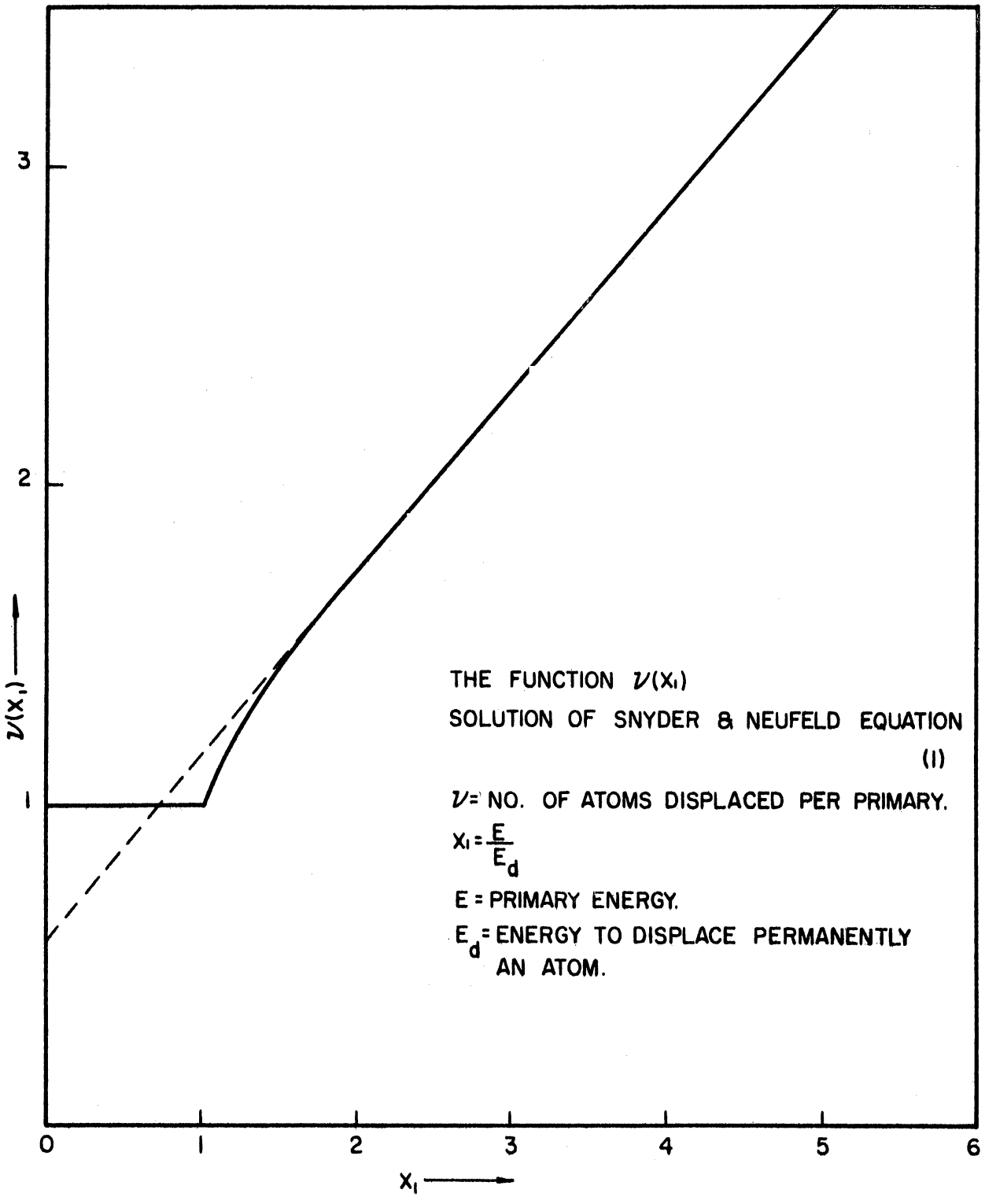
3
2
1
0
1
2
3
4
5
6
$\nu(X_1)$
X_1
THE FUNCTION $\nu(X_1)$
SOLUTION OF SNYDER & NEUFELD EQUATION
(1)
ν = NO. OF ATOMS DISPLACED PER PRIMARY.
$X_1 = \frac{E}{E_d}$
E = PRIMARY ENERGY.
E_d = ENERGY TO DISPLACE PERMANENTLY AN ATOM.

Equation (1) assumes that any atom receiving 25 ev is released from its site and that the incoming knock-on always emerges from the collision.

Now, assume that, if the incoming knock-on has energy smaller than 25 ev after collision, it replaces the secondary dislodged.

The integral Equation (1) becomes

$$x_1 \nu(x_1) = \int_1^{x_1} \nu(x'_1)\, dx'_1 + \int_0^{x_1-1} \nu(x_2)\, dx_2 \ .$$

The differential Equation (2) remains unchanged, but the boundary condition (3) must be replaced by

$$\nu(x_1) = 1 \ , \quad 0 < x_1 < 2 \ .$$

An asymptotic solution $\nu(x_1) = a\,(1 + x_1)$ also exists. For $x_1 < 3$, $\nu(x_1 - 1) = 1$, so that

$$\nu(x_1) = C + \mathrm{Log}\, x_1 ; \nu(2) = C + \mathrm{Log}\, 2 = 1;$$

$$\nu(3) = 1 - \mathrm{Log}\, 2 + \mathrm{Log}\, 3 = 1 + \mathrm{Log}\, \tfrac{3}{2} \cong 4\, a;$$

this yields $a \cong 0.351$.

Finally, assume that, not only the primary replaces the secondary if $0 < x'_1 < 1$, but also that the secondary recombines with its vacancy if $0 < x_2 < 1$.

The integral Equation (1) becomes

$$x_1 \nu(x_1) = \int_1^{x_1} \nu(x'_1)\, dx'_1 + \int_1^{x_1-1} \nu(x_2)\, dx_2 \ .$$

(2) remains unchanged, but its boundary condition (3) becomes

$$\nu(x_1) = 1 \ , \quad 0 < x_1 < 3 \ .$$

For $x_1 < 4$,

$$\nu(x_1) = C + \mathrm{Log}\, x_1 \ ; \nu(4) = 1 - \mathrm{Log}\, 3 + \mathrm{Log}\, 4 \cong 5a \ .$$

This yields $a \cong 0.258$.

It is seen that these two models, assuming replacement, or replacement and recombination, would reduce the overestimate inherent to the Snyder and Neufeld method. But they remain artificial ways and means to bring calculations closer to the desired result.

APPENDIX XXIII

Direct obtention of the primary integral equation for the model used in the collision problem.

The differential cross sections used are

$$\sigma(E,T)\,dT = -\pi\frac{2\alpha}{E}\,d\,\frac{\left(1-\frac{2}{\pi}\sin^{-1}\sqrt{T/E}\right)^2}{1-\left(1-\frac{2}{\pi}\sin^{-1}\sqrt{T/E}\right)^2},$$

$$\sigma(E,E')\,dE' = -\pi\frac{2\alpha}{E}\,d\,\frac{\left(1-\frac{2}{\pi}\sin^{-1}\sqrt{(E-E')/E}\right)^2}{1-\left(1-\frac{2}{\pi}\sin^{-1}\sqrt{(E-E')/E}\right)^2}$$

Put into (38) of the text, assume a solution $\nu(E) = A + BE$ and integrate (38) by parts, to obtain

$$\begin{aligned}\sigma_s(E)\nu(E) = -\pi\frac{2\alpha}{E}\Bigg[&\nu(E-E_d)\times 0 - \nu(0)\frac{E}{2\pi\alpha}\sigma_d(E)\\ &- B\int_{E_d}^{E}\frac{\left(1-\frac{2}{\pi}\sin^{-1}\sqrt{T/E}\right)^2}{1-\left(1-\frac{2}{\pi}\sin^{-1}\sqrt{T/E}\right)^2}\,dT\Bigg]\\ -\pi\frac{2\alpha}{E}\Bigg[&\nu(0)\times 0 - \nu(E)\frac{E}{2\pi\alpha}\sigma_s(E)\\ &- B\int_{E}^{0}\frac{\left(1-\frac{2}{\pi}\sin^{-1}\sqrt{\frac{E-E'}{E}}\right)^2}{1-\left(1-\frac{2}{\pi}\sin^{-1}\sqrt{\frac{E-E'}{E}}\right)^2}\,dE'\Bigg],\end{aligned}$$

or

$$\sigma_s(E)\nu(E) = \nu(0)\sigma_d(E) + \nu(E)\sigma_s(E) + \pi\frac{2\alpha}{E}B\left[\int_{E_d}^{E} + \int_{E}^{0}\right].$$

Finally since $\nu(0) = 1$,

$$E\,\sigma_d(E)/2\pi\alpha B = -\int_{E_d}^{E} - \int_{E}^{0}$$

which is Equation (43) of the text.

APPENDIX XXIV

THE DESIGN OF A CRYOSTAT FOR PILE IRRADIATION

Note: This Appendix has been arranged as a separate, complete part of the dissertation, with its own numbering and bibliography.

INTRODUCTION
SECTION I

1-Basic idea

The application of cryogenics to particle irradiation is of general interest. Low temperature irradiation allows for eliminating the effects of thermal motion, diffusion, for example.

Because of this importance of cryogenics, in particular for pile neutron irradiation, it is considered that the design and construction of a multi-purpose low temperature cryostat for the Ford reactor is a worthwhile undertaking.

In the design of such a cryostat, to be used at liquid helium temperature--i.e. the minimum temperature practically attainable in the application proposed--one is severely limited in the mass of the experimental set up. A large mass of the components liable of supplying heat to liquid helium by conduction or radiation means a high rate of helium evaporation from gamma-ray heating in the reactor. Within this limitation, the low temperature chamber and the tube leading to it must be of such dimensions that specimens of substantial size or chemical test tubes can be inserted in the chamber, so that the installation can serve many purposes. Mass is reduced by the adoption of a practically all aluminum construction.

Diagram 1 shows the general dimensions and the arrangement of the cryostat. The low temperature chamber and helium in and out transfer tubes are placed in a vacuum jacket, reducing heat intakes other than from absorption of nuclear radiations to radiative and free molecule transfers between jacket and liquid helium chamber or helium transfer tubes. In

Diagram 1

CRYOSTAT

General arrangement and dimensions

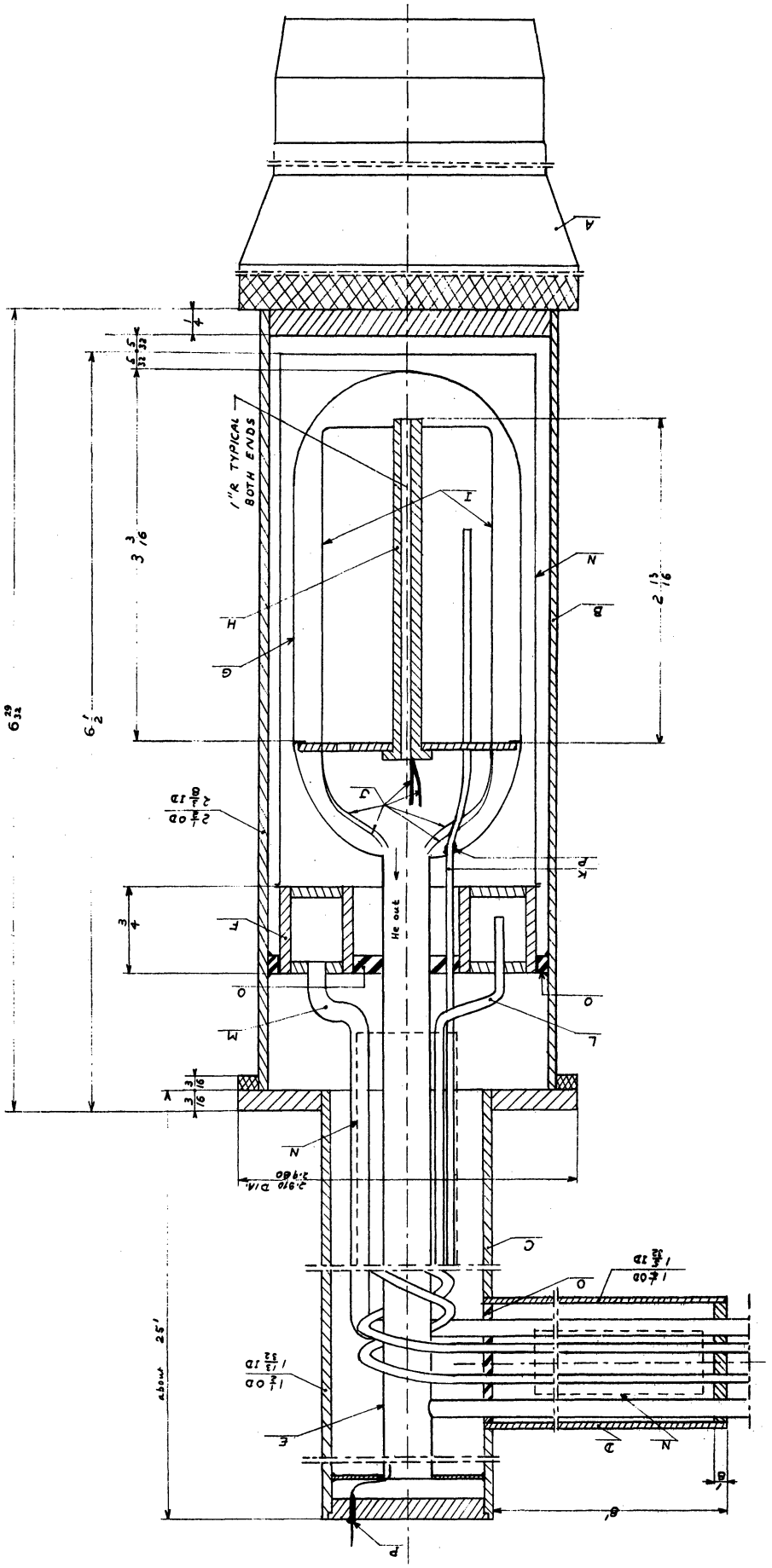

A-Support ("Mock up Fuel Element")
B-Jacket Envelope, Lower Part
C-Jacket Envelope, "Long Tube"
D-Jacket Envelope, Horizontal Tube
E-Central Tube
F-Nitrogen Chamber
G-Helium Chamber
H-Rod

I-Samples
J-Electrical Leads
K-Helium in Tube
L-Nitrogen in Tube
M-Nitrogen out Tube
N-Thermal Shields
O-Guides
P-Covers

order to save on helium,which is an expensive commodity, radiative losses are minimized by interposition of thermal shields between liquid helium chamber and jacket and, also, between helium tubes and jacket, the latter at positions which do not make construction too difficult. The shield around the liquid helium chamber is attached to a liquid nitrogen chamber, fed by in and out nitrogen transfer tubes. The shields around the tubes are welded to the nitrogen out tube. They shield the nitrogen in tube, as well as the helium in tube.

Liquid helium and nitrogen are transfered to their respective chambers by applying a light pressure of helium gas to their containers. Continuous transfer is planned and no automatic devices are provided. The liquid level in the helium chamber will be monitored by continuous measurement of a resistance and that in the nitrogen chamber by a thermocouple in contact with the nitrogen out tube. It will be noted that this arrangement is predicated upon a continuous, constant power level operation of the reactor. This is not an additional restriction placed on the operation of the reactor, since such conditions are requisite to the knowledge of the irradiation neutron integrated flux in the range of energy of interest.

2- Application to the study of atomic displacement by fast neutron bombardment

The first use that is intended for the cryostat is a low temperature neutron irradiation of thin metallic wires, in order to study atomic displacements induced by such irradiation.

It is known,[1] that, during cyclotron charged particle bombardment of metals, at liquid helium temperature, the variations of the increase in electrical resistivity induced by irradiation versus

integrated flux are represented, not by a straight line, but by a curve bending down. Since the increase in resistivity is found to be stable at helium temperature when irradiation is ceased, the recombination of defects evidenced by the curving down of the irradiation curve cannot be ascribed to thermal annealing. Hence the process is called "radiation anneal".

Considerations, developed in the text, relative to the number of atoms displaced by secondary collisions of moving atoms, per atom displaced by a bombarding particle (primary knock-on), and to the moving atom mean free path between displacing collisions, show that radiation anneal can be explained, for charged particle bombardment, in terms of interaction of defects of various generations. They show that no such explanation seem valid for neutron bombardment, where, for the fast fluxes and irradiation times practicable in experiments, the total number of primary knock ons is much smaller than the corresponding number for charged particle irradiation with integrated fluxes remaining reasonable. A low temperature, in-pile measurement experiment performed at Oak Ridge, to study, not radiation anneal, but thermal anneal after irradiation, shows as a by-result, that no radiation anneal takes place, and, thus checks the theoretical deduction recalled above.

The experiment planned will serve as a further check. Also, since samples of several metals (four different metals, as a first step) will be irradiated in the same flux conditions, indications on the dependence of the change in electrical resistivity--i.e. of the fraction of atoms displaced--on atomic number or mass number will be obtained. In addition to shedding light on these two important points of the theory of atomic displacements, the experiment will provide valuable training in cryogenic techniques.

Since heat intakes have mainly for source the absorption of prompt fission gammas and uranium capture gammas, it is important to place the experiment in a region of comparatively small thermal neutron flux. On the other hand, a maximum damage is inflicted to the sample for a displacing neutron flux (energy greater than 400 Mev for copper) as high as possible. Irradiation out of a beam hole, or within the thermal column, using a converter plate, leads to a simple design of cryostat, but only allows very small displacing fluxes, hence exigl long exposures. In addition, such set ups demand an extensive shielding, in order to prevent the escape of fast neutrons into the experimental space around the reactor.

A high fast flux is best attained in the core of the reactor and the maximum ratio fast flux-thermal flux is obtained right in the center of the core. This position of the irradiation low temperature chamber has been selected.

It will be noted that such a positioning of the experimental set up can only be obtained with a swimming pool reactor, hence the Ford reactor is ideally suited for the kind of experiment planned.

In order to maintain a reasonable rate of consumption of helium, a reactor power level of 0.1 MW has been selected. It will be shown later that meaningful results should then be obtained for 50 hr exposure.

3-Mass of cryostat-Consumption of liquid nitrogen and helium

The total mass of the cryostat is 7.35 kg, not including the "mock-up fuel element" to which the cryostat is attached at its lowest part, most of which is due to the outer vacuum jacket. Only a small part of this total mass is placed in a region of appreciable gamma flux. It

is estimated that about 38 gr absorb gammas with resulting heat flow to liquid helium and about 200 gr absorb gammas with a resulting heat flow to liquid nitrogen. A mass of 16 gr liquid helium and 30 gr liquid nitrogen, about, should be present at all times in the respective chambers.

Liquefied gases expenditure is estimated as follows: (see Section III, paragraph 5)

TABLE I

Use	Liquid He, liters	Liquid N_2, liters
Transfer tests, during construction.	25	25
Pre-experiment cooling.	15	2
Experiment.	280	26
Totals	320	53

With a figure, of about $3.00 per liter of liquid helium, the cost of preparing and running the first experiment amounts, for this commodity, to 320 x 3 = $960. This includes investment costs consisting in developing equipment and techniques, which will not be incurred for further experiments.

4-Construction schedule

The design was completed on November 22, 1957. Aluminum sheets and tubing were ordered at the same date and received a week later. Construction began in the first days of December (lower part of vacuum jacket). Welding of comparatively thin aluminum tubes commenced on February 21, 1958, when an appropriate Heliarc "torch" was received.

An aluminum transfer tube of 20 feet length, consisting of an inner tube of 1/16 in. inside diameter, 1/8 in. outside diameter (Alcoa "Utilitube") and of a peripheric outer vacuum jacket of 1/2 in. outside diameter, 0.028 in. thickness (Alcoa 3003 H 14) was completed at the end of March. This transfer tube is represented in Figure 1. It proved possible to Heliarc weld the 3003 H 14 tube, but attempts to weld the Utilitube failed and threaded compression fittings were used for the passage of the inner tube at the ends of the vacuum jacket. The transfer tube has been used to check the possibility of long transfers with tubes of small diameter and to attempt to measure liquefied gas evaporation during such a transfer. From the beginning of April to mid-May, a vacuum line was built to evacuate the vacuum jacket of the test transfer tube. The system was tested for leaks, which resulted in the replacement of the oil diffusion pump. A thermocouple vacuum gauge (RCA 1946) was installed and calibrated. In April the shop welded the flanges on the sections of the long tube which constitutes the main part of the vacuum jacket of the cryostat

After the transfer tube proved to be of too small a diameter (inner tube) to transfer nitrogen, two transfer tubes with larger diameter were ordered from the shop, on May 20. It is worth noting that a low temperature cryostat, manufactured at Hanford, has required 1 1/2 years to be completed.

5-Demand on the reactor schedule

It is re-emphasized that 50 hours at constant power level operation--0.1 MW--will be demanded by the experiment.

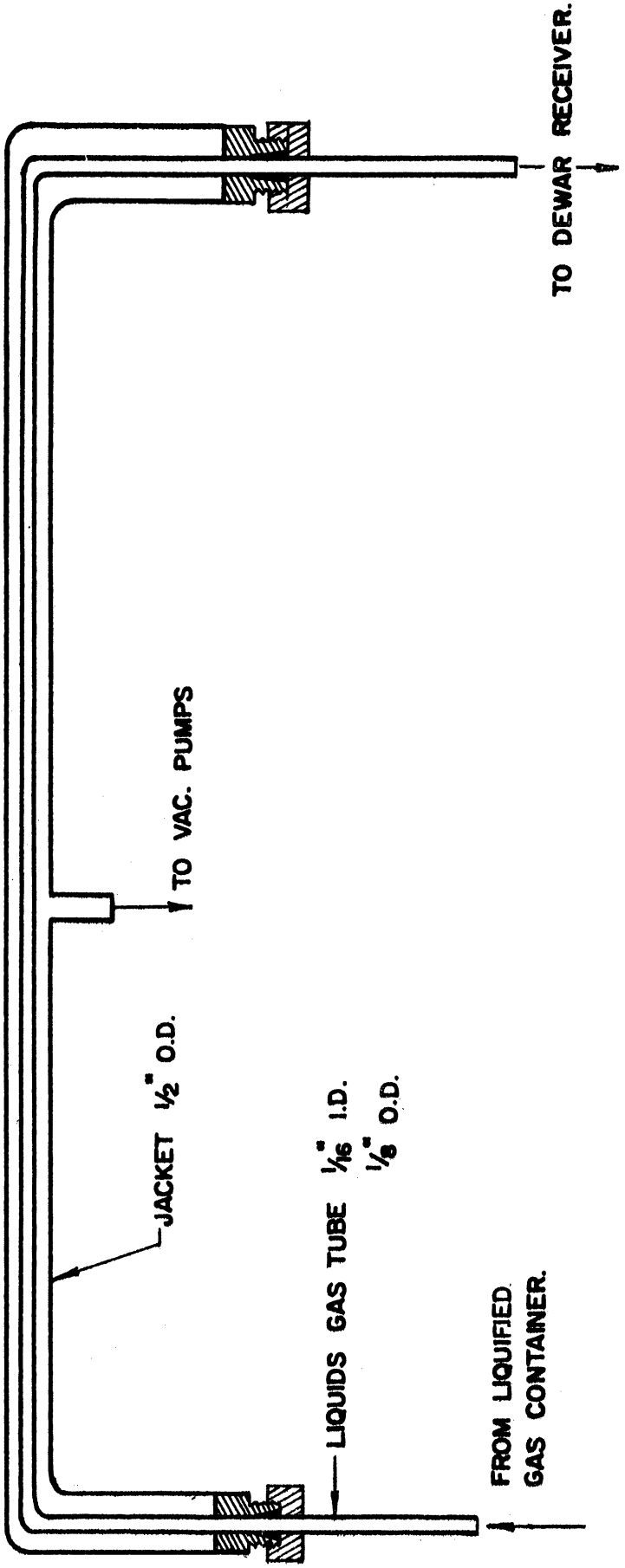

Figure 1. Test Transfer Tube.

FEASIBILITY OF IN PILE MEASUREMENT OF
CHANGE IN ELECTRICAL RESISTIVITY
DUE TO NEUTRON IRRADIATION

SECTION II

1-Fast flux available-Change in electrical resistivity expected

Even with the experimental device in place, we can expect to obtain in the samples, at a reactor power of 0.1 MW, a fast flux

$$\phi_{fast} = \int_{E_T}^{\infty} \phi(E)\,dE$$

of the order of 10^{12} neut cm^{-2} sec^{-1}. Here, E_T is the cut off energy for the thermal region. This estimate is made from information contained in the document "Research Reactors",(3) which gives data obtained of the Bulk Shielding Reactor. It is probably sufficient to admit, for the purpose of estimate, a fast flux of the form

$$\phi(E)\,dE = K\,dE/E \quad .$$

Assume, to be on the safe side, that E_T is taken equal to 1/40 ev, and take a neutron cut off energy of 2 Mev. Then, K is determined by,

$$K \int_{1/40}^{2\times10^6} dE/E = 10^{12} \quad .$$

Hence

$$K = 5.5 \times 10^{10}$$

From Equation (32) of the text, we have,

$$C \cong (t\sigma_s/E_d)(1/A)\,5.5\times10^{10}\times 2\times10^6,$$

where C is the fraction of atoms displaced after an exposure t sec.

For copper, σ_s = 3b, A = 64, E_d = 25 ev.

Since we know that the theory of displacements overestimates the fraction displaced by a factor of about 5, we shall take for estimate of C, after 50 hr irradiation,

$$C \cong \frac{1}{5} \times \frac{50 \times 3.6 \times 10^3 \times 3 \times 10^{-24}}{25 \times 64} \times 5.5 \times 10^{10} \times 2 \times 10^6$$
$$= 7.45 \times 10^{-6} = 7.45 \times 10^{-4} \text{ o/o} .$$

Taking Jongenburger value[4] of $\Delta\rho = 2.7 \mu\Omega$cm for C = 1% in copper, the estimate for the increase in electrical resistivity of copper after 50 hr irradiation is

$$\Delta\rho = 2.7 \times 7.45 \times 10^{-4} \cong 2 \times 10^{-3} \mu\Omega \text{ cm} .$$

2-Feasibility of measurement

Take, again, the typical example of copper. First calculate the electrical resistivity at the temperature of the experiment. Θ denoting the Debye temperature, T the temperature considered, ρ_T the thermal component of the resistivity at temperature T, ρ_Θ the thermal component of the resistivity at temperature Θ, ρ_T/ρ_Θ varies practically linearly with T/Θ for $T/\Theta \geqslant 0.3$ and ρ_T is expected to vary like T^5 for $T \ll \Theta$ (Gruneisen function, see Figure 2).

For copper, $\Theta = 333$°K and, from the curve ρ_T/ρ_Θ versus given by Kittel,[4] it is found that $\rho_\Theta \cong 1.9 \mu\Omega$cm, and that $\rho_T/\rho_\Theta \cong 5 \times 10^{-3}$ for $T/\Theta = 0.1$. The coefficient K of $\rho_T = KT^5$ is determined by $5 \times 10^{-3} \times 1.9 = K \times (33.3)^5$, i.e. $K = 2.24 \times 10^{-10}$. The temperature of the helium chamber will be maintained at about 5°K while liquid helium will fill the chamber. At this temperature, the thermal component of ρ should be about,

$$\rho\ 5°K = 2.24 \times 10^{-10} \times 5^5 \cong 7 \times 10^{-7} \mu\Omega \text{ cm} .$$

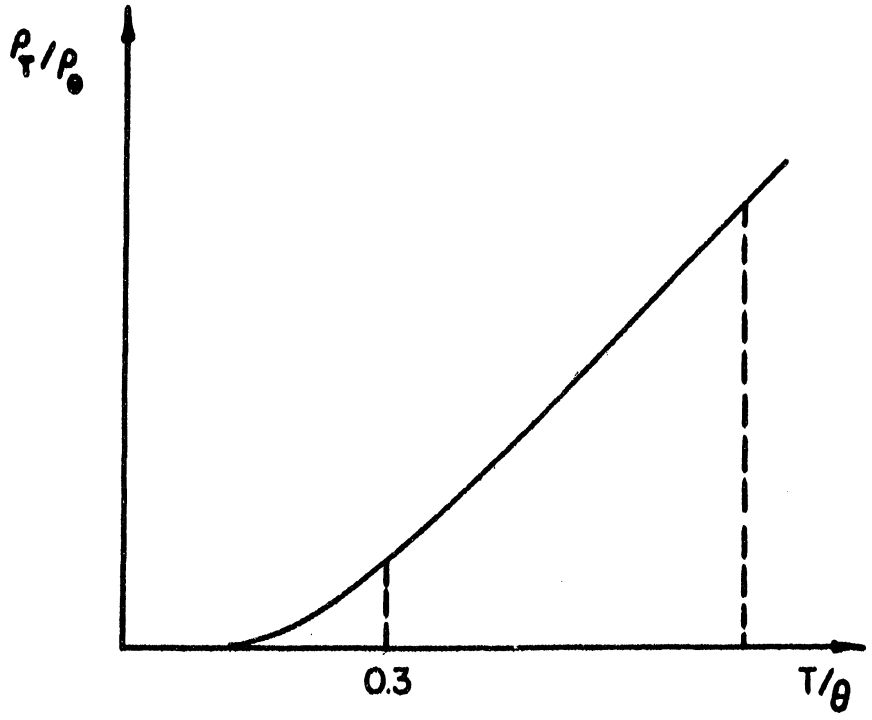

Figure 2. Gruneisen **Function.**

Should the supply of liquid helium fail to maintain the level and the temperature of the samples rise to 15°K, the thermal component of the resistivity of the samples would become

$$\rho\ 15°K = 2.24 \times 10^{-10} \times (15)^5 \cong 1.72 \times 10^{-4}\ \mu\Omega\,cm\ .$$

It is quite feasible to obtain commercially metallic samples whose residual resistivity--i.e. non thermal component, due to impurities and crystalline imperfections--is 5×10^{-4} times the total resistivity at 0°C. For copper this residual resistivity would then be about

$$1.69 \times 5 \times 10^{-4} \cong 8.5 \times 10^{-4}\ \mu\Omega\,cm\ .$$

Hence the total resistivity of the copper samples may be taken as

$$\rho_{Tot,}\ 5°K \cong 7 \times 10^{-7} + 8.5 \times 10^{-4} \cong 8.5 \times 10^{-4}\ \mu\Omega\,cm \text{ at } 5°K,$$

and

$$\rho_{Tot,}\ 15°K \cong 1.72 \times 10^{-4} + 8.5 \times 10^{-4} \cong 1.02 \times 10^{-3}\ \mu\Omega\,cm \text{ at } 15°K.$$

At one tenth of full irradiation, $\Delta\rho$ would be about

$$2 \times 10^{-4}\ \mu\Omega\,cm\ .$$

As we have seen before, ρ should be of the order 8.5×10^{-4} at 5° K, so that there is no difficulty in obtaining a meaningful measurement of $\Delta\rho$, provided the temperature is maintained reasonably constant. For example, if the temperature in the helium chamber should jump from 5°K to 15°K between two measurements, the thermal component ρ_T would pass from $7 \times 10^{-7}\ \mu\Omega$ cm to $1.72 \times 10^{-4}\ \mu\Omega$ cm and the two measurements could not be compared (i.e. plotting their representative points on the same curve would be meaningless). However, a change of 2°K, about 5°K between two measurements distant of 1/20 of the total irradiation time would be permissible, since the $\Delta\rho$ corresponding to that length of irradiation would be of order 10^{-4}, while the change in ρ_T due to the temperature

change would be of order

$$7 \times 10^{-7}\left[(7/5)^5 - 1\right] \cong 3.08 \times 10^{-6},$$

i.e. only 1/30 of the increase in $\Delta\rho$. If the level of liquid helium is maintained above the samples at all times, the temperature of the samples can only change if the pressure changes. At the pressure envisaged (slightly above atmospheric pressure), the temperature of saturated liquid helium is fairly insensitive to changes in pressure, hence constancy of temperature is not considered a difficulty, provided the samples are alway immersed in liquid helium.

DESIGN OF THE CRYOSTAT

SECTION III

1-General considerations

The design of the cryostat has proceeded along the following lines. The general feature of the cryostat were first selected, starting from the basic ideas expressed in Section I, Paragraph 1. Diagram 1 shows the layout. The material selected was aluminum, at least for the parts in or near the core, for reason of small mass, hence comparatively low gamma absorption and also because, with this metal, there is no activation problem. The criterion used to select the dimensions was that the mass of the portion of the cryostat placed in high gamma flux should be as small as possible, in order to limit gamma heating and, therefore, liquefied gas consumption. The dimensions selected must meet the requirements of mechanical resistance, unrestricted flow of liquids and gases, and usability of the cryostat as a multi-purpose low temperature reactor irradiation device. The selection was therefore made by trial and error calculations. Diagram 1 shows the dimensions arrived at.

2-Calculation of gamma-heating

The cryostat will be placed in the core, in such a way that the center of the helium chamber will be approximately at the center of gravity of the core. To simplify the calculation, since the geometry of the cryostat is quite complicated, it was decided to consider as concentrated at the center of gravity of the core the whole gamma-absorbing portion of the mass of the device. This is equlivalent to assuming a space independent gamma flux around the experimental device. This is probably not a

bad assumption within the core. Since the gamma flux should fall rather fast outside the core with distance from the core face, the gamma absorbing portion of the cryostat is assumed to extend only about the one foot above the top of the core. The portions of the helium and nitrogen systems so considered are shown schematically in Figure 3. Since the experiment is placed in the center of the core, for gammas originated in the reactor itself we shall consider only gammas born in the core, i.e. we assume, which is reasonable, that gammas born in the reflector will be absorbed by the core and will never reach the experiment. The cross sections for capture and fission are much greater for thermal neutrons than for fast neutrons, hence only the thermal neutron flux will be considered.

Core gammas are:

-thermal fission prompt gammas and uranium capture gammas,

-fission product decay gammas,

-aluminum capture and decay gammas,

-water capture gammas.

The first two sources can be lumped together, as, for example, in the work of Clairborne et al.[6]

Call $N_i(E)\,dE$ the number of photons with energy in dE about E produced, per interaction, by kind i of the processes mentioned above, and Σ_i the macroscopic thermal cross section for that process.

Call $S(E)dE$ the number of photons with energy in dE about E produced per second, per MW, by all (total) the processes above. Call ϕ the thermal flux per MW, averaged over the core.

Then the source corresponding to a volume dV of the core is,

$$S(E)\,dE = \phi\, dV \sum_i \left[\Sigma_i N_i(E) dE \right] \qquad (1)$$

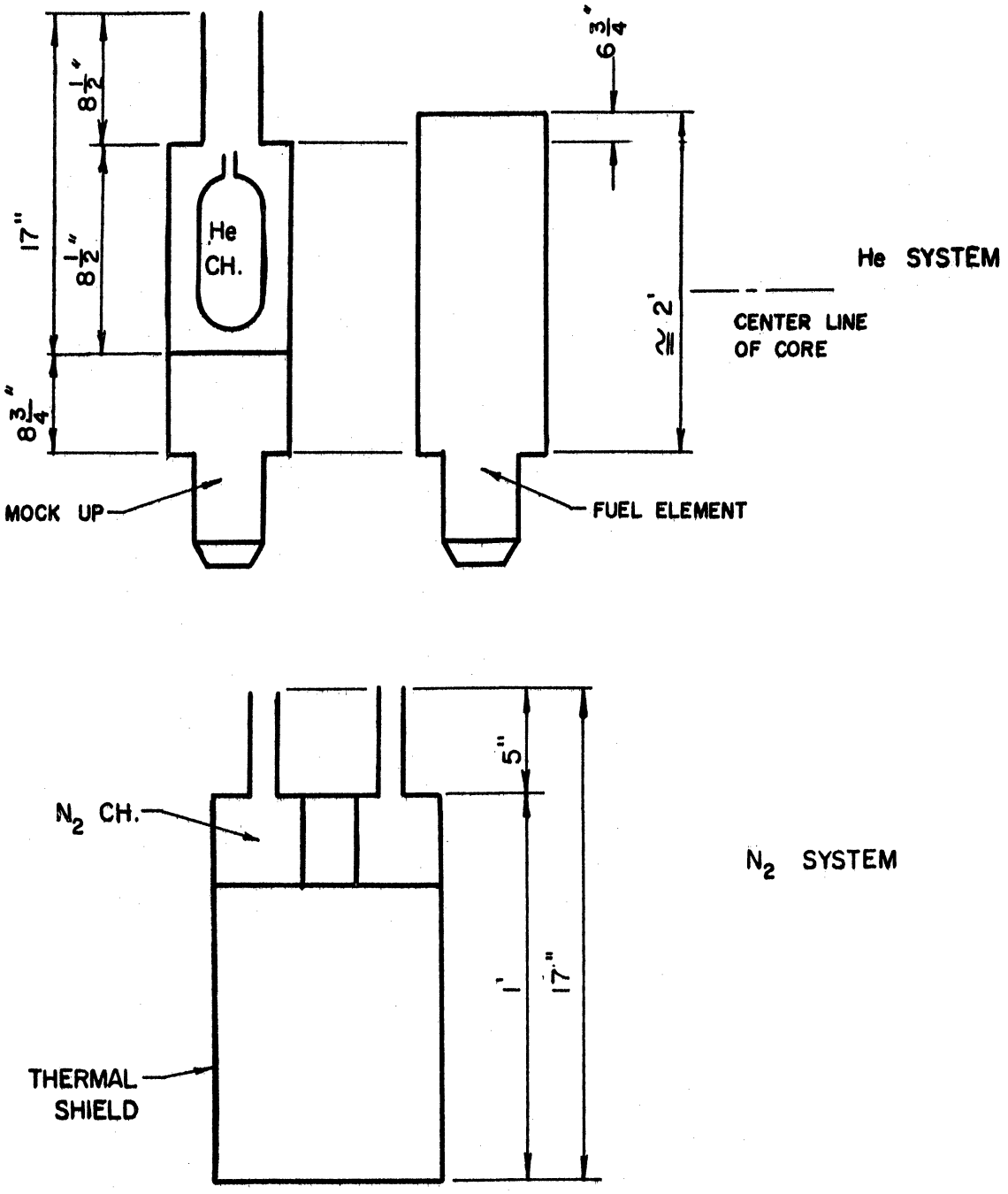

Figure 3. Gamma Absorbing Portion of N_2 and He Systems.

Consider (Figure 4) the experiment concentrated at 0, center of the core. Consider a volume dV of the core, concentrated around a point P, as a punctual source. Call r the distance OP, μ_c (E) the linear absorption coefficient of the core, and μ_e (E) that of the experimental set up (homogeneized) for gammas of energy E. Call ρ_e the density of the homogeneized experimental set up. Neglect build up in the experimental set up, since it is mainly made of thin aluminum walls. In aluminum, for 1 Mev gammas, $\mu/\rho \cong 0.09$g cm^2 x gr^{-1} (5) hence $\mu \cong 0.09$g x $2.7 \cong 0.24$ cm^{-1}. The thickness is smaller than 0.2 cm, hence $\mu x < 0.24$ x 0.2 = 0.048 and the build up factor B(1 Mev, x) is about unity (B = 2.0. for $\mu x = 1$, E = 1 Mev, and B = 1.53 for $\mu x = 1$, E = 4 Mev.(5)) .

Call B(E) the build up factor in the core, admitting that it varies little with r. If the core is assimilated to an homogeneous mixture of water and aluminum, the build up factor is taken equal to

$$B(E,r) \cong (\text{Vol Al}/\text{Vol core})B_{Al}(E,r)+(\text{Vol H}_2\text{O}/\text{Vol core})B_{H_2O}(E,r) \quad (2),$$

where E is the energy of the gammas considered and r the distance from the gamma source considered. Uranium will be neglected.

In the Ford reactor, the following approximate ratios obtain,

$$\text{Vol Al}/\text{Vol core} = 0.42\ ;\ \text{Vol H}_2\text{O}/\text{Vol core} = 0.58. \quad (3)$$

Hence,

$$B(E,r) \cong 0.42\, B_{Al}(E,r) + 0.58\, B_{H_2O}(E,r). \quad (4)$$

From simple arguments (in particular, isotropy of emission of gammas is assumed), it can be shown(6) that the energy spent in the homogeneized set up, per unit mass of its material, per MW of reactor power, by gammas with energy in dE about E and originated in a volume element

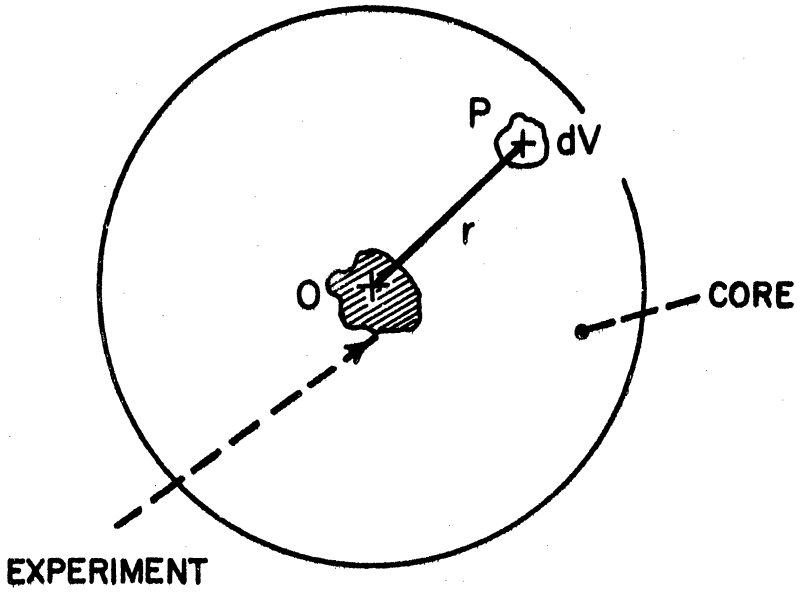

Figure 4. Volume Element of Core Source of Gamma-rays.

dV at distance r from the set up (concentrated) is, in Watts,

$$h(E)dE = 1.6\times10^{-13}\frac{\mu_e(E)B(E,r)}{4\pi\rho_e r^2}e^{-\mu_c(E)r}ES(E)dE \quad (5),$$

where S(E) is given by Equation (1), and the other symbols have been defined above.

We write

$$h(E)dE = F(E,r)\,E\,S(E)\,dE \quad , \quad (6)$$

with

$$F(E,r) = 1.6\times10^{-13}\frac{\mu_e(E)\,B(E)}{4\pi\rho_e r^2}e^{-\mu_c(E)r} \quad . \quad (7)$$

Now in the work of Clairborne et al.,[6] the energy is divided into seven groups, setting an arbitrary average energy in each group, and defining an equivalent number of photons for each group and each process, such that the average energy $E_{av,n}$ in the n-th group, limited by energies E_{n-1} and E_n (n, 1, 2, ...7) and the equivalent number of photons $N_{eq,n,i}$ for the same group and for process i are related by

$$N_{eq,n,i}\,E_{av,n} = \int_{E_{n-1}}^{E_n} E\,N_i(E)\,dE \quad . \quad (8)$$

From Equation (6) and Equation (1) we can obtain the total energy expended in the experiment by gammas with energy in the n-th group, produced in dV by all processes, namely,

$$h_n = \int_{E_{n-1}}^{E_n} F(E,r)\,E\,S(E)\,dE \quad , \quad (9)$$

$$h_n = \int_{E_{n-1}}^{E_n}\left\{F(E,r)\,E\,\phi\,dV\sum_i\left[\Sigma_i N_i(E)\right]\right\}dE \quad , \quad (10)$$

$$h_n = \phi\,dV\sum_i \Sigma_i \int_{E_{n-1}}^{E_n} F(E,r)\,E\,N_i(E)\,dE \quad . \quad (11)$$

If we can consider F(E,r) independent of E, i.e. equal to a function $F_n(r)$ in each group n, then,

$$h_n = \phi dV F_n(r) \sum_i \Sigma_i \int_{E_{n-1}}^{E_n} E N_i(E) dE \ , \qquad (12)$$

$$h_n = \phi dV F_n(r) E_{av,n} \sum_i \left(\Sigma_i N_{eq,n,i} \right) . \qquad (13)$$

We therefore look into the possibility of considering F(E,r) constant in each group.

Table II gives, in the six columns at the left, $E_{av,n}$ and $N_{eq,n,i}$

TABLE II

n	Energy group	$E_{av,n}$ Mev	$N_{eq,n,i}$ i = 1 Fission (prompt, U capture, fission product decay*)	i = 2 Al capture and decay	i = 3 Water capture	E Mev	(μ/ρ) H_2O	(μ/ρ) Al
1	0.00- 0.75	0.5	5.680	0.000	0.000	0.1	0.171	0.169
						0.6	0.089	0.078
2	0.75- 1.50	1.0	4.000	0.425	0.000	1.0	0.071	0.061
3	1.50- 3.00	2.0	2.345	1.113	1.115	3.0	0.049	0.043
4	3.00- 5.00	4.0	0.441	0.727	0.000	4.0	0.034	0.031
5	5.00- 7.00	6.0	0.054	0.202	0.000	6.0	0.028	0.027
6	7.00- 9.00	8.0	0.007	0.344	0.000	8.0	0.024	0.024
7	9.00-11.00	10.0	0.0009	0.000	0.000	10.0	0.022	0.023

* Note - The decay term is variable with time of operation. The value adopted is an average for the decay at 85% saturation. Strictly, the rate of consumption of helium should vary somewhat as irradiation progresses.

from Clairborne et al.[6] and μ/ρ for water and aluminum from the Reactor Handbook[5] in the two columns at the right. It is seen that the μ's of water and aluminum may be taken as constant in any energy group except the first one (n equal to one). The error made by taking the μ's constant in group 1 may be appreciable, since $N_{eq,1,i}$ is important for i = 1. However, to be on the safe side, i.e. overestimating rather than underestimating μ_e, hence h_n, we shall take a high value for μ_e in this group. We denote by subscript n the constant values adopted. The values selected appear in Table III below.

TABLE III

Group, n	$(\mu/\rho)_{H_2O}$	$(\mu/\rho)_{Al}$
1	0.150	0.150
2	0.065	0.055
3	0.055	0.045
4	0.034	0.031

Since, for $E > 5$ Mev, μ has changed in the ratio 0.034/0.17 = 0.2 for both aluminum and water, and since $N_{eq,5,1}/N_{eq,1,1} \cong 0.05/5 = 0.01$[6] for the most important process of gamma production, we shall consider only n = 1, 2, 3, 4.

B(E), given by Equation (4), is very sensitive to changes in E at energies smaller than 2 Mev. We shall adopt rather strong values of B(E) in the various intervals. Call $B_{H_2O,n}$, $B_{Al,n}$, B the build up factors, considered constant, for the n-th group, in water, aluminum, and the core. The values of B_n for the different groups is calculated in the following way. First an appropriate value for the linear gamma-

absorption coefficient of the core $\mu_{c,n}$ is calculated for each group n. The core is assimilated to an homogeneous mixture of water and aluminum, and $\mu_{c,n}$ is calculated by

$$\mu_{c,n} = \left(\frac{\mu}{\rho}\right)_{H_2O,n} \rho_{H_2O,m} + \left(\frac{\mu}{\rho}\right)_{Al,n} \rho_{Al,n} \quad)$$

where the $\left(\frac{\mu}{\rho}\right)$'s are for the pure component in the mixture. Uranium is neglected. For aluminum, $\rho_{pure} = 2.7$.

$$\rho_{H_2O,m} = \frac{1 \times V_{H_2O}}{V_{core}} = 0.58 \; ; \; \rho_{Al,m} = \frac{2.7 \times V_{Al}}{V_{core}} = 1.13 .$$

Hence,

$$\mu_{c,n} = 0.58 \left(\frac{\mu}{\rho}\right)_{H_2O,n} + 1.13 \left(\frac{\mu}{\rho}\right)_{Al,n}$$

Table IV below gives the values of $\mu_{c,n}$ obtained.

TABLE IV

Group	H_2O		Al		
	$\frac{\mu}{\rho}$	$0.58\frac{\mu}{\rho}$	$\frac{\mu}{\rho}$	$1.13\frac{\mu}{\rho}$	$\mu_{c,n}$
1	0.150	0.087	0.150	0.169	0.256
2	0.065	0.038	0.055	0.062	0.100
3	0.055	0.032	0.045	0.051	0.083
4	0.034	0.020	0.031	0.035	0.055

Now the B's are calculated

Group 1 $E_{av,1} = 0.5$ Mev; $\mu_{c,n} = 0.256$.

For r = 10 cm, $\mu_{c,n} r = 2.56$, $e^{-\mu_{c,n} r} = 0.08$.

For r = 5 cm, $\mu_{c,n} r = 1.28$, $e^{-\mu_{c,n} r} = 0.27$.

We certainly can neglect all volume elements ar distance greater than 10 cm. Hence, the maximum values of the B's are,

Water- $\mu = 0.150$, $\mu r = 1.5$, $B_{H_2O}(0.5, 1.5) \cong 3.5$,

Aluminum- $\mu = 0.405$, $\mu r = 4.05$, $B_{Al}(0.5, 4) \cong 9.5$.

$$B = 6.00 \ .$$

Group 2 $E_{av,2} = 1$ Mev; $\mu_{c,n} = 0.100$.

For r = 10 cm, $\mu_{c,n} r = 1$, $e^{-\mu_{c,n} r} = 0.332$.

For r = 15 cm, $\mu_{c,n} r = 1.5$, $e^{-\mu_{c,n} r} = 0.223$.

We take values at 15 cm .

Water- $\mu = 0.065$, $\mu r = 0.975$, $B_{H_2O}(1, 0.98) \cong 2.13$.

Aluminum- $\mu = 0.148$, $\mu r = 2.220$, $B_{Al}(1, 2.22) \cong 3.50$.

$$B = 2.70 \ .$$

Group 3 $E_{av,3} = 2$ Mev; $\mu_{c,n} = 0.083$.

We take r maxi. equal to 15 cm .

Water- $\mu = 0.055$, $\mu r = 0.825$, $B_{H_2O}(2, 0.825) \cong 1.60$.

Aluminum- $\mu = 0.121$, $\mu r = 1.810$, $B_{Al}(2, 1.81) \cong 2.40$.

$$B = 1.93 \ .$$

Group 4 $E_{av,4} = 4$ Mev; $\mu_{c,n} = 0.055$.

Again, we take r maxi. equal to 15 cm .

Water- $\mu = 0.034$, $\mu r = 0.510$, $B_{H_2O}(4, 0.5) \cong 1.20$.

Aluminum- $\mu = 0.084$, $\mu r = 1.260$, $B_{Al}(4, 1.26) \cong 1.70$.

$$B = 1.415 \ .$$

With these adopted values, we can write Equation (7), for $E_{n-1} \leq E \leq E_n$,

$$F_n(r) = 1.6 \times 10^{-13} \frac{\mu_{e,n} B_n}{4\pi \rho_e} \frac{e^{-\mu_{c,n} r}}{r^2} \qquad (14)$$

The total energy expended in the target (experimental set up) by all gammas originated in dV (i.e. with all energies), per unit mass of target, per MW, is obtained by summing Equation (13) over n and using Equation (14), thus,

$$h = \phi dV \frac{1.6\times10^{-13}}{4\pi\rho_e}\sum_{n=1}^{4}\left[\mu_{e,n}B_n E_{av,n}\frac{e^{-\mu_{c,n}r}}{r^2}\sum_{i=1}^{3}\left(\Sigma_i N_{eq,n,i}\right)\right]. \quad (15)$$

Call M the total mass of the target, P the reactor operating power in in MW, then the total energy expended by core gammas in the target is,

$$H_\gamma = MP\phi\frac{1.6\times10^{-13}}{4\pi\rho_e}\sum_{n=1}^{4}\left[\mu_{e,n}B_n E_{av,n}\sum_{i=1}^{3}\left(\Sigma_i N_{eq,n,i}\right)\int_{core}\frac{e^{-\mu_{c,n}r}}{r^2}dV_c\right]. \quad (16)$$

in Watts.

Now, for the sake of simplicity, we assimilzte the core to a sphere whose center is the point at which the experiment is concentrated and of radius 15 cm (Figure 5). This does not introduce a large error, compared to the actual geometry, since for group 1, the largest contributor, and for r = 10 cm, $e^{-\mu_{c,n}r} = e^{-2.56} = 0.077$.

Now,

$$\int_{core}\frac{e^{-\mu_{c,n}r}}{r^2}dV_c = \frac{4\pi}{\mu_{c,n}}\left(1-e^{-15\mu_{c,n}}\right).$$

Hence Equation (16) becomes,

$$H_\gamma = MP\phi\times1.6\times10^{-13}\sum_{n=1}^{4}\left[\frac{1}{\mu_{c,n}}\left(\frac{\mu_{e,n}}{\rho_e}\right)B_n E_{av,n}\left(1-e^{-15\mu_{c,n}}\right)\sum_{i=1}^{3}\Sigma_i N_{eq,n,i}\right]. \quad (17)$$

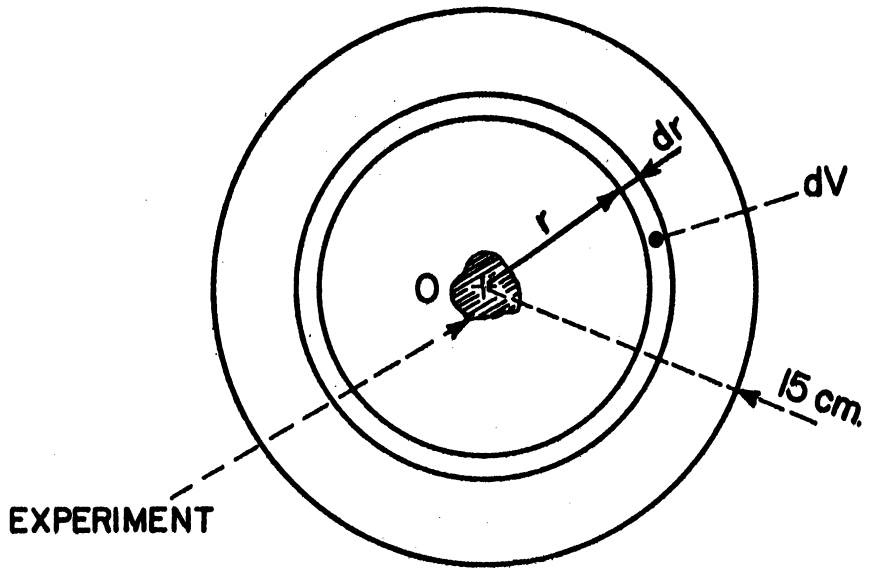

Figure 5. Reduction to a Spherical Core.

Since the only parameter of Equation (17) depending on the nature of the target is $\mu_{e,n}/\rho_e$, and since it is known that, at a given energy, μ/ρ is about the same for all elements, we can use for M the total mass which absorbs gammas, whatever the nature of the materials contributing to it and replace $\mu_{e,n}/\rho_e$ by $(\mu/\rho)_{Al,n}$. Equation (17) can be written,

$$H_\gamma = MP\phi \times 1.6 \times 10^{-3} A \quad \text{watts} \quad , \quad (18)$$

with,

$$A = \sum_n A_n \quad , \quad (19)$$

and,

$$A_n = \frac{1}{\mu_{c,n}} \left(\frac{\mu}{\rho}\right)_{Al,n} B_n E_{av,n} \left(1 - e^{-15\mu_{c,n}}\right) \sum_{i=1}^{3} \Sigma_i N_{eq,n,i} \quad . \quad (20)$$

The macroscopic cross sections to consider are,

i	Σ_i
1	Thermal fission, U 235
2	Thermal capture, Al
3	Thermal capture, Water

If v_{nT_0} is the most probable speed of neutrons at temperature T_0, assuming a Maxwell Boltzman energy distribution and that the Σ_i's follow a B/v law, calling $\Sigma_i(v_{nT_0})$ the cross section for process i at speed v_{nT_0}, we have at temperature T_n,

$$\Sigma_{iT_n} = \frac{\sqrt{\pi}}{2} \sqrt{\frac{T_0}{T_n}} \Sigma_i (v_{nT_0}) \quad .$$

BNL 325 gives $\sigma_i (v_{nT_0})$ for $T_0 = 20°C$, i.e. for $v_{nT_0} = 2200$ m sec^{-1}.

If we admit that T_n is the moderator temperature and is equal to 50°C, then,

$$\Sigma_{iT_n} = \frac{\sqrt{\pi}}{2}\sqrt{\frac{293}{393}}\,\sigma_{i\,2200}\,N_i = 0.845\,\sigma_{i\,2200}\,N_i \quad .$$

From BNL 325 and its supplement, the following values are found, at 2200 m sec,

$$\sigma_{f\,U\,25} = 582\ b\ ;\ \sigma_{a\,Al\,27} = 230\ mb\ ;\ \sigma_{a\,H} = 332\ mb\ ;\ \sigma_{a\,O} < 0.2\ mb.$$

A schematic description of the core of the Ford reactor is given in Figure 6. The volume percentages in the core are:

vol. water 57.7%; vol. aluminum 42.3%.

The active length of the elements (and of the core) is 60 cm. Each element contains 140 gr of U 235. Σ_i is calculated from the formula above where

$$N_i = \frac{m_i}{A_i} N_o \frac{1}{V} \quad ,$$

m_i mass of constituent i, A mass number of constituent i, V total volume (core or cell), N_o Avogadro's number.

The calculation of the Σ_i's is made in the Addendum. The results are,

$$\Sigma_1 = 4.75 \times 10^{-2}\ cm^{-1}$$

$$\Sigma_2 = 4.83 \times 10^{-3}\ cm^{-1}$$

$$\Sigma_3 = 1.09 \times 10^{-2}\ cm^{-1}$$

The value of the quanity A, defined by Equations (19) and (20), is calculated in Table V. It is found that A = 0.922.

The mass M to consider in Equation (18) is obtained as follows. Two "systems" are considered. A "helium system", in which gamma absorption results in helium evaporation, and a "nitrogen system", in which gamma absorption results in nitrogen evaporation.

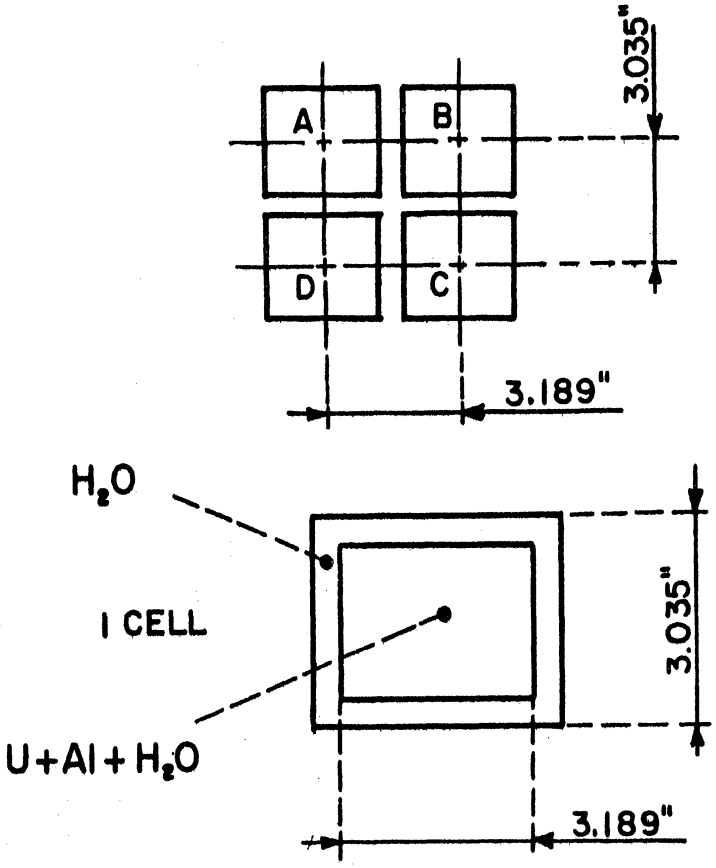

Figure 6. Spacing of Fuel Elements.

TABLE V

HEAT FROM CORE GAMMAS

Group	$\mu_{c,n}$	$\frac{\mu_{e,n}}{\rho_e}$	1 $\frac{1}{\mu_{c,n}} \frac{\mu_{e,n}}{\rho_e}$	B_n	$E_{av,n}$	2 $B_n E_{av,n}$	3 = 1 x 2 $\frac{1}{\mu_{c,n}} \frac{\mu_{e,n}}{\rho_e} B_n E_{av,n}$	$15\mu_{c,n}$	$e^{-15\mu_{c,n}}$	4 $1-e^{-15\mu_{c,n}}$	5 = 3 x 4 $\frac{1}{\mu_{c,n}} \frac{\mu_{e,n}}{\rho_e} B_n E_{av,n}(1-e^{-15\mu_{c,n}})$	6 $\sum_i (\Sigma_1 \ldots)$	5 x 6 A_n
1	0.256	0.150	5.85×10^{-1}	6	0.5	3	1.655	3.84	0.021	$\tilde{=}$ 1.00	1.655	2.7×10^{-1}	0.468
i Σ_i			i Σ_i		$N_{eq,n,i}$	$\Sigma_i N_{eq,n,i}$							
1 Fission			1 4.75×10^{-2}		5.68	0.270							
2 Al Capture } Thermal			2 4.82×10^{-3}		0	0	$\sum_i$						
3 H_2O Capture			3 1.0×10^{-2}		0	0	0.270						
2	0.100	0.055	5.5×10^{-1}	2.70	1.0	2.70	1.485	1.50	0.223	0.777	1.154	1.92×10^{-1}	0.222
			i Σ_i		$N_{eq,n,i}$	$\Sigma_i N_{eq,n,i}$							
			1 4.75×10^{-2}		4.00	0.190							
			2 4.82×10^{-3}		0.425	0.002	$\sum_i$						
			3 1.09×10^{-2}		0	0	0.192						
3	0.083	0.045	5.42×10^{-1}	1.93	2.0	3.86	2.092	1.24	0.300	0.700	1.464	1.28×10^{-1}	0.187
			i Σ_i		$N_{eq,n,i}$	$\Sigma_i N_{eq,n,i}$							
			1 4.75×10^{-2}		2.345	0.111							
			2 4.82×10^{-3}		1.113	0.005	$\sum_i$						
			3 1.09×10^{-2}		1.115	0.012	0.128						
4	0.055	0.031	5.65×10^{-1}	1.42	4.0	5.680	3.209	0.825	0.44	0.560	1.797	2.5×10^{-2}	0.045
			i Σ_i		$N_{eq,n,i}$	$\Sigma_i N_{eq,n,i}$							
			1 4.75×10^{-2}		0.441	0.021							
			2 4.82×10^{-3}		0.727	0.004	$\sum_i$						
			3 1.09×10^{-2}		0	0	0.025						

A = 0.922

$H_\gamma = MP\Phi \times 1.6 \times 10^{-13} \quad A \quad W$

$A = \sum_n A_n$

For the helium system (see Figure 3), the upper part of the chamber, the cryostat central tube, the electrical wires, are intensively cooled by helium gas leaving the chamber. This gas has a specific heat of 4.99 cal/gram atom, or 4.99/4 cal/gr. Assume a helium consumption of 3 liter per hr (liquid), i.e. $3 \times 10^3 \times 0.126 = 378$ gr/hr. If helium gas warms up to 10°K above liquid helium temperature, then it can absorb

$$(4.99/4) \times 378 \times 4.18 \times 10 \quad \text{joule hr}^{-1}$$

or

5.5 Watts.

For a gamma absorption of 0.1 watt/gram of experimental set up, it is seen that the leaving gas could possibly evacuate the gamma from 55 grams of material. This is more than the gamma absorbing mass of the helium system. It was decided that 1/4 of the mass in the upper part of the gamma-absorbing region (i.e. above the liquid helium level in the helium chamber) would convey heat to the liquid helium by convection and the whole mass of the lower part would do so. Then, the gamma absorbing mass of the helium system is of 22 gr of aluminum and samples plus 16 grams of liquid helium, or a total of 38 gr. In order to limit to an acceptable value the rate of consumption of liquid helium, the power level of the reactor is chosen to be P = 0.1 MW, i.e. the thermal flux of the order of 7×10^{11} neut cm^{-2} sec^{-1} (average).

Equation (18) gives, for the gamma heat per gram,

$(H_\gamma)_{gr} = 7 \times 10^{11} \times 1.6 \times 10^{-13} \times 0.922 = 0.103$ watt/gr.

For the gamma heat in the helium system,

$(H_\gamma)_{He} = 38 \times 0.103 = 3.92$ watts.

For the nitrogen system, it was considered that the total gamma absorbing mass contributed to nitrogen evaporation. This total mass is found to be 200 gr, including 30 gr of liquid nitrogen. Hence the gamma heat in the nitrogen system is estimated to be

$$(H_\gamma)_{N_2} = 200 \times 0.103 = 20.6 \text{ Watts.}$$

The latent heat of vaporization of helium is 24 cal/gr atom at - 268°C, i.e. 6 cal/gr, or 25.11 Joule/gr. The mass consumption of helium is then,

$$(C_\gamma)_{He,mass} = 3.92/25.11 \text{ gr He/sec}$$

The volume consumption is

$$(C_\gamma)_{He,vol} = \frac{3.92 \times 3.6}{25.11 \times 0.124} \text{ lit He/hr} = 4.6 \text{ lit/hr}$$

The latent heat of vaporization of nitrogen is 42.8 cal/gr near atmospheric pressure, or 4.96×10^{-2} Watt hr/gr, or 40 Watt hr/liter of liquid nitrogen.

Hence the volume consumption of nitrogen due to core gamma heating is,

$$(C_\gamma)_{N_2,vol} = \frac{20.6}{40} = 0.52 \text{ liter/hr liquid } N_2 .$$

3-Other sources of radiation heating

Heat is also introduced into the system by the following processes,

-scattering of neutrons, particularly fast neutrons. This effect is small and usually neglected;

-self-absorption of gammas originated in the experimental device by (n,γ) reaction Al 27 (n,γ) Al 28;

-self-absorption of betas produced by the decay of Al 28.

The calculations by Clairborne et al.[6] show that, for an aluminum test sample placed on the face of the BSR core, while the heat due to core gammas is 0.177 Watt/gr MW, the heat due to self-absorption of gammas is 0.0027 Watt/gr MW and the heat due to self-absorption of betas is 0.023 Watt/gr MW.

Since a significant part of the absorbing mass of the helium system is constituted by liquid helium and the absorbing mass of the nitrogen system has been willingly overestimated, and since the core gamma heating has also been overestimated, it is concluded that self-absorption of gammas and betas can be neglected.

4-Heat transfers into the system

The cryostat will be jacketed by a vacuum space at a pressure of the order of 0.1μ mercury. Heat transfer from the outer wall of the vacuum jacket into the helium and nitrogen systems can take place through the following processes,

-radiative transfer;

-free molecule convection;

-conduction at the upper end of the cryostat, where helium and nitrogen systems are in contact with the outer envelope through the central tube and the helium and nitrogen in and out tubes.

There exist formulae to calculate, for simple geometries, heat transfer by the first two processes.[8-9] However, they employ assumptions and empirical coefficients which render doubtful the accuracy of the resutls. On the whole, it appears safer to adapt to the system under study experimental observations made on other cryostats. For a

large volume cryostat with short transfer lines,[10] it was observed that, when irradiation was turned off, the helium consumption, including transfer losses, amounted to 4.7 liters per day. The volume of the helium chamber and of the liquid helium transfer tube is much smaller for the cryostat planned, although the transfer line is much longer. It seems safe to admit that the transfer losses will not exceed five times the loss of helium by heat transfer (other than due to absorption of radiations) into the chamber and to adopt a global consumption of 1 liter per hour of liquid helium for all these contributions. Paragraph 2 of Section IV indicates what liquid helium transfer experiments are being performed to check this point.

For nitrogen, since the problem is less critical, no such contributions will be added, in this estimate.

5-Total volume rate of consumption of liquid helium and nitrogen and total consumption.

Our estimate of the volume rate of consumption of liquid helium and nitrogen is then,

$$C_{He,\ vol} = 5.6 \text{ liters/hr} ,$$

$$C_{N_2,\ vol} = 0.52 \text{ liters/hr} .$$

For 50 hours exposure in the reactor, the estimate of liquefied gas consumption is,

280 liters helium

26 liters nitrogen

6-Cooling prior to experiment.

First, the cryostat will be cooled by liquid nitrogen and nitrogen exchange gas produced by evaportion, then by liquid helium and helium exchange gas. It is computed that the mass (practically all aluminum) to cool from, say, room temperature, or about 300°K, to liquid nitrogen, or 77°K, is 850 gr and that the mass (also all aluminum) to cool from 77°K to temperatures between 4°K and, say, 15°K, is 636 gr.

For aluminum, $C_{\omega} = 5.78$ cal/gr atom = 0.214 gal/gr, at 20°C. Actually, it is much less than that at low temperature. For example,(11) $C_{\omega} \cong 0.5 \times 3R$ for $T/\Theta \cong 0.25$, where Θ is the Debye temperature of the metal, R Mayer constant, or Boltzman constant for a gram-molecule. For aluminum, $\Theta = 394$°K, hence, at 100°K, $C_{\omega} \cong 0.5 \times 6 = 3$ cal/gr atom. For simplicity we shall keep $C_{\omega} = 0.214$ cal/gr atom.

We can treat the cooling problem in the following way. Suppose the mass M to cool, of specific heat C_{ω}, is placed in the cooling liquid, whose latent heat of vaporization is L. The gas produced by the evaporation contributes to cool the mass M. Call C_{p} its specific heat. When a mass dm of the liquid vaporizes, L dm is furnished to cool M. Further, if T_0 is the temperature of the liquid and T that of the mass M, the gas produced by evaporation brings a contribution which we may estimate as

$$\alpha\, C_{p}\, dm\, (T - T_0)$$

In view of the geometry, it is not exaggerated to take $\alpha = 0.1$. We can write,

$$- M\, C_{\omega}\, dT = dm\, [L + \alpha C_{p} (T - T_0)]$$

or, with $T - T_0 = \Theta$,

$$- M\, C_{\omega}\, d\Theta = dm\, [L + \alpha C_{p} \Theta] \quad .$$

Call T_i the initial temperature. The mass m_o of liquid needed to cool the mass M from T_i to T_o is

$$M_o = (M C_v / \alpha C_p) \text{ Log } [1 + (\alpha C_p / L)(T_i - T_o)]$$

We first apply this for the cooling of 850 gr of aluminum from 300°K to 77°K with nitrogen. For nitrogen L is comparatively large, 42.8 cal/gr, so that for α small,

$$m_o \cong (M C_v / L)(T_i - T_o) = (850 \times 0.214/42.8) \times 233 \cong 956 \text{ gr}$$

This represents a volume

$$(965/0.808) \times 10^{-3} = 1.195 \text{ liters liquid nitrogen.}$$

We shall consider that a volume of 2 liters liquid nitrogen will be needed for this phase of the cooling.

Next, we calculate the mass m'_o of liquid helium needed to cool 630 gr of aluminum from 77°K to, say, 4°K. For helium, $C_p \cong 1.25$ cal/gr, L = 6 cal/gr.

$m'_o = [636 \times 0.214/(0.1 \times 1.25)] \times 2.3 \log [1 + 0.1 \times 1.25 \times 73/6] \cong 10^3$ gr.

The volume of liquid helium needed for this phase of the cooling will be,

$$1/0.124 = 8.1 \text{ liters}$$

As a safe estimate we shall count on spending 15 liters of liquid helium for this operation.

7-Expenditure of liquefied gases during construction. Total expenditure of liquid helium and nitrogen.

Transfer tests through long transfer tubes have been made with liquid nitrogen and are being made with liquid helium. A total consumption of 25 liters of each liquefied gas is estimated for these tests.

The various consumptions are summarized in Table I (Section I, Paragraph 3). The estimated global consumption of liquid helium, including construction tests, amounts to 320 liters, that of liquid nitrogen to 53 liters.

8-Selection of aluminum alloys

For most parts it is not possible to use the series 1... of Alcoa because of low mechanical strength and welding difficulty (practically pure aluminum). Commercial Alcoa aluminum alloys are aluminum with copper (2...), aluminum with manganese (3...), aluminum with magnesium and silicon (6...), aluminum with silicon.

Al 27, abundance 100%, has a thermal reaction cross section of 0.23 b. Al 28, formed by (n, γ) reaction, undergoes beta decay (2.865 Mev), half life 2.27 min, with a gamma transition of 1.782 Mev.

The only isotope of silicon which captures thermal neutrons to form a radioactive product is Si 30, abundance 3.05%, with a thermal reaction cross section of 0,4 b. Si 31, formed by (n, γ) reaction, decays by beta emmision (1.48 Mev), half life 2.62 hr, gammas 0.17 and 0.52 Mev.

The only isotope of magnesium which captures thermal neutrons to form a radioactive product is Mg 26, abundance 11.29%, giving Mg 27 by (n, γ) reaction (reaction cross section 60 mb). Mg 27 decays by beta emmision (1.8 Mev), with gamma transitions of 1.01 and 0.84 Mev, half life 9.45 min.

Mn 55, abundance 100%, has a thermal reaction cross section of 13.4 b. Mn 56, formed by (n, γ) reaction, decays by beta emission (2.87 Mev), 2.576 hr half life, gamma transition 0.822, 1.77, and 2.06 Mev.

Cu 63, abundance 69.1% , has a cross section of 4.3 b for thermal reaction. By (n,γ) reaction it gives Cu 64, which decays by electron capture, beta, and positron emmision, with half life 12.8 hr (betas 0.571 Mev, positrons 1.65 Mev, gammas 1.34 Mev). Cu 65, abundance 30.9%, has a thermal reacton cross section of 2.11 b. By (n,γ) reaction, it gives Cu 66, which decays by beta emmision (2.63 Mev), half life 5.10 min, gamma transition 1.05 Mev.

The above data have been collected from standard texts on neutron reactions data.[5, 12,13] Because of comparatively high thermal reaction cross sections coupled with non-negligible half life of the radiosotope formed, it is advisable to use alloys containing copper and manganese, i.e. for example the series 2... and 3... of Alcoa, only where necessary. We may note, however, that even the activation of a large sample containing 5% in volume of copper would not create very serious problems. Take a hollow cylindrical sample of 5 cm diameter, thickness 0.2 cm, length 100 cm. Assume the whole sample placed in a thermal neutron flux 10^{13} neut/cm^2 sec for 50 hrs. The half life of Cu 64 is about 13 hours, hence we may consider that saturation is attained.

For simplicity, consider that all the copper present is Cu 63. The activation cross section is 4.3 b. The rough estimate of the activity of the sample at the end of the exposure is

$$\frac{1}{3.7 \times 10^{10}} \times 5 \times 10^{-2} \times 0.75 \times 10^{23} \times 4.3 \times 10^{-24} \times 10^{13} \times 3.14 \times 5 \times 0.2 \times 10^{2} = 1.2 \times 10^{4} \quad \text{curies.}$$

If the sample is left in the pool, away from the core, for 20 days, i.e. about 40 half lives, the activity at the end of this period is

$$1.2 \times 10^{4}/(2)^{40} = 1.2 \times 10^{-8} \quad \text{curie.}$$

The alloys selected are 6061 T 6, 5052 0 for most parts, 3003 H 14, 2024 T 3 and 2024 0 for components which may pose problems of weldability (helium chamber) or are not in the neutron flux,as well as 1100 aluminum (all Alcoa). In addition, during construction, it was decided to build the long tube of the cryostat in three sections assembled by flanges. The lower section is made of 2024 T 3, the upper section, the horizontal section and the T for assembling the horizontal section are made of brass (see Diagram 1). These last sections are not placed in the neutron flux.

9-Mechanical resistance

The following values are admitted[12] for the yield strength of aluminum and various aluminum alloys,

Al (more than 99%) annealed	1.22×10^8 dyne cm^{-2}
Al 75% rolled	10.60×10^8 dyne cm^{-2}
Al 5 Si, cast	9.65×10^8 dyne cm^{-2}
Al 3.8 Mg	11.00×10^8 dyne cm^{-2}
Al 12 Si	12.40×10^8 dyne cm^{-2}

The following critical parts were calculated for mechanical strength.

Helium chamber

On the cylndrical body the stress is greater than on the spherical caps. It is given by,

$$R = p\ r\ /\ 2\ h$$

with p internal pressure, r radius, h thickness. r = 1 inch, $p < 2$ atm $= 2 \times 0.981 \times 10^6$ dyne cm^{-2}. We try h = 0.03 cm $\cong$ 12 mils.

This gives

$$R < 1.64 \times 10^8 \text{ dyne cm}^{-2}$$

We can try Alcoa 1100 in 12, 16, and 20 mils, and 2024 0 and 5052 0 in 12 mils.

Nitrogen chamber

The critical parts are the two annular discs that form the bottom and the cover of the chamber. The stress is maximum along the small circumference of the discs. It is given by(14)

$$R \; K \; p \; r^2 / h^2$$

K is a coefficient equal to 0.9 for a disc built in at the inner edge and prevented from rotating at the outer edge, and for a ratio outside diameter/inside diameter equal to 2.2, p is the internal pressure in psi, r the outside diameter, h the thickness.

We consider using a silicon or magnesium alloy, hence we take a yield strength of 9×10^8 dyne cm^{-2}. We have already selected r = 5.62 cm. Take p = 2 atm. The formula gives h = 2.5 mm $\simeq$ 0.083 in. The alloy selected is 6061 T 6.

Envelope of the vacuum jacket

Similar considerations as those above lead to adopt a thickness of 5 mm = 1/4 in. for the disc closing the envelope at the bottom of the cryostat and 4 mm = 3/16 in. for the annular disc that forms the top of the lower part of the envelope (liaison with the long tube).

Another consideration, for the envelope, is that of possible collapsing of the long tube under extermal pressure. At the bottom end of the long tube the water head is about 23 feet or 690 cm, hence the pressure 1 + 0.69 = 1.70 kg cm^{-2}. The critical pressure(15) is given by

$$p_c = \frac{E}{4} \left(\frac{h}{r}\right)^3$$

E elasticity modulus, r radius, h thickness.

$E = 0.98 \times 10^6$ dyne cm^{-2} is a good value for Al Si, Al Mg Si, Al Mg.

With this value one obtains,

$$h > 1.32 \text{ mm}$$

The above results were used in addition to the requirement that the dimensions selected should permit multiple use of the cryostat and yet lead to an acceptable gamma absorption, for the trial and error selection of these dimensions

10-Thermal contraction on cooling

Due to the different temperatures of helium and nitrogen systems, in their coldest parts, and the cryostat envelope, and since appreciable lengths are involved, relative positions of these elements will change appreciably from the beginning of cooling, at room temperature, to the end of cooling, when the various components have reached their operating low temperatures.

Consider a linear distribution of temperature along a given element, from top to bottom, the top (top of the cryostat) being roughly at room temperature T_o, the bottom being at the operating low temperature T_l. Call x the abscissa of the point on the element, counted vertically, from top to bottom. Let T_x be the temperature at that point. Call l the length of the element, from top to bottom, and α the average linear coefficient of expansion of the material at the temperatures considered. The change δl of length of a portion dx at x is

$$\delta l = \alpha \, dx \, (T_o - T_x) = \alpha \, dx \, \frac{T_o - T_l}{l} x ,$$

and the total contraction of the element is $\alpha l \, \frac{T_o - T_l}{2}$

Central tube

This is the tube leading to the helium chamber (see Diagram 1). Say that $T_\ell = -269°C$, $T_o = 24°C$. For aluminum, $\alpha = 18 \times 10^{-6}$. The length is about 696 cm. This gives

$$\Delta\ell \cong 1.83 \text{ cm}$$

This is an upward motion, since the central tube is attached at the top.

The helium out tube will contract of about the same quanity. The helium in tube, colder at the upper part, will contract more. The differential contraction will be absorbed by an appropriate bend in the helium tube.

Nitrogen out tube and thermal shield

The bottom of the thermal shield is at distance about 707 cm from the top of the cryostat. Take the temperature at the bottom as -190°C and that at the upper part of the nitrogen out tube as 24°C. Then,

$$\Delta\ell \cong 1.36 \text{ cm}$$

Hence, the clearance to provide between bottom of nitrogen chamber and top of helium chamber is

$$1.83 - 1.36 = 0.47 \text{ cm}$$

For safety, we shall leave o.6 cm.

The nitrogen out tube is suspended from a support (lucite) at the top of its vertical portion. Its contraction will pull upward the nitrogen chamber. The nitrogen in tube will contract more than the nitrogen out tube. The differential contraction will be absorbed by a bend in the nitrogen in tube and the nitrogen chamber will be guided in the jacket envelope.

The helium in tube is cooled roughly from 24 to -269°C. Its length is about 270 cm. The contraction, with respect to the envelope, is 1.41 cm. This will be absorbed by the bend in the helium tube already provided to compensate the central tube contraction. The nitrogen in tube also possesses a bend, as seen before, which will absorb its contraction.

11-Activation of nitrogen-14

Radioactive N 13 is formed by (γ, n) or (n, 2n) reaction on N 14. C 14 is formed by (n, p) reaction on N 14. The latter does not constitute an activation problem, since its half life is 5568 years. The N 14 (γ, n) N 13 reaction has a threshold of 10.5 Mev. The N 14 (n, 2n) reaction has a threshold of 11.3 Mev. The total reaction cross section of N 14 at 10 Mev is smaller than 1.5 b.

(γ, n) reaction

μ/ρ is of the order of 0.02 for 10 Mev gammas.(5) We certainly have

$$\Sigma_{(\gamma,n)} < \mu = 0.02 \times 1.25 \times 10^{-3} = 2.5 \times 10^{-5} \text{ cm}^{-1}$$

for nitrogen gas, and,

$$\Sigma_{(\gamma,n)} < 0.02 \times 0.81 = 1.62 \times 10^{-2} \text{ cm}^{-1}$$

for nitrogen liquid. We may neglect the reaction in the gas phase and consider that the reaction with liquid nitrogen only takes place in the nitrogen chamber, since the volumes of nitrogen in and out tubes are small. The liquid nitrogen chamber may be considered as a point absorber of volume 37.5 cm^3, concentrated in the center of the core. It is found(6 that the equivalent number of gammas of energy greater than 10 Mev, per fission, is 9×10^{-4}.

Consider a volume element dV of the core and, at distance r, a surface element dS, normal to the line joining it to the volume element and subtending a solid angle $d\Omega$. Call the average thermal neutron flux in the core, Σ_f the thermal macroscopic fission cross section of the core, μ_c the linear absorption of the core for 10 Mev gammas, B(r) the build up factor of the core for 10 Mev gammas and penetration r.

The number of gammas of energy greater than 10 Mev which cross dS per sec is,

$$\phi \, \Sigma_f dV \times 9 \times 10^{-4} \times e^{-\mu_c r} \, dS \, B(r)/4 \pi r^2 ,$$

and the number of gammas with energy greater than 10 Mev absorbed in a colume element dV' = dS dr is,

$$\phi \, \Sigma_f \, dV \times 9 \times 10^{-4} \, e^{-\mu_c r} \, B(r) \, \Sigma_{(\gamma,n)} \, dV' / 4 \pi r^2 .$$

Take $\Sigma_{(\gamma,n)} = \mu = 1.62 \times 10^{-2}$ cm^{-1}, and consider a spherical core of radius 30 cm. The number of (γ,n) reactions per sec in the liquid nitrogen chamber is,

$$3.75 \times \phi \Sigma_f \times 9 \times 10^{-4} \times 1.62 \times 10^{-2} \, B(r) \, (1 - e^{-30\mu_c})/\mu_c$$

μ_c, for a water-aluminum core, may be taken equal to

$$(0.58 + 1.13) \times 2 \, 10^{-2} = 3.42 \times 10^{-2} \text{ cm}^{-1}$$

An overestimated value for B(r) is 1.4; Σ_f has been calculated previously and found equal to 4.75×10^{-2} cm^{-1}. Take $\phi = 7 \times 10^{11}$. We obtain, as an overestimate of the number of N 13 atoms formed per sec,

$$N = 3.75 \times 10 \times 7 \times 10^{11} \times 4.75 \times 10^{-2} \times 9 \times 10^{-4} \times 1.62 \times 10^{-2}$$
$$\times 1.4 \times (1 - e^{-1})/3.42 \times 10^{-2} = 4.7 \times 10^{8},$$

For a nitrogen consumption of 0.5 liter/hr, the time of exposure in the nitrogen chamber (volume 37.5 cm^3) is

$$37.5/(5 \times 10^2/3.6 \times 10^3),$$

or about 250 sec. Since this is smaller than the half life, 10 min, of N 13, we shall disregard N 13 decay. Hence, the number of N 13 atoms continuously formed is 1.18×10^{11}.

The 37.5 cm^3 of liquid nitrogen correspond to a volume

$$37.5 \times 0.808/(1.25 \times 10^{-3}) = 22 \times 10^3 \text{ cm}^3$$

of the nitrogen gas at atmospheric pressure and 0°C. In a tube of 4 mm I D, this volume occupies a length,

$$L = 22 \times 10^3/(3.142 \times 16 \times 10^{-2}/4) \text{ cm} \cong 1.8 \times 10^3 \text{ m}$$

The number of N 13 atoms per meter is, disregarding decay, in this overestimate,

$$(1.18/1.8) \times 10^8 = 10^8$$

N 13 has a half life of 10 min, hence a disintegration constant of

$$0.692/(6 \times 10^2) = 1.15 \times 10^{-3} \text{ sec}^{-1}$$

The linear activity of the nitrogen out tube is much smaller than

$$10^8 \times 1.15 \times 10^{-3}/3.7 \times 10^{10} = 10^{-5} \text{ curies/meter}$$

<u>(n, 2n) reaction</u>

$\Sigma_{(n, 2n)}$ is smaller than Σ_{tot} (10 Mev) for all possible reactions. Again, consider reactions in the liquid nitrogen chamber alone. Then, Σ_{tot} (10 Mev) $= 1.5 \times 10^{-24} \times 0.81 \times 6.02 \times 10^{23}/14 = 5.3 \times 10^{-2}$ cm^{-1} .

It is difficult to obtain a reasonable estimate for the integrated flux at energies above 10 Mev. It has been observed(3) that, for the BSR, while the thermal flux at the center of the core is $\cong 10^{12}$, the flux of neutrons with energy greater than 8.1 Mev (Al [n,α] Na 24 threshold reaction) is about 7×10^9 at the same position. Operating at 0.1 MW,

i.e. with a thermal flux of order 10^{12} at its maximum, we expect a flux of neutrons with energy greater than 10 Mev of less than 5×10^{9} at the center of the core. Hence the rate of formation of N 13 atoms is certainly much smaller than

$$37.5 \times 5.3 \times 10^{-2} \times 5 \times 10^{9} \cong 10^{10}$$

This is about 22 time what was found for a maximum estimate of the (γ, n) yield.

Hence, we expect that the activity of the nitrogen out pipe will be much smaller than 2.3×10^{-4} curies/meter. This should give no great shielding difficulty.

PRELIMINARY EXPERIMENTS

SECTION IV

1-Measurement of electrical resistance

The length of the samples will be about 8 cm, their diameter 1 mil, i.e. their cross sectional area 5.06×10^{-6} cm^2. The measuring circuit to be used during the experiment is represented schematically in Figure 7. Actually, the potential difference will be measured across the sample and the rod which supports it in series. This is permissible, since the resistance of the rod is very small compared to that of the sample.

With $\rho_{Tot} = 8.5 \times 10^{-4}$ $\mu\Omega$ cm at 5°K for copper, the resistance of a copper sample would be, at that temperature,

$$R_{5°K} = 8.5 \times 10^{-4} \times 8/(5.06 \times 10^{-6}) = 1.34 \times 10^{3} \ \mu\Omega$$

After 50 hours exposure, the increase in resistivity due to irradiation is expected to be 2×10^{-3} $\mu\Omega$ cm, i.e. the total resistivity at 5°K is expected to be

$$8.5 \times 10^{-4} + 2 \times 10^{-3} = 2.85 \times 10^{-3} \ \mu\Omega cm,$$

and the resistance of the sample,

$$2.85 \times 10^{-3} \times 8/(5.06 \times 10^{-6}) = 4.5 \times 10^{3} \ \mu\Omega .$$

After 5 hours exposure (1/10 total irradiation), the estimated increase in resistivity is 2×10^{-4} $\mu\Omega$ cm, i.e. the total resistance of the copper sample at 5°K is expected to be

$$1.05 \times 10^{-3} \times 8/(5.06 \times 10^{-6}) = 1.66 \times 10^{3} \ \mu\Omega .$$

Leeds and Northrup potentiometers reading down to 10^{-7} V are available in the Department of Electrical Engineering of the University. These would in principle allow to take readings every hour. The change in resistance between readings would then be

$$4 \times 10^{-5} \times 8/(5.06 \times 10^{-6}) = 63.1 \ \mu\Omega .$$

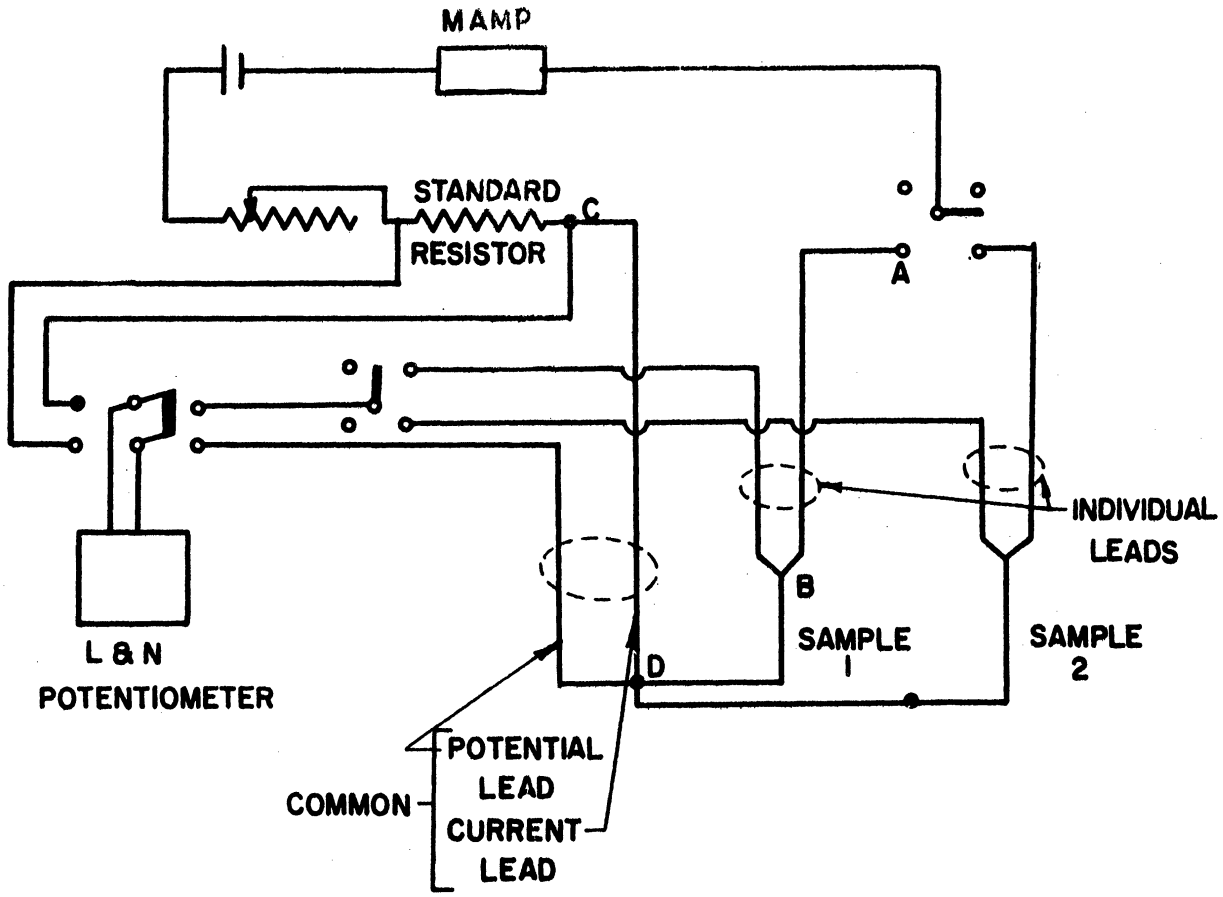

Figure 7. Measuring Circuit.
(4 samples)

With a current of 0.1 A--small enough to prevent heating of the samples--this is an increase of the drop of potential across the sample of 6.31 V. The lowest range of e.m.f. that can be read with the potentiometer corresponds to 1 μV per large division of the drum. To read 10^{-7} V, the tenth of a division must be estimated. This is problematic. However, even an accuracy of one large division is sufficient, since we want to read increases of 6 divisions. However, account must be taken of the accuracy with which the galvanometer can be read and the value of the current can be measured. A check of the accuracy obtained was made, using a Leeds and Northrup potentiometer type K. A standard resistor of 0.1 Ω was placed in series with a resistor of 0.01Ω, to be measured, two dry cells of 1.5 V in parallel furnished a current through the circuit set at o.1 A by a slide potentiometer. A sensitive wall galvanometer was used in connection with the measuring potentiometer. In a first series of readings, the e.m.f. for the measuring potentiometer was furnished by a dry cell of 1.5 V. Table VI shows the readings and the value of the resistance obtained. It is seen that the value obtained is 0.01Ω, exact to the fifth decimal, i.e. $10^{-5}\,\Omega = 10\,\mu\Omega$ can be measured. This is sufficient, although with not much accuracy to spare, for precise measurements of ΔR every hour during irradiation.

A second series of readings was made with a stable power supply as e.m.f. for the potentiometer. Table VII shows the readings and the value of the resistance obtained. This gives the same accuracy as the first series.

Attempts to measure small resistances with other galvanometers than a spot deflection galvanometer, namely using two electronic galvanometers, failed to give the accuracy of 10 $\mu\Omega$ desired.

TABLE VI

Measurement of resistance-e.m.f. for potentiometer:dry cell

Current A	e.m.f. V	Resistance Ω
0.09906	0.0009906	0.0100000
9903	9908	50
99045	99045	00
9902	9902	00
9902	9904	20
9900	9902	20
9900	9902	20
9900	9903	30
98985	98985	00
9897	9905	81
9899	9899	00
98975	98975	00
9894	9895	10
98835	9884	05
9884	98849	09
98849	9885	01
9885	9885	00
9885	9885	00
9886	98865	05
9885	9886	10
9886	9886	00
98835	98915	81
9885	9885	00
98855	98865	10
9885	98855	05
98855	98855	00
98855	98865	00
9885	9887	20
9887	9888	10
98805	98825	20
9880	9882	20 ↑MΩ

TABLE VII

Measurement of resistance
e.m.f. for potentiometer: stable voltage supply

Current A	e.m.f. V	Resistance Ω
0.09885	0.0009885	0.0100000
9880	98805	05
98705	98705	00
9864	9864	00
9855	9856	10
9849	98505	15
9842	9844	20
98375	98385	10
9834	9835	10
9832	9832	00
9830	9830	00
98275	98275	00
9826	98265	05
9822	98225	05

↑μΩ

It may be concluded that, irradiating thin samples (1 mil diameter, at least for copper) and using a sensitibe wall galvanometer, the measurement of change in resistance may be made with about 50 experimental points for 50 hr irradiation, per sample. However, this is using the available equipment to the limit of its possibilities. A more sensitive potenetiometer (10^{-8} V; Rubicon, for ex.) would permit the use of a galvanometer less cumbersome than a wall-type model and the adoption of thicker samples (5mils diameter, for ex.).

2-Transfer tests of liquid nitrogen and helium

Since the loss of liquid during transfer cannot be estimated on the paper with a reasonable degree of accuracy, it was decided to measure the fraction of liquid helium which evaporates during a transfer through a long tube. Figure 8 represents the principle of the measurement. A transfer tube of 20 feet length, diameter of the vacuum jacket 1/2 inch, inside diameter of the helium tube 1/16 inch, was built, as explained in Section I, Paragraph 4. The envelope is in Alcoa 3003 H 14, the helium tube in Alcoa "Utilitube". The vacuum jacket is pumped down to less than 1 μ mercury by an oil diffusion pump and a mechanical pump. Vacuum is read with a RCA 1946 thermocouple tube. The calibration curve obtained for this thermocouple, using a McLeod mercury gauge, is given in Figure 9.

An attempt to pass liquid nitrogen through this tube showed that the mass flow was extremely slow, even applying a pressure of 20 lbs psi nitrogen gas on the Dewar containing the liquid nitrogen. After two hours no liquid nitrogen was collected at the outlet of the transfer tube. The volume flow of nitrogen gas out of the transfer tube was too small

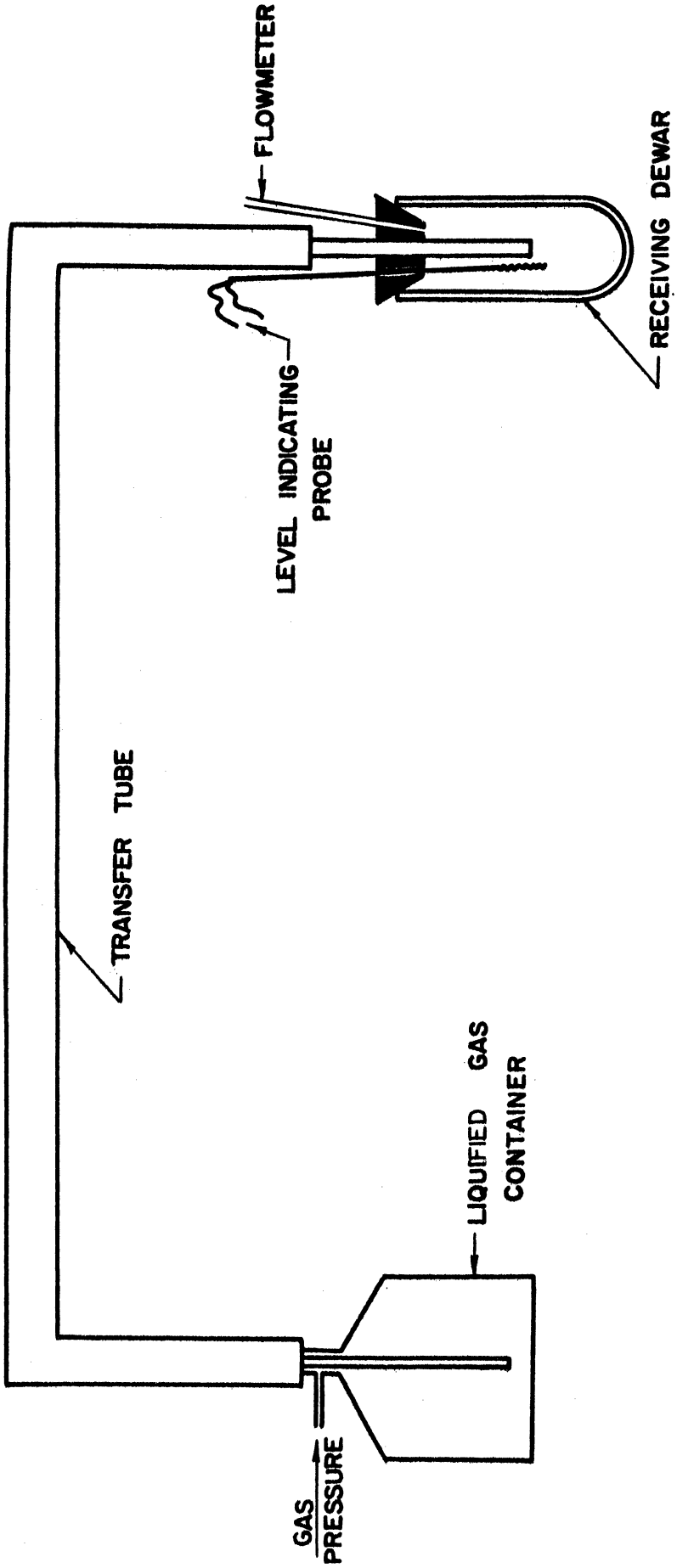

Figure 8. Principle of Measurement of Evaporation During Transfer.

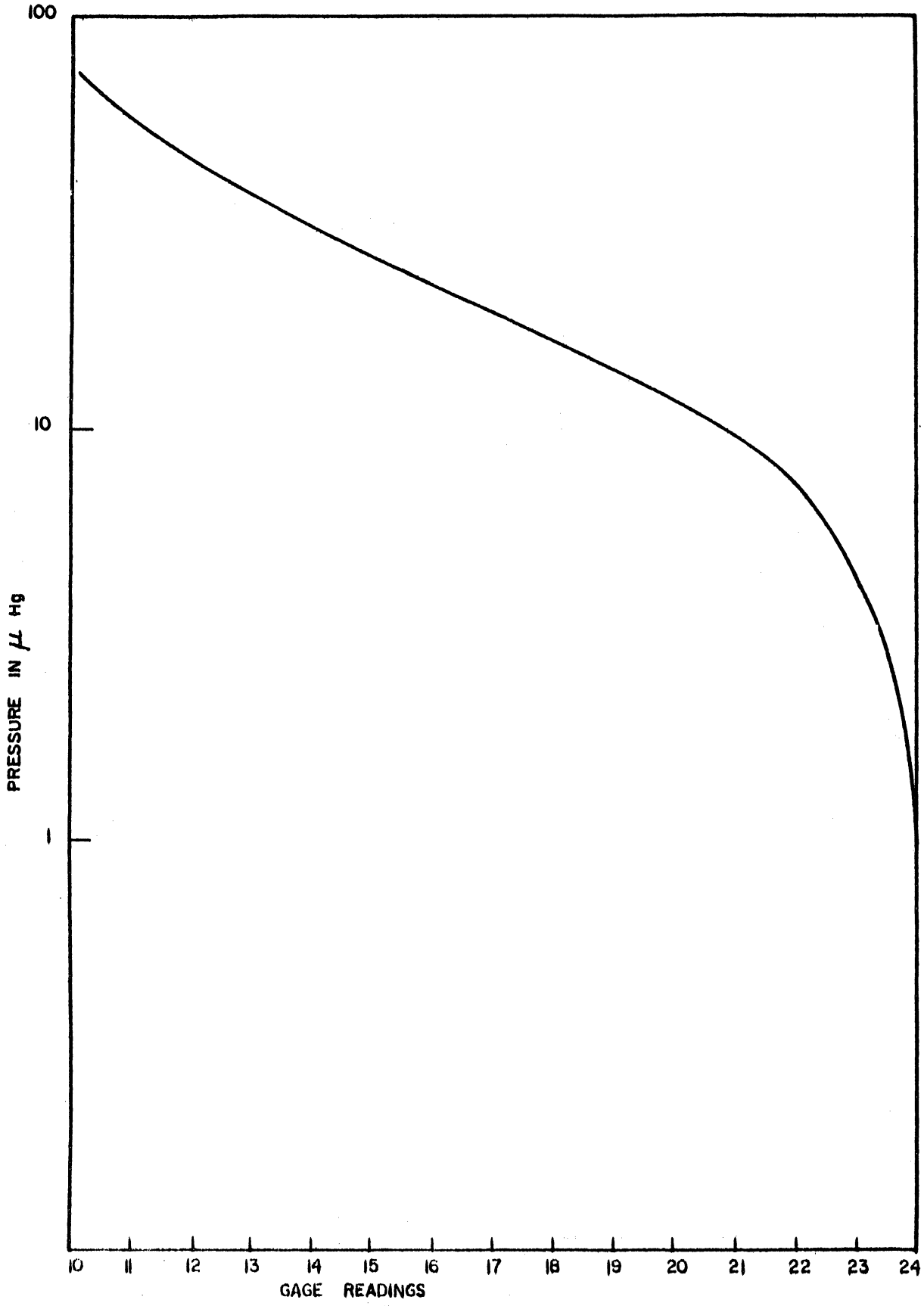

Figure 9. Calibration of Thermocouple.

to be measured. Although there is a serious reduction in the section of the inner tube caused by the use of threaded compression fittings, it was decided that the diameter of 1/16 inch was too small for the transfer of liquid nitrogen. Two transfer tubes for nitrogen, with a nitrogen tube of diameter of 1/8 and 3/16 inch, respectively, were ordered from the laboratory shop. Inasmuch as their use is only a test of dimensions, steel has been selected as the material.

There remain, however, the possibility that the aluminum tube would be adequate for the transfer of liquid helium, whose viscosity is extremely low.

ADDENDUM

Calculations of the macroscopic cross sections

U_{25} $$N_{25} = \frac{140}{235} \times \frac{1}{(3.189 \times 3.035) \times (2.54)^2 \times 60} N_o$$

$$= 1.6 \times 10^{-4} N_o ,$$

$$\Sigma_1 = \Sigma_{f\ th,\ 25} = 0.845 \times 582 \times 10^{-24} \times 1.6 \times 10^{-4} \times 6.03 \times 10^{23}$$

$$= \underline{4.75 \times 10^{-2}\ cm^{-1}}$$

Al $$N_{Al} = \rho_{Al,\ m} \times \frac{N_o}{27} = \frac{1.13 \times 6.03 \times 10^{23}}{27} = 2.49 \times 10^{22} ,$$

$$\Sigma_2 = \Sigma_{a\ th,\ Al} = 0.845 \times 0.23 \times 10^{-24} \times 2.49 \times 10^{22}$$

$$= \underline{4.82 \times 10^{-3}\ cm^{-1}}$$

H_2O $$\Sigma_{a\ H_2O} = N_H \sigma_H + N_{ox} \sigma_{ox} = 2\vartheta \sigma_H + \vartheta \sigma_{ox} ,$$

$$\vartheta = \rho_{H_2O,\ m} \times \frac{N_o}{18} = \frac{0.58}{18} N_o = 3.22 \times 10^{-2} \times 6.03 \times 10^{23}$$

$$= 1.942 \times 10^{22} ,$$

$$(\Sigma_{a\ H_2O})_{core,\ 2200} = 1.942 \times 10^{22} (2 \times 0.332 + 0.0002) \times 10^{-24}$$

$$= 1.29 \times 10^{-2} ,$$

$$\Sigma_3 = \Sigma_{a\ th,\ H_2O} = 0.845 \times 1.29 \times 10^{-2}$$

$$= \underline{1.09 \times 10^{-2}\ cm^{-1}}$$

BIBLIOGRAPHY TO APPENDIX XXIV

1. Cooper, H. G., Koehler, J. S., and Marx, J. W., "Irradiation Effects in Copper, Silver, and Gold Near 10°K," Phys. Rev., 97, No. 3, (1955).

2. Marx, J. W., Cooper, H. G., and Henderson, J. W., "Radiation Damage and Recovery in Copper, Silver, Gold, Nickel, and Tantalum," Phys. Rev., 88, No. 1, (1952).

3. Selected Reference Material, United States Atomic Energy Program, Research Reactors, (1955).

4. Kittel, C., Introduction to Solid State Physics, John Wiley and Sons, Inc., New York, (1956).

5. The Reactor Handbook, Vol. 1, Physics, declassified edition, published by Technical Information Service, U.S. Atomic Energy Commission, (May 1955).

6. Clairborne, H. C., Copenhaver, C. M., Bertini, H. W., and Fowler, T. B., "Calculating Gamma Heating in Reactor Structures," Nucleonics 15, No. 10, (1957).

7. Blewitt, T. H., Coltman, R. R., Holmes, D. K., and Noggle, T. S., "Mechanism of Annealing in Neutron Irradiated Metals," ORNL 2188, p. 52, (December 1956).

8. Wexler, A., "Evaporation Rate of Liquid Helium 1," Proceedings of the NBS Semicentennial Symposium on Low-Temperature Physics, NBS Circular 519, (1952).

9. Dushman, S., Scientific Foundations of Vacuum Technique, John Wiley and Sons, Inc., New York, (1949).

10. Mapother, D. E., and Witt, F. E. L., "Cryostat for Cyclotron Irradiation at Liquid Helium Temperatures," Rev. Sci. Instr., 26, No. 9, (1955).

11. DeLaunay, J., "The Theory of Specific Heats and Lattice Vibrations," Solid State Physics, Advances in Research and Applications, Vol. 2, Academic Press Inc., New York, (1956).

12. Hughes, D. J., and Harvey, J. A., Sect. 8, Nuclear Physics, Para. 8h, Neutrons, American Institute of Physics Handbook, Gray, D. E., Editor, McGraw-Hill, New York, (1957).

13. Hughes, D. J., and Harvey, J. A., Neutron Cross Sections, BNL 325, (July 1, 1955).

BIBLIOGRAPHY TO APPENDIX XXIV (CONT'D)

14. Marks, L. S., Mechanical Engineers' Handbook, McGraw-Hill, New York, (1941).

15. Föppl, A., Résistance des Matériaux et Elements de la Théorie Mathématique de l' Elasticité, Gauthier-Villars et Cie, Paris, (1930).

BIBLIOGRAPHY

1. Planeix, J. M., Preliminary Study, University of Michigan, (1958).

2. Brinkman, J. A., "On the Nature of Radiation Damage in Metals," J. Appl. Phys., 25, No. 8, (1954).

3. Snyder, W. S., and Neufeld, J., "Disordering of Solids by Neutron Irradiation," Phys, Rev., 97, No. 6, (1955), Phys. Rev., 99, No. 4, (1955).

4. Jongenburger, P., "The Extra-Resistivity Due to Vacancies in Copper, Silver, and Gold," Appl. Sci. Research B, 3, No. 4-5, (1953).

5. Blatt, F. J., "Effect of Vacancies and Interstitials on the Electrical Properties of Copper," Bulletin Am. Phys. Soc., 29, No. 7, (1954).

6. Dexter, D. L., "Scattering of Electrons from Point Singularities in Metals," Phys. Rev., 87, No. 5, (1952).

7. Marx, J. W., Cooper, H. G., and Henderson, J. W., "Radiation Damage and Recovery in Copper, Silver, Gold, Nickel, and Tantalum," Phys. Rev., 88, No. 1, (1952).

8. Cooper, H. G., Koehler, J. S., and Marx, J. W., "Irradiation Effects in Copper, Silver, and Gold Near 10°K," Phys. Rev., 97, No. 3, (1955).

9. Seitz, F., and Koehler, J. S., "Displacement of Atoms during Irradiation," Solid State Physics, Advances in Research and Applications, Vol. 2, Academic Press Inc., New York, (1956).

10. Cooper, H. G., "Irradiation Effects in Copper, Silver, and Gold, Near 10°K," PhD Dissertation, University of Illinois, (1954).

11. Redman, J. K., Noggle, T. S., Coltman, R. R., and Blewitt, T. H., "Very Low-Temperature Irradiation of Metals: Change in Electrical Resistivity," Bul. Am. Phys. Soc., II, 1, No. 3, (1956).

12. Huntington, H. B., "Creation of Displacements in Radiation Damage," Phys. Rev., 93, No. 6, (1954).

13. Eggen, D. T., and Laubenstein, M. J., "Displacement Energy for Radiation Damage in Copper," Phys. Rev., 91, No. 1, (1953).

14. Dixon, C. E., and Bowen, D. B., "Radiation Ordering by Cyclotron Particles," Phys. Rev., 94, No. 5, (1954).

15. Wruck, D., and Wert, C., "Crystal Structure as a Factor in Radiation Damage," Phys. Rev., 94, No. 5, (1954).

16. Dieckamp, H., and Crittenden, E. C., "Shear Modulus of Irradiated Copper," Phys. Rev., 94, No. 5, (1954).

17. McDonnell, W. R., and Kierstead, H. A., "Expansion of Copper Bombarded by 21-Mev Deuterons," Phys. Rev., 93, No. 1, (1954).

18. Overhauser, A. W., "Isothermal Annealing Effects in Irradiated Copper," Phys. Rev., 90, No. 3, (1953).

19. Tucker, C. W., and Senio, P., "On the Nature of Thermal Spikes," J. Appl. Phys., 27, No. 3, (1956).

20. McReynolds, A. W., Augustyniak, W., McKeown, M., and Rosenblatt, D. B., "Neutron Irradiation Effects in Copper and Aluminum at 80°K," Phys. Rev., 98, No. 2, (1955).

21. Denney, J. M., "Experimental Evidence for Melted Regions in Metal Crystals Resulting from Particle Bombardment," Phys. Rev., 94, No. 5, (1954).

22. Cottrell, A. H., "Effects of Neutron Irradiation on Metals and Alloys," Metallurgical Reviews, Vol. I, Part 4, (1956).

23. Rutherford, E., "The Scattering of Alpha and Beta - Particles by Matter and the Structure of the Atom," Phil. Mag., 21, p. 669, (1911). Reprint of original paper in Foundations of Nuclear Physics, Beyer, R. T., Editor, Dover, New York, (1949).

24. Ozeroff, J. D., "Atomic Displacements Produced by Fission Fragments and Fission Neutrons in Matter," KAPL-205, AECD-2973, (1949).

25. Bohr, N., "The Penetration of Atomic Particles Through Matter," Det. Kgl. Danske Videnskab. Selskab. Mathematisk-fysiske Medd., XVIII, 8, (1948).

26. Kaplan, I., Nuclear Physics, Addison-Wesley, Cambridge, Mass., (1956).

27. Cooper, H. G., Koehler, J. S., and Marx, J. W., "Resistivity Changes in Copper, Silver, and Gold Produced by Deuteron Irradiation Near 10°K," Phys. Rev., 94, No. 2, (1954).

28. Geiger, H., and Marsden, E., "The Laws of Deflection of Alpha-Particles Through Large Angles," Phil. Mag., 25, p. 604 (1913).

29. Hughes, D. J., and Harvey, J. A., Neutron Cross Sections, BNL 325, (July 1, 1955).

30. Seitz, F., "Disordering of Solids by Action of Fast Massive Particles," Discuss. Faraday Soc., 5, p. 271 (1949).

31. Blewitt, T. H., Coltman, R. R., Holmes, D. K., and Noggle, T. S., "Mechanism of Annealing in Neutron Irradiated Metals," ORNL 2188, p. 52, (December 1956).

32. Waltson, G. N., "Fission Recoil and Its Effects," Progress in Nuclear Physics, Vol. 6, Pergamon, London, (1957).